Development of a Global Statistical Framework for Estimating Landscape Freeze-Thaw under Changing Climate Conditions with Application to Québec

Shadi Hatami Majoumerd

A Thesis
in
the Department
of
Building, Civil & Environmental Engineering

Presented in Partial Fulfilment of the Requirements
For the Degree of
Doctor of Philosophy (Building Engineering) at
Concordia University
Montréal, Québec, Canada

September 2021

CONCORDIA UNIVERSITY
SCHOOL OF GRADUATE STUDIES

This is to certify that the thesis prepared

By: Shadi Hatami Majoumerd

Entitled: Development of a Global Statistical Framework for Estimating Landscape Freeze-Thaw under Changing Climate Conditions with Application to Québec

and submitted in partial fulfillment of the requirements for the degree of

Doctor of Philosophy

complies with the regulations of the University and meets the accepted standards with respect to originality and quality.

Signed by the final examining committee:

_____ Chair
Dr. John Xiupu Zhang

_____ External Examiner
Dr. Farshid Vahedifard

_____ External to Program
Dr. Farnoosh Naderkhani

_____ Examiner
Dr. Attila Michael Zsaki

_____ Examiner
Dr. Biao Li

_____ Thesis Supervisor
Dr. Ali Nazemi

Approved by _____
Dr. Mazdak Nik-Bakht, Graduate Program Director

September 13, 2021 _____
Dr. Mourad Debbabi, Dean,
Gina Cody School of Engineering and Computer Science

Abstract

Development of a Global Statistical Framework for Estimating Landscape Freeze-Thaw under Changing Climate Conditions with Application to Québec

Shadi Hatami, Ph.D.
Concordia University, 2021

Seasonal Freeze-Thaw (FT) dynamics are among the most important landscape processes, influencing ground thermal and hydrological characteristics across cold regions. These impacts can further affect the environmental processes, socio-economic, and cultural activities developed around the use of lands and waters. From a physical perspective and at the large spatial and regional scales, temperature and snow depth are the key drivers of variability in the timing and distribution of FT dynamics. However, climate change has significantly affected both temperature and snow depth over the past decades, and thus FT dynamics in time and space. As a result, it is of a great importance to understand and quantify the control of changing climate on FT characteristics and project future states of FT characteristics subject to future climatic projections. This knowledge and modeling capability can provide an invaluable information for agricultural activities, infrastructure design and maintenance, monitoring the ecosystem's livelihood, and estimating land-induced greenhouse gas emissions due to permafrost degradation. This thesis provides a generic and globally relevant statistical framework to quantify the compound control of temperature and snow depth on FT dynamics over different spatiotemporal scales. A set of gridded observed temperature and snow depth data with the remotely sensed state of the frozen soil are utilized as basis for understanding the climate control on FT dynamics and their spatiotemporal variability. Using these gridded data records, it is possible to greatly overcome the limitations in using station-based data, particularly at higher latitudes. Utilizing future projections of climate models along with a rigorous data processing step and different statistical methodologies, future projections of precipitation type, snow depth, and FT can be obtained over the required spatial and temporal resolutions. Although statistical models have been widely used to address the impact of changing climate on different environmental processes, to the best of our knowledge, there was no previously known formal framework to pair the hydroclimatic data with FT patterns. In this work, bivariate and multivariate copula methodologies are used to statistically model the interdependencies between a relevant set of hydroclimatic variables and different FT characteristics and consequently quantify the control of climate on FT patterns over observed and future time episodes. By considering Québec as a case study, it is demonstrated that how this methodology can be fused with available bottom-up and top-down impact assessment approaches. In the bottom-up impact assessment approach, the response of FT characteristics to a range of feasible future climate conditions is quantified using various forms of stress tests in the form of what-if scenarios. To implement the model in the context of top-down impact assessments, a dynamic copula model with time-varying parameterization is advised and accordingly, future FT characteristics are projected conditional to future air temperature and snow depth in Québec.

"The wide world is all about you: you can fence yourselves in, but you cannot forever fence it out"[1]

J.R.R Tolkien

[1] The Fellowship of the Ring: Being the first part of The Lord of the Rings. 1954.

Dedication

To my colleague, friend and husband, Masoud

Acknowledgments

First, I would like to express my special gratitude to my supervisor Dr. Ali Nazemi, for his help, guidance, availability and persistent support throughout my Ph.D. and giving me the golden opportunity to do this wonderful project. He always guides and motivates me to work hard and keep pursuing the path toward perfection. I will be always thankful for his critical review of my works and the continuous encouragement through the course of this long journey.

I would also like to extend my deepest gratitude to my examining committee members – Dr. Attila Michael Zsaki, Dr. Biao Li, Dr. Farnoosh Naderkhani, Dr. Javad Sadri, and Dr. Farshid Vahedifard – for their invaluable time, comments, and feedback on my thesis work.

I also wish to thank the Concordia University Faculty of Engineering and Computer Science for granting me the "International Tuition Award of Excellence" scholarship, "Conference & Exposition Award", and "Accelerator Award" that enabled me to conduct this research. I also would like to acknowledge the "Fond de Recherche Nature et technologies through Établissement de la relève professorale" and "Canada Natural Science and Engineering Research Council" for providing part of the funding and support during my Ph.D. program.

I would like to express my profound appreciation to Dr. Elmira Hassanzadeh of Polytechnique Montréal for her valuable support and constructive suggestions.

Many thanks to all my colleagues and friends in Water Security and Climate Change Lab (WSCC) for the great group discussions and the time we shared that made this trip more enjoyable.

Last but not least, my deepest gratitude goes to my beloved husband, Masoud; wonderful parents, Ashraf and Hossein; and my precious little sister, Donya, for their unconditional love and support.

Statement of Contribution

Published and Submitted Journal Papers:

1. Hatami, S., Zandmoghaddam, S., Nazemi, A. (2019). Statistical Modeling of Monthly Snow Cover Loss in Southern Canada. *Journal of Hydrologic Engineering*, 24.3, 04018071. Link
2. Hatami, S., Nazemi, A. (2021). A statistical framework for assessing temperature controls on landscape freeze-thaw: application and implications in Québec, Canada (1979-2016). *Journal of Hydrology*, 126891. Link
3. Hatami S., Nazemi, A. (2021). On Complex Responses of Landscape Freeze-Thaw to Compound Climatic Changes: Lines of Evidence from Québec, Canada. *Scientific Reports*, (Submitted on June 9th, 2021).

Working Papers:

1. Hatami, S., Nazemi, A. (2021). A Multivariate Statistical Framework for Top-down Projections of Freeze-Thaw under Changing Climate Conditions – Part 1: Key Considerations and Development of a Gridded Snow Depth Model. *Earth's Future*, (In preparation – to be submitted).
2. Hatami, S., Nazemi, A. (2021). A Multivariate Statistical Framework for Top-down Projections of Freeze-Thaw under Changing Climate Conditions – Part 2: Development of a Time-varying Dependence Model and an Integrated Impact Assessment. *Earth's Future*, (In preparation – to be submitted).

Published and Accepted Conference Papers:

1. Hatami, S., Nazemi, A. (2021). The Compound Impacts of Changing Temperature and Snow Cover on Freeze and Thaw Patterns across Québec. *Geo-Extreme 2021*, Savannah, Georgia. (Accepted).
2. Hatami, S., Nazemi, A. (2019). Temperature controls of the freeze and thaw patterns in Québec. *CSCE2019 Conference Proceedings*, Montréal, Canada. Link
3. Hatami, S., Nazemi, A., Amirjabbari, A. (2019). Evolving trends of rain over precipitation in Canadian cold season during the late 20th century. *CSCE2019 Conference Proceedings*, Montréal, Canada. Link – recipient of ***"Student Best Paper Award"***. Link

Conference Presentations:

1. Hatami, S., Nazemi, A. "21st Century Projections of Snow Depth over the Province of Québec, Canada". *CWRA Abstract*, Oral presentation, June 2021, Virtual.
2. Hatami, S., Nazemi, A. "21st Century Projections of Soil Freeze and Thaw over the Province of Québec, Canada". *AGU Fall Meeting Abstract*, Poster presentation, December 2020, Virtual. Link
3. Hatami, S., Nazemi, A. "Temperature control on Freeze and Thaw Patterns in Québec". *27th IUGG General Assembly*, Oral presentation, July 2019, Montréal, Canada.
4. Hatami, S., Zandmoghaddam, S., Nazemi, A. "A Statistical Framework for Estimating Monthly Loss of Snow Depth in Southern Canada". *CGU Abstract*, Oral presentation, June 2018, Niagara Falls, Canada.

Table of Contents

List of Figures

List of Tables

List of Abbreviations, Nomenclature, Greek Symbols, and Subscripts

Table I. Abbreviations

Abbreviations		Unit
ANOVA	ANalysis Of Variance	(-)
CCDAP	Canadian Climate Data Accessibility Portal	(-)
CDF	Cumulative Distribution Function	(-)
CMC	Canadian Meteorological Center snow depth data	(-)
CMIP5	5th phase of the Coupled Model Intercomparison Project	(-)
EFA	Expected daily extent of Frozen Area	(%)
ETA	Expected daily extent of Thawed Area	(%)
EZ	EcoZone	(-)
FD	Number of Frozen Days	(days)
FT	Freeze-Thaw	(-)
FTD	Number of transient Days	(days)
FT-ESDR	Freeze and Thaw Earth System Data Records	(-)
GCM	Global Climate Model	(-)
GMFD	Global Meteorological Forcing Dataset	(-)
GPCIS	Global Partial Correlation Input Selection	(-)
HBV	Hydrologiska Byråns Vattenbalansavdelning hydrological model	(-)
LANDSAT	LAND Remote-Sensing SATellite	(-)
IPCC	Intergovernmental Panel of Climate Change	(-)
LPCIS	Local Partial Correlation Input Selection	(-)
METAR	Meteorological aviation	(-)
MLR	Multiple Linear Regression	(-)
MODIS	MOderate Resolution Imaging Spectroradiometer	(-)
NEX-GDDP	NASA Earth Exchange Global Daily Downscaled Projections dataset	(-)
NSIDC	National Snow and Ice Data Center	(-)
Obs.	Observed	(-)
PCIS	Partial Correlation Input Selection	(-)
PDF	Probability Density Function	(-)
PE	Permafrost Extent	(%)
RCPs	Representative Concentration Pathways	(-)
SA	Special Aviation	(-)
SD	Snow Depth	(cm)
SDL	Snow Depth Loss	(cm)
Sim.	Simulated	(-)
SM	Snow Melt	(cm)
SMRS	Satellite Microwave Remote Sensing	(-)
SSM/I	Special Sensor Microwave/Imager	(-)

Table I. Continued.

Abbreviations		**Unit**
SSMIS	Special Sensor Microwave Imager/Sounder	(-)
SSMR	Scanning Multichannel Microwave Radiometer	(-)
SWAT	Soil & Water Assessment Tool	(-)
SWE	Snow Water Equivalent	(cm)
SYNOP	surface SYNOPtic	(-)
TD	Number of Thawed Days	(days)
VFA	Variability in expected daily extent of Frozen Area	(%)
VTA	Variability in expected daily extent of Thawed Area	(%)
WEAP	Water Evaluation And Planning system	(-)
WMO	World Meteorological Organization	(-)

Table II. Nomenclature

Nomenclature		**Unit**
BIC	Bayesian Information Criterion	(-)
$C(.)$	Copula function	(-)
$c(.)$	Copula density	(-)
Cov^{-1}	Inverse of the covariance matrix	(-)
Cum(.)	Cumulation operator	(-)
CV	Coefficient of variation	(%)
DOY	Day of year	(-)
e	error	(-)
E(.)	Long-term expected value over any time-episode	(-)
$F(.)$	Marginal CDFs of random variables	(-)
$f(.)$	Marginal PDFs of random variables	(-)
FD_{year}	Annual number of frozen days	(days)
FTD_{DJF}	Number of transient days in the winter season	(days)
k_1, k_2	Densification parameters	(-)
$H(.)$	Joint dependencies structure	(-)
O_{FT}	Centroid of FT data record	(-)
$O_{T/SD}$	Centroid of temperature of snow depth data record	(-)
m_f	Melt factor	(-)
n_c	Number of concordant pairs	(-)
n_d	Number of discordant pairs	(-)
NSE	Nash and Sutcliffe coefficient of efficiency	(-)
Pricip / P	Daily precipitation	(cm)
R	Rainfall	(mm)
$R(.)$	Correlation function	(-)

Table II. Continued.

Nomenclature		Unit
R^2	Coefficient of determination	(-)
RE	Relative Error	(-)
RMSE	Root Mean Squared Error	(-)
S	Snowfall	(cm)
S/P	Partitioning of precipitation	(-)
S_w	Water stored in monthly snowfall	(mm)
T_b	Brightness temperature	(°K)
$\bar{T}$	Mean temperature (at different temporal scales)	(°C)
T_{mean}	Mean daily temperature	(°C)
T_{min}	Minimum daily temperature	(°C)
T_{max}	Maximum daily temperature	(°C)
$T_{max} - \bar{T}$	Surplus from average thermal energy	(°C)
$\bar{T} - T_{min}$	Deficit from average thermal energy	(°C)
$T_{max} - T_{min}$	Range of available thermal energy	(°C)
T_l	Melting temperature thresholds	(°C)
T_s	Freezing temperature thresholds	(°C)
X , Y	Pairs of random variables	(-)
ρ_w	Density of water	(g/cm^3)
ρ_b	Bulk density of snowpack	(g/cm^3)
ρ_{max}	Maximum bulk density	(g/cm^3)
ρ_0	Initial bulk density	(g/cm^3)
Ψ(.)	Standardization operator	(-)

Table III. Greek symbols

Greek Symbols		Unit
θ	Copula model parameters	(-)
τ	Kendall's tau dependence coefficient	(-)
Δ	Change in the value of a variable	(-)
∂	Partial derivative	(-)
ε / ϵ	Residuals	(-)
ρ	Density	(g/cm^3)

Table IV. Subscripts

Subscripts		Unit
year	Annual scale	(-)
DJF	Winter	(-)
i, j, k, n	index	(-)
c, d	Concordant and discordant pairs	(-)
max	maximum	(-)
min	minimum	(-)
mean	average	(-)

Chapter 1.
Introduction

1.1 Introduction

Landscape Freeze-Thaw (FT) is one of the most important cryosphere components in cold regions, capable of profoundly impact various eco-hydrological processes (Kim et al., 2019). Changes in FT dynamics can alter regional hydrology (Karlsson et al., 2012), permafrost extent (Hachem et al., 2012; Park et al., 2016a) as well as land-surface fluxes (Bochove et al., 2000; Schaefer et al., 2011; Yi et al., 2014) particularly over northern latitudes where the frozen temperatures and available snow depth are significant parts of the annual hydroclimatic cycle. Around 50% of the land across the northern hemisphere undergoes seasonal transitions from frozen to thawed conditions annually (Kim et al., 2011). This forms a recurring phenomenon determining the occurrence of ecological, hydrological, pedological, and biological activities within the active layer of soil (X. Wang et al., 2019).

Physically, as the state of soil changes from frozen to thawed conditions and vice versa, soil properties such as density, hydraulic conductivity, and infiltration change (M. Wang et al., 2018; Weng et al., 2020; Zhang and Cui, 2017). For instance, frozen soil reduces the hydraulic conductivity, leading to either more runoff due to decreasing infiltration or higher soil moisture as a result of restricted drainage (Iwata et al., 2010; Qi et al., 2019). This can affect surface and sub-surface connectivity (Bechmann et al., 2005) and alters pathways in which water, carbon, and other matters travel (Bosson et al., 2013; Jones et al., 2011) altering the regional hydrology (Karlsson et al., 2013). The FT dynamics can also impact the soil moisture which is of great importance to understand land-atmospheric feedbacks since soil moisture affects the precipitation, temperature, and the motion field of the atmosphere at regional and global scales (Entekhabi et al., 2004; Vogel et al., 2017; Walvoord and Kurylyk, 2016) – see Figure 1.1. Extended thawing can also impact the size, number, and distribution of thermokarst lakes (Jones et al., 2011).

The changes in soil structure as a result of FT cycles could also be in the forms of disruptions of soil aggregates, the release of aggregate protective organisms, and death of soil microorganisms due to excessive pressure (A. Edwards and Cresser, 1992). Sharma et al. (2006), for instance, observed an evident shift in microbial communities of a sample soil from a Greenland area located in southern Germany, due to the events of FT. The changes observed in soil microbial structure can further lead to soil denitrification patterns contributing significantly to the greenhouse effect. Margesin et al. (2007) provided a literature review about the impacts of FT on the growth rate and metabolic activity. C. M. Williams et al. (2015) also studied the effects of climate change on FT patterns and consequently the terrestrial organisms. In addition, FT cycles can contribute to changes in the plant community. Kreyling et al. (2006), for instance, investigated the effects of five more FT cycles on the productivity of grassland community and soil enzymatic activity over the following growing season. The changes in plants' productivity can further alter ecosystem stability and ecosystem services, such as nutrient retention.

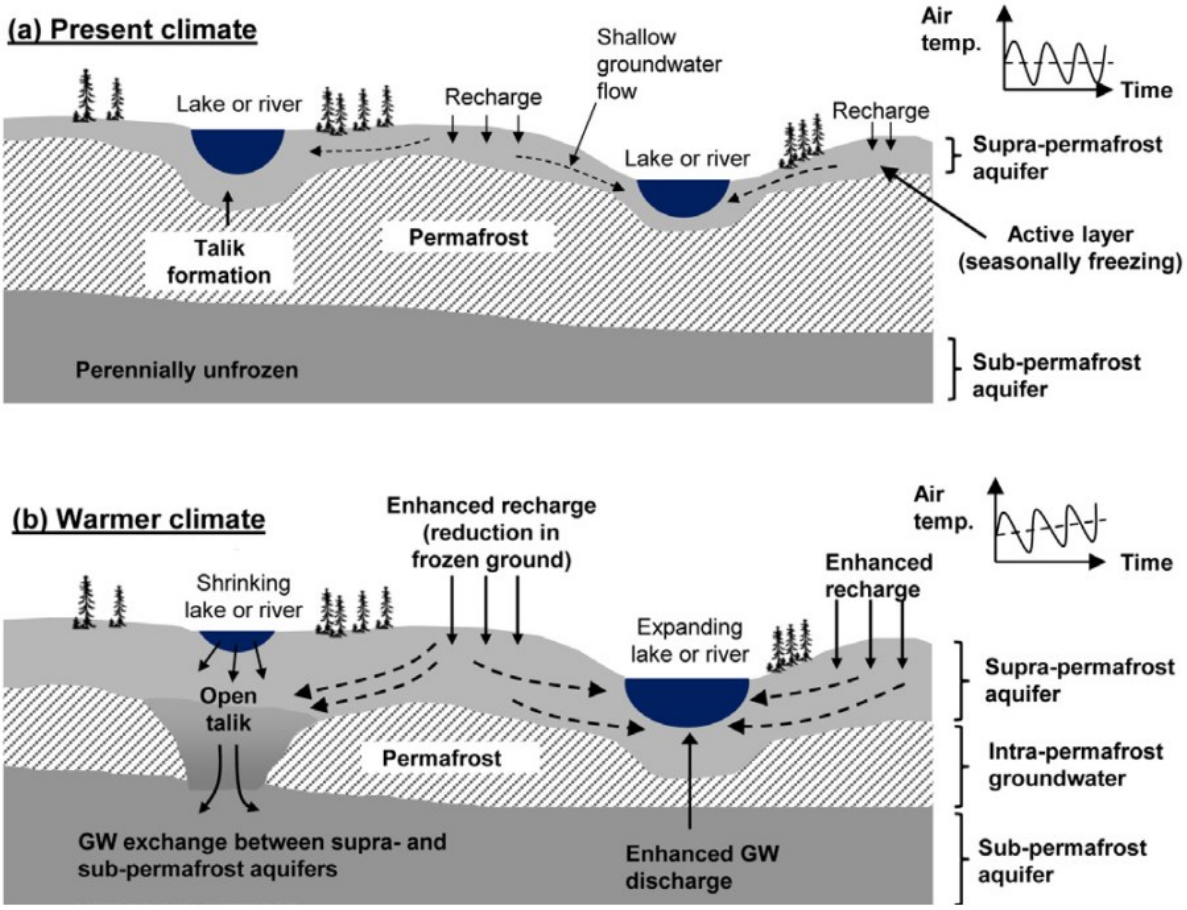

Figure 1.1. The evolution of hydrologic conditions due to thaw in discontinues permafrost region for (a) present climate and (b) warmer climate. The effects of thawing of both active layer and permafrost can be observed on the groundwater level, surface water flow paths, and the terrestrial water balance (Walvoord and Kurylyk, 2016).

There are numerous ways that FT can impose seasonal constraints on environmental activities. The surge of CO_2 and N_2O are among these effects. Figure 1.2 shows the schematic of feedbacks between frozen land and the carbon and nitrogen emission. As the figure clearly illustrates, the higher amount of CO_2 and/or N_2O emission are mainly due to the changes in frozen soil extent and depth as a result of FT dynamics. The reduction in future soil freezing days may stimulate soil respiration and organic matter decomposition (Sjursen et al., 2005). Skogland et al. (1988), for instance, explored the changes in respiratory gasses, due to the FT dynamics. By finding a sudden burst of CO_2 emission after the thawing of soil, they concluded that consideration of FT cycles must be an essential step of greenhouse emission models in cold regions. Later, Bochove et al. (2000) showed the importance of including the FT cycles in N_2O emission models, specifically in areas in which the freezing of the top layer of soil is a frequent event. The changes in FT patterns moreover showed to be significant in the future due to global warming. The thaw and decay of permafrost carbon in near future, for instance, require larger reductions in fossil fuel consumption to reach a target CO_2 emission (Schaefer et al., 2011).

FT dynamics at high latitudes are also a key consideration point for geotechnical engineering applications as well as socio-economic activities such as design, operation, and durability of civil engineering infrastructure (McCartney et al., 2019; Roseen et al., 2012; Shahrajabian and Behfarnia, 2018; Zapata and Houston, 2008). The expansion of water molecules due to freezing can affect the human infrastructure in various aspects. For instance, human infrastructure, in particular, is vulnerable to the number of expansion events in soil and therefore the increasing number of transient FT cycles. This has been the subject of numerous studies. Feng et al. (2010) tried to monitor the residual life of different mixtures of asphalt pavements under the influence of FT cycles in coastal regions of China. They concluded the fact that different types of asphalt mixtures have fixed residual lives after a number of FT cycles due to the damaging effect of ice expansion load and the interfacial damage between asphalt and aggregate or fracture of asphalt mortar. Mills et al. (2009) also considered the future changes in FT cycles as a factor of alterations in pavement deterioration rates. According to their results, in the next 50 years, the structures will freeze later and thaw earlier with a shorter freezing period, which will raise the potential for rutting. FT can also affect roads and pavements (Roseen et al., 2012) and therefore have an impact on human transportation systems (Zapata and Houston, 2008). The FT-driven changes in soil hydraulic conductivity can be also important for designing hydraulic structures (Chamberlain et al., 1990; Kraus et al., 1997) and runoff management infrastructures (Zheng and Flerchinger, 2001). As another example of the FT impacts on human infrastructure, Mohamed et al. (2002) studied the effects of FT cycles on the stability of mine tailing. They observed a considerable reduction in compressive strength of the mine tailing samples, attributed to high tailing moisture suction developed in freezing soil. Their results also indicated changes in tailing soil permeability due to FT cycles providing valuable information for future mining activities in cold regions.

Changes in landscape FT can result in other socio-economic challenges that can be accompanied by opportunities for new development in northern countries such as Canada (Ho and Gough, 2006). For instance, frozen landscape and short growing seasons that have constrained agricultural activities in the north are about to be replaced by warm and extended growing seasons, making new opportunities for growing crops over northern lands (King et al., 2018; Parry, 2019). Moreover, warmer temperature with the help of technological advancements makes other resources, such as oil and gas and minerals accessible (Poppel et al., 2015). More days with frozen state, on the other hand, can negatively impact agricultural activities by damaging agricultural products (Harrison et al., 2020; Zhou et al., 2015). From the cultural perspective, FT dynamics can directly or indirectly affect the archaeological and cultural sites (Andrews et al., 2016), community relocations (Maldonado et al., 2013; Gibson et al., 2021), the use of traditional travel routes (Proverbs et al., 2020), and wildlife distribution (Tape et al., 2016) particularly in northern-region communities. As an example, since the agriculture and natural resources industry enters northern regions, environmental risk particularly in terms of contamination increases (Ali, 2009). In addition, as soil thaws near a hillside or a stream, it can trigger erosions and landslides causing the relocation of indigenous communities (Lewkowicz and Way, 2019; Patton et al., 2019).

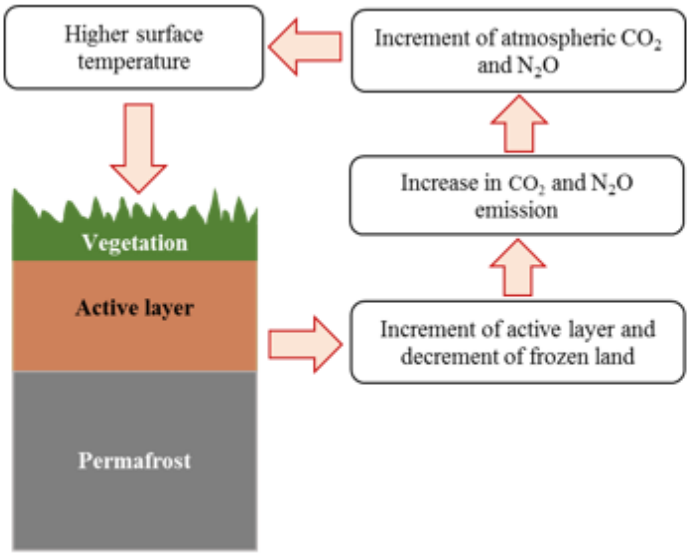

Figure 1.2. The schematic for basic dynamics of frozen land and carbon emission feedback.

Having said that, there are several physical and biological processes affecting the dynamics of soil moisture and soil freezing and thawing. The interplays between these variables, ranging from solar radiation to the characteristics of the organic soil layer, determine the dynamics of FT (Bonan, 1989; Gibson et al., 2018; Slater et al., 1998). Vegetation, for instance, can act as a buffer for climatic warming and regulate the amplitude and duration of diurnal soil FT cycles (Hu et al., 2020; Niu et al., 2019). Different vegetation types have distinct structures and consequently affect energy balance differently (Guo et al., 2018). Additionally, a large proportion of organic matter in the soil can affect the FT dynamics, heighten microbial decomposition in a warming climate and consequently alter the FT dynamic (Walz et al., 2017). Land surface albedo can also influence the energy budget and regional climate, particularly at higher latitudes where there is a significant snow season (Fletcher et al., 2009; Kattsov et al., 2007; Kim et al., 2018). Additionally, solar radiation, the forest floor organic layer, and wildfire are among important physical processes affecting the dynamics of soil moisture and soil freezing and thawing (Bonan, 1989; Gibson et al., 2018; Slater et al., 1998). Having said that, it has been shown that temperature and snow depth are the two most influential drivers of FT dynamics (Henry, 2008; Larsen et al., 2007; Peng et al., 2016). On the one hand, near-surface air temperature can affect the timing and duration of FT states as well as the depth of frozen layer (Frauenfeld et al., 2004; Henry, 2007; Hirota et al., 2006; Sinha and Cherkauer, 2008; Wei et al., 2017; Yi et al., 2015) . On the other hand, the depth of snow cover can control the thermal regime of the soil layer through interfacing with the atmosphere (Iwata et al., 2010; Zhang, 2005) and influence the energy balance through albedo (Fletcher et al., 2009; Kattsov et al., 2007; Kim et al., 2018).

The global mean surface temperature, however, has shown an upward trend specifically since the mid-20th century (Huang et al., 2017). The rate of warming is even higher across northern latitudes and over winter and spring (IPCC, 2001; Rosenzweig et al., 2008). This warming in recent decades, which is mainly associated with increasing anthropogenic CO_2 emission (Francey et al.,

2010), significantly changes the cryosphere and its components such as snow depth and FT states (IPCC, 2014; Y. Qin et al., 2016). Higher temperature results in the lengthening of thaw season, deepening the active layer, and poleward retreat of permafrost boundaries in northern latitudes (Anisimov and Nelson, 1996; Zhang et al., 2011). Reduced precipitation associated with warming temperature can also increase the frequency and intensity of FT cycles (Brown and Degaetano, 2011). Decreasing snow depth reduces the thermal insulation of soil surface and increases soil vulnerability to fluctuations in air temperature (Chen et al., 2020; Hirota et al., 2011). This can in turn contribute to decreasing frost depth and increasing the frequency of transitions in FT states (Henry, 2008; Iwata et al., 2010; Zhang, 2005).

As FT dynamics alter due to elevating air temperature and thinning snow depth, natural processes and socio-economic activities are affected (Krogh et al., 2017; J. Liu et al., 2009; Wolf et al., 2010). For instance, increased transitions between frozen and thawed conditions can cause soil erosion (Y. Wu et al., 2018) and deteriorate critical community infrastructures such as pipelines, roads, and other built environments (Melvin et al., 2017; Nelson et al., 2001; Raynolds et al., 2014). Climate change impacts of FT condition can also result in emerging feedback processes between land and atmosphere as the thawing permafrost releases significant amount greenhouse gasses that can even intensify the rate of a warming climate (Schaefer et al., 2014; E. Schuur et al., 2015; Wagner-Riddle et al., 2017). As a result, quantifying possible changes in FT characteristics under future climate conditions can be important for a variety of problems related to land and water management, ranging from local infrastructure design and maintenance to the regional potential for agriculture and natural resource development to global warming.

1.2 Problem Statement

Over past decades many studies have investigated the control of climate on FT patterns, specifically in northern regions (Hachem et al., 2012; Williams et al., 2015). Some studies focused on understanding the relationship between different hydroclimatic variables (mostly near-surface temperature) and FT characteristics such as the number of frozen and thawed days (Wu and Zhang, 2010; Zhao et al., 2010). Smith et al. (2004), for instance, studied the similarity between near-surface air temperature and FT patterns in a large area in northern Eurasia and America. They found a strong positive correlation between spring temperature anomalies and thaw dates, associated with a significant negative correlation between fall air temperature anomalies and freezing dates. The effects of warming temperature on less number of days with the frozen state (Kim et al., 2015), increasing the length of the thawed season (Kim et al., 2014) and poleward retreat of permafrost boundaries (Anisimov and Nelson, 1996) are among other subjects studied over the past years. Other studies investigate the effect of snow depth and snowpack on FT dynamics. Henry (2008), for instance, investigate the impact of snowpack on FT dynamics, demonstrating that reducing snowpack can make soil vulnerable to air temperature which contributes to an increased frequency of FT cycles. However, it is not yet clear whether changes in the FT characteristics are solely due to changes in these influential variables; or, it is due to a more profound change in the relationship between them and FT characteristics at landscape scale.

The current dominant paradigms to assess the impacts of changing climate on FT dynamics are mostly based on physically-based approaches, often involving soil water content, latent heat of water, and even soil properties (Guo et al., 2018; Zhang et al., 2008). Such approaches are often developed based on coupling simultaneous heat and water models, embedding the complex processes of heat convection induced by the water migration (Flerchinger and Hanson, 1989; Kang et al., 2005; Zhang et al., 2021). Qi et al., (2016a,b), for instance, developed a physically-based soil temperature module to simulate the FT dynamics by considering the soil thermal status and snow insulation effects. Peng et al. (2018) used future climate projection to assess the impact of climate change on active layer thickness in permafrost regions across the entire Northern Hemisphere, showing an increase in active layer thickness over all permafrost regions. Wei and Dong (2015), used an ensemble of climate model projections to simulate the projected changes in the snow depths in Qinghai-Tibetan Plateau, indicating decreases in snow depths for most of the climate models. Although physically-based models often lead to accurate results at the local scale, such approaches are limited due to uncertainty in the model parametrization (Li et al., 2012), the possibility of poor process representation (Cao et al., 2020; Walvoord and Kurylyk, 2016), being hugely data-intensive (McCarty et al., 2020; Tape et al., 2018), the requirement for site evaluation for compatibility with original assumption, and limitations in data support at larger scales (Hayashi et al., 2007; Romanovsky and Osterkamp, 1997).

Additionally, current studies focusing on the impacts of changing climate on FT dynamics under historical and future conditions are mainly based on in-situ data (Henry, 2008; Wang et al., 2015). The in-situ data can provide insights on the impacts of changing climate on FT dynamics at the local scale. However, the sparse distribution of station-based data network and lack of continuous data availability can considerably constraint the ability of observation-based data in capturing the spatiotemporal patterns in FT dynamics at larger temporal and spatial scales, particularly at higher latitudes (Takala et al., 2009; K. Zhang et al., 2007). Data interpolation into data-sparse regions, moreover, will result in ignoring the role of geographic features in contributing to heterogeneity in FT states over the landscape (Williams et al., 2000).

In response to these limitations, alternative approaches for impact assessment of FT dynamics have been suggested. These approaches are mainly through the use of statistically-based impact assessment paradigm (Hatami and Nazemi, 2021b, 2019; Lemoine and Kapnick, 2016). Statistical approaches are generally more computationally efficient and require less data support than process-based models and thus often have a better transferability as well as scalability at large temporal and spatial scales (Ni et al., 2021; Zheng et al., 2020). The key advantage of such approaches is in providing the opportunity for the modeling of FT characteristics across coarser temporal and spatial scales instead of continuous modeling of FT dynamics using complex physically-based approaches. Despite the advantages of statistically-based approaches, developing a global statistical framework for estimating FT dynamics under changing climate conditions at coarse temporal and spatial scales is not a straightforward task. Hence, several issues need to be addressed.

First, there is a need for gridded data products for climatic, snow depth, and Freeze/Thaw available at coarse temporal and spatial scales. Although the advent of publically available gridded data products, such as satellite remote sensing data, can overcome such issues, the size and centroid of these datasets are not the same. Therefore, the raw data should be matched in a common grid system before further use.

Second, conventional approaches often assess the individual impact of one event on FT characteristics. The impacts of climate change on FT dynamics, however, can be through more than one individual event. This requires methodologies that can characterize the compound impacts of events on FT dynamics. One key feature of the response to compound events is the nonlinear nature of the response, meaning that the impact of compound events can be more intense compared to the cumulative impacts of individual events when occurring independently. This should be taken into account for the development of statistical framework for a multivariate modeling of FT dynamics.

Third, gridded downscaled climate projections are widely available, it is not yet clear whether they can readily support impact assessment studies, particularly when representing the dynamics of impacts in time are needed. Studies showed that although downscaled climate projections can reproduce long-term statistics and evolution in climate variables, they may need further bias-correction for the purpose of impact assessment when representing the year-to-year dynamics are sought (Ehret et al., 2012; Jaramillo and Nazemi, 2018).

Fourth, there is a need for methodologies for representing snow depth dynamics over the future time episodes at the grid scale. Conventional methodologies such as temperature-index models are widely used due to their computational simplicity, wide availability of air temperature data, and good modeling performance. Nonetheless, such models cannot perform well in complex conditions such as the occurrence of rain over snow and in environments with heterogonous land cover (Bengtsson, 1984; Garen and Marks, 2005). Therefore, a parsimonious model is needed to be developed which is then applied in conjunction with downscaled projections of future climate to produce future scenarios of snow depth required for projection of FT dynamics in future.

Fifth, traditional statistical methodologies are based on the fundamental assumption of stationarity in which it is assumed that probabilistic characteristics of hydrometeorological processes and the dependence structures between variables will not change over time. This is in contrast to the empirically observed time-varying dependence structures between hydroclimatic variables (Chebana and Ouarda, 2021; Dong et al., 2021; Jiang et al., 2015). Although modeling the nonstationary features of individual variables such as trends in the moments of a single variable is often taken into account in the literature, the nonstationarity in the dependence structure is often overlooked. Hence, suitable statistical methodologies are required to identify and incorporate the nonstationarity features such as the time-varying dependence structure.

1.3 Freeze-Thaw, climatic, and snow depth gridded data

It is argued that the advent of publically available gridded data products along with powerful statistical approaches can overcome some of the limitations noted above. Satellite Microwave Remote Sensing (SMRS), which has become extensively popular in recent decades, is well suited for monitoring the spatiotemporal variability of global FT dynamics. They provide a continuous data record with a synoptic view, highly sensitive to signal degradation and contrasting properties of frozen and liquid water in landscape (Nghiem et al., 2012; Z. Qin et al., 2012). The availability of several global and regional gridded datasets under current and future conditions such as reanalysis gridded dataset (e.g., Sheffield et al., 2006; Dile and Srinivasan, 2014), satellite product (e.g., MODIS Terra/Aqua; https://modis.gsfc.nasa.gov/data; Landsat; https://landsat.gsfc.nasa.gov; Huffman et al., 2007), and projected climate model simulation (e.g., Giorgi et al., 2009; Thrasher et al., 2012) provide viable sources for impact assessment under historical and future climatic conditions. With direct relevance to our work here, currently, there is a publically-available data for daily FT states retrieved from satellite imageries (see Kim et al., 2017). If this data product paired with climate and/geographic data, it can provide synoptic, homogeneous, and globally relevant data with a continuous record (Kim et al., 2012; McDonald et al., 2004; Smith et al., 2004) and an opportunity to formally quantify the spatiotemporal variability of FT dynamics and its dependencies with driving climatic and/or geographic variables (Park et al., 2016b). To develop a global statistical framework capable of estimating FT dynamics under changing climate conditions, a database consisting of the observed gridded climatic data, snow depth data, and FT data as well as future projections of climatic data had to be put together. The data set used in this research is presented in Table 1.1. Detailed information on each data record is also provided as follows.

1.3.1 Freeze and Thaw Earth System Data Records (FT-ESDR)

Satellite Microwave Remote Sensing can provide a continuous data record with a synoptic view of FT dynamics. SMRS considerably reduces the sensitivity to signal degradation by atmospheric cloud/aerosol contamination and solar illumination effects as well as increasing the sensitivity to contrasting properties of frozen and liquid water in landscape (Kim et al., 2011; Tucker et al., 2005). One of the reliable sources of FT state data is the global landscape FT Earth System Data Record (FT-ESDR) available from National Snow and Ice Data Center (NSIDC) archive (https://doi.org/10.5067/MEASURES/CRYOSPHERE/nsidc-0477.004). The data set is available on the daily temporal scale with the spatial resolution of 25×25 km over the period of 1979-2017. The microwave radiation emitted from the surface of snow or ice cover is measured to provide the state of FT at each grid. This parameter is referred to as brightness temperature (T_b). The primary record is derived by 37GH, vertically polarized T_b observations. T_b is acquired from three different satellite-based passive microwave sensors of Scanning Multichannel Microwave Radiometer (SMMR), Special Sensor Microwave/Imager (SSM/I), and Special Sensor Microwave Imager/Sounder (SSMIS). The FT state is then classified in the daily morning (AM) and evening

(PM) overpass based on the value of T_b. The combination of the resulting classification produces a daily composite (CO) FT state for each day with four discrete classification levels. The classes are frozen (AM and PM frozen), non-frozen (AM and PM non-frozen), transitional (AM frozen and PM thawed), and inverse-transitional (AM thawed and PM frozen) – see Kim et al. (2017).

Table 1.1 The detailed information on the data record used in this study.

Section	Data set	Considered variables	Spatial coverage	Spatial resolution	Temporal coverage	Temporal resolution	Data format
2.1	FT-ESDR	FT state	Global	25 km x 25 km	1979-2017	Daily	GIF HDF GeoTIFF
2.2	GMFD	Precipitation Minimum temperature Maximum temperature	Global	0.25 deg	1948-2016	3-hourly, daily, monthly	NetCDF
2.3	CMC	Snow depth	Northern hemisphere	24 km x 24 km	1998-2020	Daily	ASCII GeoTIFF
2.4	NEX-GDDP	Precipitation Minimum temperature Maximum temperature	Global	0.25 deg	1950-2100	Daily	NetCDF

A set of FT characteristics can be obtained by knowing the composite daily state of FT. The defined characteristics need to have physical relevance and the ability to describe the FT dynamics in different spatial (grid, ecozone, and province) and temporal (monthly, seasonal, and annual) scales. The list of derived FT characteristics is presented in Table 1.2 (Hatami and Nazemi, 2021b). These FT characteristics fall into two main groups of temporal and special characteristics. Temporal FT characteristics are those acquired in each grid while spatial ones are derived over regions with variable sizes (e.g. ecozones or province). The temporal variables consist of the number of frozen days (*FD*), the number of thawed days (*TD*), and the number of transient days (*FTD*). These variables are studied over different temporal scales. Spatial FT characteristics, on the other hand, are only defined in a specific temporal scale. Permafrost extent (*PE*), for instance, is an annual variable showing the percentage of grids with available permafrost over each year. Permafrost is defined as the ground with a temperature of 0 °C or below over two consecutive years and where the *FD* in each year is higher than the summation of *TD* and *FTD* (Dobinski, 2011; Park et al., 2016b). Mean and variations in the area of frozen/thawed land are among other spatial characteristics defined in monthly scales. These characteristics are shown with *EFA* and *VFA* for expected and standard deviation of daily percentage of grids in each region with the frozen state. Similar notations are used for the mean and standard deviation of thawed area (*TA*).

Table 1.2 Extracted FT characteristics along with their notation, physical relevance, and temporal scale.

Abbreviation	Type	Relevance	Temporal Scale
FD	**Temporal**	Number of frozen days	Monthly/Seasonal/Annual
TD		Number of thawed days	Monthly/Seasonal/Annual
FTD		Number of transient days	Monthly/Seasonal/Annual
PE	**Spatial**	Permafrost extent	Annual
EFA		Expected daily extent of frozen area	Monthly
VFA		Variability in expected daily extent of frozen area	Monthly
ETA)		Expected daily extent of thawed area	Monthly
VTA		Variability in expected daily extent of frozen area	Monthly

1.3.2 Global Meteorological Forcing Dataset (GMFD)

Determining accurate climate variables has central importance to understanding the climate control on FT dynamics. Global Meteorological Forcing Dataset (GMFD) is a long-term, high-resolution, near-surface meteorological dataset that can be easily matched with FT-ESDR data. GMFD climate data are intended to form a benchmark forcing dataset by combining the reanalysis data from the National Centers for Environmental Prediction, the National Center for Atmospheric Research, and a group of recent global observation-based data. This data set has considerably higher accuracy comparing to the initial reanalysis variables as well as better consistency over time and space (Sheffield et al., 2006). The climate variables needed for this study are acquired from a public repository hosted by Princeton University; (http://hydrology.princeton.edu/data.php). The dataset provides gridded climate records with different spatiotemporal resolutions over the period of 1948 to 2016. Due to the availability of FT-ESDR from 1979 to 2017, the period of 1979-2016 is considered as the common period between GMFD and FT-ESDR data records. The abbreviation, name, the spatial and temporal resolution of obtained variables are presented in Table 1.3. The mean daily temperature (T_{mean}) is calculated as the average of daily maximum and minimum temperature at each grid.

Table 1.3 The climate variables obtained from the GMFD dataset as well as their temporal and spatial resolution.

Abbreviation	Relevance	Temporal Resolution	Spatial Resolution
Precip	Precipitation	Daily	0.25 deg
T_{min}	Minimum temperature	Daily	0.25 deg
T_{max}	Maximum temperature	Daily	0.25 deg

1.3.3 Canadian Meteorological Center snow depth data

Snow Depth (SD) is the second important controller of FT dynamics. The gridded snow depth data for the historical period is available with different temporal and spatial resolutions. One of the most comprehensive and accurate sources of gridded SD data is obtained from the Canadian Meteorological Center (CMC; https://doi.org/10.5067/W9FOYWH0EQZ3). The dataset contains analyzed snow depth (SD; in cm) at daily and monthly scales as well as estimated snow water equivalent (SWE; in mm) at monthly scale. CMC data record is provided over the period of 1998 to 2020 with daily and monthly temporal resolution and spatial resolution of 24×24 km across the northern hemisphere. The CMC dataset is obtained by combining the information from a set of in-situ SD measurements and optimal interpolation results of a simple physical snow accumulation and melt model. The physical melt model itself utilized the analyzed daily temperature and precipitation data from the Canadian forecast models. In-situ SD observations are also received from three different sources of surface synoptic (SYNOP) observations, meteorological aviation (METAR), and special aviation (SA) from the World Meteorological Organization (WMO) information system (Brasnett, 1999). The monthly SD values as well as monthly mean snow density from Canadian snow course observations are then used to derive the monthly values of SWE in October to June of each year (Brown and Mote, 2009; Strum et al., 1995). The results of CMC dataset verification show the considerable accuracy of this data set in the northern hemisphere with 94% accuracy in detecting the snow cover detected by SSM/I. For this project, only the monthly SD data record is required over the common period of 1998 - 2016.

1.3.4 NASA Earth Exchange Global Daily Downscaled Projections dataset (NEX-GDDP)

The future climate conditions can be provided by complex computational models, known as Global Climate Models (GCMs) or more recently Earth System Models (ESMs). These models are coupling the numerical models of atmosphere, land, and ocean to simulate large-scale fluid motion and key physical processes such as cloud formation, convection, and radiative transfer (Edwards, 2011; Foley, 2010). The fifth phase of the Coupled Model Intercomparison Project (CMIP5), by the Intergovernmental Panel of Climate Change (IPCC), is currently one of the latest generations of publically available GCMs (Taylor et al., 2012). CMIP5 used the results of multiple GCMs to provide different future climate scenarios of change in emission of greenhouse gases referred to as Representative Concentration Pathways (RCPs). CMIP5 projections are available through (https://esgf-node.llnl.gov/search/cmip5/; Leong et al., 2017; Ouyang et al., 2015). Although the RCP runs embedded in CMIP5 provide a range of future projections of climate at global daily scale and can be utilized for climate change impact assessment; the coarse spatial resolution of these projections (around 100 km) pose considerable limitation at regional scales (Kharin et al., 2013; Koven et al., 2013). Further downscaling is therefore required for bringing the coarse GCMs' projections to a finer scale (Hamlet et al., 2010; Sunyer et al., 2015).

There are available data sources that are already downscaled. NASA Earth Exchange Global Daily Downscaled Projections dataset (NEX-GDDP) is one of the main sources of these downscaled future projections of climate data. This data set includes the downscaled daily maximum and minimum near-surface air temperature and precipitation for the period of 1950 to 2100, obtained from the RCP4.5 and RCP8.5 scenarios of GCM runs of CMIP5. The high scenario (RCP8.5) is defined as an increase of radiative forcing throughout the 21st century before reaching the level of 8.5 Wm^{-2} at the end of the century. The intermediate scenario (RCP4.5) is, however, the scenario of stabilized radiative forcing at 4.5 Wm^{-2} without ever exceeding that value over the 21st century (Meinshausen et al., 2011; Thomson et al., 2011). The downscaling is conducted using the Bias Correction Spatial Disaggregation methodology which falls into the pool of linear statistical downscaling algorithms. These algorithms are aiming at addressing the limitations of global GCM projections such as local biases and coarse spatial resolutions (Thrasher et al., 2013, 2012). The NEX-GDDP data are directly available through (https://www.nasa.gov/nex) with spatial resolution of 0.25°. However, it is so far no clear consensus on whether this already downscaled data record should be further localized for studying the impact of climate on FT dynamics.

1.3.5. Regridding

The size and centroid of different sources of gridded data mentioned above are often not the same. As a result, these data should be regridded before pairing them with FT data. The *k*-nearest neighbor interpolation methodology is widely used to match the spatial resolution of different sets of data (Hodgson, 1989; Östh et al., 2015). In simple words, the *k*-nearest neighbor methodology searches for several nearby cells of original space within a specific radius of the center of desired space. Then a distance-weighted technique is used to interpolates the selected cells (Fekete et al., 2001; Grant et al., 2008). In an attempt to match the climatic data with FT characteristics, I found four as the optimum number of nearest neighbors to achieve the highest accuracy in modeling the mean and standard deviation in these variables across Québec (Hatami and Nazemi, 2019). The Mahalanobis metric is used as the distance measure for this analysis (Mahalanobis, 1936). The Mahalanobis distance between the centroid of FT-ESDR data (O_{FT}) set and GMFD or CMC data ($O_{T/SD}$) can be calculated as:

$$d(O_{FT}, O_{T/SD}) = (O_{FT} - O_{T/SD})^{T}.Cov^{-1}.(O_{FT} - O_{T/SD}) \quad \textbf{(1.1)}$$

where $(O_{FT} - O_{T/SD})^{T}$ is the vector of transposition of difference between the centroid of mentioned gridded data and Cov^{-1} is the inverse of the covariance matrix of the centroid of FT-ESDR data record.

1.4 Methodology

The key methodological elements of this extended statistical framework for estimating landscape FT under changing climate conditions are summarized as follows:

1.4.1 Assessing the empirical dependence

To quantitatively measure the interdependencies between pairs of variables, the Kendall's tau dependence coefficient is utilized. Kendall's tau is a non-parametric dependence test with the empirical formulation as (Kendall, 1938):

$$\tau_{X,Y} = \frac{n_c - n_d}{\binom{n}{2}} \quad \textbf{(1.2)}$$

where n_c and n_d are the number of concordant and discordant pairs, respectively and X, Y are the pair of random variables (Genest and Favre, 2007). The significance of the dependence is evaluated by a formal p-value associated with Kendall's tau dependence coefficient. In this study, p-value = 0.05 is considered as the level of meaningful dependence.

1.4.2 Multiple linear regression

MLR assumes that the properties of a given dependent variable is linearly related to a set of predictors and that each predictor has a positive effect on the performance of the simulation (Holder 1985). The MLR can be formulated as:

$$y(t) = \alpha_0 + \sum_{i=1}^{m} \alpha_i . x_i(t) + e(t) \quad \textbf{(1.3)}$$

where α_0 is the intercept and α_i, $i = 1, \dots, m$ are the linear coefficients; e is the error term and m is the number of predictors. Apart from simplicity, the key advantage of MLR is the fact that the validity of underlying assumptions and the predictive uncertainty can be formally explored and addressed. The MLR mappings used for this study are dimensionless; therefore, the predictors and predictand are standardized using their observed ranges. Here I consider scaling both predictors and predictands in the range of [0.1 0.9] instead of standard [0 1] interval before model application. The considered 0.1 buffer at the upper and lower ends of the scaling space can facilitate accommodating outliers and the data points that may occur beyond the range of calibration data (Hsu et al. 1995). Maximum Likelihood Method (Uss et al. 2012; Giles et al. 2016) is used to find the optimal parameters of MLR models (including uncertainty bounds), and to calculate the predictive uncertainty.

1.4.3 Literature review of copula methodology

It has been shown that statistical and machine learning approaches – if appropriately applied in the right domains – can provide an alternative approach to conventional modeling approaches (Crane-Droesch, 2018; Lemoine and Kapnick, 2016; Sarhadi et al., 2018; Towler et al., 2010; W. Wang et al., 2018). While some machine learning approaches such as neural networks and/or other methods under the umbrella of artificial intelligence may suffer from the lack of transparency (Abrahart et al., 2012; Creel, 2020; Kuwajima et al., 2019), the curse of dimensionality (Trunk, 1979) and/or parametric and predictive uncertainty (Khosravi et al., 2011; Nourani et al., 2019), there are still need for a parsimonious and well-established statistical approach that can address some of the limitations in physically-based and/or conceptual approaches.

There has been a growing interest in different applications of copulas in hydrology over the past decades, knowing the fact that copula could be an effective tool for describing the dependence among multiple hydrological variables (Favre et al., 2004). The copulas are used in earlier hydrological studies to model the interdependence between two variables. Hao and AghaKouchak (2014), for instance, used copulas to model the dependency between soil moisture and precipitation across the continental United States. The empirical copula was used in their study to overcome the limitation of parametric families such as rigorous parameter estimation and goodness-of-fit tests. De Michele and Salvadori (2003) also showed the ability of copulas structure in intensity-duration modeling of storm rainfall. In other investigations, Salvadori and De Michele (2004) presented theoretical aspects of rainfall frequency analysis based on copulas. Gebremichael and Krajewski (2007) used copula for simulation of remotely sensed rainfall data. Moreover, many studies used copula functions in streamflow modeling and flood frequency analysis. Nazemi et al. (2013), for instance, used the methodology for streamflow reconstruction and further assess the response of a real-world water resources system to possible changes in the flow regime. Some studies also focus on applying the copula on analysis of the maximum flow and hydrograph behavior (De Michele et al., 2005; Poulin et al., 2007). Salvadori and De Michele (2004) discussed the use of copulas to assess the joint return period. Finally, Nazemi and Elshorbagy (2012), used copula for investigating as conditional quantities of the maximum annual water deficit (Nazemi and Elshorbagy, 2012).

Besides the application of bivariate copulas, multivariate copulas gain popularity in hydrology to model the interdependencies between three or more hydro-climatological variables. As an example, the multivariate copula was found to be effectively used for determining the effect of climate on different hydroclimatic variables. Salvadori and De Michele (2006) extended their previous models, using trivariate copulas, for examining the role of moisture conditions in rainfall modeling. Salvadori and Michele, (2007) also presented a trivariate copula to model the temporal structure of sequences of storms. AghaKouchak et al. (2010) used copula for simulation of remotely sensed rainfall data. Kao and Govindaraju (2008), Grimaldi and Serinaldi (2006) applied copulas in the analysis of extreme rainfall behavior. Bárdossy and Pegram (2009) find multivariate copula a suitable tool to successfully model both the rainfall amount and its occurrence. Later,

Nguyen-Huy et al. (2017), employed a multivariate vine copula for investigating the impacts of multiple large-scale climate indices such as El-Nino Southern Oscillation and Inter-decadal Pacific Oscillation on spring precipitation forecasting over parts of Australia. Khedun et al., (2014) employed the trivariate form of different copula families to find the impacts of climate on monthly precipitation patterns and then present a precipitation forecasting model.

In another context, Madadgar and Moradkhani (2014) employed trivariate copula function for spatiotemporal drought forecasting while there are other investigations considering the copula application on drought duration and severity analysis (Cheng et al., 2016; Kao and Govindaraju, 2010; Madadgar et al., 2013; Madadgar and Moradkhani, 2014). Genest and Favre (2007), used Elliptical copulas to analyze flood peak, volume, and duration data for the Romaine River, Québec. L. Zhang et al., (2007) used the trivariate Archimedean copula for the same purpose using the flood data from the Amite River Basin in Louisiana. Shafaei et al., (2017), employed a multivariate copula to model the interdependencies between different flood characteristics, such as flood peak, duration, volume, and peak time. Moreover, many studies used multivariate copula functions in flood frequency analysis (Salvadori and De Michele, 2010; Serinaldi and Grimaldi, 2007; Yue, 2001). Furthermore, the multivariate copula is applied extensively for other hydrologic investigations such as multi-site streamflow modeling (Pereira et al., 2017), annual peak snow water equivalent and peak reservoir elevation (Bracken et al., 2018), concurrent drought, and heatwaves (AghaKouchak, 2015) and groundwater quality (Bárdossy, 2006; Bárdossy and Li, 2008).

However, to the best of the author's knowledge, there has been no study yet to use copula for quantifying the climate control on FT dynamics. Copula framework can provide the capability of modeling the interdependencies between hydroclimatic variables and FT characteristics as well as assessing the changes in long-term FT events due to changing climate. Moreover, comparing the absolute effect of the same magnitude of warming and cooling on expected FT characteristics can highlight the linearity/nonlinearity of the FT response to changing temperature.

1.4.4 Bivariate copula

To quantitatively describe the joint dependencies between two variables, bivariate copulas are used. In simple words, a copula is a continuous parametric function, coupling Cumulative Distribution Functions (CDFs) of two or more marginal variables to come up with a joint CDF (Salvadori et al., 2016). If X and Y are two random variables with marginal CDFs of $F_1(X)$ and $F_2(Y)$, then the joint dependencies structure $H(X,Y)$ can be described as:

$$H(X,Y) = C\{F_1(X), F_2(Y)\} \quad \textbf{(1.4)}$$

where C is the bivariate copula, describing the joint dependence between $F_1(X)$ and $F_2(Y)$. The theoretical work of Sklar (1959) shows that the joint CDFs formulated by copulas are equivalent to the joint CDFs of the initial random variables, from which the marginal CDFs are inferred. An

important benefit of the copula methodology is in separating the description of marginal distribution from the joint dependence structure. The procedure of model identification, parametrization, and validation of copula models has been discussed in detail in several other sources, e.g., Genest and Favre (2007), Nazemi and Elshorbagy (2012) as well as Sadegh et al. (2017) and is not repeated again here.

The parametrized copula model can serve as a probabilistic impact model, with which the control of any impactful variable on the target variable can be described through the general rule of conditional probability. Y can be conditioned to X at a given X^* within the empirical range as (Nelsen, 2006; Bouezmarni et al., 2019):

$$F_2(Y \leq Y^* | X = X^*) = \frac{H(X = X^*, Y \leq Y^*)}{F_1(X = X^*)} = \frac{C\{F_1(X = X^*), F_2(Y)\}}{F_1(X = X^*)} = \frac{\partial(C\{F_1(X), F_2(Y)\})}{\partial(F_1(X))}_{X=X^*} \quad \textbf{(1.5)}$$

The above conditional modeling is generic and has been applied in several studies in hydrology (Grimaldi and Serinaldi, 2006a, b; Salvadori and De Michele, 2007; Nazemi et al. 2013, 2020) among several others. The procedure of quantifying the conditional control can be described as the following:

I. Obtain the marginal CDFs, i.e. $F_1(X)$ and $F_2(Y)$, of random variables X and Y.
II. Seek and establish the joint distribution using bivariate copula $C\{F_1(X), F_2(Y)\}$
III. Estimate the copula parameter(s) using observed datasets.
IV. Obtain the conditional CDF of the target variable (here Y), subject to a particular value of the conditioning variable (here X) at $X = X^*$, using Equation (1.5).
V. Back transform the conditional CDF of the target variable, i.e., $F_2(Y \leq Y^* | X = X^*)$, from the CDF space to the quantile space using the inverse cumulative distribution function.

1.4.5 C-vine copula

To model the joint dependencies between three variables, trivariate copulas can be used. Based on the Sklar's Theorem, the extended form of Equation 1.4 for modeling the joint dependencies between the three variables is defined as:

$$F(X, Y, Z) = C\big(F_1(X), F_2(Y), F_3(Z)\big) \quad \textbf{(1.6)}$$

where $F_1(X)$, $F_2(\mathrm{Y})$ and $F_3(Z)$ are the Cumulative Distribution Functions (CDFs) for X, Y and Z, respectively and C is the trivariate copula function (Sklar, 1959). Among different alternative multivariate copulas, canonical vine (C-vine) is employed to represent joint distribution between the three variables of Equation 1.6 (Bedford and Cooke, 2002). In brief, C-vine copulas decompose a d-dimensional joint distribution into a $d(d-1)/2$ bivariate pairs of copulas

arranged into $(d-1)$ trees; and accordingly the joint distribution between X, Y and Z can be described as:

$$f(X,Y,Z) = f_2(Y) f_{3|2}(Z|Y) f_{1|2,3}(X|Y,Z) \quad \textbf{(1.7)}$$

where $f(.)$ is the marginal PDFs and the conditional distributions that can be estimated as (Aas et al., 2009):

$$f_{3|2}(Z|Y) = \frac{f(Z,Y)}{f(Y)} = \frac{c_{2,3}\big(F_2(Y), F_3(Z)\big) f_2(Y) f_3(Z)}{f_2(Y)} = c_{2,3}\big(F_2(Y), F_3(Z)\big) f_3(Z) \quad \textbf{(1.8)}$$

and

$$f_{1|2,3}(X|Y,Z) = \frac{f(X,Z|Y)}{f(Z|Y)} = \frac{c_{1,3|2}\big(F(X|Y), F(Z|Y)\big) f(X|Y) f(Z|Y)}{f(Z|Y)} = c_{1,3|2}\big(F(X|Y), F(Z|Y)\big) c_{1,2}\big(F_1(X), F_2(Y)\big) f_1(X) \quad \textbf{(1.9)}$$

where $c(\cdot)$ is the 3-dimensional copula density. As a result, the three dimensional joint density can be represented in terms of bivariate copulas as the following (Joe, 1997):

$$f(X,Y,Z) = f_1(X).f_2(Y).f_3(Z).c_{2,1}.c_{2,3}.c_{1,3|2} \quad \textbf{(1.10)}$$

where $c_{2,1}(F_2(Y), F_1(X))$ and $c_{2,3}(F_2(Y), F_3(Z))$ are simply written as $c_{2,1}$ and $c_{2,3}$; and the conditional pairwise copulas between $F_1(X)$ and $F_3(Z)$ conditional to $F_2(Y)$, i.e. $c_{1,3|2}\big(F_1(X), F_3(Z)|F_2(Y)\big)$ is shown by $c_{1,3|2}$. In addition, $c_{2,1}$, $c_{2,3}$ and $c_{1,3|2}$ are the densities of bivariate pairs. Having the C-vine copulas, the probability distribution of target variable due to different quantitative change in impactful variables can be obtained through conditional modeling as:

$$h = F(X|Y,Z) = \frac{\partial C_{1,3|2}\big(F(X|Y), F(Z|Y)\big)}{\partial F(Z|Y)} \quad \textbf{(1.11)}$$

where $F(X|Y,Z)$ is the conditional distribution function. Moreover,

$$F(X|Y) = h(X|Y) = \frac{\partial C_{1,2}\big(F(X), F(Y)\big)}{\partial F(Y)} \quad \textbf{(1.12)}$$

and

$$F(Z|Y) = h(Z|Y) = \frac{\partial C_{3,2}\big(F(Z), F(Y)\big)}{\partial F(Y)} \quad \textbf{(1.13)}$$

Using Equations 1.12 and 1.13, Equation 1.11 can be rewritten as:

$$h = F(X|Y,Z) = h[h(X|Y)|h(Z|Y)] \quad \textbf{(1.14)}$$

The estimated CDF of characteristics can be back transformed to the original quantile space using the inverse CDF function, assuming empirical or parametric distributions for X, Y and Z. The inverse form of h-function given in Equation 1.14 is applied for this purpose. To extract the probability distribution of the target variable, a Monte Carlo-based simulation is adopted by generating 1,000 random set of target variable under known values of impactful variables (Roy and Gupta, 2021). Given random uniform random numbers of ε, the target variable can be sampled as:

$$X = F^{-1}\left\{h^{-1}\left[\left(h^{-1}(\varepsilon|h(Z|Y))\right)|Y\right]\right\} \quad \textbf{(1.15)}$$

1.4.6 Climate change impact assessment

To assess the impacts of climate change on any target variable, two generic impact assessment paradigms under changing conditions are suggested. These paradigms are generally known as top-down (scenario-led) and bottom-up (scenario-neutral) approaches. In simple words, top-down approaches mainly rely on using downscaled projections of Global Climate Models (GCMs), obtained under different greenhouse gas emission scenarios (Nakicenovic et al., 2000), as the basis of impact assessment (Hickel and Zhang, 2006). Top-down assessments commonly determine the response of a hydrological process using a physical and/or statistical model that is forced with downscaled climatic variables obtained from GCM projections (Bhave et al., 2014; Hassanzadeh et al., 2016). Hence, the information is cascading from one step to the other in this approach (Girard et al., 2015). In the context of this study, a top-down approach is employed to understand the future state of FT conditioned to future climate projections. For this purpose, the future projection of temperature and future simulation of snow depth data, as the most influential hydroclimatic variables on FT dynamics, are fed to the copula models calibrated over the observed period to project the future FT characteristics under changing climate – see Figure 1.3.

Bottom-up approaches, on the other hand, focus on analyzing climate change using different forms of stress tests without considering the future climate projections directly (Roach et al., 2016). Using these approaches the response of the target variable to various feasible future climate conditions can be investigated across different spatial and temporal scales. The results of bottom-up stress tests can provide the response of FT characteristics to a range of feasible future climate conditions. Copula methodology can provide a basis for performing the stress test through conditional probability modeling. Using copula, the FT characteristics at any temperature and/or snow depth can be stochastically generated through resampling from the copula space. In our study, we inter-compared the changes in FT characteristics due to negative and positive changes in long-term average temperature and/or snow depth, i.e. $E(\bar{T})$ and $E(SD)$. With the help of conditional resampling, the corresponding probability distribution of FT characteristics to any temperature and/or snow depth can be obtained. Accordingly, the change in probability

distribution of FT characteristics can be obtained under any shift in the long-term average of temperature and snow depth, i.e. $E(\bar{T}) \pm \Delta T$ and $E(SD) \pm \Delta SD$. The changes in corresponding statistics characterize the extent to which FT characteristics respond to changing hydroclimatic variables.

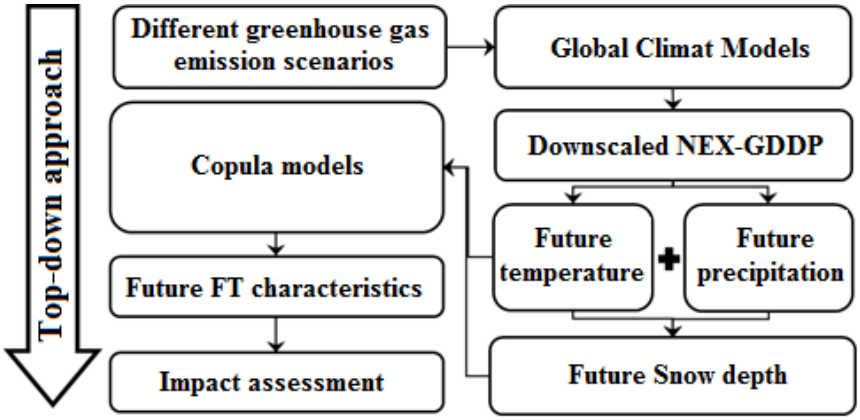

Figure 1.3. A schematic representation of the proposed top-down approach for addressing the compound impacts of temperature and snow depth on FT characteristics.

1.5 Scope of the thesis

The research presented in this thesis is focused on providing a comprehensive statistical framework to quantify the impacts of changing climate on FT dynamics. The driving questions can be summarized as follows:

(i) As mentioned earlier, the dynamics of FT largely depend on the air temperature. However, the global air temperature has been increasing in the recent past due to the increased anthropogenic greenhouse gas emissions since the mid-19th century. It is hence of great importance to investigate the linkage between FT characteristics and temperature and understand the impacts of changes in FT characteristics under changing temperature.

(ii) Snow depth is the second influential hydroclimatic variable on FT dynamics at larger temporal and spatial scales. As the second research question, I aim to address the compound impacts of changing temperature and snow depth on FT characteristics. This is of great importance due to the nonlinear nature of the response as one of the key features of compound events, meaning that the impact of compound events can be more intense compared to the cumulative impacts of individual events when occurring independently.

(iii) As the future dynamics of snow depth are not available with good accuracy, it is important to find the relationship between the dynamics of snow depth and the climatic variables, which are available over future periods. To find this relationship there should be a simple framework capable of linking the snow depth dynamics to the climatic data.

The simplest form of this framework should be capable of capturing the snow depth characteristics using the in-situ based data.

(iv) Having the statistical framework capable of capturing the dynamics of snow depth over the observed period at station scale, the calibrated models can be extended to regional scale and fed with gridded climate data rather than in-situ observations. These models can be finally linked with future climate projections. This can provide an understanding of the future state of snow depth dynamics, as one of the most important climatic drivers of landscape FT, due to future projections of changing climate.

(v) Finally, although the statistical frameworks can provide a generic approach for conditioning FT characteristics to temperature and snow depth over the observed period, they are based on the fundamental assumption of stationarity. Under stationarity, it is assumed that probabilistic characteristics of hydrometeorological processes and the dependence structures between variables will not change over time. This is in contrast to the empirically observed time-varying dependence structures between hydroclimatic variables. Hence, there is a need for a statistical framework which is capable of incorporating the nonstationarity in the dependence structure.

1.6 Overview and Layout

This thesis follows a manuscript-based format including a collection of five manuscripts along with two conference papers that are published, submitted, or in preparation. The five journal papers compose Chapters 2 to Chapter 6, each aims to address one of the above mentioned questions and are slightly edited to unify the format of the thesis. The references of all papers and the conclusion are combined at the end of the thesis.

(i) Chapter 2 presents a statistical framework to assess the control of temperature on FT dynamics. Here, I focus on describing the joint interdependencies between temperature and various FT characteristics with physical relevance. Consequently, the impacts of temperature alterations on FT characteristics are addressed using conditional probabilities inferred from copula models across different spatial and temporal scales.

(ii) Chapter 3 takes a closer look at the compound impacts of changing temperature and snow depth on FT cycles. In this chapter, the methodology proposed in Chapter 2 is extended into multivariate form to look into the joint interdependencies between temperature, snow depth, and FT characteristics. Here, I investigate the nonlinearity and non-symmetry in the response of FT characteristics to changing temperature and/or snow depth.

(iii) Chapter 4 presents a statistical framework for the determination of monthly snow depth using a set of climatic proxies. This framework fuses a regression-based model with a forward input selection algorithm to describe the dynamics of snow depth. The proposed

framework stands as a parsimonious, accurate, and robust model which is capable of describing the monthly dynamics of snow depth at the station scale.

(iv) In Chapter 5, the future dynamics of monthly snow depth are projected, using the generalized form of the framework that is previously introduced at the local scale in Chapter 4. The development and application of this procedure include classifying the type of precipitation, identifying the best set of climate proxies for representing the dynamics of snow depth at the regional scale, developing parsimonious regression models for representing monthly snow depth dynamics at the grid scale, and linking the developed models with future projections of climate variables.

(v) In Chapter 6, a top-down impact assessment scheme is employed to address the future state of FT characteristics due to the future projection of climatic variables. A multivariate statistical framework is proposed to investigate the changes in future FT characteristics conditional to future air temperature and snow depth. To accommodate the nonstationarity in the dependence structure under future conditions, a regression-based algorithm is employed to update the parameters of the proposed model. Although the proposed methodology is performed to investigate the impacts imposed by changes in temperature and snow depth conditions on FT dynamics across the province of Québec, Canada, we make a particular effort to develop a generic framework that can include other variables and be applicable in other regions and/or globally.

(vi) Finally, Chapter 7 summarizes the main contribution of this thesis and research needs.

Chapter 2.

A Statistical Framework for Assessing Temperature Controls on Landscape Freeze-Thaw: Application and Implications in Québec, Canada (1979-2016)[2]

The contents of this chapter have been published as "Hatami, S., Nazemi, A. (2021). A statistical framework for assessing temperature controls on landscape freeze-thaw: application and implications in Québec, Canada (1979-2016)" in the Journal of Hydrology. The contents are slightly modified.

Synopsis

Climate change has already made significant alterations to various elements of the hydrologic cycle. One relatively less attended hydrologic impact of climate change is on the landscape Freeze-Thaw (FT), which largely affects surface and sub-surface hydrology, phenology, and land-atmospheric interactions, particularly in cold regions. Understanding the impacts of climate change on FT patterns, however, is not trivial due to sparse networks of in-situ measurements as well as limitations in current physically-based modeling schemes, aiming at continuous simulations of FT states in time and space. Here, we propose shifting the focus of FT modeling from continuous simulations to statistical representations of FT characteristics at larger temporal and spatial scales. We accordingly suggest using copulas to formally describe the impacts of temperature alterations on FT characteristics using conditional probabilities. To showcase the application of this framework in practice, we pair datasets of satellite-based FT with gridded temperature over Québec, Canada. The results show strong and rather unique dependencies between temperature and FT characteristics across different regions and/or timeframes and demonstrate copulas as effective tools to capture such dependencies and reconstruct marginal FT characteristics. Through a set of impact assessments, it was shown that a similar change in temperature conditions can result in different regional responses in landscape FT. These responses are often nonsymmetric, meaning that the magnitude of change in FT conditions can be different under warming and cooling conditions. In addition, we highlight intensifications in FT responses to a similar magnitude of change in temperature under more recent years, which is linked to alterations in dependencies between temperature and FT. This study provides another line of evidence for complex responses of landscape to climate change in cold regions.

[2] Hatami, S., Nazemi, A. (2021). A statistical framework for assessing temperature controls on landscape freeze-thaw: application and implications in Québec, Canada (1979-2016). *Journal of Hydrology*, 126891.

2.1 Introduction

Landscape Freeze and Thaw (FT) is arguably one of the most important land-surface characteristics in cold regions. FT acts as a controller to various natural processes taking place in the critical zone (Kim et al., 2019; Wang et al., 2019), including bulk density and hydraulic conductivity that determine the storage and movement of moisture and nutrients (Elliott and Henry, 2009; Han et al., 2020; Henry, 2013). When soil freezes, hydraulic conductivity reduces (Mccauley et al., 2002), leading to decreasing infiltration and increasing surface transport (Iwata et al., 2010; Qi et al., 2019; Zheng et al., 2018). When the landscape thaws, water pathways are formed below and above the land surface; and in some regions, surface and sub-surface water reserves connect to one another (Johansson et al., 2015; Karlsson et al., 2013). Transitions between frozen and thawed states are also important drivers for erosion in natural and built environments (Kimiaghalam et al., 2015; Kreyling et al., 2006), and therefore are important considerations for the design and operation of infrastructure in cold regions (Roseen et al., 2012; Shahrajabian and Behfarnia, 2018). FT dynamics also control the vegetation growth, posing seasonal constraints on agriculture and ecosystem livelihood (Sharma et al., 2006; Zhou et al., 2015).

Statistical characteristics of FT states such as its timing and duration can be determined by the soil temperature dynamics, depending largely on the air temperature (Frauenfeld et al., 2004; He et al., 2015; Shati et al., 2018). The global air temperature has been increasing in the recent past due to the increased anthropogenic greenhouse gas emissions since the mid-19th century (Francey et al., 2010; Huang et al., 2017). The warming pattern has higher rates across northern latitudes (IPCC, 2013; Rosenzweig et al., 2008), particularly during winter and spring (Smith et al., 2004). This unprecedented warming has already affected FT dynamics by decreasing frozen periods (Kim et al., 2014, 2015), deepening active soil layer (Qin et al., 2016; Wu and Zhang, 2010; Zhao et al., 2010) as well as retreating permafrost boundaries (Lawrence et al., 2008; Schuur and Abbott, 2011). These changes can impact regional hydrology (Genxu et al., 2017; Krogh et al., 2017; Liu et al., 2009), Pedology (Hachem et al., 2012; Park et al., 2016a), phenology (White et al., 2009; Williams et al., 2015), water quality (Meshesha et al., 2020; Wei et al., 2017), and land-atmospheric interactions (Entekhabi et al., 2004; Vogel et al., 2017).

Changes in landscape FT can result in environmental and socio-economic challenges that can be accompanied with opportunities for new development in northern countries such as Canada (Ho and Gough, 2006). For instance, frozen landscape and short growing seasons that have constrained agricultural activities in the north are about to be replaced by warm and extended growing seasons, making new opportunities for growing crops over northern lands (King et al., 2018; Parry, 2019). Warmer temperature with the help of technological advancements makes other resources, such as oil and gas and minerals accessible (Poppel et al., 2015). On the other hand, the changing FT dynamics can also pose considerable challenges. As the agriculture and natural resources industry enters in northern regions, environmental risk particularly in terms of contamination increases (Ali, 2009). In addition, as soil thaws near a hillside or a stream, it can trigger erosions and landslides (Lewkowicz and Way, 2019; Patton et al., 2019). Localized thawing, especially in northern

villages undermines roads and schools, cracks pipelines, and deteriorates infrastructures (Hjort et al., 2018; Melvin et al., 2017; Teufel and Sushama, 2019). This has major societal implications as these communities, mainly Indigenous, have faced longstanding inequalities. Moreover, as the north thaws and businesses are spreading northward, the unique way of life and cultural values of Indigenous people become largely vulnerable (Andrews et al., 2016). Last but not the least, thawing soil can unleash substantial amounts of carbon into the atmosphere (Butterbach-bahl and Wolf, 2017; Mu et al., 2015) – a threat that has not been fully accounted for in climate models (Knoblauch et al., 2018; Plaza et al., 2019).

While current studies provide clear lines of evidence for impacts of warming temperature on FT states across cold regions, they are mainly based on in-situ data (Fang et al., 2019; Smith et al., 2004; Tran et al., 2018). For instance, Henry (2008) studied the impacts of winter's temperature on soil frozen days and FT cycles in 31 in-situ stations across Canada, indicating higher impacts of warming on FT dynamics in southern regions. While in-situ observations provide valuable local knowledge on the linkage between FT characteristics and air temperature, sparse observation networks and the lack of continuous data availability limit capturing spatial and temporal patterns of FT at the larger scales (Takala et al., 2009; Williams et al., 2000; Zhang et al., 2007). In addition, current physically-based modeling capability is limited due lack of process representations (Cao et al., 2020; Walvoord and Kurylyk, 2016) and limited data availability for model parametrizations (McCarty et al., 2020; Tape et al., 2018).

This study is an effort to address some of the gaps in in-situ data and physically-based models. We recognize that the advent of satellite technology provides a new opportunity to overcome some of the limitations of in-situ observations, at least at larger scales (Kim et al., 2011; Tucker et al., 2005; Zhang and Armstrong, 2001). The remotely-sensed FT data can be further paired with the gridded temperature records to investigate the statistical link between air temperature and FT dynamics. In addition, quantifying FT response to changing climate conditions requires implementing mathematical models that can project the future states of FT based on relevant climate and/or environmental variables (Sinha and Cherkauer, 2008). Here, we shift the purpose of modeling from continuous simulations of FT states to statistical modeling of FT characteristics over coarser temporal and spatial scales using joint dependencies with temperature. If the joint dependence between FT and temperature characteristics can be formed, then the statistical properties of FT, conditioned to temperature, can be quantified. We suggest using copulas to represent and quantify these dependencies and their changes in time and space. The copula methodology is a formal framework to describe joint distribution between two or more variables (Favre et al., 2004) and has gained enormous popularity in hydrology in recent years (Chen et al., 2019; De Michele and Salvadori, 2003; Jalili Pirani and Najafi, 2020), particularly to assess the changes in the depednece structure over time (Singh et al., 2021; Tebaldi and Sansó, 2009) as well as investigating the conditional control of one variable on another (Huning and Aghakouchak, 2018; Madadgar et al., 2013).

We showcase the application of the proposed framework in the province of Québec, the largest province in Canada, with diverse ecological and landscape characteristics. We specifically illustrate: (i) how FT characteristics and temperature are linked across a range of spatial and temporal scales in Québec; (ii) how such interdependencies can change in time and space; and (iii) how changes in temperature conditions can affect FT characteristics across different regions and timeframes in Québec. The paper is organized as follows: Section 2.2 presents the proposed methodology. Section 2.3 introduces the case study and datasets used. Section 2.4 provides results with respect to the first and second research questions outlined above. In Section 2.5 various examples are presented to pursue the third research question. Section 2.6 summarizes and concludes this study and provides some further remarks.

2.2 Methodology

Our proposed framework is developed to serve two key purposes. First, we aim at formal inspection of the dependencies between temperature and FT characteristics and their variations in time and space. Second, we aim at providing a bottom-up basis for addressing the impact of changing temperature on FT characteristics. The proposed framework is shown in Figure 2.1 and starts with a preprocessing step for matching gridded FT and temperature datasets. We skip describing this step and will come back to it in Section 2.3. Methodologically, the framework starts with measuring dependence between FT and temperature characteristics. We use Kendall's tau, a non-parametric measure for quantifying the associations between a pair of random variables (Nelsen, 2006). Kendall's tau is calculated using Equation 2.1, where X, Y are considered random variables; n_c and n_d are the number of concordant and discordant pairs of X and Y. The significance of a Kendall's tau measure is assessed by a p-value (Genest and Favre, 2007), chosen in this paper as 0.05.

$$\tau_{X,Y} = \frac{n_c - n_d}{\binom{n}{2}} \quad \textbf{(2.1)}$$

To quantitatively describe the joint dependencies between temperature and FT characteristics, we use bivariate copulas. In simple words, a copula is a continuous parametric function, coupling Cumulative Distribution Functions (CDFs) of two or more marginal variables to come up with a joint CDF (Salvadori et al., 2016). If X and Y are two random variables with marginal CDFs of $F_1(X)$ and $F_2(Y)$, then the joint dependencies structure $H(X, Y)$ can be described as:

$$H(X, Y) = C\{F_1(X), F_2(Y)\} \quad \textbf{(2.2)}$$

where C is the bivariate copula, describing the joint dependence between $F_1(X)$ and $F_2(Y)$. The theoretical work of Sklar (1959) shows that the joint CDFs formulated by copulas are equivalent to the joint CDFs of the initial random variables, from which the marginal CDFs are inferred. An important benefit of the copula methodology is in separating the description of marginal distribution from the joint dependence structure. This provides an opportunity for addressing

whether changes in FT characteristics are solely related to marginal changes in the air temperature or the changes in the association between air temperature and FT states. The procedure of model identification, parametrization, and validation of copula models has been discussed in detail in several other sources, e.g., Genest and Favre (2007), Nazemi and Elshorbagy (2012) as well as Sadegh et al. (2017) and is not repeated again here. The specific setups for model identification and parametrization of copula models in this study are introduced in Section 2.3.

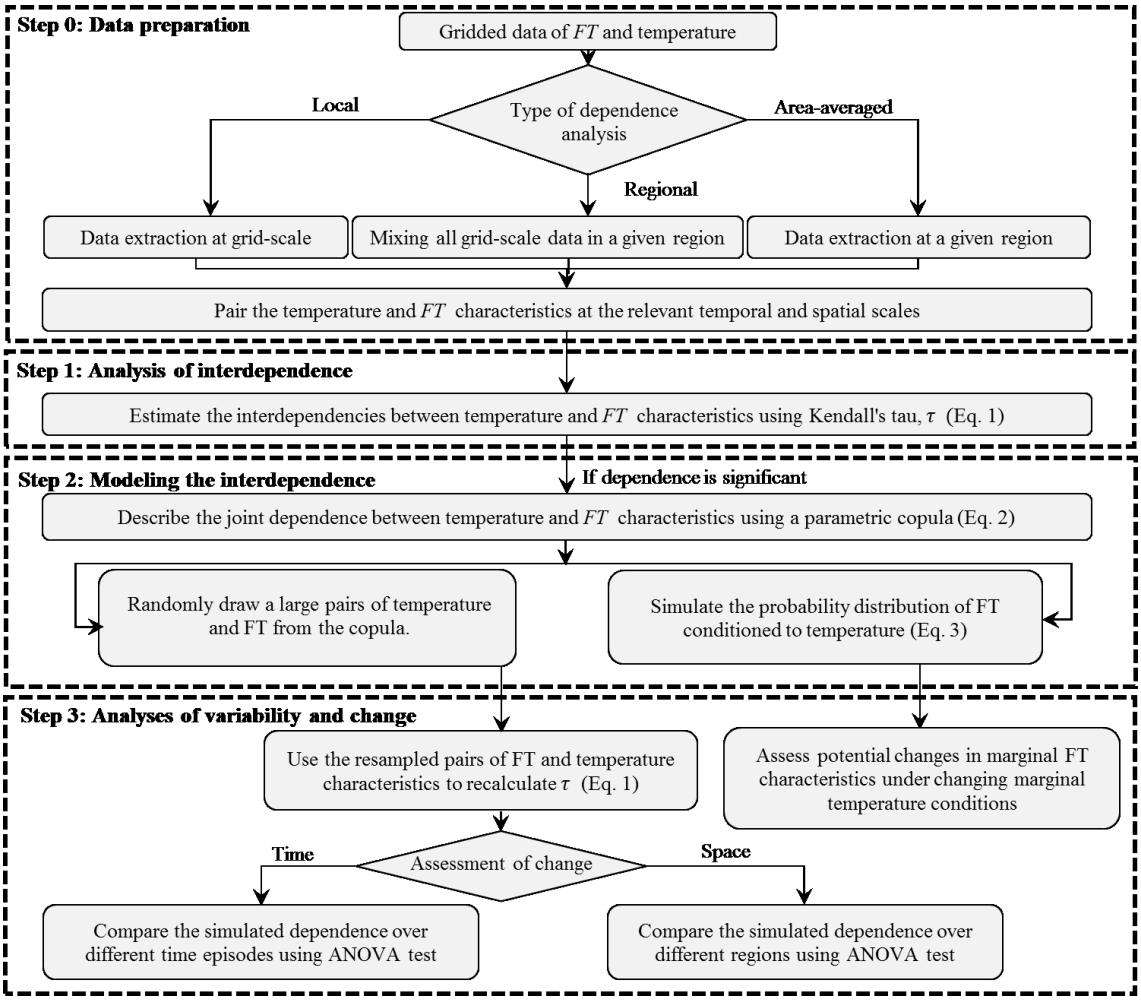

Figure 2.1 Workflow of the proposed copula-based framework for diagnosing, quantifying and analyzing variations in temperature control on landscape FT characteristics.

When the copula model is established (Figure 2.2a), it can be used for two purposes: (1) as a stochastic simulator to regenerate pairs of temperature and FT conditions from the copula space (Figure 2.2b); and (2) as a basis to estimate the probability distribution of FT characteristic, under a known temperature condition (Figure 2.2c). Regarding the first purpose, the resampled pairs of temperature and FT characteristics can be used to re-estimate the Kendall's tau coefficient (Eq. 1), which can accordingly demonstrate how well the copula model is able to reconstruct the empirical dependence. This can be used as a basis for validating the parametrized copula model (Aas and

Berg, 2009; Berg and Aas, 2007; Hatami and Nazemi 2019). In addition, if the same analysis is repeated in a different timeframe and/or region using an identical copula structure, then the difference in characteristics of simulated samples of Kendall's tau coefficients can be used as a basis to formally inspect the variations in the dependence structure across time and space. Here, we use the one-way ANalysis Of VAriance (ANOVA) with Bonferroni correction (Bland and Altman, 1995; Stuart and Jones 2006; Nazemi et al., 2020) to formally examine the changes in the simulated samples of Kendall's tau coefficients between FT characteristics and temperature conditions obtained in different regions and/or timeframes. Here, the ANOVA test analyzes the probability distribution of resampled Kendall's tau coefficients over different regions and/or timeframes to find a notion for statistical difference in the dependence structure in time and space. The null hypothesis of the ANOVA test in this study is that the expected Kendall's tau coefficients in two samples of simulated Kendall's tau coefficients, obtained at two different regions and/or timeframes, are the same. The test can be rejected at a particular significance level, indicating meaningful differences in the dependence structure of temperature and FT characteristics. Here, we choose *p*-values = 0.05 as the threshold in which the null hypothesis of the ANOVA test is rejected verifying a meaningful difference in estimated Kendall's tau coefficients in different regions and\or timeframes. The Bonferroni correction allows for multiple pairwise comparisons among samples with more than two variable (Maity et al., 2016; Nayak and Villarini, 2018). Changes in the dependence structure obtained during a unique time period over different regions can show the impacts of land-surface characteristics such as vegetation type, elevation, slope, and latitude on regulating the control of temperature on FT characteristics. In parallel, changes in the dependence structure in a given region but in different timeframes can highlight temporal variations in the dependence between FT characteristics and temperature conditions and can be taken as the revelation of climate change.

The parametrized copula model can also serve as a probabilistic impact model, with which the control of temperature on FT characteristics can be described through the general rule of conditional probability. Considering the same notation as Equations (1) and (2), Y can be conditioned to X at a given X^* within the empirical range as (Nelsen, 2006; Bouezmarni et al., 2019):

$$F_2(Y \le Y^* | X = X^*) = \frac{H(X = X^*, Y \le Y^*)}{F_1(X = X^*)} = \frac{C\{F_1(X = X^*), F_2(Y)\}}{F_1(X = X^*)} = \frac{\partial(C\{F_1(X), F_2(Y)\})}{\partial(F_1(X))}_{X=X^*} \quad \textbf{(2.3)}$$

The above conditional modeling is generic and has been applied in several studies in hydrology (Grimaldi and Serinaldi, 2006a, b; Salvadori and De Michele, 2007; Nazemi et al. 2013, 2020) among several others; here it can provide a generic basis for quantifying the impact of changing temperature on altering the FT conditions. The procedure of quantifying the conditional control can be described as the following:

I. Obtain the marginal CDFs, i.e. $F_1(X)$ and $F_2(Y)$, of random variables X and Y.
II. Seek and establish the joint distribution using bivariate copula $C\{F_1(X), F_2(Y)\}$
III. Estimate the copula parameter(s) using observed datasets.
IV. Obtain the conditional CDF of target variable (here Y), subject to a particular value of the conditioning variable (here X) at $X = X^*$, using Equation (2.3).
V. Back transform the conditional CDF of target variable, i.e., $F_2(Y \leq Y^*|X = X^*)$, from the CDF space to the quantile space using the inverse cumulative distribution function.

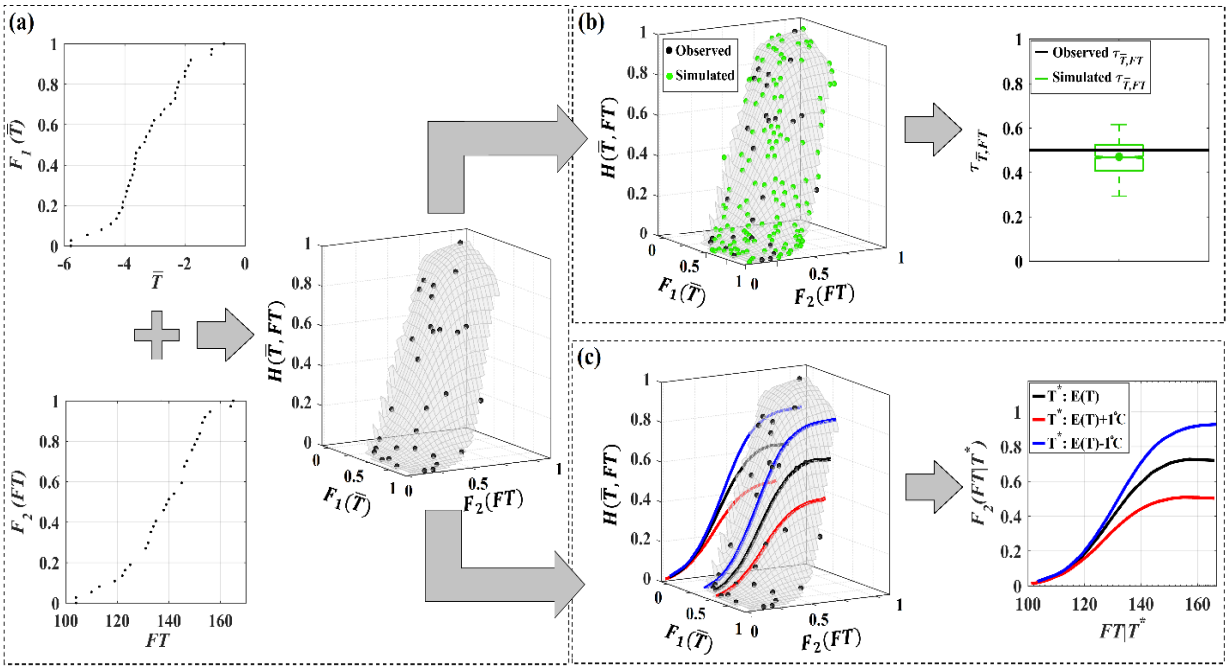

Figure 2.2 The process of (a) identification, parametrization, and validation of copulas models, along with their implementation for (b) re-sampling from the copula space and re-estimating the Kendall's tau coefficient; and (c) addressing the impact of changing temperature conditions on freeze-thaw characteristics given the dependence structure captured by the copula model. $\overline{\boldsymbol{T}}$ and FT are temperature and freeze-thaw characteristics respectively. $\boldsymbol{F_1}(.)$ and $\boldsymbol{F_2}(.)$ are Cumulative Distribution Functions of $\overline{\boldsymbol{T}}$ and FT respectively and $\boldsymbol{T}^*$ is the given temperature condition.

2.3 Case study and implementation

To showcase the application of the proposed framework, we consider the largest province in Canada, Québec (QC). With the elevation varying from 0 to 1652 meters, Québec has a total area of 1,542,056 km^2, from which 176,928 km^2 are waterbodies, making Québec the richest Canadian jurisdiction in terms of available surface water resources (Atlas of Canada, 2016). With eight distinct ecological units, known as ecozones (Wiken, 1986), Québec is the richest Canadian region in terms of ecosystem diversity. Delineating the whole Québec area to ecozones provides an opportunity to assess the potential changes in temperature control on the FT characteristics across different ecological sub-regions. The eight ecozones covering Québec include Northern Arctic (2.3% of the area; Coops et al., 2008), Southern Arctic (10.4% of the area; Coops et al., 2008),

Arctic Cordillera (0.8% of the area; Lespinas et al., 2015), Taiga Shield (34.8% of the area; Marshall et al., 1999), Hudson Plains (2.4% of the area; Goodbody et al., 2020), Boreal Shield (42.7% of the area; Rowe and Sheard, 1981; Ireson et al., 2015), Mixed-Wood Plains (1.7% of the area; Kerr and Cihlar, 2004) and Atlantic Maritime (4.3% of the area; Lespinas et al., 2015). These ecozones are named from north to south by IDs of EZ1 to EZ8, respectively – see Figure 2.3.

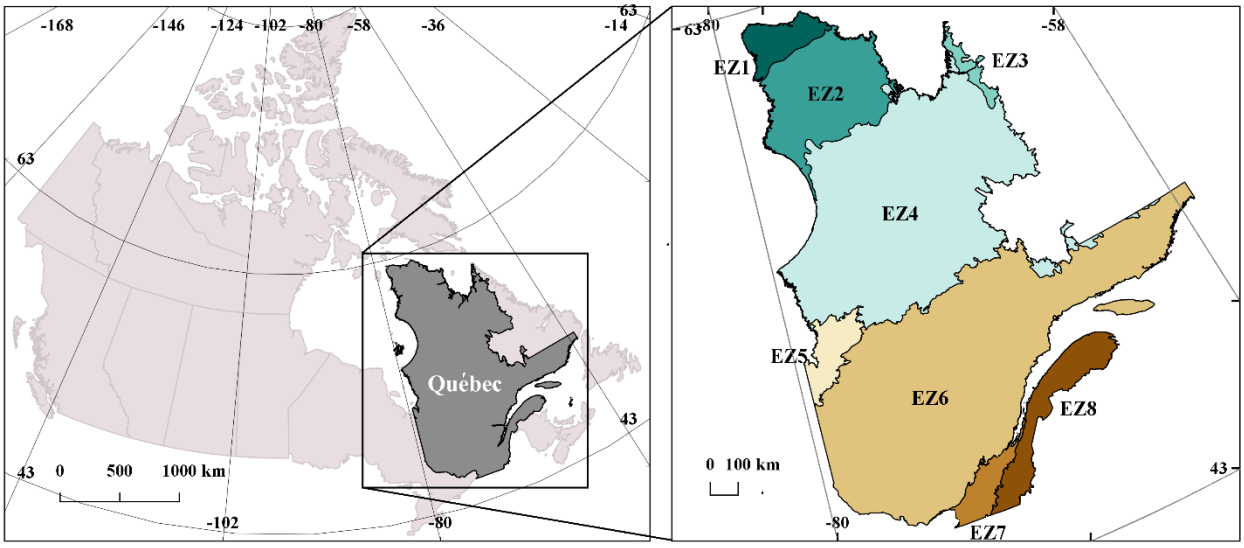

Figure 2.3 The province of Québec, Canada, and its eight ecozones.

To extract FT characteristics, we use the global landscape FT Earth System Data Record (FT-ESDR) available from National Snow and Ice Data Center (NSIDC; https://doi.org/10.5067/MEASURES/CRYOSPHERE/nsidc-0477.004). The dataset includes daily FT states, based on four classes of (1) AM and PM frozen, (2) AM and PM non-frozen, (3) AM frozen and PM thawed (transitional), and (4) AM thawed and PM frozen (inverse transitional) with spatial resolution of 25×25 km^2 over the period of 1979-2017 (Kim et al., 2017). By having the gridded daily FT states, various FT characteristics can be extracted across multiple temporal and spatial scales, each having different relevance and implications. As an example, annual number of frozen days at each grid can reveal the temporal alterations in the frozen period at the grid scale. Similarly, the number of frozen days from all grids in one ecozone can provide a notion for spatiotemporal variations in the number of frozen days in a given ecozone/period. As another example, the expected daily percentage of frozen area can be calculated at each ecozone to provide a notion for how the total area of frozen land can change across different regions. Table 2.1 summarizes the list of FT characteristics considered in this study, which can be categorized into three categories. The first category of FT variables includes three FT characteristics related to the duration of events at the grid and/or ecozone scales, namely number of Frozen Days (hereafter *FD*), number of Thawed Days (hereafter *TD*), and number of transient days, either as transitional or inverse-transitions (hereafter *FTD*). *FD*, *TD*, and *FTD* are defined as the total number of days with the above-mentioned states at annual, seasonal, and monthly scales. Note that the annual FT

characteristics are calculated from the month of September of each year to the month of August of the year after, in contrast to a Julian and/or hydrologic years. This FT year in suggested to capture the time in which the majority of the landscape is thawed and a fresh cycle of FT is recurring (Kim et al., 2017; Park et al., 2016a). For monthly FT characteristics and for the sake of brevity, we only focus on the months of April, October, and January as the representative months in the spring, fall, and winter seasons. The second category of variables includes expected monthly extents of daily frozen and thawed areas (hereafter *EFA* and *ETA* respectively) as well as the monthly variability in daily extents of frozen and thawed areas (hereafter *VFA* and *VTA* respectively). The variables are only calculated in representative months of April, October, and January as their seasonal and annual estimates are not informative due to high variability of daily FT extents over coarser temporal scales. The last variable investigated is the annual Permafrost Extent (hereafter *PE*), defined as the percentage of the land, where the annual *FD* is higher than sum of annual *TD* and *FTD* (Dobinski, 2011; Park et al., 2016b). *PE* is relevant in the northern ecozones (EZ1 to EZ4).

Table 2.1 The freeze-thaw characteristics calculated using the gridded FT-ESDR data over Québec.

Name	Abbr.	Unit	Temporal scale	Spatial scale
Number of frozen days	*FD*	days	monthly (April, October, January) seasonal annual	grid ecozone, province
Number of thawed days	*TD*			
Number of transient days	*FTD*			
Expected daily extent of frozen area	*EFA*	%	monthly (April, October, January)	ecozone province
Variability in expected daily extent of frozen area	*VFA*			
Expected daily extent of thawed area	*ETA*			
Variability in expected daily extent of frozen area	*VTA*			
Permafrost extent	*PE*	%	annual	EZ1, EZ2, EZ3, EZ4

We obtain the temperature dataset from the Global Meteorological Forcing Dataset (GMFD; https://hydrology.princeton.edu/data.pgf.php). GMFD includes global near-surface meteorological data with various spatial resolutions and is constructed by combining the reanalysis products from National Centers for Environmental Prediction, National Center for Atmospheric Research, and a group of global observation datasets, providing higher global accuracy as well as better temporal and spatial consistency comparing to conventional reanalysis products (Sheffield et al., 2006). The data has been widely used to support large-scale hydrologic and land-surface modeling efforts (Funk et al., 2015; Haile et al., 2019; Sheffield et al., 2012). We consider gridded records of daily maximum and minimum temperature from GMFD to estimate the daily mean temperature at 0.25°×0.25° from 1979 to 2016, overlapping with the available data for the FT characteristics.

Prior to any further analysis, we transfer the temperature and FT data into a unique spatial scale. By considering the grids of FT-ESDR as the reference, we use the *k*-nearest neighbor interpolation (Steinfeld et al., 2020) to estimate the mean daily temperature at the same grid resolution as FT data. In brief, *k*-nearest neighbor is a non-parametric geostatistical method to

estimate a variable in an unknown point based on its known neighborhood (Fekete et al., 2001; Grant et al., 2008). The nearest neighbors are identified here as those with the smallest Euclidian distance to the centers of FT-ESDR grids. By performing a series of numerical experiments, we find that considering four nearest neighbors can provide the highest accuracy in modeling the mean and standard deviation of daily temperature dataset over different ecozones as well as the Québec as a whole (Hatami and Nazemi, 2019). The regridded estimations of mean daily temperature are then used to estimate temperature conditions and to pair them with FT characteristics at the same temporal and spatial scales. The utilized dataset in this study along with additional data related to snow cover and snow depth, elevation, land-use and land-cover, as well as existing in-situ climatic and hydrometric networks are available through the Cold Region Data Accessibility Portal for Québec (CRDAP – QC; Nazemi et al., 2021).

We apply the proposed methodology in Figure 2.1 to diagnose, represent, and quantify the control of temperature on FT characteristics. As the marginal variables should be independent and identically distributed random variables, we first study the existence of autocorrelation in the temperature and FT data. Based on the results, the autocorrelation is only relevant in annual gridded temperature and less than 17% of grids with no obvious geographic concentration. These grids are excluded from the analysis at the annual scale. Note that autocorrelation could have been theoretically removed using e.g. a simple regression model (see Jalili Pirani and Najafi, 2020); however, this would have caused the issue of heterogeneity in our comparing our results with those grids in which autocorrelation was not removed. Considering other spatial and temporal scales, no significant autocorrelation structure is found in neither temperature nor FT characteristics.

We consider three frequently-used and parsimonious bivariate copula structures, i.e. Gaussian, Frank, and Clayton copula families (Arns et al., 2017; Liu et al., 2020; Shi et al., 2020), to find the best copula to describe the joint interdependencies between FT and temperature characteristics across Québec. These copulas are considered due to their simplicity as well as generation properties and the fact that they together can represent a wide range of dependencies with different characteristics (Nelsen, 2006). We use empirical distribution to describe marginal characteristics of FT and temperature; as a result, any difference between the performances of copula models can be referred to the difference in considered copula structures. The Method of Moments is implemented to parametrize the considered copula structures (Oh and Patton, 2013). After fitting the copula models, we consider comparing the simulated and observed Kendall's tau coefficients between FT characteristics and temperature at the spatial and temporal scales noted in Table 2.1. Considering the overall performance for other FT characteristics as well, the Frank copula is found as the best bivariate copula structure with a good performance in modeling all cases of interdependencies considered – see Appendix-B. It should be noted that here our focus is not on extremes and therefore representing the Kendall's tau can be sufficient. In studies focusing on extremes and tail dependencies, other goodness-of-fit measures should be used to assess the performance of the fitted model (Genest et al., 2009; Nazemi and Elshorbagy, 2012; Singh and Najafi, 2020).

Considering $F_1(X)$ and $F_2(Y)$ as the marginal CDFs of random variables X and Y, Frank copula can be described as (Chen et al., 2017; Favre et al., 2004):

$$C_\theta\{F_1(X), F_2(Y)\} = -\frac{1}{\theta} log\left[1 + \frac{\left(e^{-\theta F_1(X)} - 1\right)\left(e^{-\theta F_2(Y)} - 1\right)}{\left(e^{-\theta} - 1\right)}\right], \theta \neq 0 \quad \textbf{(2.4)}$$

where θ is the copula parameter, which is directly linked to the Kendall's tau through the following equations (Acar et al., 2011; Ghotbi et al., 2020):

$$\tau = 1 + \frac{4}{\theta}\left\{\left(\int_0^\theta \frac{t}{e^t - 1} dt\right) - 1\right\} \quad \textbf{(2.5)}$$

We first inspect the grids with significant dependencies between temperature and FT characteristics across considered temporal and spatial scales. Accordingly, a statistical analysis is performed to quantify the changes in dependencies over space and time. To address spatial variations, we look into changes in the Kendall's tau across different ecozones. To demonstrate temporal variation, we look at differences in Kendall's tau between two non-overlapping, equally long, and consecutive sub-periods of 1980-1997 (1 September 1979 to 31 August 1997) and 1998-2016 (1 September 1997 to 31 August 2016). The analysis of spatial and temporal variations in the dependence structure is presented in Section 2.4. In parallel, using developed copulas, we perform a set of impact assessments to illustrate how changes in temperature condition would result in changes in FT characteristics. These examples are presented in Section 2.5.

2.4 Large-scale dependencies between freeze-thaw and temperature conditions

2.4.1 Empirical dependencies across temporal and spatial scales

We first quantify the empirical dependencies between FT characteristics and temperature conditions at the grid scale and during the entire data period. Figure 2.4 summarizes the results for the annual (Figure 2.4a), seasonal (Figure 2.4b), and monthly (Figure 2.4c) time scales, in which red and blue colors indicate significant positive and negative dependencies. Regions with no colors are where dependencies are not significant. Black dots indicate grids where significant autocorrelations in temperature data are seen. As noted above, this condition only appears in annual temperature and in less than 17% of grids with no particular regional pattern.

Considering annual and seasonal scales, the dependencies are stronger for the case of $\bar{T}$ and *FD* as well as $\bar{T}$ and *TD* compared to $\bar{T}$ and *FTD* except for summer. The strongest dependencies between $\bar{T}$ and these FT characteristics are observed in the annual time scale as well as in spring for *FD* (≈-0.45) and *TD* (≈0.4). Considering *FTD*, the largest magnitude for expected dependence between $\bar{T}$ and *FTD* across Québec is observed over winter (≈0.20). Regarding the dependencies between $\bar{T}$ and *FD* as well as $\bar{T}$ and *TD* at monthly scale, it is clear that the dependencies are stronger in April (≈-0.50 and ≈0.37, respectively). In April, significant negative and positive

dependence between $\bar{T}$ and *FD* as well as $\bar{T}$ and *TD* are pronounced across the province in contrast to $\bar{T}$ and *FTD* for which a clear departure is observed in the sign of dependence in the north (positive) and south (negative). While positive dependencies between $\bar{T}$ and *FTD* are stronger in northern Québec in April, statistically significant negative dependencies mainly take place in October across southern parts of the province.

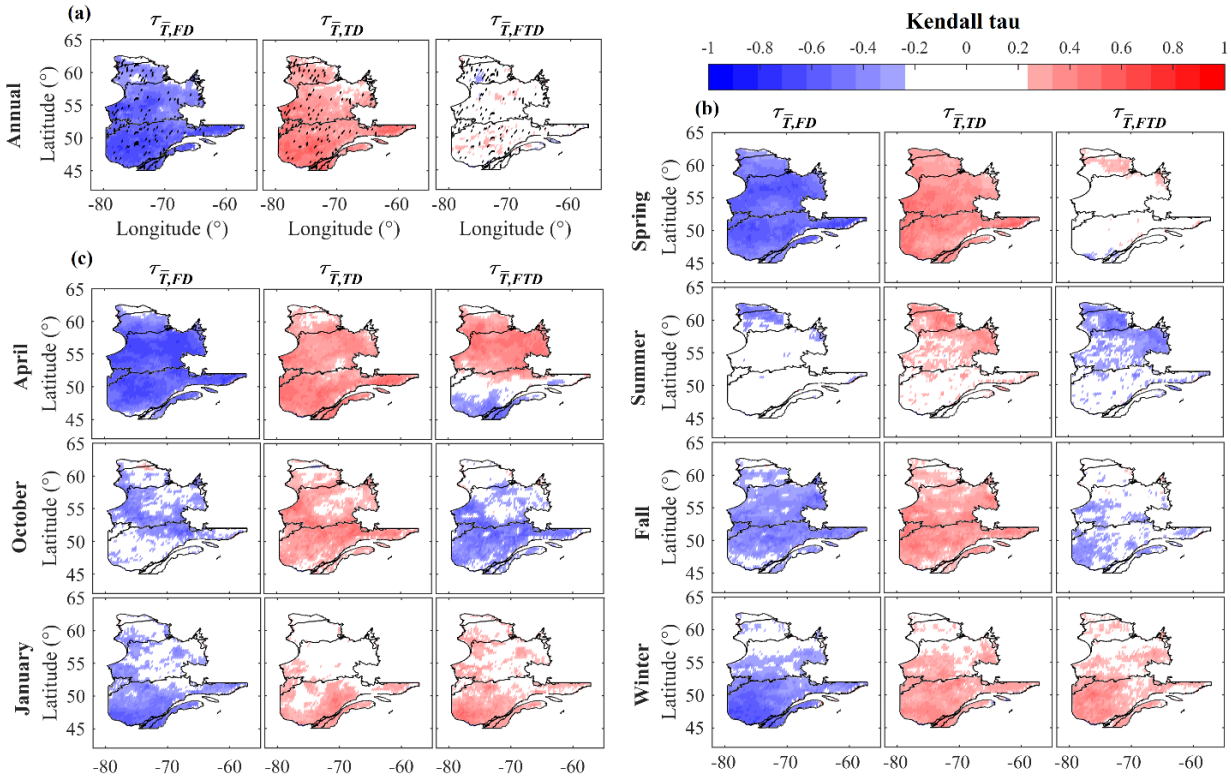

Figure 2.4 Significant dependencies between temperature and FD, TD, as well as FTD across (a) annual, (b) seasonal, and (c) monthly scales in Québec. In each sub-figure, the interdependence between temperature and FD, TD, as well as FTD are presented in columns from left to right. Red and blue colors show positive and negative dependencies, respectively.

Figure 2.4 also points at spatial variations in the dependencies between $\bar{T}$ and FT conditions at the grid scale. To take a closer look, in Figure 2.5, we monitor changes in regional dependencies between $\bar{T}$ and FT characteristics across ecozones and the province as a whole. In each panel, color bars show the sign and magnitude of significant Kendall's tau during the complete data period. The color code used for bars corresponds to those used for identifying ecozones in Figure 2.3. The gray bars also show the results for Québec. Panels (a), (b), and (c) correspond to the duration of FT states, the spatial extent of FT states as well as the extent of permafrost area, respectively.

Considering the dependence between $\bar{T}$ and duration of FT states, it is clear that the dependencies are stronger for the case of *FD* and *TD* compared to *FTD*. In addition, there is a clear increase in the magnitude of dependencies between $\bar{T}$ and *FD* as well as $\bar{T}$ and *TD* by moving from north to south in all time scales considered. Similar to the analysis made at the grid scale, the

dependence between $\bar{T}$ and *FD* as well as $\bar{T}$ and *TD* are stronger during spring, particularly in April. In contrast, statistically significant dependencies between $\bar{T}$ and *FTD* mainly happen during winter, particularly in January. Similar to the case of *FD* and *TD*, the magnitude of dependence between $\bar{T}$ and *FTD* increases in southern ecozones over the winter season. Regarding the dependence between temperature and spatial extent of FT states, the dependence between temperature and *EFA*, *ETA*, *VFA* as well as *VTA* are more pronounced in April. In the case of *VFA* and *VTA,* there are clear departures between the sign of dependence in the north (positive) and south (negative). Considering the dependence between $\bar{T}$ and *PE*, the negative dependencies exist in all four northern ecozones, however, the dependence is insignificant in EZ3, and the magnitudes of dependencies are stronger in EZ2 and EZ4 compared to EZ1.

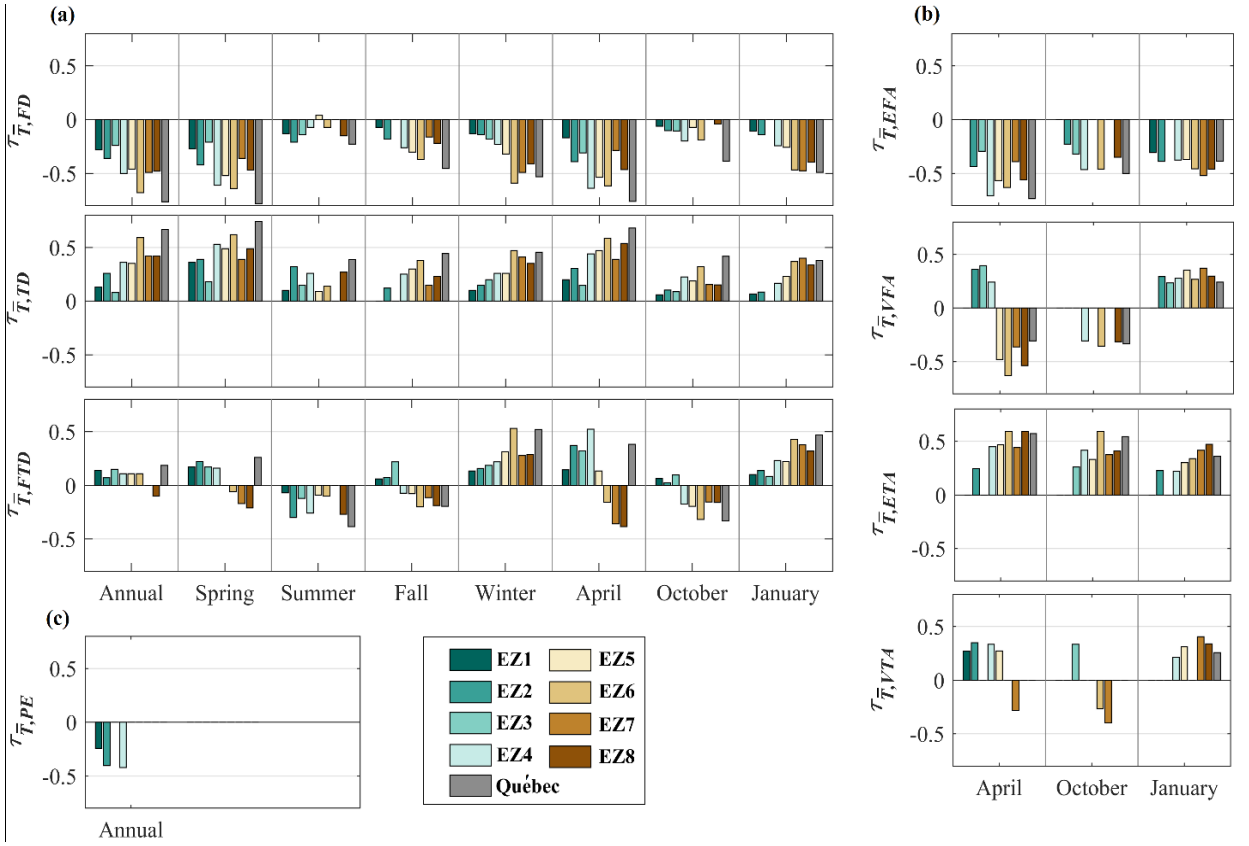

Figure 2.5 Variations in annual, seasonal, and monthly dependencies between temperature and (a) duration of FT states, (b) spatial extent of FT states, and (c) extent of the permafrost area across various ecozones and Québec as a whole. Only the significant dependencies are shown.

Overall, duration-based FT characteristics, i.e. *FD*, *TD*, and *FTD*, demonstrate more significant dependencies with temperature, particularly in annual and seasonal scales. The dependence between seasonal temperature and duration-based FT characteristics (spring for *FD* and *TD*, winter for *FTD*) are significant in all ecozones as well as the province as a whole. Considering the spatial extent of FT states during April, significant dependencies are observed between mean temperature and *EFA* and *VFA* in all ecozones except EZ1. During the same month, the dependence between

ETA and temperature is significant across all ecozones except EZ1 and EZ3 and the dependence between *VTA* and temperature is only significant across EZ1, EZ2, EZ4, EZ5, and EZ7. From now on, we only consider these strong and significant seasonal and monthly dependencies, along with significant annual dependencies between average temperature and *PE* for further investigation.

2.4.2 Variations of dependencies in time and space and the suitability of copula methodology

Although Figure 2.5 reveals significant dependencies between temperature and FT characteristics in most of the investigated cases; two important issues require more attention. First, it is still unknown how well parametrized copulas can capture the observed dependence between temperature and FT characteristics across different ecozones. Second, although empirical Kendall's tau measures for the considered dependency cases are changing across different ecozones, it is not yet clear how significant these differences are. To address these, we recalculate Kendall's taus using randomly synthesized pairs of temperature and FT characteristics, generated using parametrized copulas in each ecozone, and compare the expected values of sampled Kendall's taus with observed ones. In addition, by comparing the probability distributions of sampled Kendall's taus across different ecozones, it would be possible to formally address how dependence between temperature and FT characteristics varies across space. Figure 2.6 presents the results of this analysis, in which the interquartile range and mean values of simulated Kendall's taus are shown in different ecozones as well as the province. Positive and negative dependencies are shown with red and blue colors, respectively. The black dots and the solid lines within interquartile ranges represent the observed and mean values of simulated Kendall's taus in each region. The results show that parametrized copulas are able to capture the empirical dependencies fairly well with an overall mean relative error of 1.6% (0.7% and 2.1% for duration- and spatial-based characteristics, respectively). In general, ranges of simulated dependencies are less for duration-based characteristics, revealing more robust simulations compared to spatial indices.

Using the one-way ANOVA, we formally assess the difference between simulated Kendall's taus across various ecozones. The results are provided in Table A1 in the Appendix-A, highlighting the uniqueness of dependence between temperature and FT characteristics in the majority of cases, particularly for duration-based characteristics. The spring's dependence between temperature and *FD* is unique across all considered regions in Québec. For the case of *TD*, the spring's dependence is similar only between EZ2 and EZ7; For *FTD* during winter this is only the case between EZ3 and EZ4. For the *EFA* during April, there are similarities between EZ2 and EZ7, QC and EZ4, as well as EZ5 and EZ8. For the dependence between temperature and *ETA* during April, there are clear pairwise similarities in southern regions, particularly across EZ4, EZ5, EZ6, and EZ7. For dependencies between *VFA* and temperature during April, there are similarities between the dependence structures in EZ2 and EZ3 as well as EZ5 and EZ8. For the case of dependencies between temperature and *VTA* during April, there are similarities between EZ1 and EZ5 as well as EZ2, EZ4 and EZ5. Dependence is similar between the annual *PE* and temperature only in EZ2 and EZ4. These significant differences in dependencies between temperature and FT

characteristics across Québec ecozones can reveal the role of ecosystem conditions in regulating the impact of temperature on FT characteristics. In Section 2.5, we will show how these spatial differences in dependencies between temperature and FT characteristics can translate into different responses to changing temperature conditions.

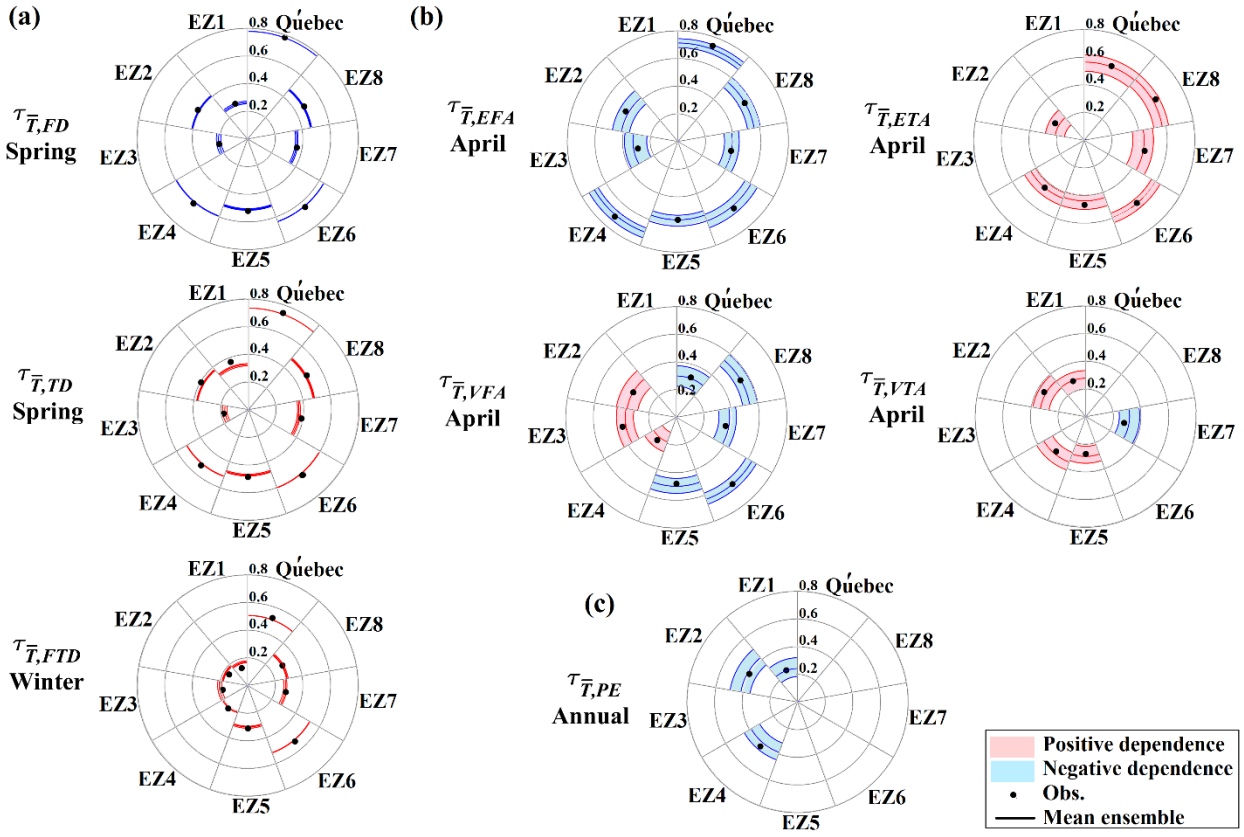

Figure 2.6 Examples for changes in the dependencies between temperature and FT characteristics over different ecozones and Québec as a whole. Colored envelopes show interquartile ranges and lines within envelopes show expected values of simulated Kendall's tau coefficients. Red and blue color are indicators of positive and negative dependence, respectively. Observed Kendall's tau coefficients are presented as black dots.

Apart from spatial variations in the dependence structure, the dependence in a given region can be also subject to change in time. To assess this and using observed pairs of temperature and FT conditions in the first and second sub-periods (i.e., 1980-1997 *vs.* 1998 to 2016), we parametrize copula models and recalculate Kendall's tau dependence using randomly generated pairs of temperature and FT characteristics. We accordingly compare the expected values of simulated Kendall's taus with observed values. Figure 2.7 summarizes the results, in which the boxplots of simulated Kendall's taus related to the first and the second time episodes are displayed with gray and pink colors, respectively. The black dots and gray crosses represent the observed empirical and the mean of simulated dependence coefficients in each sub-period.

As it can be seen, parametrized copulas are able to capture the empirical dependencies fairly well. Based on the expected Kendall's taus obtained through simulation, parametrized copulas are able to capture the observed values of dependencies between temperature and FT characteristics with overall relative mean error of 1.2% (1.9% for duration-based characteristics, 0.7% for spatial-based characteristics). Similar to the results obtained in Figure 2.7, it is clear that the range of simulated dependencies is strictly lower for duration-based FT characteristics. Considering the dependency between temperature and *FD*, there is a substantial increase in negative dependence over time in all ecozones as well as Québec. For dependency case between temperature and *TD*, the dependence is also strengthening over the second period (1998-2016) with higher rates of increase in northern ecozones. The same conclusion is drawn from the results of *PE*.

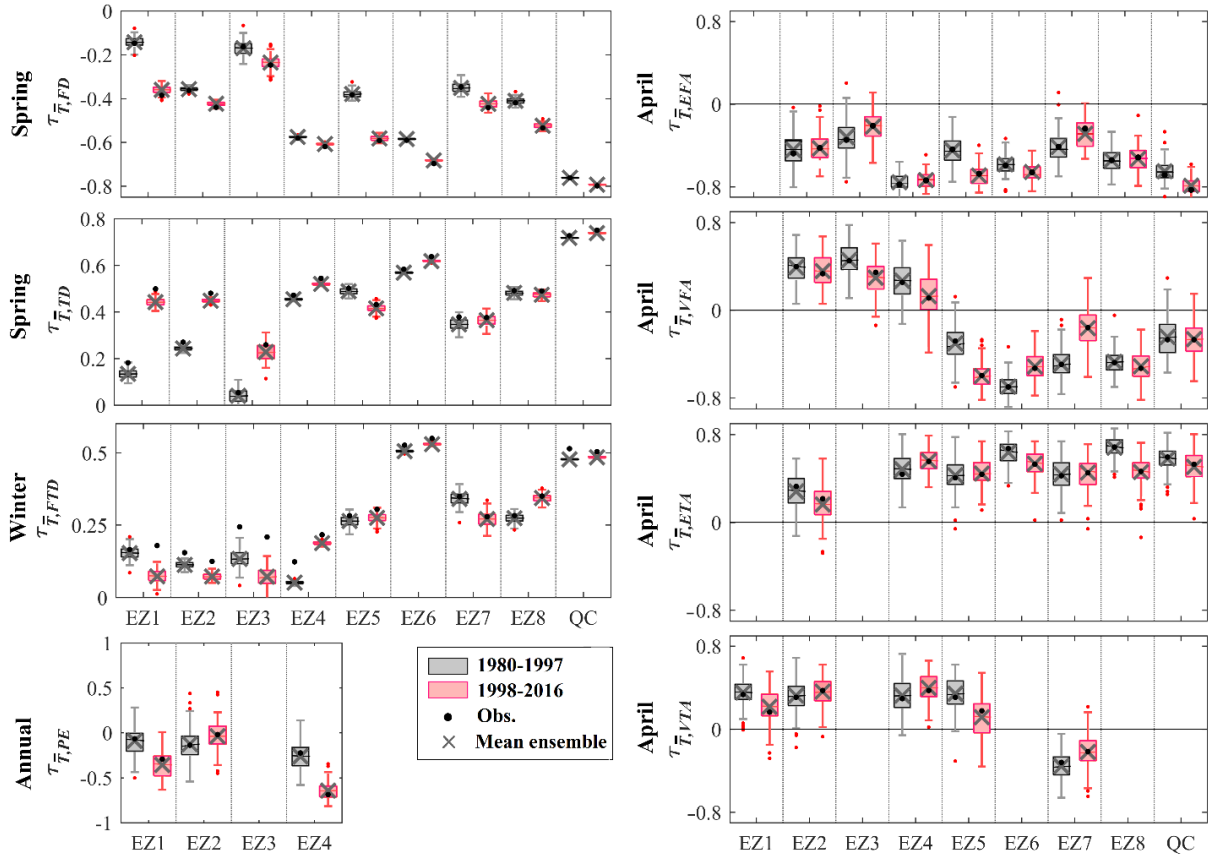

Figure 2.7 Changes in dependencies between temperature and FT characteristic during 1980-1997 and 1998-2016 at ecozone and province scales. Gray and pink colors correspond to the simulated Kendall's tau over the first and second periods, respectively. The observed and mean of simulated dependence coefficients at each region/period are marked with black dots and gray crosses.

To formally assess the temporal changes in the dependence structure between temperature and FT characteristics, we use the corrected one-way ANOVA. The results are provided in Table A2 in the Appendix-A, highlighting the uniqueness of dependence between temperature and FT characteristics in the majority of comparison cases. There are significant differences between temperature and duration-based FT characteristics, i.e. *FD*, *TD*, and *FTD*, during the first and the

second sub-periods across all considered regions. There are more cases of similarity in dependencies between temperature and other spatial-based characteristics, i.e. *EFA*, *ETA*, *VFA*, and *VTA* during the first and the second sub-periods. In brief, the dependence between temperature and *EFA* during April is similar over time in EZ2 and EZ8. The dependence between temperature and *ETA* during April is not changing in time across EZ7 as well as the province. Although the dependence between temperature and *VFA* changes temporally across all ecozones of Québec except EZ2, it stays unchanged in the province. The dependence between temperature and *VTA* as well as the dependence between annual average temperature and *PE* is significantly different during the first (1980-1997) and second (1998-2016) sub-periods in all considered ecozones. Significant temporal changes in the interdependencies between temperature and FT characteristics can be an indicator for a profound change that is not only related to the marginal characteristics of temperature and FT but the change in their joint characteristics. Below, we discuss how these variations can result into a changing landscape response to alterations in temperature conditions.

2.5 Application examples for impact assessment

Section 5.4 provides several lines of evidence for strong dependencies between statistical properties of temperature and FT that are significantly variant in time and space. In this section we demonstrate (i) how such dependencies can be used as a basis for assessing the impacts of temperature change on FT characteristics; and (ii) what implications spatial and temporal variations in joint dependencies have on FT characteristics. We pursue these questions through a set of illustrative examples. The first two examples showcase how developed copula models can be used as a basis for estimating temporal and spatial FT characteristics given a known alteration in expected temperature conditions. The third and fourth case studies demonstrate how spatial and temporal changes in dependencies can impact the FT response to changing temperature conditions.

2.5.1 Impacts of unit degree change in average temperature at the grid scale on the duration of frozen and thawed days in spring

The Kendall's tau coefficients presented in Figure 2.4(b) show strong grid-base dependencies between temperature and *FD* as well as *TD* during spring. Developed copulas can provide a basis to estimate changes in these FT conditions under a prescribed change in average temperature at the grid scale (Equation 2.3). Figure 2.8 summarizes the results for 1℃ change in average temperature, in which the top and bottom rows are related to *FD* and *TD*, respectively. The left column shows the expected grid-base *FD* and *TD* during spring under current temperature conditions using shades of gray. The middle and right columns show changes in expected FT conditions under 1℃ cooling and warming, respectively. Shades of red (blue) represent increasing (decreasing) *FD* and *TD* as a result of 1℃ change in temperature conditions. Looking at expected values under historical condition, the period of *FD* in spring is considerably longer in the north (i.e., EZ1 to EZ4) compared to the south (i.e., EZ5 to EZ8). The variation in FD period in spring

is ranging from 14 to 83 days in EZ7 and EZ1 respectively, with an average of 42 days over the whole province. This pattern is reversed for period of *TD* during spring (panel e), in which longer thawed periods are observed in southern grids (maximum of 75 days in EZ8), with the mean of 34 days in the province.

The Kendall's tau coefficients presented in Figure 2.4(b) show strong grid-base dependencies between temperature and *FD* as well as *TD* during spring. Developed copulas can provide a basis to estimate changes in these FT conditions under a prescribed change in average temperature at the grid scale (Equation 2.3). Figure 2.8 summarizes the results for 1℃ change in average temperature, in which the top and bottom rows are related to *FD* and *TD*, respectively. The left column shows the expected grid-base *FD* and *TD* during spring under current temperature conditions using shades of gray. The middle and right columns show changes in expected FT conditions under 1℃ cooling and warming, respectively. Shades of red (blue) represent increasing (decreasing) *FD* and *TD* as a result of 1℃ change in temperature conditions. Looking at expected values under historical condition, *FD* period in spring is considerably longer in the north (i.e., EZ1 to EZ4) compared to the south (i.e., EZ5 to EZ8), ranging from 14 to 83 days in EZ7 and EZ1, respectively and with an average of 42 days over the whole province. This pattern is reversed for spring's *TD* (panel e), in which longer thawed periods are observed in southern grids (maximum of 75 days in EZ8), with the average of 34 days over the province.

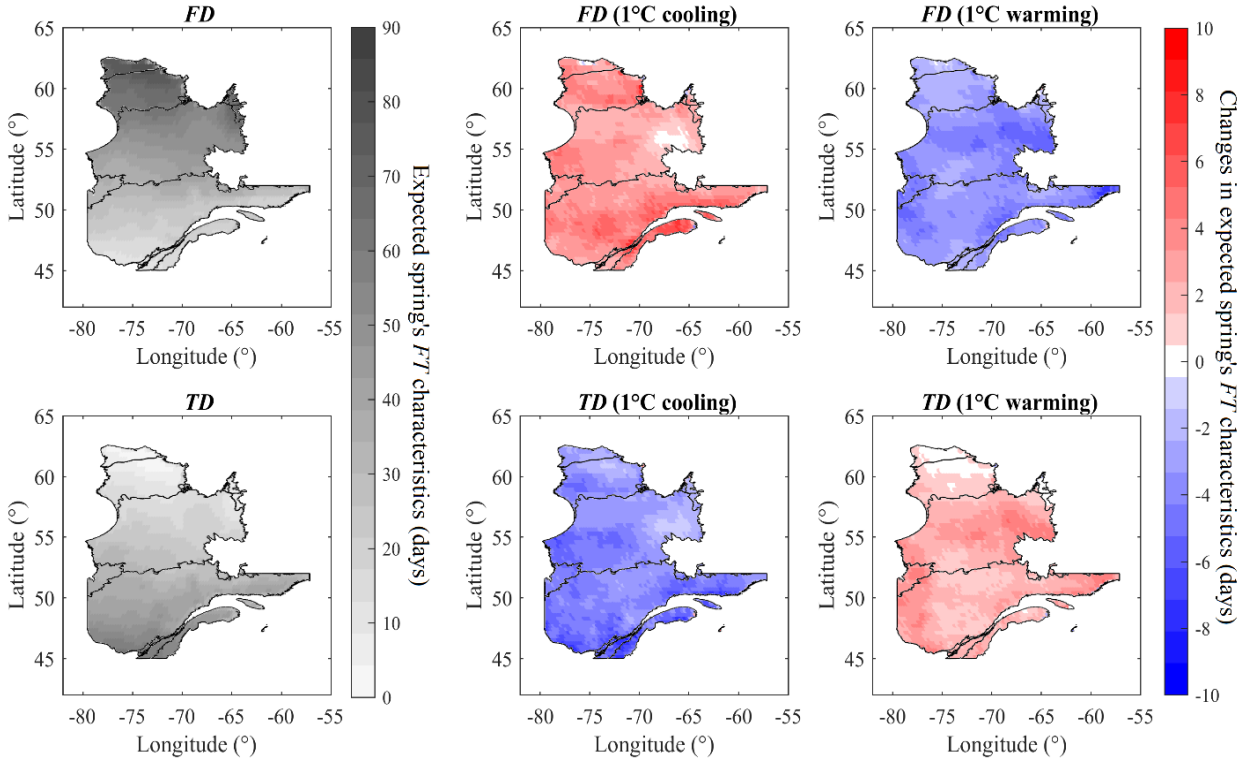

Figure 2.8 Impacts of unit degree change in spring's mean temperature on expected *FD* and *TD* at the grid scale in Québec. The expected *FD* and *TD* values under historical conditions are shown in shades of gray (left hand panels). The middle and right panels show the impacts of **1**℃ cooling and warming respectively. Red (blue) colors illustrate positive (negative) shifts in expected FT characteristics.

The comparison of the change in expected *FD* and *TD* in spring under 1℃ alteration in average temperature indicates the higher impacts of cooling than warming. For instance, the impacts of 1℃ cooling on *FD* are higher compared to that of 1℃ warming in about 61% of grids. Over the province, 1℃ cooling leads to an average of roughly 5 more frozen days in spring, while the same magnitude of warming causes 4 less non-frozen days. Similarly for *TD*, higher impacts of 1℃ cooling are observed in more than 66% of grids. One degree cooling causes the expected *TD* to decrease by 5 days over the province, while 1℃ warming increases the expected *TD* by 3 days over Québec. More details related to spatial differences in the response of *FD* and *TD* to temperature change in spring are discussed in Section 2.5.3.

2.5.2 Impacts of unit degree temperature change on the annual permafrost extent in northern ecozones

Here we use the empirical dependence between *PE* and annual temperature as a basis to assess the impacts of changing temperature on annual *PE* across Québec's northern ecozones. Similar to the example presented in Section 2.5.1, we assume that joint dependencies and marginal distributions of temperature and *PE* remain unchanged in each ecozone; and aim at quantifying alterations in the Probability Density Function (PDF) of *PE* due to 1℃ change in expected annual temperature. This analysis is performed in EZ1, EZ2, and EZ4, where dependencies between *PE* and temperature are significant. We use the parametrized copula model in each ecozone to estimate the PDF of *PE*, corresponding to $\pm$1℃ change as well no change in the expected temperature. Figure 2.9 summarizes the results, in which panels (a) to (c) show this analysis for EZ1, EZ2, and EZ4, respectively. PDFs corresponding to 1℃ cooling, no change, and 1℃ warming are shown in blue, black, and red. PDF of observed values over each ecozone is displayed with a dashed black line.

Comparison between the observed PDFs with simulated ones for no change conditions (dashed *vs.* solid black PDFs), highlights the ability of the proposed framework to capture the observed statistics of *PE*. Over three studied ecozones, the parametrized copulas can effectively represent the 1st, 2nd and 3rd moments of *PE* with overall expected relative errors of 1.7%, 7.8%, and 11.2%. Considering changes in temperature conditions, the results show considerably higher impacts of 1℃ warming compared to the same magnitude of cooling in EZ1 (9% decrease *vs.* 5.7% increase) and EZ2 (12.9% decrease *vs.* 11% increase). This is different in EZ4, where the expected shift in *PE* due to unit degree cooling is higher than warming (2.5% increase *vs.* 0.9% decrease). In panel (d), the likelihood of *PE* being larger than the expected *PE* during historical condition is presented under the three temperature scenarios. In EZ1, the exceedance probability decreases from 67.5% (for 1℃ cooling) to 34.1% (for 1℃ warming). This alteration is more intense in EZ2, where the exceedance probability decreases from 73.9% (for 1℃ cooling) to 15.5% (for 1℃ warming). In EZ4, the rate of change is from 63.5% (for 1℃ cooling) to 13.4% (for 1℃ warming). The results clearly show the nonsymmetric response of *PE* to a unit degree changes in temperature.

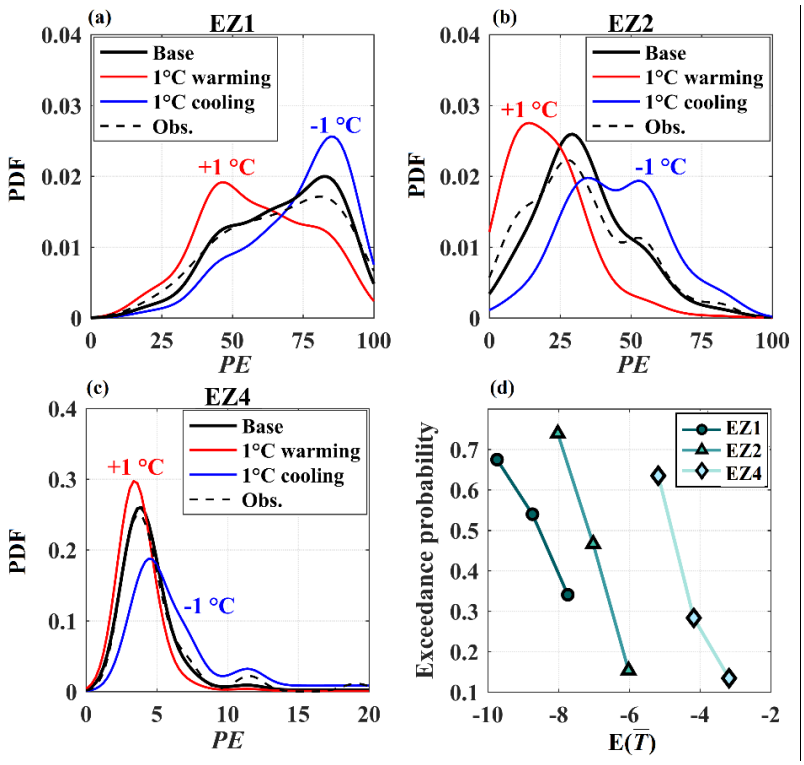

Figure 2.9 Probability Density Functions (PDFs) of *PE* in (a) EZ1, (b) EZ2, and (c) EZ4 under 1°C warming, no change and **1**°C cooling, shown in red, black, and blue colors. The PDF of observed values in each ecozone is displayed with dashed black lines. The likelihood of *PE* being larger than the expected value under historical condition given the three temperature conditions are shown in panel (d).

2.5.3 Regional impact of changing temperature on duration of frozen and thawed periods in spring across ecozones

To showcase how FT characteristics can change spatially due to unique changes in temperature characteristics, we implement a bottom-up assessment to quantify expected changes in the long-term average of *FD* and *TD* in spring, given a range of changes in expected temperature at each ecozone, we consider the change in mean temperature at each ecozone from -2°C to $+2$°C with a sampling step of 0.5°C. Figure 2.10 summarizes the results of this analysis, in which the left and right panels are related to *FD* and *TD*, respectively. Each row is related to specific ecozones, ordered from north (top) to south (bottom). Red (blue) color is the indicator of increasing (decreasing) changes in the long-term average of *FD* and *TD* at each ecozone. Considering unique changes in temperature conditions, it is clear that the changes in spring's *FD* due to identical change in regional temperature is considerably higher in northern ecozones, while *TD* is more sensitive to changes in expected temperature in southern ecozones. Due to 2°C cooling (warming), for instance, the increase (decrease) in the long-term average of spring's *FD* is ranging from 10 (8) to 6 (5) days in EZ1 and EZ8, respectively. These shifts for *TD* are -4 (4) and -10 (9) days in EZ1 and EZ8 for 2°C cooling (warming), respectively.

Moreover, the comparison of changes in expected spring's *FD*, as a result of a unique magnitude of positive and negative changes in average temperature conditions, indicates the higher impacts of cooling than warming. The average increase in *FD* over all ecozones due to 2℃ cooling temperature conditions is ≈7 days while due to 2℃ warming the average decrease in *FD* is ≈6 days. Similarly, looking at changes in expected *TD*, the results highlight the higher sensitivity to cooling temperature conditions comparing to the same magnitude of warming. Over all ecozones on average, 2℃ cooling (warming) leads to an average of ≈7 less (≈6 more) thawed days in spring. The higher impacts of cooling is consistent with the results obtained at grid scale in Section 2.5.1.

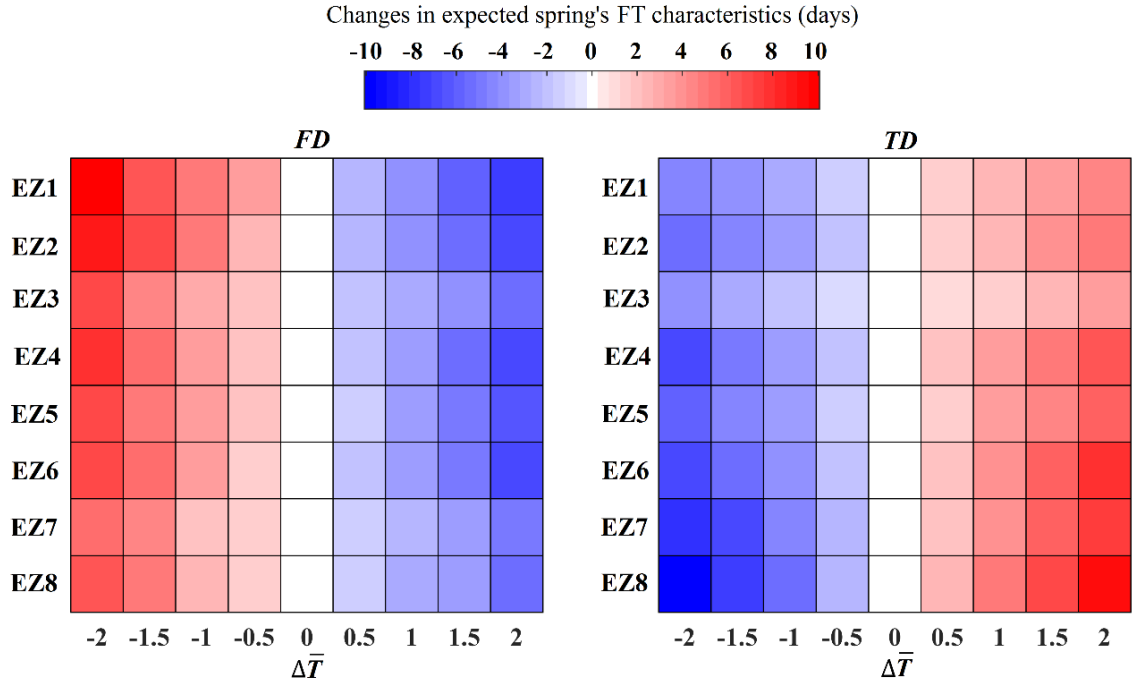

Figure 2.10 Impacts of -2 to $+2$℃ of change in expected regional temperature on *FD* and *TD* durations in spring across different ecozones of Québec. The rows are related to the different ecozones sorted from north (top row) to south (bottom row). Columns are related to the degree of shift in $\boldsymbol{E}(\overline{\boldsymbol{T}})$. The red (blue) color spectrum is an indicator of increase (decrease) in the long-term average of spring's *FD* or *TD*.

2.5.4. Impacts of changing dependencies on mean and variance of frozen area during April across Québec's ecozones

As noted in Section 2.4.2, dependencies between temperature and FT characteristics are subject to significant temporal changes in the majority of comparison cases. Here we investigate how temporal changes in dependence structures can alter the response of FT characteristics to unique changes in temperature conditions. To showcase this, we quantify the impact of unit degree warming on *EFA* and *VFA* during April in two distinct time episodes of 1980-1997 and 1998-2016 across Québec's ecozones and the province as a whole. The results are shown in Figure 2.11, where the top and bottom panels correspond to *EFA* and *VFA*, respectively. Four colored interquartile ranges are shown for each region, except for EZ1 where the dependencies are not significant. For

each region, light gray and red show the interquartile ranges corresponding to historical temperature conditions for the periods of 1980-1997 and 1998-2016, respectively. In parallel, dark gray and red show the impact of 1℃ warming during each sub-period. For each range, the corresponding mean ensemble is depicted with black dots and the long-term average of FT characteristics during the entire data period is displayed with black lines.

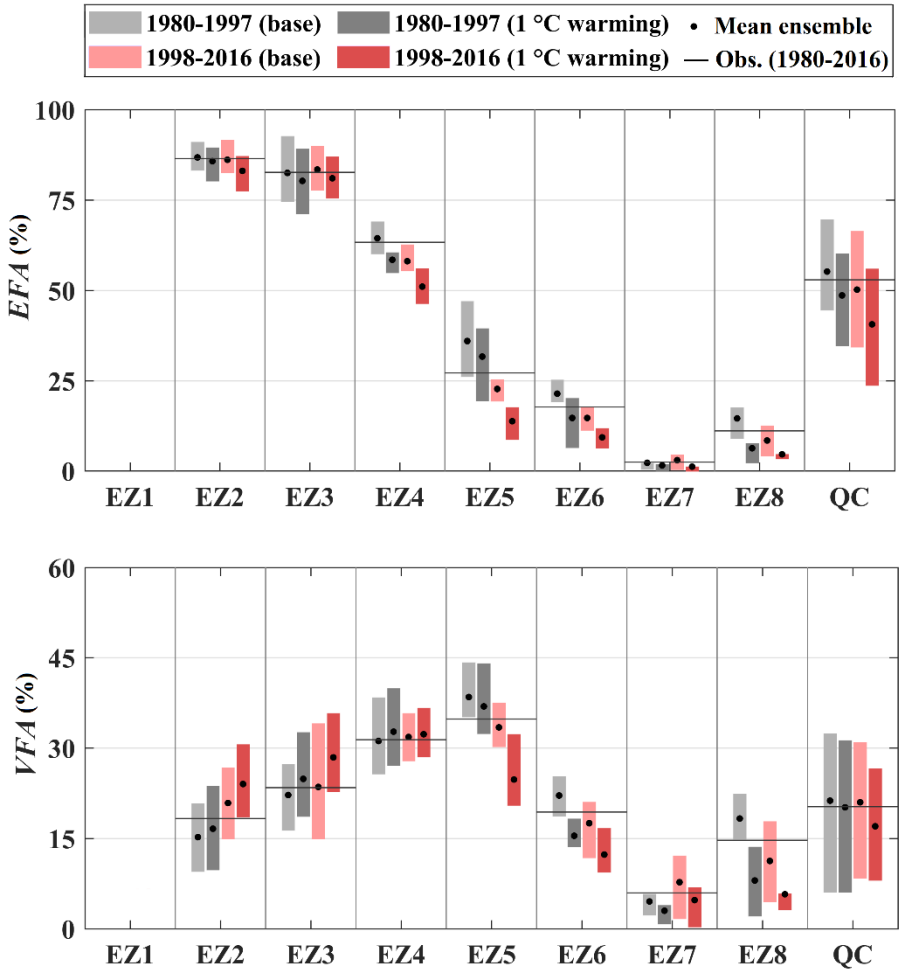

Figure 2.11 Temporal changes in the impact of a unit degree warming on April's *EFA* and *VFA* over different ecozones. The light and dark colors are indicators of the interquartile ranges corresponding to $\boldsymbol{E}(\overline{\boldsymbol{T}})$ and unit degree warming, respectively. The ranges over the first and the second sub-periods are shown with gray and pink. Black dots are the long-term average of FT characteristics over each time episode. Black lines show the long-term average of FT characteristics over the whole period of 1980 to 2016 in each region.

By looking at the shifts in interquartile ranges and the mean values of both *EFA* and *VFA*, higher alterations are observed during the second period in most regions, particularly in southern ecozones as well as the province as a whole. Over Québec, for instance, the decline in long-term average *EFA* due to 1℃ warming is 6.6% for 1980-1997, compared to 9.6% for 1998-2016. These shifts are, respectively, -1% (1980-1997) *vs.* -4% (1998-2016) for *VFA* over Québec. The

intensifying impact of 1°C warming on *EFA* during the second period is vividly observed in EZ5, where there are shifts of ≈-9% in long-term average values over 1998-2016 comparing to only ≈-4% over 1980-1997. For *VFA* over EZ5, decreases of ≈9% and ≈2% in expected values are estimated over the second and first half sub-periods, respectively. Also, by looking at *VFA* over both time episodes, a unit degree warming leads to an increase (decrease) in interquartile ranges as well as expected values over northern (southern) ecozones. This effect is consistent with the changes in sign of dependence between temperatures *VFA* over the different region (Figure 2.5b). The nonstationary in the dependence structure has been reported in some other studies looking at climate variables in Canada (e.g. Singh et al., 2020, 2021) and deserves giving more attention.

2.6 Summary and conclusion

Recurring cycles of FT are among the most important landscape features in cold regions, controlling various environmental processes below and above the soil. As the dynamics of FT are largely governed by the near surface air temperature, warming climate can alter historical characteristics of FT quite substantially; and such changes have been already observed across cold regions. Having said that, there are still several rooms for improving our knowledge about the effects of warming climate on FT patterns under current and future conditions. First and foremost, the current understandings about the alterations in FT patterns, and how they relate to the warming climate, are mainly built on in-situ measurements that are crucial, yet sparse and locally relevant. Second, projecting FT characteristics under future conditions is not trivial due to the limitations in available datasets and/or process representations in current hydrology and land-surface models. Third, it is not yet clear whether changes in the FT characteristics are solely due to changes in temperature conditions; or, it is due to a more profound change in the relationship between temperature and FT characteristics at the landscape scale. To tackle these questions, we suggest shifting the focus of FT modeling from continuous descriptions of FT states in time and space to quantifications of statistical properties of FT variables at coarser temporal and spatial scales. We accordingly propose using copulas, a set of generic multivariate mathematical functions that quantify dependence between random variables, to formally account for the link between temperature and FT variables at relevant scales. Using copulas, we can (1) describe the statistical dependence between temperature and FT variables, (2) diagnose temporal and spatial variations in the dependence, and (3) estimate FT characteristics, conditioned to a given change in temperature.

To showcase the application of the developed modeling framework, we consider the province of Québec, the largest province in Canada, over the period between 1979 and 2016. We consider pairing a global satellite-based FT with a gridded climate datasets and extract a number of FT variables across a range of temporal and spatial scales. The results of this study reveal the existence of strong dependencies between temperature and FT characteristics. Relatively speaking, the dependence between temperature and duration of frozen and thawed states are stronger, particularly during spring and in April, when significant dependencies between temperature and spatial extent of FT are also observed. The empirical dependencies that are extracted from the

gridded datasets can be reconstructed using the parameterized copulas. In general, the ranges of simulated dependencies are less for duration-based FT characteristics, revealing better capability of copula models in representing the empirical dependence between temperature and duration-based compared to spatial FT characteristics.

Our findings clearly highlight significant variations in the dependencies across time and space. Most importantly, the magnitudes of dependencies between temperature and duration of FT states increase by moving from north to south and in more recent time episodes (1998-2016). These changes can reveal the role of ecosystem conditions and/or climate change in regulating the impact of temperature on FT characteristics. Using parametrized copula models, we show the nonsymmetric response of FT characteristics to temperature change. As an example, the comparison of the change in expected *FD* and *TD* in spring under 1℃ alteration in average temperature indicates the higher impacts of cooling than warming across spatial scales from grid, to ecozone, to the whole province. We also show that a similar magnitude of change causes higher impacts under more recent dependencies, particularly in southern ecozones as well as the province as a whole. The intensifying impact of temperature change under changing dependence conditions can be vividly seen in Hudson Plains areas within Québec for which the impact of 1°C warming on *VFA* is up to 4.5 times more under dependencies observed in 1998-2016 compared to 1980-1997. These findings point at a complex and multifaceted nature of climate change impacts on FT conditions, caused by both variations in marginal characteristics of temperature, as well as joint dependencies between temperature and FT characteristics.

Although this method is applied in Québec and using a particular dataset, it is globally relevant and can be implemented through pairing other relevant datasets too. Having said that, still, several improvements can be made. First and foremost, although air temperature is the most influencing climate variables on FT characteristics, other variables such as snow cover and depth, can also influence FT patterns (Iwata et al., 2010; Yi et al., 2015). Including more climate variables require going beyond bivariate copulas and inevitably lead to more computational complexities, particularly with respect to conditional modeling, but it is a necessary step toward a better understanding of FT patterns under changing conditions. Second, it is not yet clear how much the findings are sensitive to specific datasets, from which temperature and FT characteristics along with their joint dependencies are inferred. This requires performing systematic sensitivity and intercomparison studies, which is an important step towards quantifying uncertainty in our findings in Québec and should be also considered in other regions. We hope that this study can inspire more efforts towards better understandings of landscape responses in changing cold regions.

Chapter 3.

On Complex Responses of Landscape Freeze-Thaw to Compound Climatic Changes: Lines of Evidence from Québec, Canada[3]

The contents of this chapter are submitted as "Hatami, S., Nazemi, A. (2021). On Complex Responses of Landscape Freeze-Thaw to Compound Climatic Changes: Lines of Evidence from Québec, Canada" in Scientific Reports. The contents are slightly modified.

Synopsis

Cycles of Freeze-Thaw (FT) are among the key landscape processes in cold regions. Under current global warming, understanding the alterations in FT characteristics is of a great importance for advising land management strategies in northern latitudes. Using a generic statistical approach, we address the impacts of changing air temperature and snow depth on FT responses across Québec, a Canadian province ~2.5 times larger than France. Our findings show significant yet complex responses of landscape FT to changing climate conditions. We note a vivid spatial divide between northern and southern regions and point out two important features, namely non-symmetry and nonlinearity, in the FT response. In general, the response of sensitive FT characteristics to changing climate is more intense under warming compared to corresponding cooling conditions. In addition, FT responses include nonlinearity, meaning that compounding changes in temperature and snow depth have more severe impacts compared to the cumulative response when temperature and/or snow depth change separately. These nonsymmetric and nonlinear responses have important implications for the future environment and socio-economy in a thawing Québec. Our study provides a fresh look at complex landscape responses to climatic changes in Québec and a generic methodology that can be applied in other regions.

3.1 Introduction

Freeze-Thaw (FT) dynamics, i.e. the fluctuations of soil state between frozen and thawed conditions (Frauenfeld et al., 2004), is one of the most important land-surface characteristics in northern regions, which plays a major role in determining soil properties (Mccauley et al., 2002), hydrologic response (Jones et al., 2011) as well as ecosystem diversity and productivity (Jansson and Taş, 2014). Due to these critical impacts, FT dynamics are among key considerations for human activities such as agriculture (Margesin et al., 2007) as well as the construction and operation of infrastructures in cold regions (Hjort et al., 2018). Heightened climate variability and change, however, have significantly affected soil temperature patterns and consequently the dynamics of FT cycles (Plaza et al., 2019). Changing climate can impact FT patterns in several ways. Increasing air temperature, for instance, can affect the FT dynamics through decreasing the

[3] Hatami, S., Nazemi, A. (2021). On Complex Responses of Landscape Freeze-Thaw to Compound Climatic Changes: Lines of Evidence from Québec, Canada. *Scientific Reports*, (Submitted on June 9th).

length of frozen season (Henry, 2008), increasing depth of the active soil layer (Wu and Zhang, 2010), and permafrost retreat (Schuur et al., 2009). Decreasing snow depth, in parallel, reduces the thermal insulation of soil interface with atmosphere and increases soil vulnerability to fluctuations in air temperature (Iwata et al., 2010). This can in turn contribute to decreasing frost depth and increasing the frequency of swinging in FT states (Zhang, 2005). Climate-induced changes in FT dynamics, therefore, can result in widespread alterations in regional hydrology (Liu et al., 2009), phenology (Williams et al., 2015), geology (Park et al., 2016b), water quantity, and quality (Meshesha et al., 2020) as well as socio-economic activities (Melvin et al., 2017). In addition, some of these alterations can create feedback effects with other elements of the environment. For instance, thawing landscapes in northern regions can affect the climate system through the emission of an excessive amount of greenhouse gas fluxes (Wagner-Riddle et al., 2017), which can intensify the rate of global warming unprecedentedly (Schaefer et al., 2014). These impacts together can pose challenges to northern communities, where not only natural processes and socio-economic activities but also cultural values and ways of life are strongly tied with dynamics of FT cycles (T. D. Andrews et al., 2016).

One example of such regions is the province of Québec in Canada. Spanning from 57º 15ˈ to 79º 23ˈwest and 44º 59ˈ to 62º 09ˈ north (*Atlas of Canada*, 2016), Québec is the largest Canadian province and the richest in terms of the ecosystem diversity and availability of freshwater resources. Almost the entire 1,542,056 km^2 of the Québec's landmass undergoes three states of FT during a typical year, including continuous periods of frozen and thawed states, divided by a transit period in which the landscape switches between frozen and thawed conditions throughout a diurnal cycle. Having said that, as the area is massive and landscape characteristics are diverse, regional FT characteristics are subject to large spatial variability (Hatami and Nazemi, 2021a, 2021b, 2019). This becomes crucial in light of significant alterations in regional temperature and snow depth (Amir Jabbari and Nazemi, 2019), the two most influential climatic controls of FT at larger temporal and spatial scales (Henry, 2008; Iwata et al., 2010; Park et al., 2016b). At this stage, similar to many other cold regions, it is not yet clear how FT cycles across Québec respond to individual and compound changes in temperate and snow depth. This is a major gap as urgent management decisions are required to face the consequences of the thawing landscape in Québec and other regions in Canada, Alaska, Russia, and Northern Europe.

The knowledge gap in accounting FT response to changing climate stems from different sources. Firstly, most of our current findings are based on in-situ data that are rather sparse spatially and discontinuous temporally (Fang et al., 2019; Henry, 2008). Secondly, in order to quantify the impact of changing climate on FT dynamics, physically-based approaches, implemented in the current generation of land-surface schemes, are typically used. Despite current advancements, this framework is rather incomplete due to limitations in both data availability and modeling capability (Walvoord and Kurylyk, 2016). While in-situ data provide valuable information on the local control of climate on FT dynamics, the lack of data, especially in higher latitudes, pose significant constraints on the ability of in-situ data to capture the characteristics of changing FT patterns in

time and space (K. Zhang et al., 2007). In addition, while physically-based models are theoretically sound, they often suffer from oversimplified process representations and require large data support that are often unavailable.

We argue that recent advancements in remote sensing technology along with the advent of powerful statistical tools can address some of the above limitations. On the one hand, satellite remote sensing data can overcome the limitations in in-situ observation of FT state at larger spatial and temporal scales, by providing a synoptic and continuous monitoring of FT dynamics. This can provide an opportunity to systematically inspect temporal and spatial dependencies in FT dynamics, and their dependence with relevant climate variables (Park et al., 2016b; Tucker et al., 2005). On the other hand, if the purpose of modeling is shifted from continuous representations of FT states to representations of FT characteristics, then various statistical frameworks with much more flexibility can be used to describe functional links between FT and climate characteristics.

One approach of such kinds is the copula methodology, a formal framework to represent statistical dependence, which is widely used in recent hydrologic and environmental studies (Favre et al., 2004; Nelsen, 2006). Copulas can provide a generic solution to formal conditioning of FT states to marginal and joint characteristics of temperature, snow depth, and other relevant variables if needed. The data support for setting up such a framework is currently available through various publicly available gridded data (Brown and Brasnet, 2010; Kim et al., 2011; Sheffield et al., 2006). This allows for setting up a bottom-up impact assessment framework, with which the impacts of changing climatic conditions on FT characteristics can be quantified systematically across different spatial and temporal scales – see Methods below.

3.2 Methods

3.2.1 Data support

We use the global landscape FT Earth System Data Record (FT-ESDR) available from the publicly available archive of the National Snow and Ice Data Center (https://doi.org/10.5067/MEASURES/CRYOSPHERE/nsidc-0477.004). This dataset includes the daily state of soil at the spatial resolution of 25×25 km^2 over the period of 1979-2017. The remotely-sensed brightness temperature is used to classify FT states into four distinct classes of frozen (AM and PM frozen), non-frozen (AM and PM thawed), transitional (AM frozen and PM thawed), and inverse-transitional (AM thawed and PM frozen) (Kim et al., 2017). We categorize transitional and inverse-transitional states into one combined transient state that shows whether landscape switches between the frozen and thawed conditions in a diurnal cycle. Knowing the gridded daily states of FT, FT characteristics, in this paper annual number of frozen days and the number of transient days in winter (FD_{year} and FTD_{DJF}), can be extracted at the grid scale or each ecozone, and accordingly paired with corresponding gridded temperature and snow depth data – see Appendix-D for the results of annual number of thawed days. For air temperature data, we use the Global Meteorological Forcing Dataset (GMFD) provided by Princeton University available

at https://hydrology.princeton.edu/data.pgf.php. GMFD dataset is constructed by blending the reanalysis data from the National Centers for Environmental Prediction, National Center for Atmospheric Research with a group of recent global observation-based data (Sheffield et al., 2006). GMFD provides daily maximum and minimum air temperature at 0.25°×0.25° for the period of 1948-2016. The daily mean temperature is calculated by averaging the daily maximum and minimum temperature at each grid. Monthly snow depth data are obtained from the Canadian Meteorological Center (CMC; https://doi.org/10.5067/W9FOYWH0EQZ3). CMC dataset is constructed by combining the information from in-situ snow depth measurements with optimal interpolation results of a simple physical snow accumulation and melt model (Brown and Brasnet, 2010). The data is provided for the period of 1998-2020 with the grid resolution of 24×24 km^2 across the northern hemisphere.

As the grid size and centroid locations of the three considered data sources are not the same, we implement *k*-nearest neighbor interpolation to re-grid the three data sets into a unique spatial scale and over the common period of 1998-2016. In brief, the *k*-nearest neighbor is a non-parametric approach to estimate a variable in a given point in time and space based on its neighboring values (Cover and Hart, 1967). The nearest neighbors are identified as those with the smallest Euclidian distance to the center of a reference grid, here the grid of FT to which climate data are re-gridded. After finding the optimal nearest neighbors, a weighted averaging is applied to rescale the variables. The weight function gains its maximum value where the distance from the interpolated point is zero and decreases as the distance increases (Fekete et al., 2001). By implementing some numerical experiments, we find k=4 as the optimal number of nearest neighbors to achieve the highest accuracy in modeling the mean and standard deviation of temperature and snow depth over different ecozones of Québec. The re-gridded monthly mean temperature and monthly mean snow depth are then matched with the corresponding FD_{year} and FTD_{DJF} at the same temporal and spatial scales. Before developing copula models, we investigate the existence of autocorrelation in temperature, snow depth, and FT characteristics and exclude those grids in which the autocorrelation is significant. We find that this is the case in less than 17% of grids, and only for annual temperature. These grids are excluded from our analysis.

3.2.2 Proposed copula-based impact assessment framework

To model the joint dependencies between FT characteristics, air temperature, and snow depth, trivariate copulas can be used. Based on the Sklar's Theorem, the joint dependencies between FT characteristics (FT), mean temperature ($\bar{T}$), and snow depth (SD) can be described as:

$$F(FT, \bar{T}, SD) = C\big(F_1(FT), F_2(\bar{T}), F_3(SD)\big) \quad \textbf{(3.1)}$$

where $F_1(FT)$, $F_2(\bar{T})$ and $F_3(SD)$ are the Cumulative Distribution Functions (CDFs) for FT, $\bar{T}$ and SD, respectively and C is the trivariate copula function (Sklar, 1959). Among different alternative multivariate copulas, we employ canonical vine (C-vine) to represent joint distribution between the three above-mentioned variables in Equation 3.1 (Bedford and Cooke, 2002). In brief,

C-vine copulas decompose a high-dimensional joint distribution into a $d(d-1)/2$ bivariate pairs of copulas arranged into $(d-1)$ trees; and accordingly the joint distribution between FT, $\bar{T}$ and SD can be described as:

$$f(FT,\bar{T},SD) = f_2(\bar{T})f_{3|2}(SD|\bar{T})f_{1|2,3}(FT|\bar{T},SD) \quad \textbf{(3.2)}$$

where $f(.)$ is the marginal PDFs and the conditional distributions that can be estimated as(Aas et al., 2009):

$$f_{3|2}(SD|\bar{T}) = \frac{f(SD,\bar{T})}{f(\bar{T})} = \frac{c_{2,3}\big(F_2(\bar{T}),F_3(SD)\big)f_2(\bar{T})f_3(SD)}{f_2(\bar{T})} = c_{2,3}\big(F_2(\bar{T}),F_3(SD)\big)f_3(SD) \quad \textbf{(3.3)}$$

and

$$f_{1|2,3}(FT|\bar{T},SD) = \frac{f(FT,SD|\bar{T})}{f(SD|\bar{T})} = \frac{c_{1,3|2}\big(F(FT|\bar{T}),F(SD|\bar{T})\big)f(FT|\bar{T})f(SD|\bar{T})}{f(SD|\bar{T})} = c_{1,3|2}\big(F(FT|\bar{T}),F(SD|\bar{T})\big)c_{1,2}\big(F_1(FT),F_2(\bar{T})\big)f_1(FT) \quad \textbf{(3.4)}$$

where $c(\cdot)$ is the 3-dimensional copula density. As a result, the three dimensional joint density can be represented in terms of bivariate copulas as the following (Joe, 1997):

$$f(FT,\bar{T},SD) = f_1(FT).f_2(\bar{T}).f_3(SD).c_{2,1}.c_{2,3}.c_{1,3|2} \quad \textbf{(3.5)}$$

where $c_{2,1}(F_2(\bar{T}),F_1(FT))$ and $c_{2,3}(F_2(\bar{T}),F_3(SD))$ are simply written as $c_{2,1}$ and $c_{2,3}$; and the conditional pairwise copulas between $F_1(FT)$ and $F_3(SD)$ conditional to $F_2(\bar{T})$, i.e. $c_{1,3|2}\big(F_1(FT),F_3(SD)|F_2(\bar{T})\big)$ is shown by $c_{1,3|2}$. In addition, $c_{2,1}$, $c_{2,3}$ and $c_{1,3|2}$ are the densities of bivariate pairs. Having the C-vine copulas, the probability distribution of FT characteristics due to different quantitative change in temperature and snow depth can be obtained through conditional modeling as:

$$h = F(FT|\bar{T},SD) = \frac{\partial C_{1,3|2}\big(F(FT|\bar{T}),F(SD|\bar{T})\big)}{\partial F(SD|\bar{T})} \quad \textbf{(3.6)}$$

where $F(FT|\bar{T},SD)$ is the conditional distribution function. Moreover,

$$F(FT|\bar{T}) = h(FT|\bar{T}) = \frac{\partial C_{1,2}\big(F(FT),F(\bar{T})\big)}{\partial F(\bar{T})} \quad \textbf{(3.7)}$$

and

$$F(SD|\bar{T}) = h(SD|\bar{T}) = \frac{\partial C_{3,2}\left(F(SD), F(\bar{T})\right)}{\partial F(\bar{T})} \quad \textbf{(3.8)}$$

Using Equations 3.7 and 8, Equation 3.6 can be rewritten as:

$$h = F(FT|\bar{T}, SD) = h[h(FT|\bar{T})|h(SD|\bar{T})] \quad \textbf{(3.9)}$$

The estimated CDF of characteristics can be back transformed to the original quantile space using the inverse CDF function, assuming empirical distributions for FT, $\bar{T}$ and SD at each ecozone. The inverse form of h-function given in Equation 3.9 is applied for this purpose. To extract the probability distribution of FT characteristics, a Monte Carlo-based simulation is adopted by generating 1,000 random set of FT characteristics under known values of temperature and snow depth(Roy and Gupta, 2021). Given random uniform random numbers of ε, given FT characteristics can be sampled as:

$$FT = F^{-1}\left\{h^{-1}\left[\left(h^{-1}\left(\varepsilon|h(SD|\bar{T})\right)\right)|\bar{T}\right]\right\} \quad \textbf{(3.10)}$$

Computer models for conducting this simulations are developed in *CRAN R* with the use of packages of *VineCopula*, *CDVine*, and *copula* (Brechmann and Schepsmeier, 2013; Schepsmeier et al., 2015; Yan, 2007). Tree structures for C-vine copulas are selected based on the maximum spanning tree algorithm, in which copula parameters are chosen with respect to the interdependencies between pairwise variables (Dißmann et al., 2013). A set of well-known parametric copula families (i.e. Frank, Gaussian, Student t, Clayton, Gumbel, and Joe) are used to develop, falsify and select pairwise bivariate copulas. The formulations of these copulas are provided in detail in other sources (Nelsen, 2006). These copulas are parameterized using the Maximum log-Likelihood Method and considering the Bayesian information criteria as the Goodness of Fit (Sadegh et al., 2017). The pool of developed structures at each ecozone are then compared and evaluated based on their capability in representing the marginal FT characteristics and preserving empirical dependencies between a given FT characteristic and $\bar{T}$ or *SD*. Dependencies are quantified using the Kendall's tau non-parametric dependence measure and the associated hypothetical test (Kendall, 1938). The best C-vine copula structure is then used for conditioning the control of compounding changes in temperature and snow depth on FT characteristics. The one-way ANalysis Of VAriance (ANOVA) with Bonferroni correction is used to formally examine any change in the estimated dependencies across different spatial regions (Nazemi et al., 2020).

3.3 Results

Québec includes eight ecozones that are regions with similar land, soil, vegetation, and climatic characteristics (Schultz, 2005). From the north to south, these ecozones include Northern Arctic (EZ1), Southern Arctic (EZ2), Arctic Cordillera (EZ3), Taiga Shield (EZ4), Hudson Plains (EZ5), Boreal Shield (EZ6), Atlantic Maritime (EZ7), and Mixed Wood Plains (EZ8), respectively (Wiken, 1986) – see Figure 3.1 below.

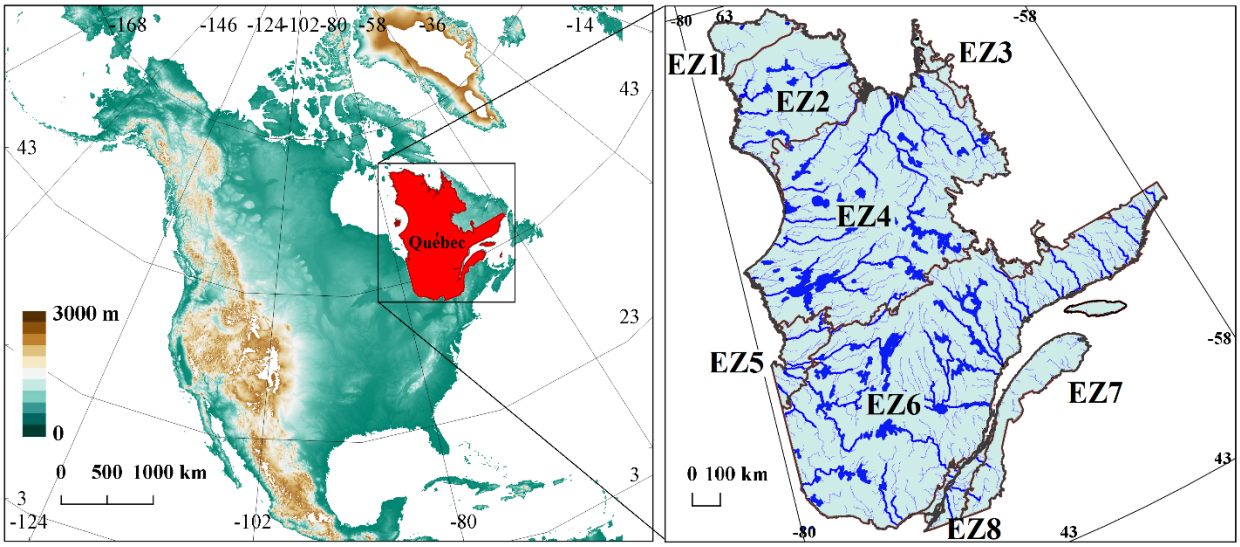

Figure 3.1 The province of Québec in Canada and its eight ecozones.

In each ecozone, the annual number of Frozen Days (FD_{year}) and the number of transient days in the winter season (December, January, and February; FTD_{DJF}) at grid scale are extracted. In line with earlier studies (Sorensen et al., 2018; Zhang et al., 2017), our empirical results also show that these characteristics are the two most sensitive regional FT characteristics to changes in climate conditions, and demonstrate the strongest interdependence with temperature and snow depth at common scales and across the eight ecozones. These FT characteristics have also direct implications for land management. The changing annual number of frozen days can affect the length of phenological and agricultural activities (Sharma et al., 2006), accessibility to natural resources (Poppel et al., 2015), and the emission of greenhouse gasses from thawing permafrost(Schuur et al., 2015). In addition, the increasing number of transient days can be a proxy for land subsidence and erosion (Kimiaghalam et al., 2015) as well as the deterioration rate of civil infrastructures such as buildings, roads, and pipelines (Melvin et al., 2017).

By applying the proposed framework (see Methods below), FT characteristics at each ecozone can be conditioned to air temperature and snow depth using developed copula models (Liu et al., 2018; Nazemi et al., 2013). Before applying these models for impact assessments, we evaluate their performance in representing the marginal and joint characteristics of the two considered FT characteristics, observed across the eight ecozones. Figure 3.2 summarizes the results, in which

the top row depicts the results for the annual number of frozen days (FD_{year}) and the bottom row is related to the number of transient days during the winter season (FTD_{DJF}). In each row, panels from left to right show the expected estimations (bars) and observed values (thresholds) for the mean, standard deviation, and skewness of the considered FT characteristics as well as their dependence with temperature and snow depth across the eight ecozones. Figure 3.2 clearly shows that the parametrized copulas can effectively represent the first three moments of the empirical probability distributions of both FT characteristics considered. For FD_{year}, the overall expected relative error of 0.2%, 2.2%, and 13.5% is observed for mean, standard deviation, and skewness, respectively. For FTD_{DJF}, the overall expected relative error for the first three moments are 0.4%, 1.1%, and 3.1%. Apart from statistical moments of marginal variables, the interdependencies between FD_{year}, temperature, and snow depth are preserved with average relative errors of 0.7% and 1.1%, respectively. Average relative errors of 0.9% and 1.1% are also observed for the interdependencies between FTD_{DJF}, temperature, and snow depth. These modeling efficiencies in reconstructing the historical FT characteristics justify the application of the proposed framework for assessing the compounding impacts of changing temperature and snow depth on the considered FT characteristics.

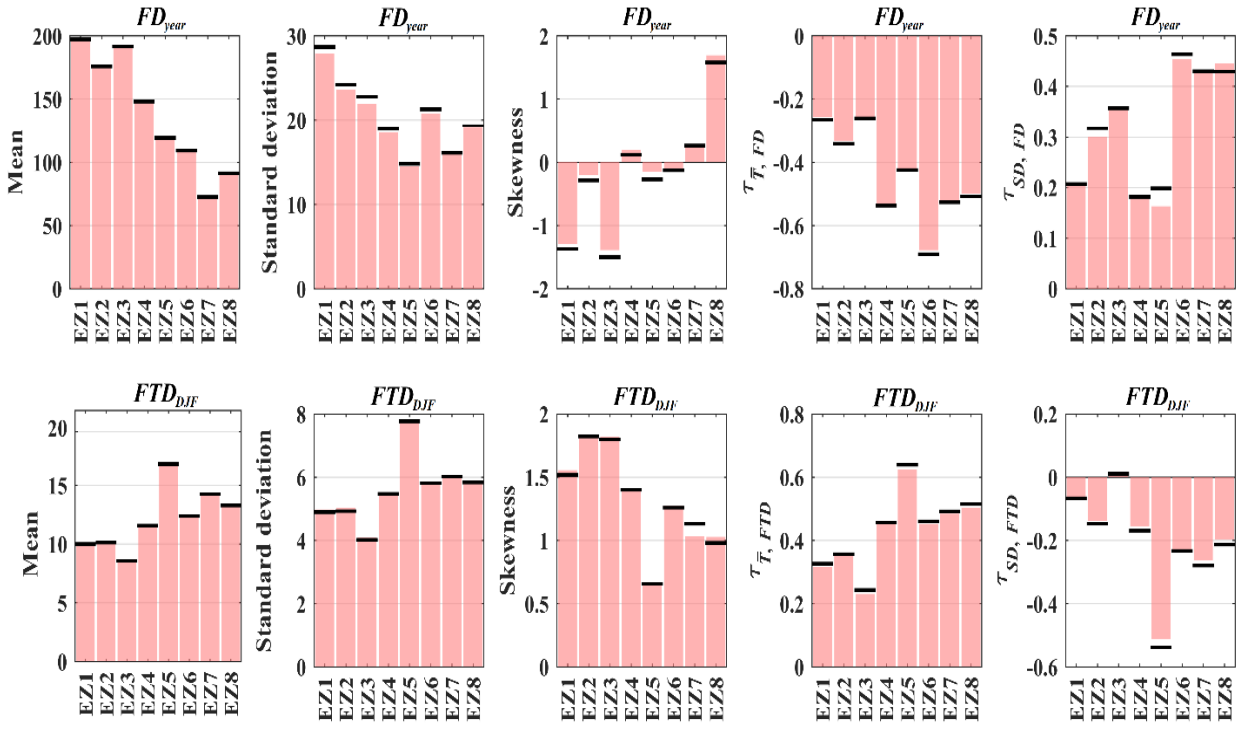

Figure 3.2 Observed (thick threshold lines) *vs.* simulated values (pink bars) for mean, standard deviation, skewness, as well as Kendall's tau dependencies between FT characteristics, temperature and snow depth across eight ecozones of Québec, displayed from left to right. The top and bottom rows depict the results for the number of frozen days in a typical year (FD_{year}) and the number of transient days in a typical winter season (FTD_{DJF}), respectively.

Apart from benchmarking the performance of copula models in reconstructing the historical dependencies between FT characteristics and climatic conditions, Figure 3.2 shows a clear increase in the magnitude of dependencies between FD_{year} and both temperature and snow depth by moving from north to south. Similarly, the magnitude of dependence between FTD_{DJF} and considered climatic drivers generally increases in southern ecozones. Using the one-way ANOVA test, we assess the differences between the estimated dependencies across different ecozones. The results highlight the uniqueness of interdependencies between FD_{year}, temperature, and snow depth across all ecozones. In addition, dependencies between FTD_{DJF} and climate drivers are almost unique. The only statistically significant similarity is in the case of FTD_{DJF} and temperature in EZ4 and EZ6. Significant variations in the dependencies between FT characteristics and hydroclimatic drivers can reveal the effect of ecosystem conditions on regulating the impacts of changing condition on FT characteristics. To showcase this empirically, we consider two compound scenarios related to opposing warming and cooling conditions. These scenarios include changes of 2°C increase in long-term mean temperature along with 10 cm thinner snow on the ground (compound warming), as well as 2°C decrease in long-term mean temperature along with 10 cm thicker snow on the ground (compound cooling). Figure 3.3 summarizes the results of this impact assessment and compares them with historical conditions, where whiskers span the range of expected FT characteristics obtained by 1,000 resampling trials – see Methods for the proposed assessment framework.

In this figure, historical baseline (no change condition) along with compound cooling and warming scenarios are shown with gray, blue, and red colors, respectively. Black dots signify the mean ensembles of simulated values. Using Figure 3.3, a couple of key findings are made. First, there is a clear geographic departure between FT responses to unique compound changes in temperature and snow depth. While the response of FD_{year} to compound cooling and warming is more vivid in the north, the impacts on FTD_{DJF} are more highlighted in the south. Considering FD_{year} and under compound warming conditions, on average between 48 (EZ1) to 22 (EZ8) fewer days with the frozen condition is expected in a typical year. The north-south decline in the response of FD_{year} is less obvious under compound cooling conditions, ranging from roughly 10 (EZ5) to 34 (EZ2) days extension in frozen conditions per year. Considering FTD_{DJF}, in contrast, the impact of compound warming increases by moving from north to south. Under this scenario and on average, it is expected to have 10 more days during a typical winter with the transient condition in EZ8, where the majority of Québec's population is inhabited, as appose to only 5 days in EZ1. Under cooling conditions, this change ranges from roughly 2 (EZ3) to 6 (EZ8) fewer days with transient conditions in a typical winter. These spatially heterogeneous impacts on FT characteristics under unique compound changes in temperature and snow depth can reveal how changes in ecozonal features (e.g. vegetation type, soil type, land cover, regional climate, etc.) can regulate FT responses to compound changes in temperature and snow depth.

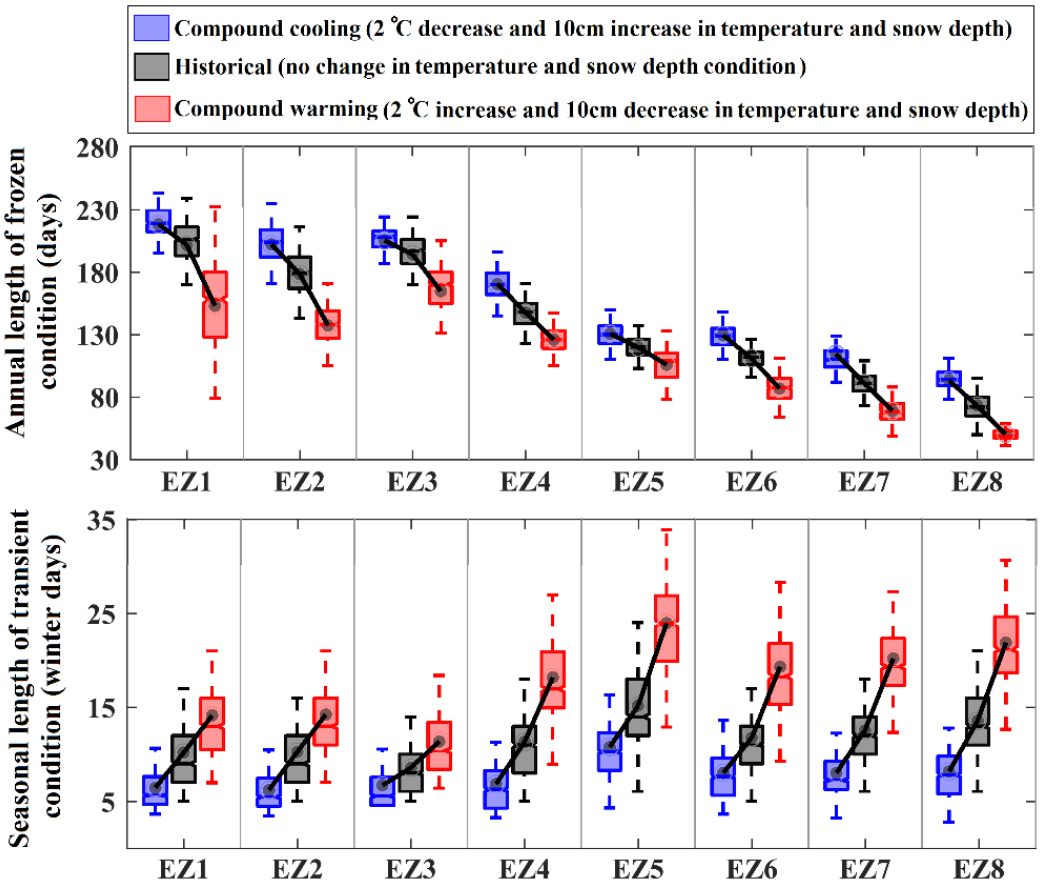

Figure 3.3 The response of FD_{year} (top row) and FTD_{DJF} (bottom row) to opposite compound scenarios of change in temperature and snow depth conditions. Historical as well as compound cooling and warming scenarios are shown with grey, blue and red boxplots obtained by 1,000 resamples. Dots signifies the simulated mean ensemble of FT characteristics at each ecozone.

Second, Figure 3.3 clearly shows that in those ecozones in which FT characteristics are more sensitive to compound changes, responses to opposite warming and cooling scenarios become more non-symmetric and are more intense under the compound warming compared to the compound cooling scenario. For instance, looking at FD_{year}, the absolute shift under compound warming scenario is 30 days more in the Northern Arctic (EZ1), compared to the shift due to compound cooling scenario in the same ecozone. The higher impact of warming on FD_{year} in northern ecozones is of great importance in the context of the land-atmospheric Carbon emissions due to permafrost degradation (Carpino et al., 2018). Similarly, in the case of FTD_{DJF}, the magnitude of positive shift due to the compound warming scenario is about 4 days more in the Mixed Wood Plains (EZ8) compared to the opposite negative shift caused by the compound cooling scenario. More sensitivity to the compound warmings has important implications regarding soil stability (Lewkowicz and Way, 2019) and deterioration of critical infrastructure (Roseen et al., 2012) that are currently under pressure due to aging (Doughty et al., 2013).

To better understand climate controls on FT characteristics, we consider additional compound and individual changes in temperature and snow depth by mixing-and-matching long-term shifts in mean temperature, ranging from −2℃ to +2℃ (sampled every 0.5º C), and mean snow depth, ranging from -10 cm to 10 cm (sampled every 2.5 cm). This results into 81 different scenarios, with which FD_{year} in the Northern Arctic (EZ1) and FTD_{DJF} in the Mixed Wood Plains (EZ8) are conditioned. We choose these two ecozones due to their largest sensitivity in changing hydroclimatic conditions with respect to FD_{year} and FTD_{DJF} (see Figure 3.3); and accordingly, they can better reveal how marginal and joint variations in temperature and snow depth can result into alterations of FT characteristics. Figure 3.4 presents the results of this analysis, in which the top (panels a to c) and the bottom rows (panels d to f) depict the results related to FD_{year} and FTD_{DJF}, respectively. Panels a and d show response surfaces for changes in FT characteristics with respect to changes in temperature and snow depth.

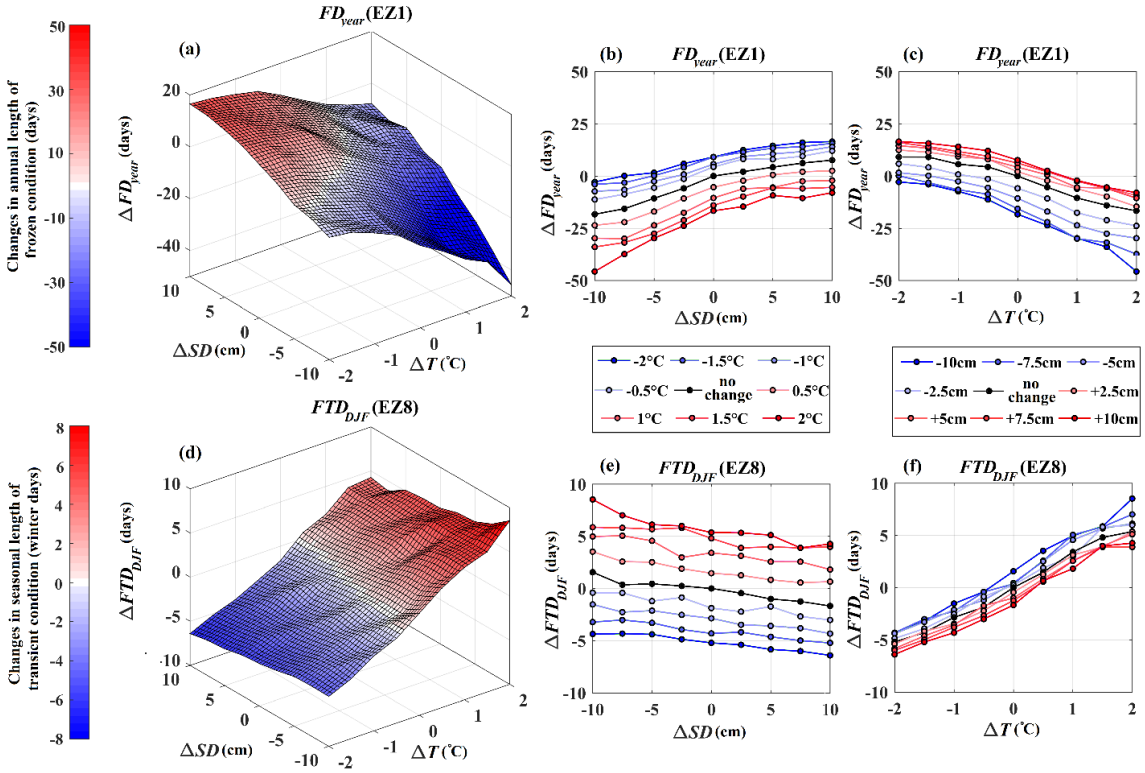

Figure 3.4 The response surfaces of FD_{year} in the Northern Arctic (EZ1, panel a) and FTD_{DJF} in the Mixed Wood Plains (EZ8, panel d) along with marginal sensitivity analyses to ±2ºC change in temperature (panels b and c) and ±10 cm change in snow depth (panels e and f) conditions.

These response surfaces are reconstructed using the proposed C-vine copula and 1,000 resampling – see Methods below. Panels b and e, as well as c and f, show the partial derivatives of these response surfaces, derived at known temperature and snow depth conditions, respectively. Looking at the results obtained for FD_{year} across EZ1 (Figure 3.4, first row), several interesting observations can be made. First and foremost, the non-symmetric response of FT characteristics

to warming *vs.* cooling is again revealed itself and is even more vivid in this round of analysis. While cooler temperature and inclined snow depth increase the length of the frozen period in a typical year by around 18 days, warmer temperature and declined snow depth can decrease the length of the annual frozen period by around 48 days. Projections of response surfaces, shown in panels (b) and (c), clearly present higher sensitivity of FD_{year} to warmer temperatures and thinner snow depth. Second, despite having different signs, the magnitude of interdependencies with temperature and snow depth is more or less the same (-0.27 and 0.22, respectively; see Figure 3.2); and therefore, the sensitivity of FD_{year} to changes in temperature and snow depth are rather similar. The expected change in FD_{year} under constant temperature conditions when snow depth is varying from -10 cm to 10 cm of its long-term average value is about 25 days (Figure 3.4b). Similarly, the expected change in FD_{year} under constant snow depth when the temperature is shifted from -2°C to +2°C of the annual long-term average is about 30 days (Figure 3.4c). Having said that, it should be mentioned that the impacts of both snow depth and temperature variations are intensified as the temperature warms and snow depth declines. This is another line of evidence for non-symmetric marginal impacts that is further controlled by the state of other driving variables.

Similar rationale can be used to interpret the results obtained for FTD_{DJF} across the Mixed Wood Plains (EZ8; the bottom row of Figure 3.4). The changes in the expected FTD_{DJF} range from 9 more transient days under warmer climate with declined snow depth to 7 fewer days with transient days under cooler climate with inclined snow depth on the ground. This observation again points at the non-symmetric response of the FT characteristics, although it is less obvious compared to FD_{year} across EZ1. In this case, however, the dependence between FTD_{DJF} and temperature is stronger than the dependence between FTD_{DJF} and snow depth; and therefore, this FT characteristic is more sensitive to temperature changes, compared to changes in the snow depth. As an example, the expected magnitude of change in FTD_{DJF} is roughly about 5 days under constant temperature conditions (Figure 3.4e), while it is about 12 days under constant snow depth conditions (Figure 3.4f). Similar to the case of FD_{year} across EZ1, the marginal impacts of change in snow depth are more intense under a warmer climate, ranging from 3 days under 2ºC cooling *vs*. 6 days under 2ºC warming. This is the case also for the marginal impacts of change in temperature under declined snow depth conditions, although with less vividity.

3.4 Discussion

The results provided above illustrate two important findings. First, the impacts of changing temperature and snow depth conditions on FT characteristics are rather unique spatially, with different manifestations and natures of response in northern and southern regions. Second, non-symmetric responses to compound warming and cooling conditions are seen across different FT characteristics and/or regions. In general, when there is a significant sensitivity to changing climate, the response is more intense under warmer and/or declined snow depth conditions. In this section, we look at another key feature of FT responses to compound changes in temperature and snow depth, which is rather overlooked in current literature. One key feature of the response to

compound events is the nonlinear nature of the response, meaning that the impact of compound events can be more intense compared to the cumulative impacts of individual events when occurring independently (Chiang et al., 2018; Mazdiyasni and AghaKouchak, 2015). Here we formally address the nonlinearity in FT responses at the grid resolution, by inspecting the deviation from the superposition principle of linear systems. This is through simulating FT responses to historical baseline and six opposing individual and compound scenarios of change in temperature and snow depth. Table 3.1 summarizes these scenarios.

Table 3.1 Individual and compound climate scenarios considered for addressing the nonlinear response of FT characteristics to individual and compound changes in temperature and snow depth conditions across Québec and at the grid scale.

Scenario description	Type	Notation
Long-term means of temperature and snow depth	Historical baseline (no-change)	(0,0)
2°C cooler compared to the long-term mean	Individual (cooling only)	(-2,0)
10 cm thicker snow compared to long-term mean	Individual (thickening snow cover only)	(0,10)
2°C cooler and 10 cm thicker snow compared to long-term means	Compound (cooling)	(-2,10)
2°C warmer compared to the long-term mean	Individual (warming only)	(2,0)
10 cm thinner snow compared to long-term mean	Individual (thinning snow cover only)	(0,-10)
2°C cooler and 10 cm thicker snow compared to long-term means	Compound (warming)	(2,-10)

In brief, we address the non-linearity in FT responses by comparing the expected values of FD_{year} under individual and compound changes in temperature and snow depth under cooling and warming conditions. For cooling, we compare the response to (-2,10) at each grid with the summation of the expected FD_{year} under corresponding (-2,0) and (0,10). Similarly for warming, we compare the (2,-10) with the summation response to (2,0) and (0,-10). Theoretically at each grid, the variation in FD_{year} under individual and compound scenarios compared to historical conditions, i.e. ΔFD_{year}, can have one of the following three conditions: (1) linear response, meaning either $\Delta FD_{year}(-2,10) = \Delta FD_{year}(-2,0) + \Delta FD_{year}(0,10)$ under cooling and/or $\Delta FD_{year}(2,-10) = \Delta FD_{year}(2,0) + \Delta FD_{year}(0,-10)$ under warming; (2) nonlinear dumping response, meaning either $\Delta FD_{year}(-2,10) < \Delta FD_{year}(-2,0) + \Delta FD_{year}(0,10)$ under cooling or $\Delta FD_{year}(2,-10) > \Delta FD_{year}(2,0) + \Delta FD_{year}(0,-10)$ under warming; or (3) nonlinear amplifying response, meaning either $\Delta FD_{year}(-2,10) > \Delta FD_{year}(-2,0) + \Delta FD_{year}(0,10)$ under cooling or $\Delta FD_{year}(2,-10) < \Delta FD_{year}(2,0) + \Delta FD_{year}(0,-10)$ under warming. Figure 3.5 summarizes the results of this analysis. The maps in the top row demonstrate the results related to deviation from the superposition principle at the grid scale under compound cooling (left column) and warming (right column). Under compound cooling, shades of blue and red show amplifying and dumping effects; whereas for compound warming, these colors represent dumping and amplifying effects, respectively. The white color highlights grids in which a linear response is observed. Black dots show the grids where the autocorrelation is present in temperature data and

accordingly these grids are excluded from our assessment. The bar charts in the bottom row show the percentage of grids at each ecozone, where amplification in compound response is observed.

Considering this figure, although the amplified response of FD_{year} to compound changes is observed across the province, it is mainly concentrated in the northern ecozones for both cooling and warming scenarios. Looking at both compound cooling and warming, more than 70% of the area in the three northern ecozones, i.e. Northern Arctic (EZ1), Southern Arctic (EZ2), Arctic Cordillera (EZ3) demonstrate an amplified response. While the expected values for amplifying effect, i.e. $\Delta FD_{year}(-2,10) - \Delta FD_{year}(-2,0) - \Delta FD_{year}(0,10)$ in EZ1, EZ2, and EZ3 are 5, 8, and 7 days, respectively, the amplified cooling effect can reach up to 16 days in some grids in northern ecozones. In contrast, the percentage of grids with amplified effect reduces to less than 10% in the EZ7 – see Figure 3.5c. Similar findings are obtained with regard to the compound warming scenario, although it should be noted that in contrast to compound cooling, the amplification can also dominate the response of FD_{year} in the south, e.g. in EZ8 (see Figure 3.5d). Having said that, still more amplifications are observed in the three northern ecozones – see Figure 3.5d. Although the expected values for amplified warming, i.e. $\Delta FD_{year}(2,-10) - \Delta FD_{year}(2,0) - \Delta FD_{year}(0,-10)$ are -4, -6, and -6 days in EZ1, EZ2, and EZ3, the amplified response can get to -11 days in a grid located in Southern Arctic. In addition, the percentage of areas with amplified warming is considerably lower in EZ4 to EZ7 with roughly 40% of grids showing some amplified response to compound warming. This finding has some important implications for the thawing landscape in the northern regions and a wide suite of environmental change that can be initiated by the amplified response of FT to compound warming. On the one hand, an amplified response can facilitate the access to untapped natural resources of the north and may unleash an opportunity for northern agriculture. On the other hand, however, it intensifies permafrost degradation, which results in unprecedented emissions of greenhouse gasses (Schaefer et al., 2014; Schuur et al., 2015; Wagner-Riddle et al., 2017).

In parallel to amplified responses in the north, the dumping effect dominates the FD_{year} response in the southern ecozones, with the exception of EZ8 under compound warming. For both cooling and warming scenarios, the most severe dumping effect is observed in the Atlantic Maritime (EZ7), with the expected and extreme dumping of -5 and -9 days under compound cooling as well as 6 and 10 days under compound warming respectively. While southern regions demonstrate significantly less amplification in FD_{year} response, it should be noted that the sensitivity of FD_{year} to compound changes in the hydroclimate conditions is rather marginal compared to northern regions. Accordingly, we look at the gridded response of FTD_{DJF} to individual and compound scenarios of change in the three most populated zones of Québec, i.e. Montréal (the grid including 45.5017ºN, 73.5673ºW), Québec City (the grid including 46.8139ºN, 71.2080ºW) and Gatineau (the grid including 45.4765ºN, 75.7013ºW). These cities are all located in the Mixed Wood Plains (EZ8), where the most significant sensitivity in the response of FTD_{DJF} to compound changes in temperature and snow depth conditions is observed – See Figure 3.3. Figure 3.6 presents the shifts in the mean and exceedance probabilities of FTD_{DJF}, i.e. ΔFTD_{DJF},

given 7 different hydroclimatic conditions in Montréal (first row), Québec City (second row), and Gatineau (third row). From left to right, the first three columns show the changes in Probability Density Functions (PDFs) of FTD_{DJF} under (+2,0) and (-2,0), (0,-10) and (0,+10), as well as (+2,-10) and (-2,+10), respectively. The right column compares the hypothetical linear response, i.e. $\Delta FTD_{DJF}(-2,0) + \Delta FTD_{DJF}(0,10)$ in the case of compound cooling and $\Delta FTD_{DJF}(2,0) + \Delta FTD_{DJF}(0,-10)$ in the case of compound warming, with expected values of $\Delta FTD_{DJF}(-2,10)$ and $\Delta FTD_{DJF}(2,-10)$, respectively.

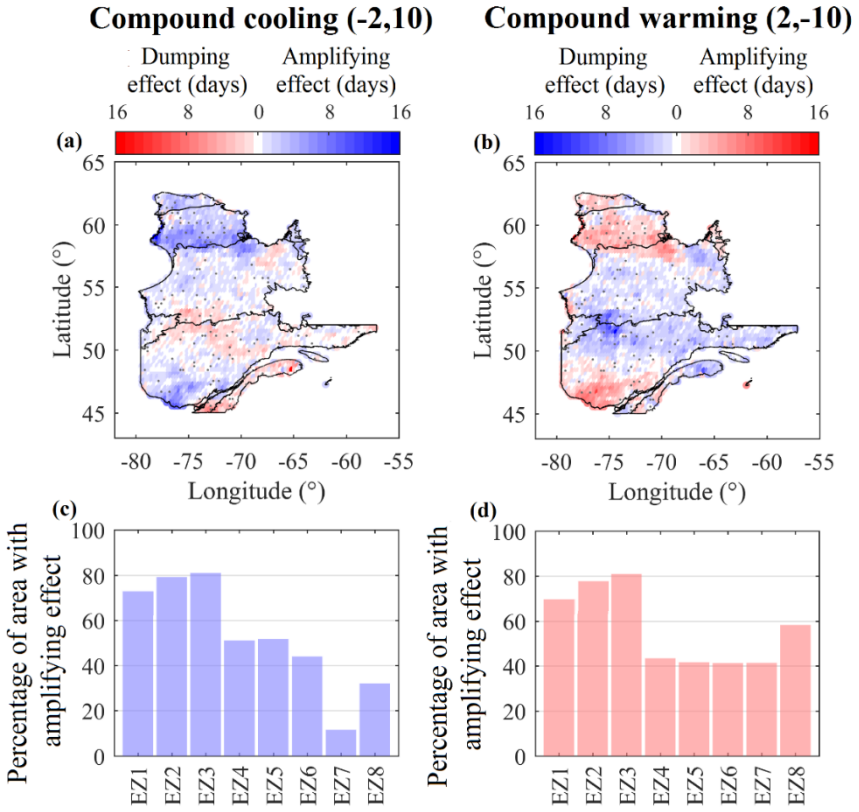

Figure 3.5 The nonlinear response of FD_{year} to considered compound cooling (left column) and warming (right column). Nonlinear responses are manifested by amplifying and dumping effects in the length of the frozen period (top row). In each map, black dots show the grids that are excluded from the study due to the existence of autocorrelation in temperature data. In the bottom row, the percentage of areas in each ecozone with an amplified response is shown.

The PDFs of FTD_{DJF} for warming, cooling, and no-change conditions are shown in red, blue, and black colors respectively; and the expected historical value of FTD_{DJF} are identified with vertical dashed lines. The highlighted regions in each PDF show likelihoods for FTD_{DJF} exceeding the long-term historical mean of FTD_{DJF} under the considered warming (red) or cooling (blue) conditions. In each panel of the right column, light colored bars show hypothetical linear responses under cooling (blue) and warming (red) conditions. Dark colored bars, in contrast, show the expected responses under compound cooling (blue) and warming (red) conditions obtained by the C-vine copula models. Both non-symmetric and nonlinear responses of FTD_{DJF} to individual and compound cooling and warming scenarios are revealed in the three cities. Under individual

scenarios, the shift in the mean of FTD_{DJF} is at least 4 days higher under (2,0) comparing to (-2,0), although these shifts are relatively symmetric under (0,-10) and (0,10). Under compound changes, the shift in the mean of FTD_{DJF} is approximately twice higher under (2,-10) comparing to (-2,10). The non-symmetric response of FTD_{DJF} to compound events is also manifested in the exceedance probabilities. For instance, in Montréal the exceedance probability of FTD_{DJF} changes by 42% under (2,-10), while the corresponding shift in the exceedance probability under (-2,10) is only -31%. This is another line of evidence for complex responses of FT characteristics to compound cooling and warming. Comparing the expected compound responses with hypothetical linear responses under cooling and warming scenarios, an amplified response to compound cooling is observed in all three cities with expected values of -2, -3, and -1 days in Montréal, Québec City, and Gatineau, respectively. Considering the compound warming scenario, the amplifying effect in Montréal and Gatineau are 2 and 1 days, respectively. It should be noted however that a dumping effect of -1 day is observed in Québec City under the considered compound warming. It should be noted that the nonlinearity in the response transcends to exceedance probabilities as well. In Montréal, for instance, the amplifying effects in exceedance probabilities under compound cooling and warming conditions are -12% and +3%, respectively. The amplifying response of FTD_{DJF} to compound warming in a place like Montréal has an important relevance to the current revelation of climate change, manifested by warmer temperature and less snowfall (Hatami et al., 2019a). Montréal marks one of the most populated regions in Canada with a high concentration of aging infrastructures, vulnerable to increasing FTD_{DJF}. In Montréal, for instance, it is shown that under the historical condition, 216 km length of the city's watermains need to be replaced while another 2,400 km will require repairing (Zangenehmadar et al., 2020). This rate will significantly change under increasing FTD_{DJF}. Findings in other cold regions indicate that more swings in FT cycles can translate to multiple million dollars to infrastructure maintenance and repair (Melvin et al., 2017). In addition, it is shown that the results of the Marshall stability test of asphalt concrete reduce by up to 57% when the materials are exposed to only 6 more transient days (Özgan and Serin, 2013). This can pressurize aging infrastructures and built environments (Farran and Zayed, 2009).

3.5 Summary and concluding remarks

Landscape FT is arguably the most important land-surface feature in cold regions, controlling physical, biological, and socio-economic processes along with their interactions with other elements of the environment. Historical characteristics of FT, however, are under unprecedented alterations due to climate change, which has important implications for land and resource management in the north. Despite existing understandings of the impact of changing climate on FT cycles, current assessment frameworks are rather limited. On the one hand in-situ data networks, often used as the main data support for understanding FT responses to changing climate conditions, are rather sparse and therefore fail to provide a synoptic view on different modes of responses. On the other hand, the current projection paradigm based on the use of physically-based

land-surface models is incomplete due to several assumptions and/or simplifications in the conceptualization, representation, and parametrization of the interacting processes that determine the state of FT at a given time and space. Our points of innovation are in the use of satellite remote-sensing data in conjunction with a formal statistical technique to overcome some of the above-mentioned limitations, at least at coarser spatial and temporal scales. First, we propose pairing gridded FT characteristics obtained from satellite retrievals with corresponding gridded data of temperature and snow depth, the two most influential hydroclimatic drivers of FT, to study the linkage between FT and climate characteristics at a common scale. Second, we suggest C-vine copulas to develop a conditional model, with which the impacts of individual and compound changes in temperature and snow depth on FT characteristics can be assessed and quantified probabilistically.

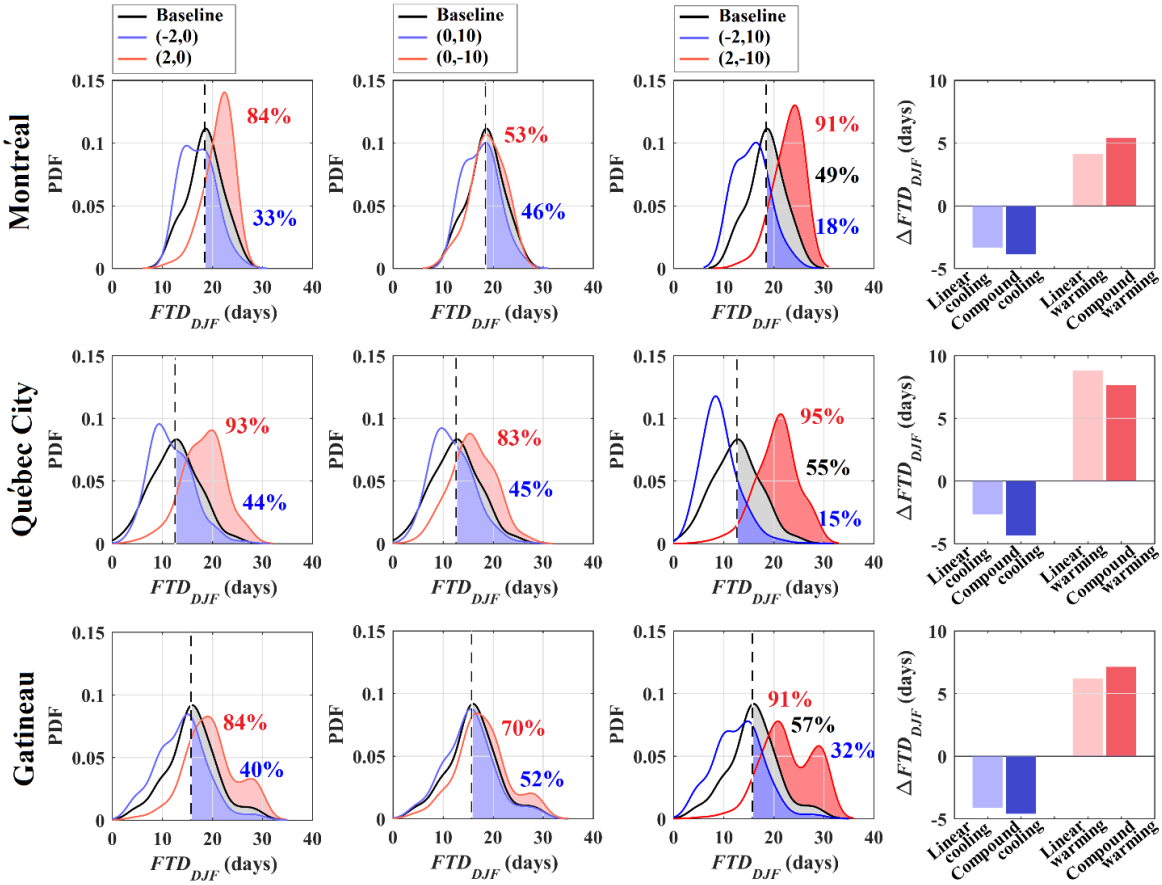

Figure 3.6 The Probability Density Functions of FTD_{DJF} along with the likelihood of exceeding the corresponding long-term historical values in Montréal (first row), Québec City (second row), and Gatineau (third row) given opposite individual and compound scenarios for climatic changes, shown in the first, second and third columns from the left, respectively.

We showcase the application of this framework in the province of Québec, Canada, a sub-country jurisdiction with an area comparable to Mongolia, the 18th largest country in the world. We show that the simulations obtained by parametrized C-vine copulas can capture the empirical moments of observed FT characteristics as well as the interdependencies between FT, temperature

and snow depth characteristics during 1998 to 2016. The application of the proposed framework for assessing the impact of individual and compound changes in temperature and snow depth reveals some important features of the FT response to climatic changes that have remained rather overlooked. First, we highlight an ecozonal uniqueness in the interdependencies between FT characteristics, temperature, and snow depth, pointing at the role of ecosystem conditions in regulating the impact of changing climate conditions on FT characteristics. Moreover, a north-south divide in the FT response to changing climate conditions is observed. While the impacts of changing climate conditions are manifested in the annual extent of the frozen period in northern regions, it is revealed through alteration in the extent of the transient period during a typical winter season in the south. Through sampling the response surfaces related to FD_{year} in Northern Arctic and FTD_{DJF} in Mixed Wood Plains, we also demonstrate a different nature of the response to changing temperature and snow depth conditions between the north and the south. Having said that, our results show a nonsymmetric response to changing temperature and snow depth conditions despite differences in FT variables, regions, and/or spatial scales. In general, where there is a considerable sensitivity in FT response, the alteration due to rising temperature and/or thinning snow depth is more intense compared to corresponding scenarios with falling temperature and/or thickening snow depth. Closer looks at the FT responses at the grid scale also revealed nonlinear, mainly amplifying, responses of FT characteristics to compound changes in climate conditions. This means that the response of FT to compound changes in temperature and snow depth is often more severe than the cumulative response of FT to changes in temperature and snow depth individually. These amplifying impacts can result in up to two weeks of alterations in the frozen period during a typical year in the north, and up to one week change in the transient period during a typical winter season in the three most populated regions of Québec, i.e., Montréal, Québec City, and Gatineau. While amplified shrinkage in the annual frozen period in the north can result into unprecedented changes in the northern environment under compound warming, the similar climatic condition can result into additional stress to already aging infrastructures in the south. We also show that the amplified response is not only observed in the expected values of the transient period in a typical winter, but also in the likelihood of this FT characteristic exceeding the long-term historical values.

Our proposed methodology is generic and can be applied globally. We encourage inspecting the non-symmetry, nonlinearity, and spatial variability of FT response to changing climate conditions in other Canadian regions and globally. In the context of Québec, landscape responses to freeze and thaw can have a wide range of implications from endangering already aging and vulnerable community infrastructures to substantial environmental changes due to amplified rates of permafrost degradation. The later can be even globally relevant due to massive land-induced carbon emissions. Facing these challenges requires integrated and inclusive, approaches that are supported by scientific information. As far as providing scientific information is concerned, we will soon report the application of the proposed framework for estimating future FT characteristics in Québec using available downscaled climate projections.

Chapter 4.
Statistical Modeling of Monthly Snow Depth Loss in Southern Canada[4]

The contents of this chapter have been published in "*Hatami, S., Zandmoghaddam, S., Nazemi, A. (2019). Statistical modeling of monthly snow depth loss in southern Canada." In the Journal of Hydrological Engineering. The contents are slightly modified.*

Synopsis

Quantifying the dynamics of snow depth is essential for understanding freshwater availability, mitigating flood and drought hazards and monitoring the effects of climate change in cold regions. Here, a statistical approach for describing the dynamics of monthly Snow Depth Loss (SDL) is developed and tested in 67 climate stations throughout southern Canada. The framework fuses an input selection scheme with multiple linear regression to approximate the SDL using a set of climate proxies, either explicitly or implicitly through modeling snow depth. Our findings suggest that statistical models – if properly developed and used – have the potential to form effective tools for describing the dynamics of SDL. In particular, the implicit statistical model, in which climate proxies are selected globally among all stations, provides an accurate model (expected $R^2 = 0.75$), which can outperform a frequently-used temperature-index model in majority of stations. In addition, model parameters can be regionalized efficiently (expected $R^2 = 0.71$ for the generalized model) using latitude, longitude and altitude. This ability can provide a basis to extend the model application into ungauged sites.

4.1 Introduction

The recurrence of snow accumulation and loss is among the most important landscape features in cold regions, controlling a large proportion of regional runoff (Young, 2006). Quantification of the dynamics of snow accumulation and loss are therefore essential for effective water resource management and the design of flood defense systems in northern latitudes (Kumar et al., 2013; Fang et al., 2014). Snow accumulation and loss, however, are highly sensitive to climate change. Warming climate results in profound alterations in timing, depth and distribution of snow and accordingly runoff in high latitudes (Barnett et al., 2005; Vicuña et al., 2011; Derksen and Brown, 2012), which can influence the ecosystem functioning (Hassanzadeh et al., 2017) and human utilization of water resources (Nazemi et al., 2017).

Although wind redistribution, also known as blowing snow, and sublimation are important physical processes affecting the dynamics of snow accumulation and loss, snowmelt is generally considered as the key physical process for transition from snow accumulation to loss, both due to its regional proportion compared to other processes (Pomeroy et al., 2009), as well as its

[4] Hatami, S., Zandmoghaddam, S., Nazemi, A. (2019). Statistical modeling of monthly snow depth loss in southern Canada. *Journal of Hydrologic Engineering*, *24*(3), 04018071.

association with important management concerns, such as spring flooding (Verdhen et al., 2013). As a result, mathematical models for describing the snow accumulation and loss mainly focus on describing snowmelt (see e.g. Yates et al., 2005; Walter et al., 2005) with only few exceptions (e.g. Pomeroy, 1989; Pomeroy et al., 1993, 2007; Liston and Sturm, 2002). Accordingly, these models can be categorized – based on the taxonomy of the snowmelt models – into two classes of temperature-index and energy balance models.

Temperature-index models, also known as degree-day schemes, assume that temperature is the fundamental driver of snowmelt and adopt a seasonal or an albedo-related melt factors to quantify the melt as a function of air temperature (Quick and Pipes, 1977). Although most temperature-index models only require temperature data, there have been attempts to improve the performance of simple temperature-index models by including other climate variables. These variables can vary from daily temperature range (Tangborn, 1984), to shortwave and net radiation (Kane et al., 1997; Brubaker et al., 1996), to combinations of other climate variables (Zuzel and Cox, 1975; Singh et al., 2005). Temperature-index models are widely used due to their computational simplicity, wide availability of air temperature data and good modeling performance, particularly at larger time scales (He et al., 2014). As a result, they have been embedded within the structure of common hydrological models such as HBV (Bergstrom, 1976), SWAT (Neitsch et al., 2011) and WEAP (Yates et al., 2005) among others. Nonetheless, temperature-index models cannot perform well in complex conditions such as the occurrence of rain over snow (Garen and Marks, 2005) and in environments with heterogonous land cover (Bengtsson, 1984). In addition, there is a substantial variation in the melt factor due to topographic effects such as slope, surface roughness and aspect/shading ratios (Hock, 2003). These limitations hinder the application of temperature-index models, particularly at finer time scales and complex landscapes (Braithwaite and Zhang, 1999; Pomeroy and Brun, 2001).

In contrast, energy balance models focus on the energy exchange between soil, snow and atmosphere, which drives the phase transition of snow accumulation to melt (Anderson, 1976; Jeníček et al., 2012). These models are known as the most comprehensive snowmelt representations; however, they are used mainly as research tools (Moghadas et al., 2016): Beside the extensive need to climate forcing data, energy-balance models require a detailed information on a wide range of physical characteristics such as internal snowpack temperature, snow surface albedo, soil heat flux and canopy density among others (Tarboton and Luce,, 1996; Garen and Marks, 2005; Burles and Boon, 2011). As such characteristics have high spatial variability, the application of these models is not trivial over large and data sparse regions (Luce et al., 1998). In addition, most energy balance models employ the uniform planar assumption (see Granger and Gray, 1990), in which governing processes of snowmelt are idealized over a plane surface. Some studies tried to refine this assumption by introducing other variables such as the solar angle and slope (Marks et al., 1999), advection (Essery, 1997) and insolation (Pomeroy et al., 2003); however, they inevitably add to the modeling complexity.

Here we aim at proposing a statistical model for representing the dynamics of snow accumulation and loss using a set of climate proxies. Statistical approaches, with different degrees of sophistication, have been extensively employed in various hydrological applications (see e.g., Adamowski et al., 2012; Hassanzadeh et al., 2013; Mekonnen et al., 2015). The simplest and most-widely used statistical approach is the Multiple Linear Regression (hereafter MLR), which can provide a baseline model for assessing more complex statistical approaches. In the context of snowmelt modeling, MLR has been used to identify the association of early snowmelt runoff timing with precipitation and/or temperature (Dettinger and Cayan, 1995; Johnson and Stefan, 2006; Moore et al., 2007). Essery et al. (2008) employed MLR to estimate daytime canopy heating as an indicator of snowmelt in forested landscapes based on above-canopy shortwave radiation. Clow (2010) applied the MLR approach to investigate the influence of temperature on snowmelt timing. Regardless of these efforts much more can be done. Most importantly, the majority of snowmelt models use the concept of Snow Water Equivalent (hereafter SWE) to describe the water available for melt in snow packs. While this approach is effective, the observed information on SWE are limited due to measurement complications in comparison with measuring snow depth. For instance, while Environment and Climate Change Canada operates 1556 sites for continuous snow depth measurements throughout the country, this number is only 27 for SWE (Sturm et al., 2010). As a result, instead of modeling the change in SWE, here we quantify the dynamics of snow accumulation and loss through representing Snow Depth Loss (hereafter SDL). In addition, choosing a set of climate proxies, with which the dynamics of SDL can be described is not trivial due to the partial understanding of underlying processes that govern the dynamics of SDL, as well as the partial information available in climate proxies in relation to the SDL. As a result, here we equip the MLR with a formal input selection scheme to choose the best set of climate predictors for describing the SDL from a pool of potential climate proxies. In this setting, however, two research questions remain unanswered. First, the dynamics of the SDL and snow depth are linked through the snow budget equation – see Equation 4.3 below; and if the information on the snowfall is available, they can equally describe one another. To the best of our knowledge, there is no study that examines which approach can be more effective to model the SDL, given the limitation in the data support as well as the MLR itself. Second, it is not still fully clear if parameters of statistical models for SDL can be regionalized (see Wagener et al., 2004 for the concept and the procedure of regionalization). If this would be possible, then there is a basis for quantifying the dynamics of SDL in ungauged sites.

By addressing the above research questions, this paper presents a step forward in using statistical approaches in modeling the dynamics of the monthly SDL. By focusing on the observed snow depth data from 67 high-quality climate stations throughout the southern part of Canada coast to coast, a fully data-driven framework is proposed that combines MLR with a formal input selection algorithm. Four model setups are developed based on matching two modeling approaches with two ways of input variable selection. The generalization capability of the proposed model is investigated with a focus on regionalizing MLR parameters using the key geographic characteristics, namely latitude, longitude, and altitude.

4.2 Rationale

As noted above, this study aims at proposing a statistical framework for quantifying the monthly dynamics of SDL in a set of gauged locations and investigating its generalization capability to extend its application to ungauged sites. The first step in building such a model is to advise a pool of climate proxies, which can be potentially used to map the dynamics of the SDL. These proxies should be able to describe both short-term (monthly) and long-term (interannual) variability in the dynamics of the SDL. Here we consider a set of temperature- and precipitation-related variables to form the pool of short- and long-term climate proxies. The crucial point is then to select effective climate predictors from this pool to establish the MLR model. Here a formal input variable selection algorithm is implemented both locally and globally. Local selection implies that climate predictors are selected at each individual site; whereas global selection refers to the selection of a common set of climate predictors to describe the SDL (or snow depth) in all stations – see Section 4.4.2 for the procedure. On one hand, local predictor selection may increase the accuracy at individual sites (this will be investigated below), but compromises generalization capability as local climate predictors are different among stations. On the other hand, global selection of predictors may compromise local accuracy (this will be further investigated in Section 4.5.1) but can provide generalization capability through parameter regionalization – see Section 4.6.3.

To describe the monthly dynamics of the SDL using the MLR, two distinct approaches can be used. In the explicit approach, the monthly SDL can be directly linked to a set of relevant monthly climate predictors at the same time step through a dimensionless mapping as the following:

$$\Psi\{\widehat{SDL}(t)\} = f(\Psi\{\boldsymbol{X}(t)\}) \quad \textbf{(4.1)}$$

$\Psi\{\widehat{SDL}(t)\}$ is the estimated dimensionless SDL at each monthly time step t; $\Psi\{\boldsymbol{X}(t)\}$ is the dimensionless vector of relevant climate predictors; and $\Psi\{.\}$ is the standardization operator. Here dimensionless mappings are advised to avoid the unit inconsistencies. The results obtained from the dimensionless mappings can be then rescaled into the actual domain using the range of the SDL in centimeter, approximated through observed data – see Section 4.3 below.

In the implicit approach, however, the aim of the dimensionless mapping is to describe the dynamics of monthly snow depth. The estimated snow depth is then embedded within the snow depth budget equation to describe the monthly SDL indirectly using the estimated snow depth (i.e. $\widehat{SD}$) and observed monthly snowfall. The implicit model can be formulated as the following, where $\Psi\{\widehat{SD}(t)\}$ is the estimated dimensionless monthly snow depth:

$$\Psi\{\widehat{SD}(t)\} = h(\Psi\{\boldsymbol{X}(t)\}) \quad \textbf{(4.2)}$$

The estimated $\Psi\{\widehat{SD}(t)\}$ can be then scaled back to the original domain using the observed range of snow depth in centimeter, and can be integrated within the snow depth budget equation to estimate the monthly SDL, where $S\ (cm)$ is the monthly snowfall:

$$\widehat{SDL}(t) = \widehat{SD}(t-1) - \widehat{SD}(t) + S(t) \quad \textbf{(4.3)}$$

Local and global predictor selections, together with explicit and implicit approaches formulated above, result in four model configurations. These models are further tested and intercompared with a temperature-index model (see Section 4.6.2).

4.3 Data

We use 67 climate stations spread over southern part of Canada. The considered stations are bounded between 41º 47' to 54º 18' north and 52º 45' to 130º 26' west, with the elevation ranging from 5 to 1080 meters above the sea level – see Figure 4.1(left) for the extent of the considered stations across Canadian landmass. All stations have the minimum of thirty years of monthly data and are situated at airports that are often well-maintained and operated – see Supplementary Materials for name, location, elevation and the data period for each station. Preliminary analysis showed that historical snow accumulation and loss typically start from beginning of November and end by late May in the considered 67 stations – see Figure 4.1(right). Monthly snow depth (recorded as the snow accumulation in cm at the end of each month) and snowfall data (in cm) are available at each site. As a result, the SDL can be calculated at each site using the Equation 4.3.

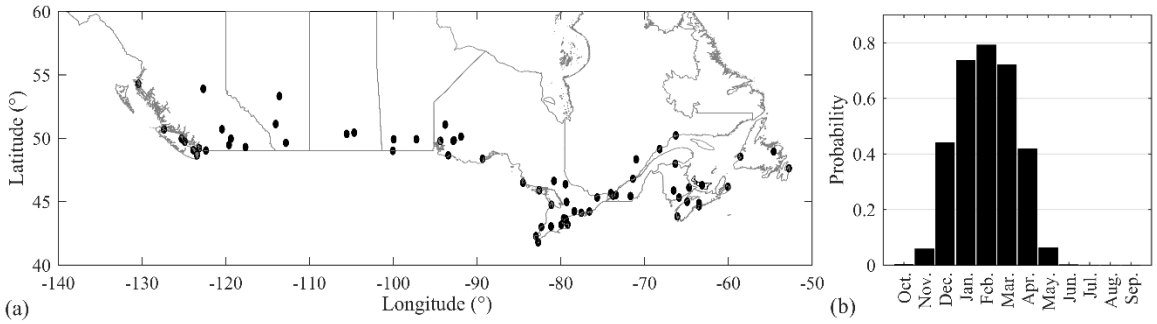

Figure 4.1 (a) The location of the 67 climate stations considered in this study; (b) the expected probability of having Snow on the Ground at the end of each month in a typical station throughout a typical hydrological year

Historical climate data are obtained through Environment and Climate Change Canada's historical climate archive (http://climate.weather.gc.ca). For each station, monthly mean of daily temperatures along with monthly extreme high and low temperatures are obtained, together with monthly sum of rainfall, snowfall and precipitation. Using these primary climate variables, a set of secondary proxies are calculated for inclusion in the pool of potential climate predictors – see Table 4.1. We also consider the cumulative values of primary and secondary variables during the cold months of each hydrologic year (i.e. November to May), meaning one value for the entire cold season in a particular year, to provide notions for interannual variability in climate proxies.

Table 4.1 Pool of monthly climate proxies, along with their notation and relevance, for representing the dynamics of the monthly SDL.

Climate proxies	Abbreviation and unit	Relevance
Mean monthly temperature	$\bar{T}$ (℃)	Average thermal energy (primary)
Maximum monthly temperature – mean monthly temperature	$T_{max} - \bar{T}$ (℃)	Surplus from average thermal energy (secondary)
Mean monthly temperature –minimum monthly temperature	$\bar{T} - T_{min}$ (℃)	Deficit from average thermal energy (secondary)
Maximum monthly temperature – minimum monthly temperature	$T_{max} - T_{min}$ (℃)	Range of available thermal energy (secondary)
Monthly rainfall	$R\ (mm)$	Form and magnitude of precipitation (primary)
Monthly snowfall	$S\ (cm)$	
Monthly precipitation	$P\ (mm)$	
Monthly ratio of snowfall to total precipitation	$S/_P$	Partitioning of precipitation (secondary)

4.4 Methodology

4.4.1 Multiple Linear Regression

MLR assumes that the properties of a given dependent variable is linearly related to a set of predictors and that each predictor has a positive effect on the performance of the simulation (Holder 1985). The MLR can be formulated as:

$$y(t) = \alpha_0 + \sum_{i=1}^{m} \alpha_i . x_i(t) + e(t) \quad \textbf{(4.4)}$$

where α_0 is the intercept and α_i, $i = 1, \dots, m$ are the linear coefficients; e is the error term and m is the number of predictors. Apart from simplicity, the key advantage of MLR is the fact that the validity of underlying assumptions and the predictive uncertainty can be formally explored and addressed. As noted in Section 4.2, the MLR mappings are dimensionless; therefore, the predictors and predictand are standardized using their observed ranges. Here we consider scaling both predictors and predictands in the range of [0.1 0.9] instead of standard [0 1] interval before model application. The considered 0.1 buffer at the upper and lower ends of the scaling space can facilitate accommodating outliers and the data points that may occur beyond the range of calibration data (Hsu et al., 1995). Maximum Likelihood Method (Uss et al., 2012; Giles et al., 2016) is used to find the optimal parameters of MLR models (including uncertainty bounds), and to calculate the predictive uncertainty. In all stations, eighty percent of the available data is used to calibrate free parameters and to extract the ranges of predictor and predictand variables for scaling purposes. The remaining twenty percent of data is used to evaluate model performance including the predictive uncertainty. Data periods for calibration and testing phases for each station are provided in Table S1 in Appendix-E.

Three goodness-of-fit measures are used to evaluate the performance of models developed in this study. These measures are Coefficient of Determination (R^2), Nash and Sutcliffe coefficient

of efficiency (NSE) and Bayesian Information Criterion (BIC). The first two measures show the accuracy of the model, while BIC considers both accuracy and complexity. In brief, R^2 defines the proportion of the described variance in the predicted compared to the observed data (Legates and McCabe, 1999). NSE is a normalized version of Root Mean Squared of Error and has been widely used in hydrological applications. Finally, the BIC is a likelihood measure that quantify the trade-off between accuracy and complexity by penalizing more complex models. The Sum of Squared Errors is considered as the error density function for BIC calculation.

4.4.2 Partial Correlation Input Selection

The performance of statistical models is largely dependent on selection of predictor variables. Correlation-based approaches are among the most popular selection methods for input selection due to their organic compatibility with the MLR (May et al., 2011; Galelli et al., 2014). In particular, Partial Correlation Input Selection (hereafter PCIS; see May et al. 2008) is used, which looks at the linear relationship between predictors and predictand by adopting a forward selection strategy based on the residual information from a new predictor. PCIS is terminated when the selection of additional predictors causes no improvement in the BIC obtained for the predictand residuals.

PCIS algorithm is implemented here in two different modes, i.e. locally to distinguish the predictors at each individual site, and globally to find a unique set of predictors in all sites. These two approaches are referred as LPCIS and GPCIS hereafter, for local and global selections respectively. LPCIS aims at choosing the best set of predictors locally. GPCIS, on the other hand, is designed to find the unique set of predictors, based on the average BIC measure in all stations. By fusing LPCIS and GPCIS with explicit and implicit modeling approaches, four model configurations can be setup – see Figure 4.2. Throughout this paper, scenarios related to explicit approach are referred to as L1 and G1, meaning direct modeling of SDL, based on local and global predictor selection, respectively. Similarly, implicit modeling scenarios are termed as L2 and G2, meaning indirect modeling of SDL through snow depth first, in which predictors for mapping snow depth are selected using LPCIS and GPCIS, respectively.

4.4.3 Temperature-Index Model

To intercompare the efficiency of statistical models with already established snowmelt models, a temperature-index model proposed by Yates et al. (2005) is implemented. In brief, the calculating snowmelt in this model is based on the concept of melt factor, defined as:

$$m_f(t) = \begin{cases} 0 & \bar{T}(t) < T_s \\ 1 & \bar{T}(t) > T_l \\ \dfrac{\bar{T}(t) - T_s}{T_l - T_s} & T_s \le \bar{T}(t) \le T_l \end{cases} \quad \textbf{(4.5)}$$

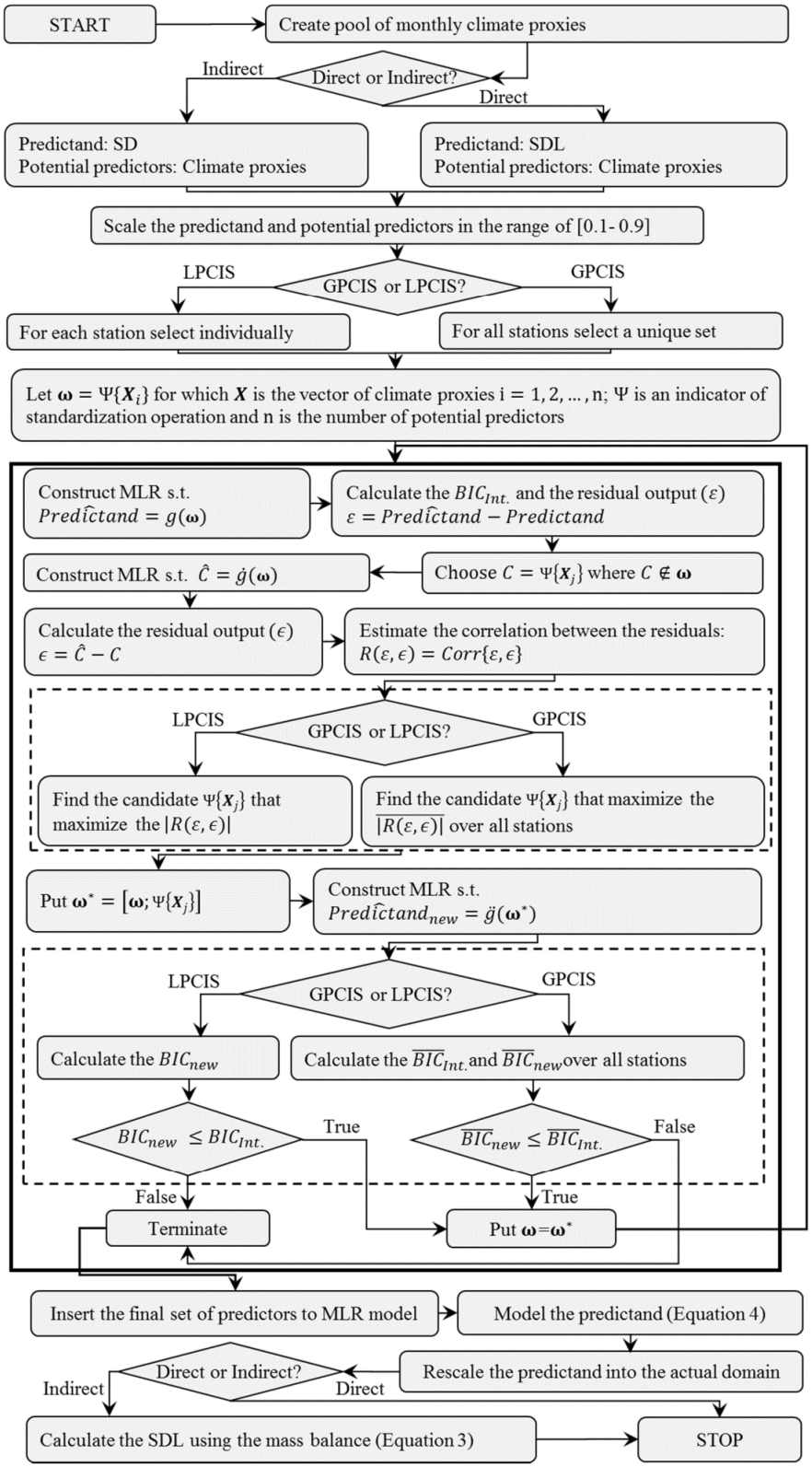

Figure 4.2 The workflow of the proposed statistical framework for estimation of the monthly SDL

where m_f is the melt factor and $\bar{T}$ (°C) is the monthly mean temperature in month t. T_l (°C) and T_s (°C) are melting and freezing temperature thresholds. Accordingly, the monthly rate of snowmelt from the accumulated snowpack, $\widehat{SM}$ (mm), can be calculated as:

$$\widehat{SM}(t) = m_f(t).\widehat{SWE}(t) \quad \textbf{(4.6)}$$

where $\widehat{SWE}$ (mm) is the estimated SWE of the snowpack at the beginning of month t, which can be described through mass balance using the water stored in the monthly snowfall S_w (mm; estimated as recorded snowfall in cm divided by 10), the melt factor and the $\widehat{SM}$ at month t:

$$\widehat{SWE}(t) = \widehat{SWE}(t-1) + \left(1 - m_f(t)\right) \times S_w(t) - \widehat{SM}(t-1) \quad \textbf{(4.7)}$$

To link the $\widehat{SWE}$ with $\widehat{SDL}$, we utilize the framework proposed by Sturm et al., (2010), which describe the relationship between estimated values of SWE and snow depth at each time step using the density of water ρ_w $\left(1\ {}^{g}/_{cm^3}\right)$ and the bulk density of the snowpack ρ_b $\left({}^{g}/_{cm^3}\right)$:

$$\widehat{SWE}(t) = \widehat{SD}(t) \times \frac{\rho_b(t)}{\rho_w} \times 10 \quad \textbf{(4.8)}$$

In which the ρ_b can be derived using the following equation:

$$\rho_b(t) = (\rho_{max} - \rho_0).\left[1 - exp\left(-k_1.\widehat{SD}(t) - k_2.DOY(t)\right)\right] + \rho_0 \quad \textbf{(4.9)}$$

where ρ_0 $\left({}^{g}/_{cm^3}\right)$ and ρ_{max} $\left({}^{g}/_{cm^3}\right)$ are the initial and maximum bulk density while k_1 and k_2 are densification parameters. The day of year is shown by DOY at the beginning of the month t. Due to spanning the winter season to two calendar years, the value of DOY varies from -62 (1st of November) to +121 (1st of May). The total SDL at the end of month t can then be estimated as the summation of loss from the old and new snowpacks:

$$\widehat{SDL}(t) = \frac{\widehat{SM}(t) + m_f(t) \times S_w(t)}{10 \times \rho_b(t)} \quad \textbf{(4.10)}$$

The free parameters in this system of equations are T_l, T_s, ρ_0, ρ_{max}, k_1 and k_2 and are calibrated at each station using Latin Hyperbolic Sampling with 1,000,000 samples. The best 1000 samples with respect to NSE during the calibration phase are then considered as the representative parametric sets, which are used to derive the predictive uncertainty during the testing phase.

4.5 Results

4.5.1 Local and global models of Snow Depth Loss

We apply the procedure outlined in Figure 4.2 to estimate the SDL in the considered climate stations – see the detailed results in Table S2 in Appendix-E. Using LPCIS, we select the local predictors for SDL and snow depth. Table 4.2 summarizes the results using the percentage of

stations, in which a predictor is selected for mapping SDL or the snow depth. Looking at the monthly climate variables S, $\bar{T}$ and $\bar{T} - T_{min}$ are selected in more than fifty percent of the stations as the monthly drivers of the SDL. Considering cumulative variables, S and $\bar{T}$ can describe the interannual variability in the SDL in more than fifty percent of stations; however, $\bar{T} - T_{min}$ is substituted by $T_{max} - \bar{T}$, which can show the effect of thermal energy surplus on interannual characteristics of the SDL. Considering the local predictor of snow depth, the key monthly driver of snow depth are monthly S, along with monthly $\bar{T}$ and S/P in majority of stations. However, assigning key local predictors of interannual variability in snow depth is not trivial as different stations are associated with different predictors. Nonetheless, there are some regional patterns; for instance, cumulative estimates of $\bar{T}$, R and S/P are mainly selected in eastern Canada. Some other variables such as the cumulative S and the cumulative $T_{max} - T_{min}$, on the other hand, do not show a strong regional pattern and are distributed uniformly over the entire region.

Using the GPCIS, we select a unique set of predictors for SDL and snow depth in all stations. These predictors are bolded in Table 4.2. For the SDL, the key local predictors noted above are also selected as global predictors along with S/P, which is chosen as an additional global driver of SDL. Regarding the snow depth, again the key local predictors are selected as monthly global predictors of snow depth. In addition, two cumulative predictors, namely the cumulative S and the cumulative $T_{max} - T_{min}$, are selected as proxies to represent the interannual variability of snow depth in the considered stations.

After calibrating both local and global models at each site, we compare the NSE of L1 and L2 during the testing phase – see Figure 4.3. The red color saturation is an indicator of the overall accuracy during the testing phase: more saturation implies higher NSE. Based on the results, L1 and L2 can quantify SDL with almost the same level of accuracy in around 91 percent of stations, in which the difference in NSE between the two model is less than 10 percent.

Table 4.2 The percentage of stations associated with potential climate predictors; the globally selected predictors are shown in bold font.

Predictors	Explicit approach (predictand is SDL)		Implicit approach (predictand is snow depth)	
	Monthly	Cumulative	Monthly	Cumulative
$\bar{T}$	**52.24%**	**62.69%**	**52.24%**	17.91%
$T_{max} - \bar{T}$	13.43%	**59.70%**	11.94%	22.39%
$\bar{T} - T_{min}$	**52.24%**	5.97%	7.46%	28.36%
$T_{max} - T_{min}$	14.93%	4.48%	8.96%	**10.45%**
R	11.94%	2.99%	20.90%	22.39%
S	**91.04%**	**71.64%**	**88.06%**	**29.85%**
P	19.40%	1.49%	26.87%	31.34%
S/P	**32.84%**	19.40%	**49.25%**	17.91%

To see how local models are comparable with corresponding global models, the NSE, R^2 and BIC are compared between L1 and G1 as well as L2 and G2 in 67 climate stations. Figure 4.4 illustrates this comparison. Top and bottom rows are related to explicit and implicit approaches whereas left, middle and right columns are related to NSE, R^2 and BIC respectively. Based on this figure it can be suggested that G1 and G2 can simulate the monthly SDL with almost the same level accuracy as L1 and L2 considering NSE and R^2. Similarly, the BIC indicate that G1 and G2 models are almost as parsimonious as their counterpart local models. Nonetheless, as G1 and G2 can quantify the SDL in all sites using unique sets of predictors, they may provide an opportunity for generalization. As a result, hereafter we limit our discussion only to G1 and G2.

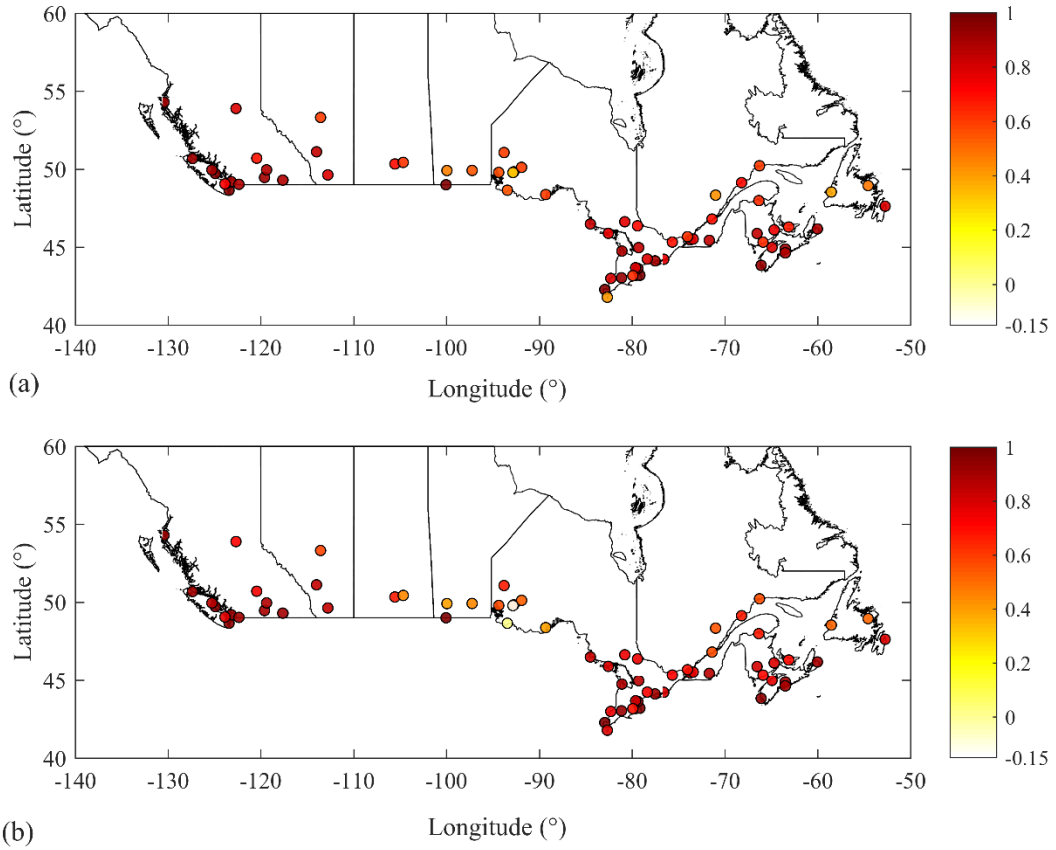

Figure 4.3 The NSE of (a) L1; and (b) L2 in representing the SDL in 67 sites in southern Canada during the testing phase. The NSE measure is shaded according to the color bar.

4.5.2 Comparison between explicit and implicit models of Snow Depth Loss

We compare global models based on the described variance, overall accuracy and predictive uncertainty during the testing phase. Figure 4.5 compares G1 and G2 based on the R^2 (top panel) and NSE (bottom panel). Looking at expected measures over all stations, the difference between G1 and G2 models is rather unnoticeable. Having said that, it was noted that both models are less accurate in the Prairie Provinces (i.e. Alberta, Saskatchewan and Manitoba) as well as the Western Ontario. The underlying processes controlling the dynamics of snow accumulation and loss in

these regions are inherently complex. For instance, Pomeroy et al. (1993) conclude that blowing snow and sublimation can result in up to 75 percent of the local SDL in the Canadian Prairies. Such processes are spatially heterogeneous and are controlled by complex interactions between wind and topography (Young, 2006). In areas such as south-western Alberta, warm and dry Chinooks often cause mid-winter snow ablation events associated with high amount of sublimation and rapid snowmelt (Pomeroy and Li, 2000; Hayashi et al., 2000; Helgason and Pomeroy, 2005). Accordingly, the low accuracy of proposed statistical models in these regions can be linked to existence of substantial nonlinearity in the dynamics of snow accumulation and loss (Holder 1985), as well as partial information available through climate proxies considered.

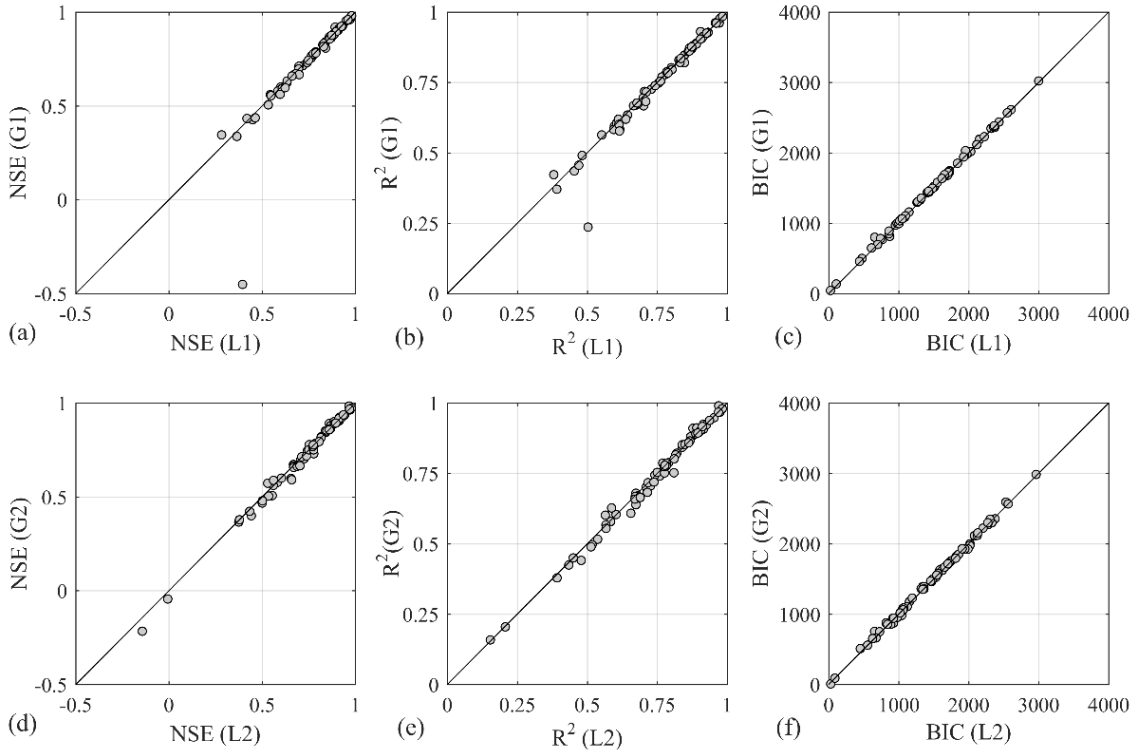

Figure 4.4 Comparison between global and local models of SDL in 67 stations in southern Canada based on NSE (a and d), R^2 (b and e) and BIC (c and f) during the testing phase; Top and bottom rows are related to explicit and implicit models of SDL, respectively.

To assess the predictive uncertainty, the 95 percent confidence intervals for model parameters are estimated at each station using Maximum Likelihood Method during the calibration. Using these intervals, the monthly SDL during the testing period and corresponding bounds of NSE are calculated at each station – see Figure 4.6. To provide a reference for accuracy of G1 and G2 during the testing phase, the best NSEs during the calibration are also shown in red dots. As noted, both G1 and G2 can capture the accuracy of the best fit during the testing phase; however, G1 has significantly thicker bound compared to G2 and therefore do not have a practical value due to substantial uncertainty in the estimations. G1, therefore, is discarded from the rest of our analysis.

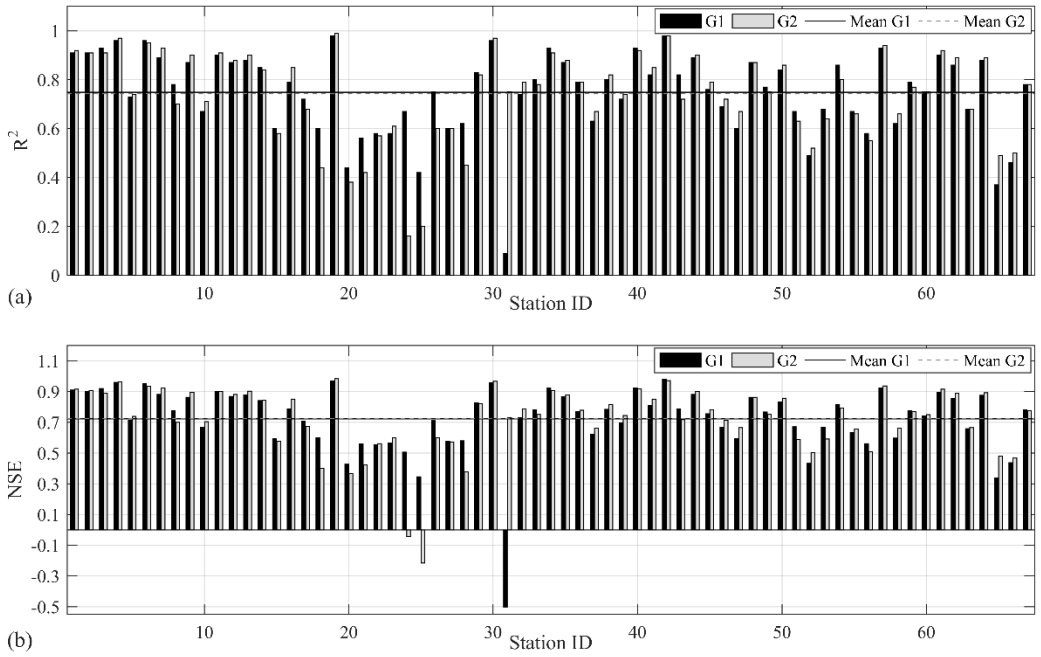

Figure 4.5 The accuracy of G1 and G2 in representing the SDL in 67 sites in southern Canada based on (a) R^2; (b) and NSE criteria during the testing phase.

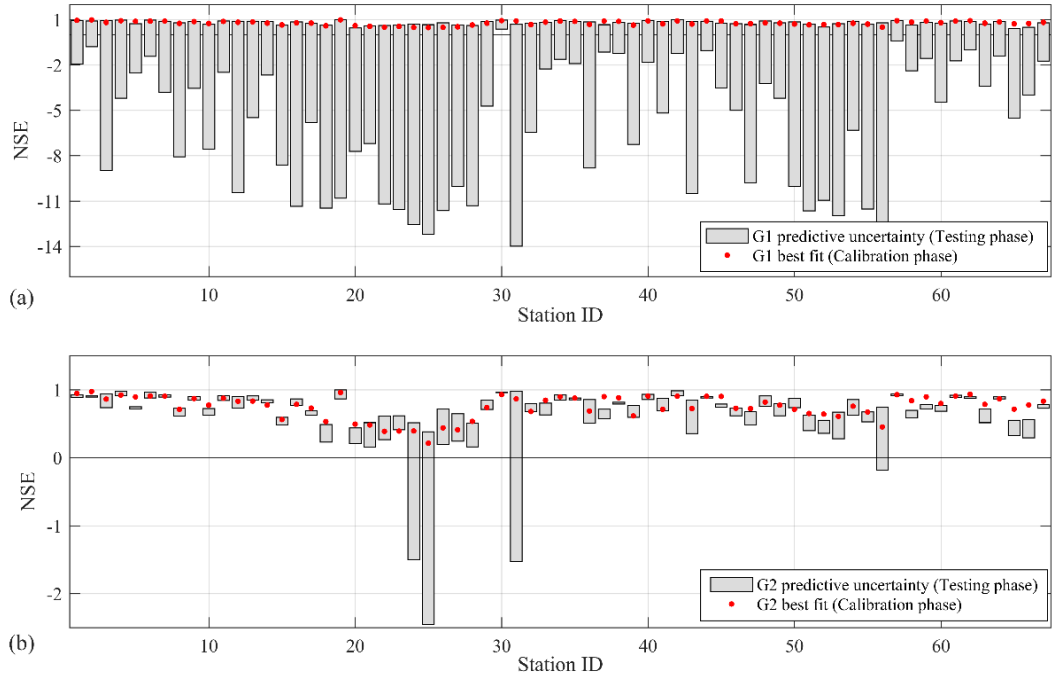

Figure 4.6 The predictive uncertainty of (a) G1; and (b) G2 in representing the SDL in 67 sites in southern Canada based on NSE criterion during the testing phase. Red dots show the best fit during the calibration period.

4.6 Discussion

Based on the above analyses, G2 stands as an accurate, parsimonious and robust statistical model for describing the dynamics of monthly SDL in southern Canada. However, it is not yet clear if G2 can satisfy the fundamental requirement of MLR, i.e. having normally distributed error vectors. In addition, the results obtained from G2 is not compared with an already established model. Finally, G2 provides an opportunity for generalization; nonetheless, this potential is not yet explored. In this section, we try to address these remaining issues.

4.6.1 Satisfying model assumptions

The validity of underlying assumptions of MLR is investigated in three stations with high, medium and low level of accuracy based on R^2 and NSE during the testing phase. These stations are Halifax (ID: 61; $R^2 = 0.92; NSE = 0.93$), Ottawa (ID: 46; $R^2 = 0.72; NSE = 0.71$) and Dryden (ID: 25; $R^2 = 0.20;\ NSE = -0.21$) – see Figure 4.7 (a-c) for comparison between observed and estimated SDL during the testing phase. We further explore associated probability distributions of errors in these stations. As can be seen, the normality of error distributions diminishes by moving from station with higher accuracy to lower – see Figure 4.7 (d-f). Further investigations show that deviation from normality of error distribution is associated with thicker uncertainty bound as shown in Figure 4.6 (b).

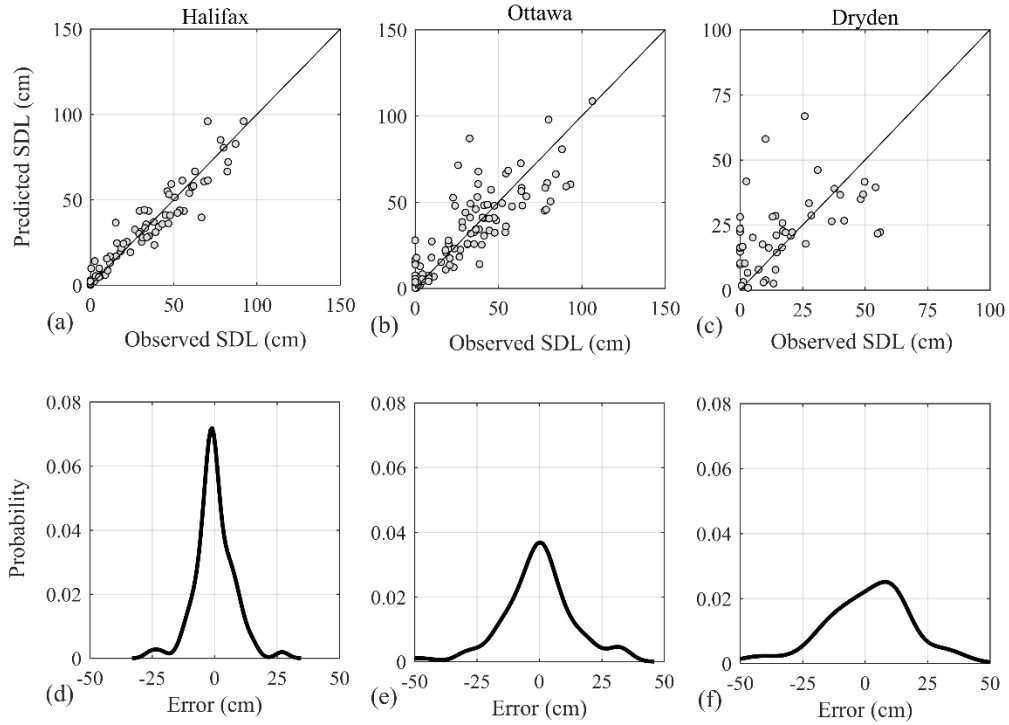

Figure 4.7 Predicted *vs.* observed SDL in three stations in which G2 performs with (a) high; (b) medium; and (c) low levels of accuracy. The empirical probability distributions of error vectors for these cases are shown in (d) through (f), respectively.

4.6.2 Comparison with the temperature-index model

Figure 4.8 compares the predictive uncertainty of G2 model with the corresponding bounds obtained by temperature-index model during the testing phase. The uncertainty bounds in the temperature-index model are extracted using the best 1000 parametric sets obtained during the model calibration. As it can be clearly witnessed, the upper bound of the range obtained for G2 is greater or equal than corresponding value for the temperature-index model in majority of stations. In addition, although the uncertainty bounds of G2 might be ticker than the corresponding ones obtained from temperature-index model in some cases, still the predictive uncertainty of G2 situates below the temperature-index model in around 85 percent of stations. This means that the lowest accuracy obtained by the G2 model is still higher than the highest accuracy of the temperature-index model. Considering these observations, it can be argued the G2 outperforms conceptual temperature-index model in majority of stations and therefore it can be a legitimate choice to estimate the monthly SDL.

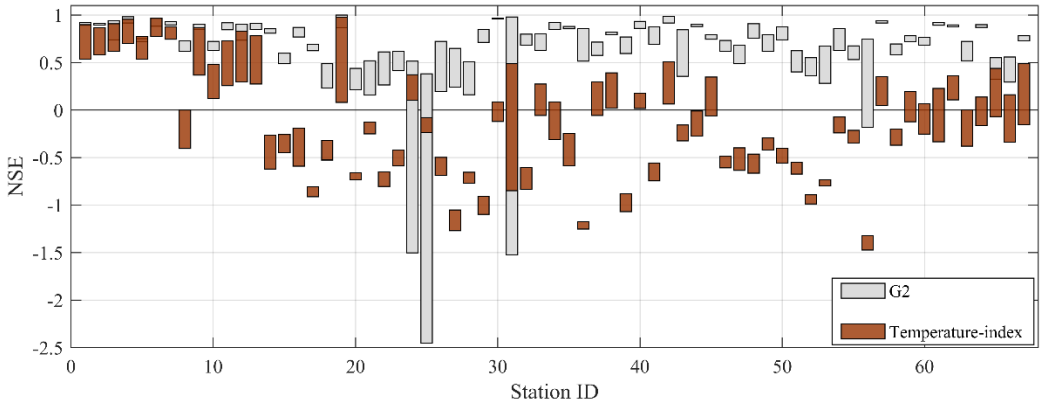

Figure 4.8 The predictive uncertainty of G2 *vs.* the temperature-index model in representing the SDL in 67 sites in southern Canada based on NSE criterion during the testing phase.

4.6.3 Generalization capability of global statistical models

Due to selecting a unique set of predictors for all stations, the parameters of G2 has the potential to be regionalized. Here we considered key geographic characteristics, i.e. latitude, longitude and elevation for the purpose of regionalization. These geographic properties are found to be effective variables for regionalization as they can be proxies for other physical characteristics (e.g., see Samuel et al., 2011; Razavi and Coulibaly, 2012; Arsenault and Brissette, 2014). According to G2 model, the monthly snow depth can be described as:

$$\Psi\{\widehat{SD}(t)\} = \alpha_0 + \alpha_1.\Psi\{\bar{T}(t)\} + \alpha_2.\Psi\{Cum\{T_{max}(t) - T_{min}(t)\}\} + \alpha_3.\Psi\{S(t)\} + \alpha_4.\Psi\{Cum\{S(t)\}\} + \alpha_5.\Psi\left\{S(t)/P(t)\right\} \quad \textbf{(4.11)}$$

where α_0 is the intercept, and α_i, $i = 1, \ldots, 5$ are the linear coefficients of climate predictors, which derived using calibration; $Cum\{.\}$ is the cumulation operator that sums up the values of the inside

variable during the cold season (November to May), in which month t is located – this means one value for the entire cold season months in a particular year. To inspect dependencies between geographic characteristics and the free parameters of G2, the Kendall's dependence coefficient is used, which is based on the ranks of paired random variables (see Genest and Favre, 2007). The significance of dependence is evaluated using the formal *p*-value associated with the measure. *p*-values equal or less than 0.05 are considered as the sign of significant dependence – see Figure 4.9. For each model parameter, a set of MLR functions are developed based on using the significantly-dependent geographic characteristics. The linear model with the least BIC is selected as the regionalization model – see Table 4.3.

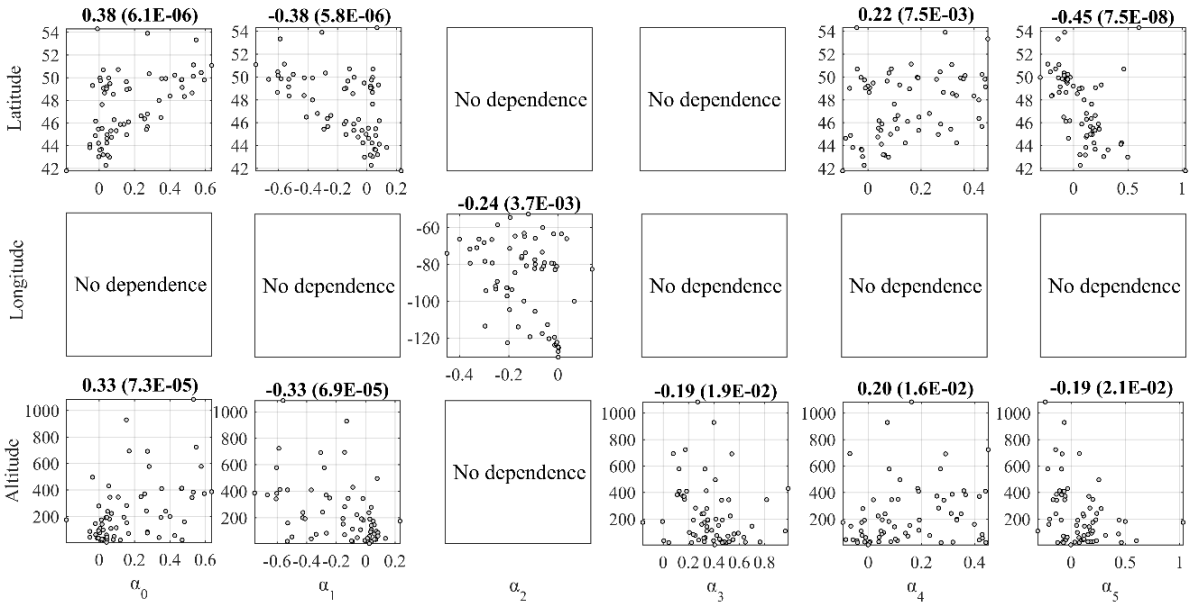

Figure 4.9 Significant dependencies between parameters of G2 and three geographic characteristics; columns are related to model parameters whereas rows are related to the three geographic characteristics. On the top of each panel, the Kendall's dependence coefficient is reported along with the associated *p*-value in the parenthesis.

By having the regionalization functions, it would be possible to estimate model parameters without calibration and recalculate monthly SDL at the considered 67 stations. To assess the accuracy of regional models, the R^2 and NSE during testing phase are compared between generalized and calibrated models – see Figure 4.10. Considering the two measures, generalized and calibrated models exhibit almost the same level of accuracy in nearly 90 percent of the sites, in which corresponding estimates of SDL obtained from the original and generalized models exhibit less than 10 percent difference. To provide a comparison between observed and simulated time series, we consider the three stations discussed in Section 4.6.1 – See Figure 4.11, which shows that the difference between original and generalized models increases as the accuracy of original model declines.

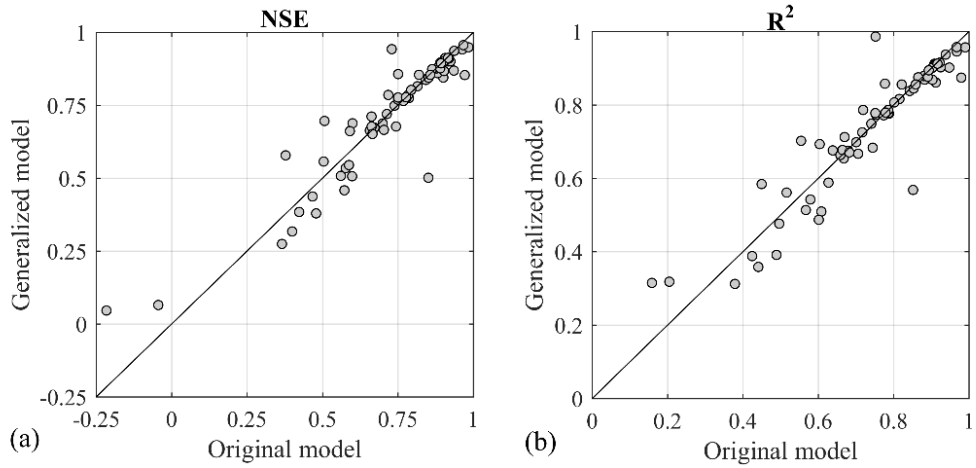

Figure 4.10 Comparison between original and generalized G2 model in 67 sites in southern Canada based on NSE and R^2 during the testing phase.

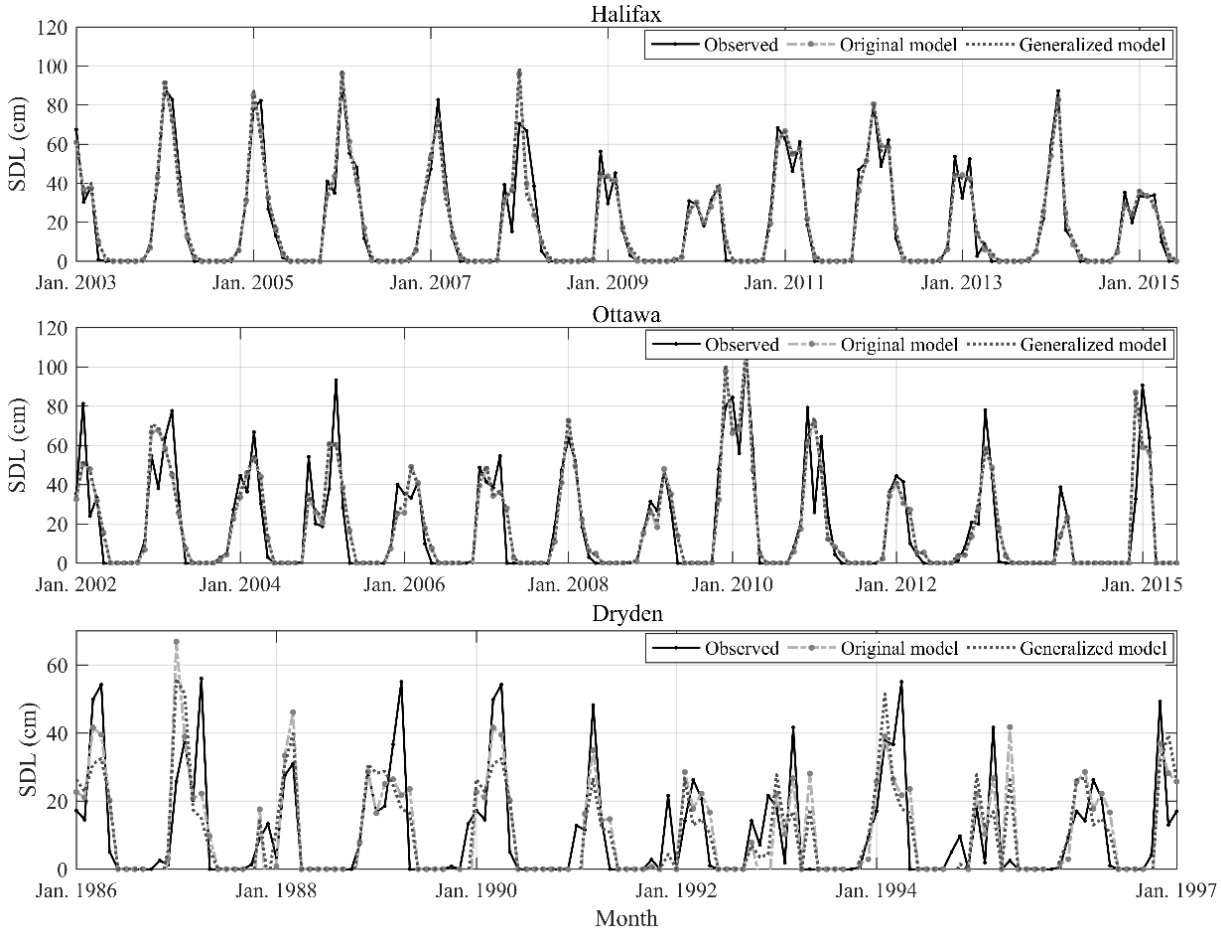

Figure 4.11 Observed *vs.* estimated SDL using original and generalized G2 model in three representative sites during the testing phase.

Table 4.3 Regionalization function for parameters of G2

Parameters	Equations
α_0	$-1.1711 + 0.0271 \times Latitude + 0.0003 \times Altitude$
α_1	$1.4956 - 0.0335 \times Latitude - 0.0003 \times Altitude$
α_2	$-0.3008 - 0.0019 \times Longitude$
α_3	$0.4057 - 0.0002 \times Altitude$
α_4	$-0.7219 + 0.0184 \times Latitude$
α_5	$1.9017 - 0.0384 \times Latitude$

4.7 Summary and conclusion

Common mathematical models for describing the dynamics of snow accumulation and loss are associated with known deficiencies. Here, a statistical framework is proposed to describe the dynamics of monthly SDL, which fuses explicit and implicit modeling approaches with global and local predictor selection schemes. The framework is tested at 67 sites throughout southern parts of Canada. The four model configurations within this framework are intercompared with one another, and with a frequently used temperature-index model using a set of goodness-of-fit measures. It is noted that in terms of the accuracy and descriptions of the observed variance, there are not that much of difference between the four setups. It is discussed, however, that global models are preferred due to their potential for regionalization. Comparing global modeling setups, it is noted that the implicit approach provides significantly less predictive uncertainty compared to the explicit configuration. Accordingly, it is concluded that in the context of MLR, climate predictors are more suitable to estimate monthly snow depth than monthly SDL.

Although the proposed implicit statistical model with global predictors, G2, is expected to describe around 75 percent of observed variance in the 67 considered stations, it is shown that the efficiency of the model declines in stations located in the Canadian Prairies and Western Ontario. This is referred to the nonlinearity in snow accumulation and loss processes and the partial information obtained by the temperature- and/or precipitation-related predictors in these regions. We envision that including other relevant climate proxies, such as the wind speed and/or relative humidity, can improve the performance of statistical models in the prairie regions. This can be the subject of the future research. Having said that, still when compared with a conceptual temperature-index model, the statistical approach outperforms in terms of accuracy in majority of 67 stations considered. Moreover, we show that the G2 model can be regionalized only with the three most primary geographic characteristics, i.e. latitude, longitude and altitude. This provides the opportunity of extending the use of model in ungauged sites, which can accordingly provide a synoptic view on the monthly SDL in the southern part of Canada, particularly in eastern and western parts of the country. This ability has enormous practical applications: it can be linked to monthly weather forecasts to provide monthly predictions of the SDL. It can be also fed by

downscaled climate model outputs to project monthly SDL under climate change condition. These estimates can be then used to approximate SWE and/or snow cover loss in short and long terms.

Considering our results, examining more sophisticated statistical techniques and/or extending model application into finer temporal resolutions are suggested. As the final remark, it should be noted that statistical models are not substitutes for conventional models. We recognize that the dynamics of snow accumulation and loss are complex, particularly under ongoing climate change, and the involving processes are subject to significant variations in time and space. As a result, we strongly believe that various models, including statistical, conceptual and/or physically-based, are required in engineers' toolkit for accurate predictions across a range of temporal and spatial scales.

Chapter 5.

A Multivariate Statistical Framework for Top-down Projections of Freeze-Thaw under Changing Climate Conditions – Part 1: Key Considerations and Development of a Gridded Snow Depth Model[5]

The contents of this chapter are in preparation as "A Multivariate Statistical Framework for Top-down Projections of Freeze-Thaw under Changing Climate Conditions – Part 1: Key Considerations and Development of a Gridded Snow Depth Model" for submission to the Journal of Earth's Future.

Synopsis

The dynamics of Freeze-Thaw (FT) significantly constrain eco-hydrological processes and socio-economic activities specifically across cold regions. Accurate quantification of the future state of FT dynamics as one of the most important features of the cryosphere in cold regions is hence essential for advising adoptive strategies for future human developments and land management. In this double feature paper, we proposed a statistical framework to formally project the FT characteristics conditioned to a wide range of air temperature and snow depth change scenarios over the province of Québec, Canada. We are determined to address the following research questions throughout this work: (1) Can we use the readily available downscaled projection of climate data in our top-down impact assessment?, (2) What are the future dynamics of snow depth over the province?, and (3) How we can formally take into the account for any possible changes in the dependence structure between air temperature, snow depth, and FT characteristics? In Part 1 of this paper, we focus on addressing the first two questions. For this purpose, we fuse an input selection scheme with Multiple Linear Regression (MLR) to project the future dynamics of snow depth across the grid scale. Partial Correlation Input selection is used to select a common set of climatic proxies from a pool of relevant forcing methodological data at each ecozone of the province. Our results suggest that MLR, if properly developed and used, has the potential to form effective tools for modeling the observed monthly dynamics of snow depth (expected $R^2 = 0.74$). The calibrated MLRs are fed with the bias-corrected future projections of climatic proxies to provide a basis for projecting the future dynamics of snow depth across Québec. The good performance of MLR models using the bias-corrected data in representing the characteristics of the historical period over the common period of 1999-2005 (ratio of errors in total snow depth = 3.7%) ensures accurate projections of future conditions. Employing the calibrated MLR models for projecting future dynamics of snow depth, we show that annual snow depth will decrease with an average magnitude of 9cm across the province due to long-term climatic scenarios (2094-2100) compared with the present day (1999-2005) and under RCP4.5. An average decrease of 18cm in annual snow depth is observed for RCP8.5. Vivid spatial patterns are observed looking at the

[5] Hatami, S., Nazemi, A. (2021). A Multivariate Statistical Framework for Top-down Projections of Freeze-Thaw under Changing Climate Conditions – Part 1: Key Considerations and Development of a Gridded Snow Depth Model. *Earth's Future*, (In preparation).

magnitude of changes in snow depth, showing the higher declines in annual snow depth in the northern ecozones of the province. We also show that the future changes in snow depth over time are amplifying, especially across northern regions. The developed MLR models over the historical period are also paired with readily available downscaled climate data to inspect the need for further bias-correction. The performance of MLR models while using downscaled gridded data is assessed based on their capability to represent the monthly dynamics of snow depth over the historical period. The low performance of MLR models obtained using the available downscaled data validates our initial assumption of the need for further bias-correction. Finally, looking at the predictive uncertainty of the proposed methodology, lower uncertainty bounds in the most southern and northern ecozones show the higher practicability of the proposed framework in these regions. The results of our research can provide useful insights into future water resources management and the design of flood defense systems in northern latitudes.

5.1 Background

The dynamics of Freeze-Thaw (FT) is one of the most important land-surface characteristics in northern latitudes. Around 50% of the land across the northern hemisphere undergoes seasonal transitions from frozen to thawed conditions annually (Kim et al., 2011). This forms a recurring phenomenon determining natural processes as well as human development in cold regions. Physically, as the state of soil changes from frozen to thawed conditions and vice versa, soil properties such as density, hydraulic conductivity, and infiltration change (M. Wang et al., 2018; Weng et al., 2020; Zhang and Cui, 2017). This can affect surface and sub-surface connectivity (Bechmann et al., 2005) and alters pathways in which water, carbon, and other matters travel (Bosson et al., 2013; Jones et al., 2011). As a result, FT matters to energy and water balance in cold regions (Guo et al., 2011; Wang et al., 2009; J. Wang et al., 2019), and controls land-atmospheric interactions (Peng et al., 2015; Schuur et al., 2015; Wu et al., 2014). FT also matters to biological processes (Congreves et al., 2018; Larsen et al., 2002) and controls vegetation growth and wildlife distribution (Hu et al., 2020; Jones et al., 2013; Niu et al., 2019; Tape et al., 2016) as well as potential impacts on agriculture (Harrison et al., 2020; King et al., 2018; Parry, 2019; Zhou et al., 2015) and resource developments (Beier and Sego, 2009; Porter et al., 2019; Qin et al., 2019). As a result, FT is key to both indigenous and modern ways of life in higher latitudes (Thomas D. Andrews et al., 2016; Gibson et al., 2021; Proverbs et al., 2020).

The interplays between multiple physical and biological variables, ranging from solar radiation to the characteristics of the organic soil layer, determine the dynamics of FT (Bonan, 1989; Gibson et al., 2018; Slater et al., 1998). Vegetation, for instance, can act as a buffer for climatic warming and regulate the amplitude and duration of diurnal soil FT cycles (Hu et al., 2020; Niu et al., 2019). Different vegetation types have distinct structures and consequently affect energy balance differently (W. Guo et al., 2018). A large proportion of organic matters in the soil can also affect the FT dynamics, heighten microbial decomposition in a warming climate and consequently alter the FT dynamic (Walz et al., 2017). Additionally, solar radiation and wildfire are among important

physical processes that can affect the dynamics of soil moisture and FT dynamics by altering the soil thermal regime (Guo et al., 2011; Michaelides et al., 2019). Having said that, it has been shown that temperature and snow depth are the two most influential drivers of FT dynamics (Henry, 2008; Larsen et al., 2007; Peng et al., 2016). On the one hand, near-surface air temperature can affect the timing and duration of FT states as well as the depth of frozen layer (Frauenfeld et al., 2004a; Henry, 2007; Hirota et al., 2006; Sinha and Cherkauer, 2008; Wei et al., 2017; Yi et al., 2015) . On the other hand, the depth of snow cover can control the thermal regime of the soil layer through interfacing with the atmosphere (Iwata et al., 2010; Zhang, 2005) and influencing the energy balance through albedo (Fletcher et al., 2009; Kattsov et al., 2007; Kim et al., 2018).

Climate change, however, has greatly impacted air temperature and snow depth and thus FT dynamics in time and space (Plaza et al., 2019; C. Wang et al., 2019). The heightened temperature in recent decades has increased the depth of the active soil layer (Connon et al., 2018), changed the timing of frozen season (Wang et al., 2015), extended the length of the thawed period (Kim et al., 2014), and retreated the permafrost (Carpino et al., 2018; Schuur et al., 2009). Decreasing the depth of the snow has also reduced the thermal insulation of soil surface and hence increased the vulnerability of soil to changing air temperature (Chen et al., 2020; Hirota et al., 2011). These changes can consequently alter the timing of the frozen period and the depth of the frozen layer (Iwata et al., 2010), causing more frequent transitions between the frozen and thawed states (Zhang, 2005). As FT dynamics alter due to elevating air temperature and thining snow depth, natural processes and socio-economic activities are affected (Krogh et al., 2017; Liu et al., 2009; Wolf et al., 2010). For instance, increased transitions between frozen and thawed conditions can cause soil erosion (Wu et al., 2018) and deteriorate critical community infrastructures such as pipelines, roads, and other built environments (Melvin et al., 2017; Nelson et al., 2001; Raynolds et al., 2014). Climate change impacts of FT condition can also result in emerging feedback processes between land and atmosphere as the thawing permafrost releases significant amount greenhouse gasses that can even intensify the rate of a warming climate (Schaefer et al., 2014; Schuur et al., 2015; Wagner-Riddle et al., 2017). As a result, quantifying possible changes in FT characteristics under future climate conditions can be important for a variety of problems related to land and water management, ranging from local infrastructure design and maintenance, to the regional potential for agriculture and natural resource development due to global warming.

International Panel for Climate Change (IPCC) suggests a top-down approach to climate change impact assessment (IPCC, 2007, 2014). These approaches are mainly based on the use of downscaled projections of Global Climate Models (GCMs) that provide the inputs for impact assessment models, with which the changes in the system under consideration can be quantified (Gizaw et al., 2017; Sunde et al., 2017). Peng et al., (2018), for instance, used future climate projection to assess the impact of climate change on active layer thickness in permafrost regions across the entire Northern Hemisphere, showing an increase in active layer thickness over all permafrost regions. Wei and Dong, (2015), used an ensemble of climate model projections to simulate the projected changes in the snow depths in Qinghai-Tibetan Plateau, indicating decreases

in snow depths for most of the climate models. The current dominant paradigm to assess the impacts of changing climate on FT dynamics is based on the use of physically-based algorithms embedded in land-surface models and often involves coupling water and energy balance equations above, at, and below the surface (W. Guo et al., 2018; Kang et al., 2005; Zhang et al., 2021, 2008). If the required data support is available, physically-based approaches can often lead to accurate results at the local scale (Karjalainen et al., 2019; Zheng et al., 2020). Such approaches are, however, limited regionally due to poor process representations (Cao et al., 2020; Walvoord and Kurylyk, 2016), the lack of scalability (Hayashi et al., 2007; Romanovsky and Osterkamp, 1997) as well as limitations in data support at larger scales (McCarty et al., 2020; Tape et al., 2018) and model parametrization (Li et al., 2012). In addition, our empirical understanding of changes in FT characteristics is mainly obtained through in-situ data that are sparse regionally and often discontinuous temporally, particularly in cold regions (Takala et al., 2009; K. Zhang et al., 2007).

We argue that the advent of publically-available gridded data products along with powerful statistical approaches can overcome some of the limitations noted above. On the one hand, the availability of several global and regional gridded datasets under current and future conditions such as reanalysis dataset (e.g., Dile and Srinivasan, 2014; Sheffield et al., 2006; Uppala et al., 2005), satellite product (e.g., Barnes et al., 2003; Huffman et al., 2007; Williams et al., 2006), and projected climate model simulation (e.g., Giorgi et al., 2009; Harding et al., 2011; Weedon et al., 2014) provide viable sources for impact assessment under historical and future climatic conditions. With direct relevance to our work here, currently, there is a publically-available data for daily FT states retrieved from satellite imageries (see Kim et al., 2017). If this data product paired with climate and/geographic data, it can provide synoptic, homogeneous, and globally relevant data with a continuous record (Kim et al., 2012; McDonald et al., 2004; Smith et al., 2004) and an opportunity to formally quantify the spatiotemporal variability of FT dynamics and its dependencies with driving climatic and/or geographic variables (Park et al., 2016b). On the other hand, it has been shown that statistical and machine learning approaches – if appropriately applied in the right domains – can provide an alternative approach to conventional modeling approaches (Adamowski, 2008; Crane-Droesch, 2018; Lemoine and Kapnick, 2016; Sarhadi et al., 2018; W. Wang et al., 2018). While some machine learning approaches such as neural networks and/or other methods under the umbrella of artificial intelligence may suffer from the lack of transparency (Abrahart et al., 2012; Creel, 2020; Kuwajima et al., 2019), the curse of dimensionality (Bach, 2017; Salimi et al., 2018; Verleysen et al., 2003) and/or parametric and predictive uncertainty (Khosravi et al., 2011; Nourani et al., 2019), there are parsimonious and well-established statistical approaches that can address some of the limitations in physically-based and/or conceptual approaches. For instance, Hatami et al. (2019b) employed a parsimonious regression-based approach fused to model snow depth dynamics using a set of climate proxies, showing better accuracy and lower uncertainty bounds compared to the common temperature-index model in more than 60 stations in southern Canada. Studies showed that such regression-based models could be parametrized efficiently using observed data and regionalized using the most primary geographic variables, i.e. latitude, longitude, and altitude. In addition, some recent studies showed

that if the focus of modeling shifts from continuous representations of FT states to estimations of FT characteristics across coarser temporal and spatial scales, then formal statistical frameworks can be used to characterize the link between FT states and driving climatic variables (Hatami and Nazemi, 2021b, 2019). These methodologies are often more parsimonious, flexible, and computationally efficient than process-based models (Ni et al., 2021; Zheng et al., 2020). The copula methodology, a generic multivariate approach to modeling statistical dependence, is one of the possible statistical tools that can provide an alternative approach for conditioning FT characteristics to climate conditions.

5.2 Scope and problem definition

Having in mind the urgent need for quantifying future FT conditions in northern latitudes, current understandings about key variables affecting the dynamics of FT, as well as the gaps and opportunities in current data supports and modeling methodologies, our aim in this double feature article is to develop an alternative statistical framework for top-down assessment of climate change impacts on FT characteristics at large temporal and spatial scales. Figure 5.1 shows the schematic of the proposed framework including two standalone sets of algorithms for the development and application of (i) a gridded snow depth model informed by a suite of climate variables (i.e. Part 1; see the left box in Figure 5.1), and (ii) regional conditioning of FT characteristics informed by temperature and snow depth (i.e. Part 2; see the right box in Figure 5.1). The required data support (see the middle box in Figure 5.1) includes gridded observations of FT characteristics, temperature and snow depth, in-situ observations of temperature, rainfall, and snowfall, as well as gridded downscaled projections of temperature and precipitation. We demonstrate the development and application of this procedure in the province of Québec, Canada, as a case study.

Our framework starts with the development of a parsimonious regression model for representing the monthly snow depth dynamics at the grid scale, which is then applied in conjunction with downscaled projections of future climate to produce future scenarios of snow depth. The development and application of this procedure include classifying the type of precipitation, identifying the best set of climate proxies for representing the dynamics of snow depth at the regional scale, developing the regression models for representing monthly snow depth at the grid scale, and linking the developed models with future projections of climate variables. This paper, which is the first part of this double feature article, reports the attempts for the development, validation, and application of the proposed gridded snow depth model. Building on previous findings of Hatami and Nazemi (2019, 2021a, 2021b), the second part of our investigation includes the development and application of a copula-based sampler for conditioning FT characteristics to temperature and snow depth. We investigate the need for updating copula parameters in time and how to link the changes in model parameters to changes in climate variables. Although we only focus on the impacts imposed by changes in temperature and snow depth conditions across the province of Québec, Canada, we make a particular effort to develop a generic framework that can include other variables and be applicable in other regions.

While developing this framework, we note four key challenges. First, IPCC-endorsed top-down impact assessments are based on the use of downscaled climate projections that are inherently uncertain. As a result, the parametric and predictive uncertainties initiated from the development and application of impact models should be trackable and quantifiable. This consideration inevitably weed out several complex machine learning approaches that are heavily parameterized and therefore full assessment of their uncertainty is complicated or even not fully possible (Kasiviswanathan and Sudheer, 2016; Srivastav et al., 2007; Tongal and Booij, 2017).

Second, although gridded downscaled climate projections are widely available and used (Giorgi et al., 2009; Lorenz et al., 2016; Mearns et al., 2007), it is not yet clear whether they can readily support impact assessment studies, particularly when representing the dynamics of impacts in time are needed. The work of Ehret et al. (2012) and Jaramillo and Nazemi (2018) showed that although downscaled climate projections can reproduce long-term statistics and evolution in climate variables, they may need further bias-correction for the purpose of impact assessment when representing the year-to-year dynamics are sought.

Third, before FT characteristics can be conditioned to future projections of temperature and snow depth, the snow depth itself should be projected based on future projections of relevant climate variables. This intermediate modeling step inherently includes uncertainty and it is not clear how the uncertainty in estimating the snow depth can propagate into the estimation of FT conditions. Finally, while previous studies showed copulas provide a generic approach for conditioning FT characteristics to temperature and snow depth, the dependence structure between these variables may change in time. Accordingly, the parameters of copula models should be updated as the dependence structure changes. At this stage of development, it is not yet clear how copula parameters can be updated in light of projected temperature and snow depth conditions.

In this paper, we focus only on those challenges that are related to snow depth modeling and address the obstacles related to conditioning of the FT to temperature and snow depth in the companion paper. Section 5.3 presents the rationale and methodology for the development of the gridded snow depth model. Section 5.4 introduces the case study and the data support used for the development and application of the proposed snow depth models. Sections 5.5 and 5.6 provide our results and discuss our findings, respectively. Finally, Section 5.7 concludes the Part 1 paper and sets the scene for our companion paper.

5.3 A framework for gridded snow depth modeling under current and future climates

The gridded snow depth model is inspired by the statistical snow depth model proposed by Hatami et al. (2019b) and rigorously tested in 67 local stations in southern Canada. Here, we attempt to extend the application of this statistical approach from local to regional scale, feed the model with gridded climate data rather than in-situ observations, and link the developed model with climate projections. This requires adding a couple of more algorithms to the previously developed framework for retrieval of the precipitation type (snow *vs.* rain) as well as potential bias-correction

for linking to climate projections rather than observation. Below, we introduce the methodological elements of this extended statistical approach.

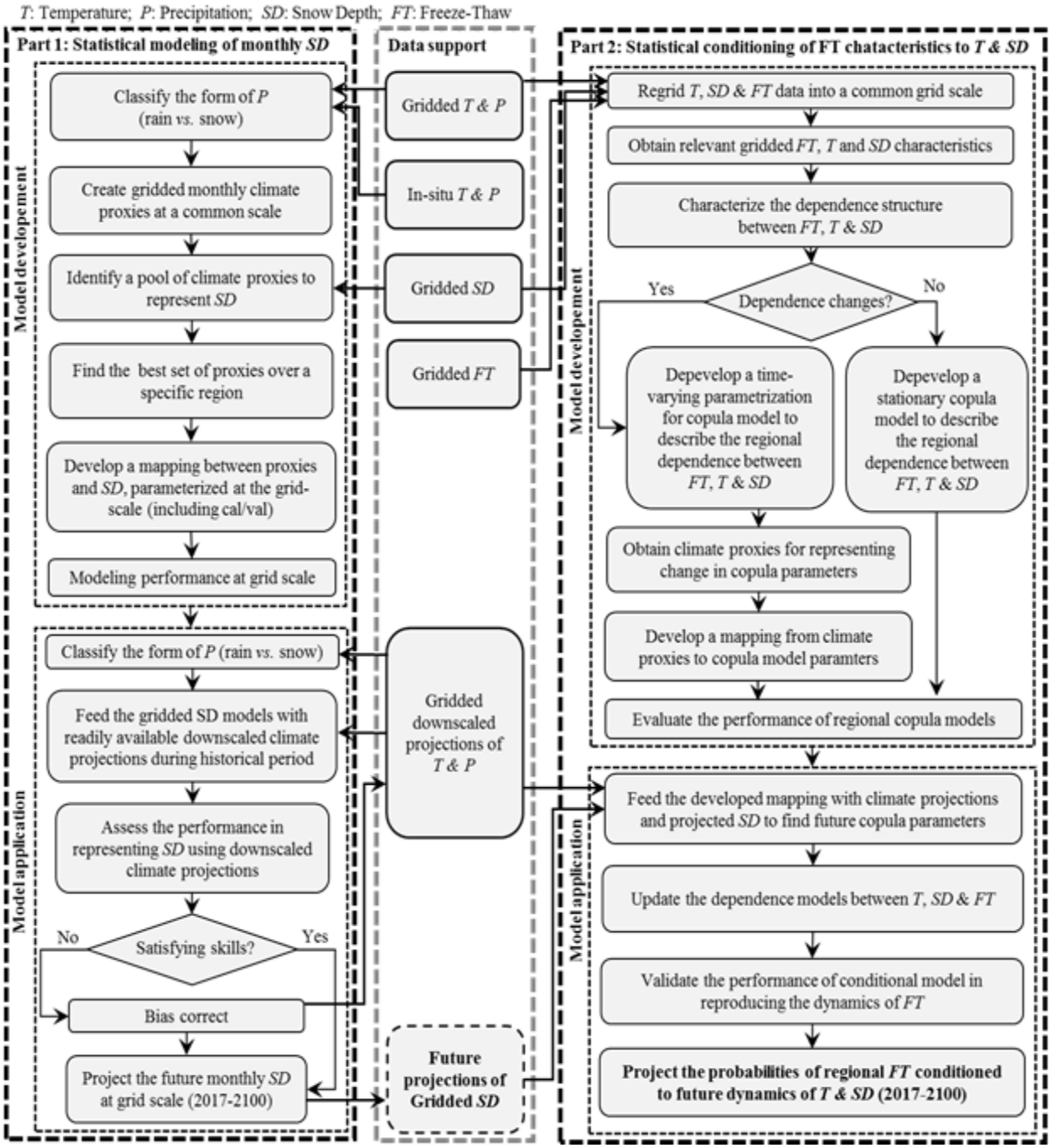

Figure 5.1 The workflow of the proposed framework for projection of FT characteristics under future projections of temperature and snow depth. The suggested framework includes a set of algorithms for gridded projections of snow depth (left box) and regional projections of FT characteristics (right box), supported by observed and projected climate variables (middle box)

5.3.1 Classification of the gridded precipitation type

The gridded climate products during historical and future climate often do not include information on precipitation type (e.g. Adler et al., 2003; Ashouri et al., 2015; Huffman et al., 2007). However, the statistical model developed by Hatami et al. (2019b) requires distinguishing between rain and snow; and therefore gridded climate products cannot be directly linked to the model. Here we use a simple Bayesian classification algorithm (Cestnik, 1990; Grams et al., 2016; Sakizadeh, 2015) to classify the type of precipitation by upscaling the information available through in-situ observations to a regional scale. This algorithm has been previously used for retrieving precipitation type (J. N. K. Liu et al., 2001; Sakizadeh, 2015) and is favorable due to being simple and non-parametric. In brief, the algorithm uses a supervised learning approach to quantify the threshold of temperature at which the type of precipitation is changing from snow to rain. This is through obtaining empirical conditional probabilities for mean daily temperature given the type of precipitation (snow *vs.* rain). The point of intersection between two class-probability distributions can be considered as the temperature threshold at which the type of precipitation is changing from snow to rain. These probability distributions can be obtained by the information available in climate stations that measure both daily snow and rainfall. Here we hypothesize that a unique regional notion for class-probability distributions can be obtained by averaging up the probability distributions of the class-probabilities at the local scale. We rigorously test the validity of this assumption through a number of experiments.

5.3.2 Statistical modeling of gridded snow depth

Statistical approaches with different degrees of complexity have recently gained popularity in modeling snow-related processes (Broxton et al., 2019; Ntokas et al., 2021; Ozga-Zielinski et al., 2016). Hatami et al. (2019b) have discussed the benefits of using statistical models over energy-balance (DeBeer and Pomeroy, 2017; Pavlovskii et al., 2019; Zaremehrjardy et al., 2020) and/or temperature-index models (Debele et al., 2010; He et al., 2014; Singh et al., 2005). With certain assumptions (see Hatami et al., 2019b), statistical models of snow depth dynamics can be described by the following dimensionless mapping:

$$\Psi\{Y(t)\} = f(\Psi\{\boldsymbol{X}(t)\}) \qquad \textbf{(5.1)}$$

where $f(.)$ is the mapping function, $\Psi\{.\}$ is the standardization operator, $Y(t)$ is the snow depth (predictand), and $\boldsymbol{X}(t)$ is the vector of forcing hydroclimatic variables (predictors) at any given timestep. The dimensionless mapping is advised to avoid the unit inconsistencies of different hydroclimatic variables. The results can be back-transformed to the actual domain using the observed range of data at each grid.

The multiple linear regression (MLR) is one of the widely used approaches for forming the functional mapping due to MLR's simplicity, effectiveness as well as quantifiability of parametric and predictive uncertainties (Clow, 2010; Essery et al., 2008; Moore et al., 2007; Parajuli et al., 2020). Here MLR is implemented to provide a basis for modeling future snow depth dynamics at the larger spatial (grid) and temporal (monthly) scales, assuming that the dependent variable (snow depth in this case) is linearly related to the climate predictors. The MLR model can be formulated as follows:

$$\Psi\{SD(t)\} = \alpha_0 + \sum_{j=1}^{m} \alpha_j . \Psi\{x_j(t)\} + e(t) \quad \textbf{(5.2)}$$

where α_0 is the intercept, α_j, $j = 1, \dots, m$ are the linear coefficients, m being the number of predictors associated with each predictor x_j, SD is the gridded monthly snow depth, and e is the error. We consider linear mapping into [0.1 0.9] for the standardization, allowing for 10% buffers below and above the observed lower and upper bounds for extrapolation. Optimal MLR parameters and associated parametric uncertainty bounds can be effectively found using the Maximum Likelihood method at each grid (Wentzell et al., 1997). The parametric uncertainty bounds can be further used for accounting for the predictive uncertainty during historical and future periods.

While the parameters of the proposed MLR model are identified at the grid scale, the vector of predictors is identified regionally. As a result, an important part of the model development is related to identifying a certain number of climate predictors from a pool of potential variables. Here, we form the pool of climate variables from a group of monthly temperature and precipitation related variables and their annual cumulative values, which is considered to provide a notion for the interannual variability in temperature and precipitation related variables. The Partial Correlation Input Selection (PCIS; May et al., 2008), a dependence-based approach for identifying predictors is used in this study (see Galelli et al., 2014; Zandmoghaddam et al., 2019). In brief, PCIS is a sequential forward selection strategy that is inspired by Granger's causality theory (see Amir Jabbari and Nazemi, 2019) and looks at the dependence between the reduction in residual and inclusion of a new predictor. The algorithm is terminated when the selection of additional predictors causes no reduction in model residuals according to the Bayesian Information Criterion (BIC). Here we choose a unique set of predictors based on the average BIC measure in all grids in a given region. The best regionally relevant predictors are then parameterized at each grid using the available data during a calibration period and tested during an independent validation phase.

5.3.3 Bias correction of gridded climate projections

While downscaled gridded climate data are able to reproduce the long-term statistical properties of the observations during a historical baseline, the sequencing of events in downscaled climate realizations can be quite different from observations (Ehret et al., 2012; Haerter et al., 2011; Johnson and Sharma, 2012; Sarhadi et al., 2018). In addition, currently available gridded

downscaled climate data are often developed globally (Giorgi et al., 2009; Karger et al., 2020; Navarro-Racines et al., 2020; Warszawski et al., 2014); and therefore, there might be regional biases in downscaled climate projections (Johnson and Sharma, 2012; Muerth et al., 2013; Ngai et al., 2017; Potter et al., 2020). As a result, there might be a need for further bias-correction when representing the monthly snow depth values as a time series are sought. Here we use the widely implemented quantile mapping bias-correction algorithm (Cannon et al., 2015; Maraun, 2013; Thrasher et al., 2012). In brief, this non-parametric algorithm uses the empirical Cumulative Distribution Functions (CDFs) of observed and downscaled climate realization to match the downscaled projections at a particular percentile level with the corresponding quantile of the observed gridded climate (Bürger, 2014; Ines and Hansen, 2006; H. Li et al., 2010). As empirical CDFs are used for bias-correction, the statistical moments of gridded observations are reproduced during bias-correction (Nsgai et al., 2017). For future periods, the procedure of bias-correction involves finding a change factor between the quantiles of future gridded projections, matching once with gridded observations and once with historical grided projections. This change factor is then applied to bias-correct future climate projection differently, depending on the nature of the variable considered. For temperature and precipitation, an additive and a multiplicative adjustments are suggested (see Bennett et al., 2011; Eisner et al., 2012).

5.4 Case study and data

With an area more than 0.9% of the global land area, Québec is the largest Canadian province. 176,928 km^2 out of 1,542,056 km^2 of Québec is covered by freshwater, making Québec the richest jurisdictionin Canada in terms of freshwater availability. Elevation in Québec varies from 0 to 1652 meters and the province includes various forms of vegetation type and landforms (*Atlas of Canada*, 2016). This diversity in land characteristics can be represented using eight distinct ecological units, known as ecozones (Lespinas et al., 2015; Schultz, 2005; Wiken, 1986). Ordered from north to south, Québec's ecozone includes Northern Arctic (EZ1), Southern Arctic (EZ2), Arctic Cordillera (EZ3), Taiga Shield (EZ4), Hudson Plains (EZ5), Boreal Shield (EZ6), Atlantic Maritime (EZ7), and Mixed-Wood Plains (EZ8). Figure 5.2 shown Québec in the Canadian context and delineates its ecozones. We select Québec as our case study because the entire area of Québec goes into FT cycles annually and the area is large enough to demonstrate the application of the proposed model at regional and global scales.

Our study benefits from various sources of publicly available gridded data products. The information related to historical snow depth is from the Canadian Meteorological Center (CMC; https://doi.org/10.5067/W9FOYWH0EQZ3). This data is provided by the National Snow and Ice Data Center archive at different spatial and temporal scales across the northern hemisphere over the period of 1999-2019. The dataset contains analyzed snow depth, obtained by combining the information from a set of in-situ snow depth measurements and optimal interpolation results of a simple physical snow accumulation and melt model. In-situ snow depth observations are also received from three different sources of surface synoptic observations, meteorological aviation,

and special aviation from the World Meteorological Organization (Brasnett, 1999; Brown and Brasnet, 2010). The snowmelt model utilizes the processed daily temperature and precipitation data from the Canadian forecast models. The data used for is study is at the monthly scale with the spatial resolution of 24×24 km^2.

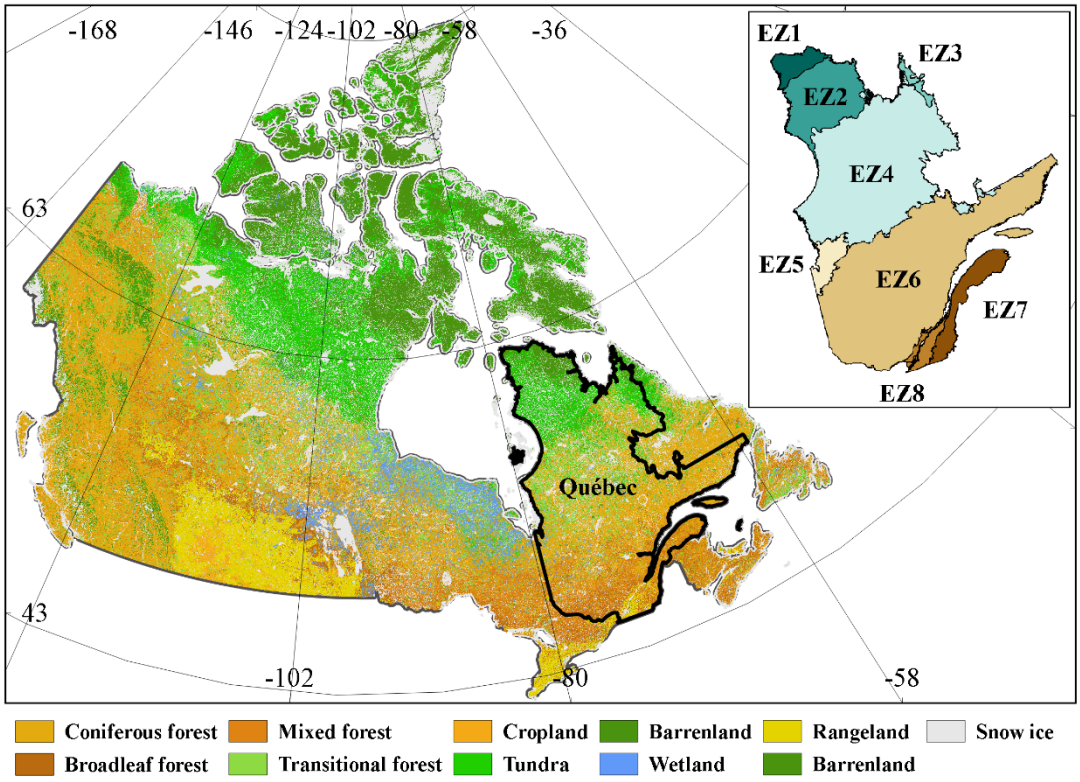

Figure 5.2 The province of Québec, Canada, and its eight ecozones.

The Global Meteorological Forcing Dataset (GMFD) hosted by Princeton University is used as the source of the observed climatic data. GMFD is available at https://hydrology.princeton.edu/data.pgf.php, with spatial resolution of 0.25°×0.25° over the period of 1950-2016. GMFD climate data are intended to form a benchmark forcing dataset by combining the reanalysis data from the National Centers for Environmental Prediction, National Center for Atmospheric Research, and a group of recent global observation-based data (Sheffield et al., 2006). It has been shown that GMFD has a higher accuracy comparing to the existing reanalysis products with better consistency over time and space (Bao and Wen, 2017; Jain et al., 2019). Daily values of maximum and minimum air temperature, from which the daily mean temperature is calculated and daily precipitation values are obtained from GMFD.

As the size and centroid of gridded snow depth and climate data are not the same, the raw data should be regridded in a common grid system before further use. Here we use the *k*-nearest neighbor interpolation methodology, which is a widely used approach to regridding (Hodgson, 1989; Östh et al., 2015). In brief, *k*-nearest neighbor is a non-parametric approach that uses the

information available from several neighboring cells in an initial grid system to estimate the information in a specific grid of the desired grid system. The cells chosen in the original domain are in the neighboring region of the desired grid in which the information should be estimated. We use the Euclidian distance to quantify the neighboring cells in the original space. A weighted distance averaging is then used to estimate the value of a given variable at the desired grid (see Cover and Hart, 1967; Steinfeld et al., 2020). Through some experimentations we identify $k = 4$, if the task is to achieve the highest accuracy in representing the first three statistical moments of the gridded data (i.e. mean, standard deviation, and skewness) across the eight ecozones of Québec (Hatami and Nazemi, 2019, 2021a, 2021b). To have a preliminary look at how regridded snow depth and temperature data are compatible, Figure 5.3 compares the monthly probabilities of temperature being below zero (panel a) against the monthly probabilities of having snow on the ground (panel b). These probabilities are obtained during the baseline period of 1999-2016, which is the common period in both GMFD and CMC. Months are shown in columns and ecozones in rows. Ecozones are ordered from the north (top) to the south (bottom). As it can be seen there is an overall match between the length of the cold season derived from temperature and snow. The cold season typically extends from September to June in the north (EZ1 to EZ3), but only from November to April in EZ8, the most south ecozone of Québec.

In addition to historical data, we obtain gridded daily maximum and minimum temperature and precipitation from NASA's Earth Exchange Global Daily Downscaled Projections (NEX-GDDP; https://www.nasa.gov/nex/). The periods of 1950-2005 and 2005-2100 are related to historical and prospective simulations, obtained from 20 climate models within the 5th Climate Model Intercomparison Phase (CMIP5) – see Jaramillo and Nazemi (2018) and Hassanzadeh et al. (2019) for specific models used. Future simulations are under two Representative Concentration Pathways (RCPs) of 4.5 and 8.5 W/m^2. NEX-GDDP uses the GMFD data for downscaling and is available at 0.25°×0.25° (Thrasher et al., 2012). The same 18-year period of 1999-2016 is considered as the historical baseline.

In parallel, in-situ data of temperature, precipitation, rainfall, and snowfall are obtained from 10 stations across the province to provide the data support needed for classifying the precipitation type (snow vs. rain) – see Table S1 for the name, location, and data period of these stations. The observed station-based climatic data are obtained from Environment and Climate Change Canada through Canadian Climate Data Accessibility Portal (CCDAP; accessible at https://www.concordia.ca/ginacody/building-civil-environmental-eng/research/water-security-climate-change-lab/data-applications/ccdap.html). We choose those climate stations with daily and finer observations that maintain long data availability (at least 20 years) and high data quality (less than 10% missing data during the data period).

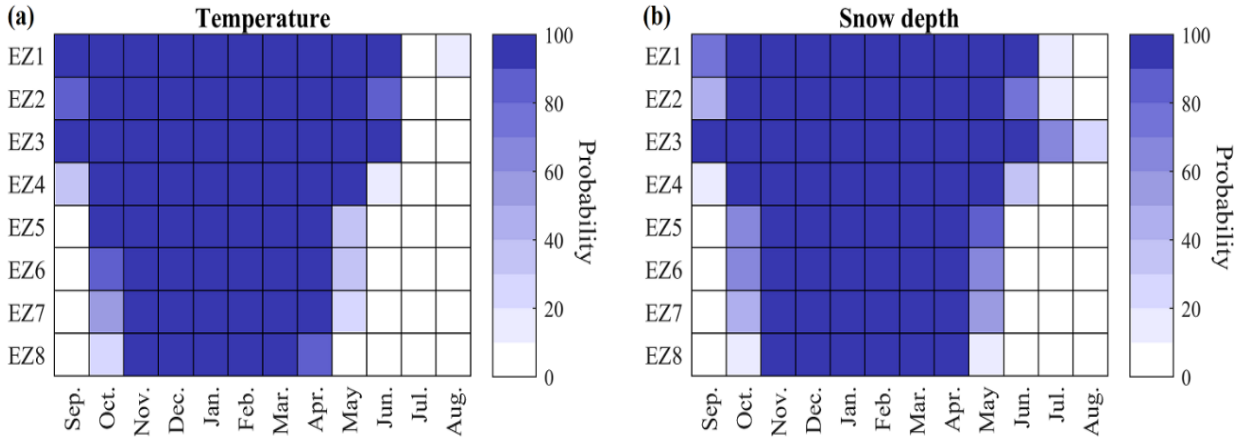

Figure 5.3 Expected probability of having (a) air temperature below 0°C, and (b) snow on the ground at each ecozone over a typical year. The data for temperature and snow depth are independent and are from GMFD and CMC respectively. Rows are related to different ecozones ordered from the north to the south. Columns are related to the months of the year.

5.5 Results

5.5.1 Model development

Classifying the precipitation type:

We use the in-situ observations in conjunction with a simple Bayesian Classifier to distinguish the form of precipitation using the approach explained in Section 5.3.1. To validate the credibility of the proposed approach, a couple of tests are performed. First, we use the developed Bayesian classifier to identify the type of precipitation in the considered stations using the observed precipitation and temperature data. Figure 5.4 demonstrates the expected percentage of misclassified daily data over each month in the 10 stations considered. The figure shows that the expected percentage of misclassified data is less than 5% in all months and across all stations considered. In general, the highest rate of misclassification is observed in April, which is the month in which precipitation swings between snow and rain quite frequently as it happens close to 0°C. As the second test, we consider the expected absolute error in the monthly ratio of snowfall to total precipitation (S/P); and accordingly, we monitor how the observed values of S/P at the 10 stations are preserved. We calculate the error in using the classifier when it is fed once with the in-situ data and once with gridded data of precipitation in which the considered station is located. This experiment can provide an understanding of the credibility of the proposed classifier when it is fed by the gridded data. The results of this experiment are depicted in Figure 5.5. The error in reproducing the historical S/P using in-situ and gridded data are shown with solid black thresholds and pink bars, respectively. As can be seen, the proposed classifier can effectively reproduce the in-situ notion of S/P using the gridded data. The overall error is reproducing S/P remains below 6% in all months and climate stations considered.

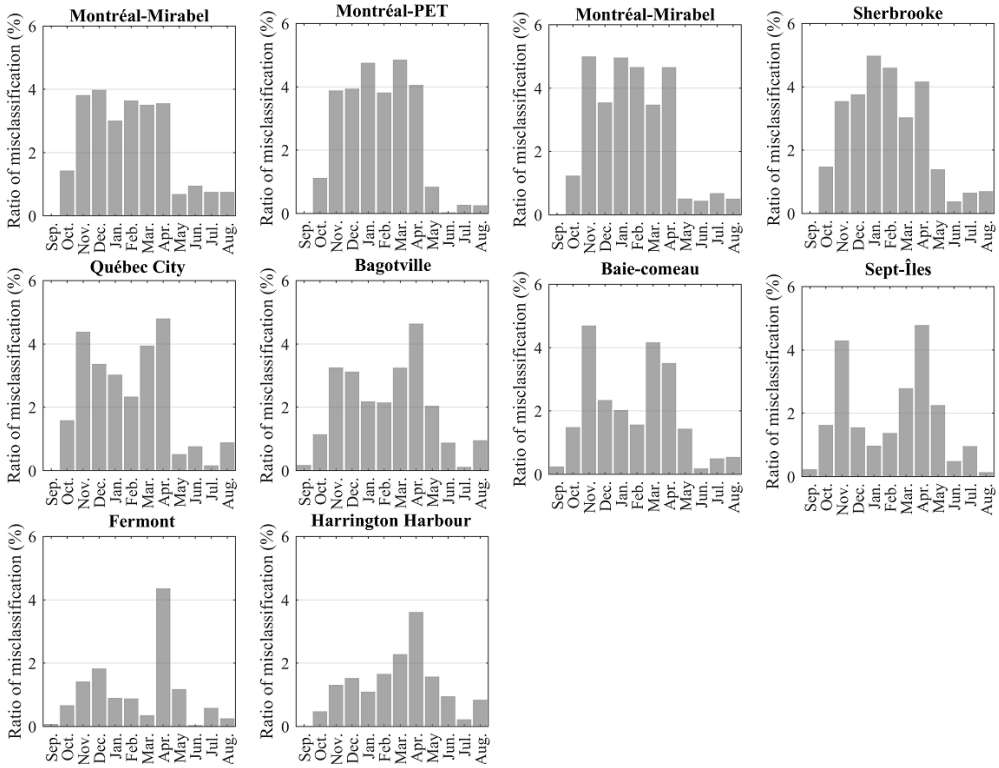

Figure 5.4 Expected percentage of misclassifying rain *vs.* snow using the proposed classifier and daily in-situ precipitation in each month and across 10 climate stations considered.

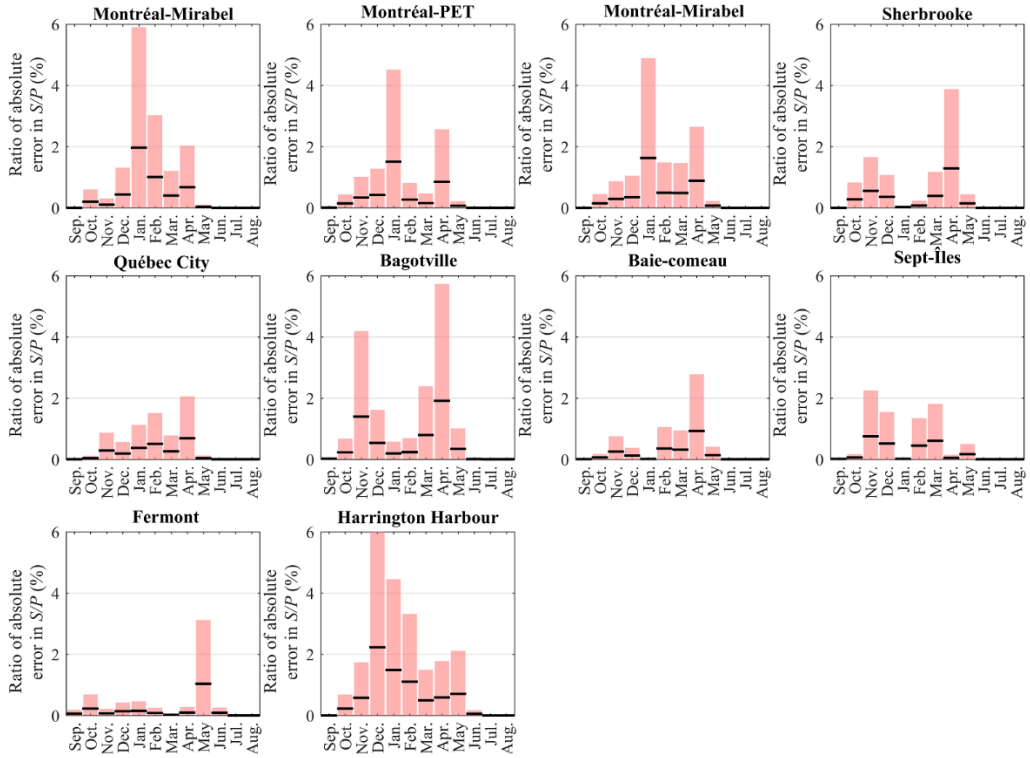

Figure 5.5 Expected absolute errors of the proposed classifier in reproducing the monthly ratios of snowfall to total precipitation in a typical year and across considered stations, when in-situ (thick threshold lines), and gridded precipitation (pink bars) are considered.

Regional climate proxies for representing snow depth dynamics:

Using the PCIS algorithm and the procedure outlined in Section 5.5.3, we extract the best set of climate proxies for modeling snow depth dynamics across each ecozone. This selection is made from a pool of primary climate variables (see Hatami et al., 2019b for the list of climatic proxies) and their cumulative values during a given year. The cumulative values representing the summation of each primary climate variable during a typical FT year (September to August; see Figure 5.3) and are considered to provide a notion for interannual variability. Table 5.1 summarizes the results for selected climatic proxies in each ecozone, in which the selected cumulative variables are shown with operator $cum\{.\}$. Looking at primary climatic variables, S/P is selected in all ecozones. S (monthly snowfall) is the second most chosen predictor from the pool of primary climatic proxies selected in half of the considered ecozones. Considering the cumulative variables, $cum\{\bar{T}\}$ and $cum\{S\}$ are the most frequent cumulative variables chosen in seven and four ecozones, respectively. It is also noted that the number of selected climate proxies strongly corresponds with the size of ecozones. While larger ecozones (e.g. EZ4 and EZ6) require more climate predictors, the dynamics of snow depth in smaller ecozones can be described by fewer climate proxies. Some regional patterns can be also witnessed. For instance, while S is selected as one of the dominant predictors in the northern ecozones (EZ1 to EZ4), $cum\{T_{max} - T_{mean}\}$ is selected as the represented of the interannual variability in the southern ecozones (EZ5 and EZ7).

Table 5.1 The list of selected climatic proxies across eight ecozones of Québec. The secondary cumulative proxies are shown with $\boldsymbol{cum}\{.\}$ operator.

Ecozones	List of selected predictors						
EZ1	$cum\{\bar{T}\}$	S	S/P	-	-	-	-
EZ2	$cum\{\bar{T}\}$	S	$cum\{S\}$	S/P	-	-	-
EZ3	$\bar{T}$	S	S/P	$cum\{S/P\}$	-	-	-
EZ4	$cum\{\bar{T}\}$	$T_{max} - T_{mean}$	$cum\{T_{max} - T_{min}\}$	$cum\{R\}$	S	$cum\{S\}$	S/P
EZ5	$cum\{\bar{T}\}$	$cum\{T_{max} - T_{mean}\}$	S/P	-	-	-	-
EZ6	$cum\{\bar{T}\}$	$T_{max} - T_{mean}$	$cum\{T_{max} - T_{mean}\}$	$cum\{R\}$	$cum\{S\}$	S/P	-
EZ7	$cum\{\bar{T}\}$	$cum\{T_{max} - T_{mean}\}$	S/P	-	-	-	-
EZ8	$cum\{\bar{T}\}$	$cum\{S\}$	S/P	-	-	-	-

Representing the monthly dynamics of snow depth at the grid and ecozone scales:

After selecting the best set of predictors for each ecozone, the observed monthly data over the period of September 2005 to August 2016 is used to extract the ranges of predictor and predictand variables for scaling purposes, calibrate the parameters of MLR models, and estimate the uncertainty bounds. The remaining of the observed period (September 1998 to August 2005) is used to investigate the model performance during an independent testing phase. Here we look at the skills in representing the monthly snow depth dynamics using the coefficient of determination (R^2) and Nash–Sutcliffe coefficient of efficiency (NSE). R^2 can assess the proportion of described variance in the simulated snow depth compared to the observed values (Legates and McCabe Jr.,

1999). In addition, NSE provides a normalized likelihood measure, similar to the Root Mean Square of Error (Ritter and Muñoz-Carpena, 2013). Figure 5.6 shows the range of NSE and R^2 at the grid scale (boxplots) during the testing phase and across each ecozone, identified with different colors. To provide a reference for the skills during the testing phase, the expected values in each ecozone during the calibration phase are shown with black dots.

Our results demonstrate that MLR can quantify the monthly dynamics of snow depth with high skills. The expected accuracy across all ecozones during the testing phase is marked by NSE $= 0.69$ and $R^2 = 0.74$. In general, the MLR models are found to be more accurate in northern or southern ecozones compared to the central regions (EZ4 to EZ6). The highest accuracy over the testing phase is observed in EZ3 (NSE $= 0.72$ and $R^2 = 0.77$) while EZ6 is the ecozone where the lowest accuracy is seen (NSE $= 0.61$ and $R^2 = 0.63$). Note here we use the best parametric estimates identified using the Maximum Likelihood Method. The issue of parametric uncertainty and how it propagates into the representation of the snow depth dynamics is discussed in Section 5.6.

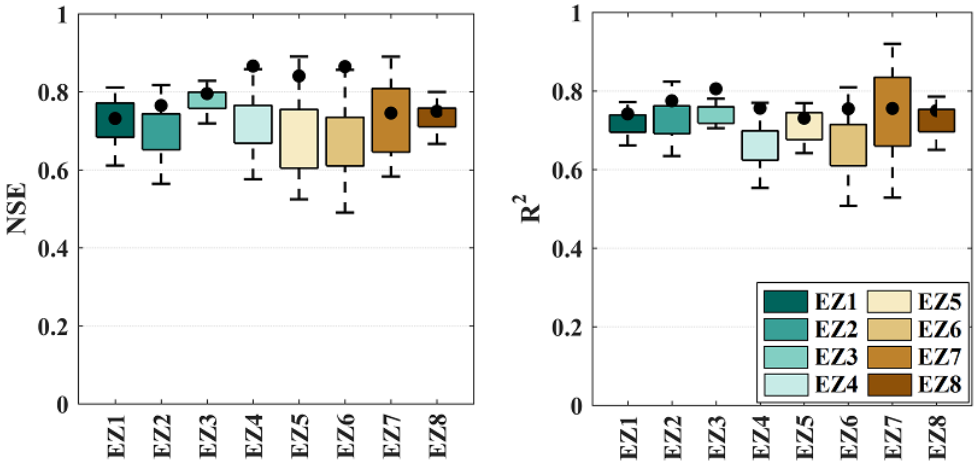

Figure 5.6 The performance of the proposed MLR models in representing gridded monthly snow depth across different ecozones measured using NSE (left) and R2 (right). The performance interval during the testing period is shown with boxplots. Dots show the average performance across each ecozone during the calibration period.

5.5.2 Model application

Quantifying the modeling performance over the historical period:

The results provided in previous section describe the use of the proposed statistical model when it is fed by the gridded observed data. When the model is applied for impact assessment, however, it should be fed by downscaled climate variables. Here we inspect how the proposed MLR models perform when they are fed with downscaled and bias-corrected climate projections. We accordingly compare the model performance with conditions in which the model is forced by

observed gridded data during the testing phase (September 1998 to August 2005). In Figure 5.7, the obtained ranges of the ratio of errors in total snow depth are displayed for each ecozone. To obtain the results using gridded downscaled climate variables, the calibrated MLR models are fed with the bias-corrected climate variables from the considered GCMs over each grid. The multimodel mean ensemble over each grid is then calculated. The relative error with respect to the gridded observed snow depth is then calculated for both cases of using gridded observed data and gridded bias-corrected data. The gray and colored boxes show the ratio of error in total snow depth using the gridded observed and gridded bias-corrected climatic data, respectively. Whiskers illustrate the range of gridded relative error over each ecozone. The filled and empty dots in each box show the mean values for relative error in each ecozone. Looking at the results, MLR show rather good performance in modeling the total snow depth in both cases of using gridded observed data *vs.* bias-corrected climatic values, with an average relative error of 3.2% and 3.7% over the ecozones. The lowest accuracy in modeling the total sow depth in both cases is observed in EZ5 (9.9% using the gridded observed data and 10.3% using the gridded bias-corrected values). The difference between the mean relative errors while using the gridded observed (filled dots) *vs.*bias-corrected data (empty dots) is higher in southern ecozones, specifically EZ7 and EZ6 with 2.7% and 1.6% difference, respectively. The good performance of the MLR models in representing the monthly dynamics of the observed period while using the bias-corrected climate variables compared to the case of using gridded observed climate data ensures the accurate projections of future conditions.

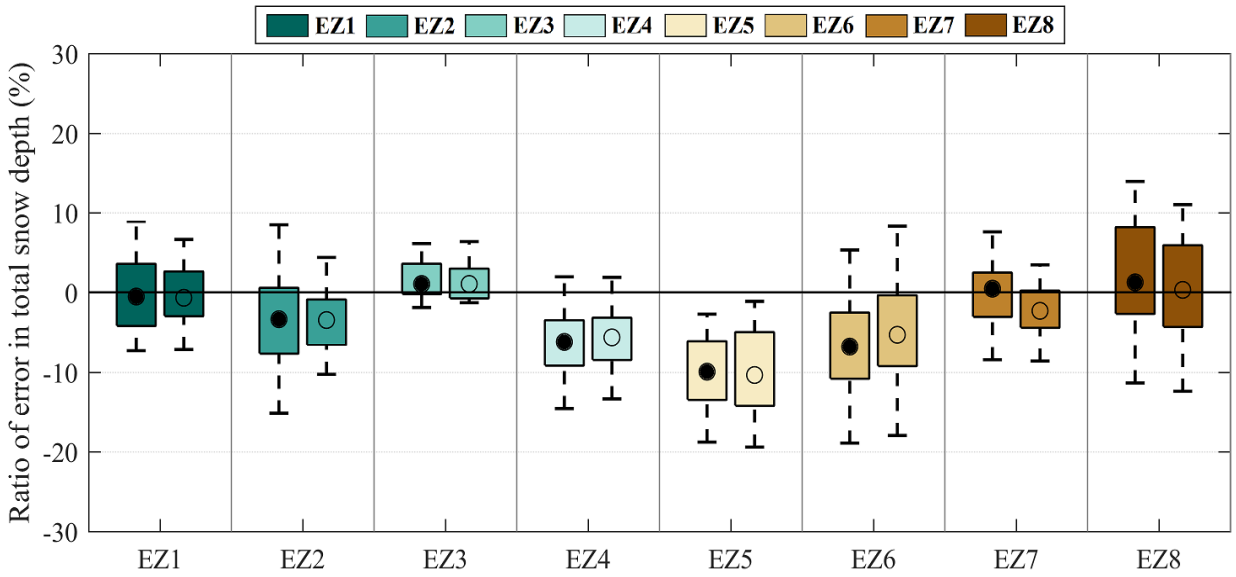

Figure 5.7 The ratio of error in total snow depth at grid scale in different ecozones using the gridded observed data (gray boxes) vs. the downscaled and bias corrected climate data (colored boxes) over the testing phase. The dots show the average values corresponding to each box.

Future changes in temperature, precipitation, and snow depth:

As discussed in previous sections, the MLR models are capable of preserving the observed dynamics of monthly snow depth over the observed period as well as capturing the statistical characteristics of snow depth over the historical period. To understand future changes in snow depth, we feed the developed regression models with the bias-corrected future projections of the 20 CMIP5 models under two RCPs. To show how changes in temperature and precipitation are translated to changes in snow depth, here, we investigate the spatial patterns of relative change in mean temperature, precipitation, and snow depth in the long-term future (2094-2100) compared with the present day. The term "present day" in this study refers to the 7-year historical period of GCM projections which is considered for the testing phase (1999-2005). Figures 5.8 and 5.9 display the multimodel mean ensemble changes in annual and winter's temperature, precipitation, and snow depth in the studied hydroclimatic variables by color hues and their agreements by color saturation, which is inversely proportional to the Coefficient of Variation (CV). The CV is defined as the percentage of the standard deviation between the expected changes in each variable from different GCMs divided by the multimodel mean values. This analysis not only reveals the information related to multimodal mean but also the uncertainty around this information (see Schewe et al., 2014). The first and second rows in Figures 5.8 and 5.9 show the results related to RCP4.5 and RCP8.5, respectively. Considering these figures, some general understandings related to future evolution in snow depth and its key climate variables can be revealed.

Considering Figure 5.8 related to annual analysis, the temperature is projected to increase under both RCP4.5 and RCP8.5. The rate of change in annual temperature is the highest in northern ecozones (i.e. EZ1 to EZ3) with an average of over 3.2℃ and 5.9℃ warming under RCP4.5 and RCP8.5, respectively. The lowest magnitude of the multimodel mean for annual temperature is observed in EZ7, experiencing an average increase of roughly 2.2℃ under RCP4.5 and 5.0℃ under RCP8.5. A relatively high level of multimodel agreement is observed between temperature projections with CV is ranging between 30 to 50% for both RCPs. Note that the quantile-based bias-correction applied to the GCM data substantially reduces the spread among the climatologies reconstructed by GCMs for the present day, but not among their future projections (Hempel et al., 2013; Schewe et al., 2014). Considering annual precipitation, relative changes in precipitation increase by moving from the south to the north, where an average change of 4 to 19% and 7 to 30% is observed in EZ8 to EZ1 under RCP4.5 and RCP8.5, respectively. Although a high agreement is observed across the northern ecozones (average CV of less than 30% for both RCPs in EZ1 to EZ3), there is substantial multimodel uncertainty in the projection of annual precipitation in the south, particularly under RCP4.5, where CV is more than 80% in some regions. Looking at future projections of snow depth, the mean ensemble of annual snow depth is projected to decrease across Québec with an average magnitude of 9cm and 18cm under RCP4.5 and RCP8.5, respectively. The rate of average change is increasing by moving from the south to the north. The highest magnitude of change is observed over EZ3 with expected changes of -13cm under RCP4.5

and -27cm under RCP8.5. A high level of agreement is observed in the projection of annual snow depth with CV ranging from 11 to 40% and 6 to 36% under RCP4.5 and RCP8.5, respectively.

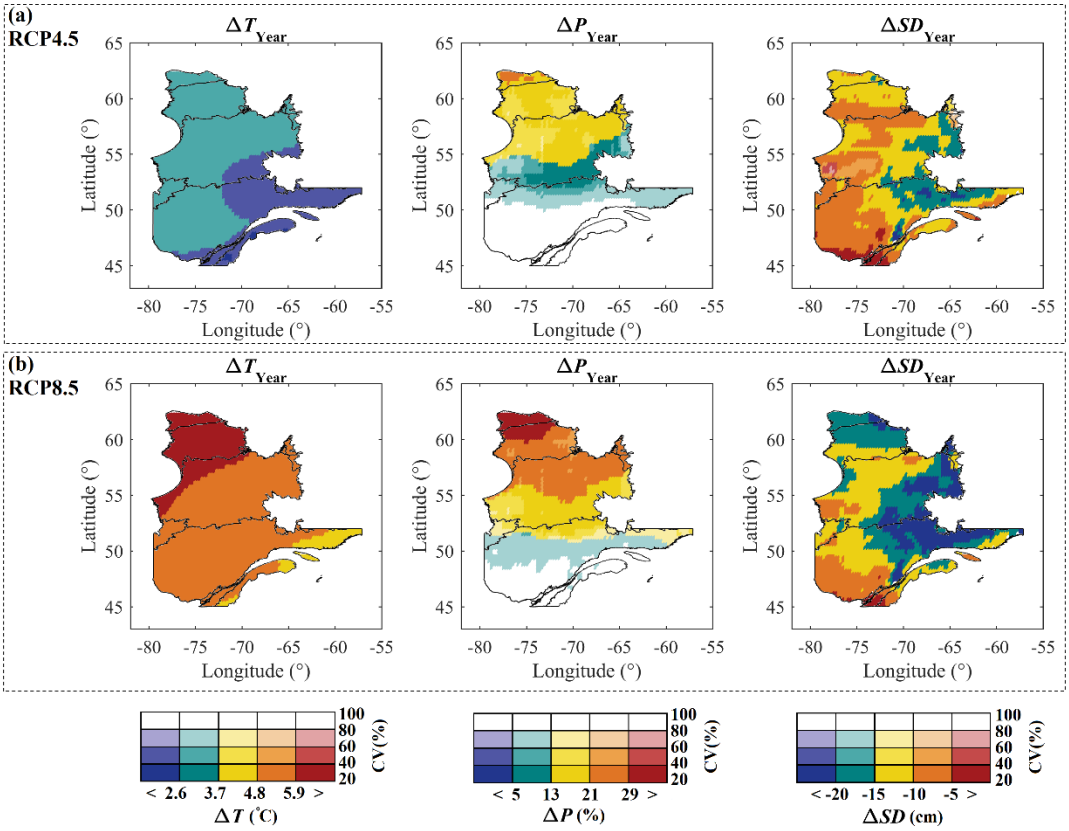

Figure 5.8 Changes in long-term annual temperature (°C), precipitation (%), and snow depth (cm) during 2094-2100 under RCP 4.5 (top) and RCP 8.5 (bottom) scenarios, compared to the present day, portrayed during 1999-2005. Color hues show the change inferred from the multimodel mean ensemble of 20 GCMs, and saturation shows the agreement between multimodel projections.

Considering Figure 5.9, warming is more intense during the winter, which is consistent with other studies across northern latitudes (IPCC, 2013; Rosenzweig et al., 2008; Smith et al., 2004). Based on our analysis and while the province experiences warming of around 6.6℃ under RCP4.5 and 9.7℃ under RCP8.5 during the winter season, the temperature in some northern regions can increase up to 9.7℃ under RCP4.5 and 14.5℃ under RCP8.5. A relatively high level of agreement across multimodel ensemble is observed during the winter, compared to the annual projection shown in Figure 8. The estimates of CV over all grids illustrate a variation of less than 20% and 17% under RCP4.5 and RCP8.5, respectively. Considering precipitation, the relative changes in precipitation increase moving from southern to northern parts of the province. Under RCP4.5 and RCP8.5, changes in winter's precipitation range from 10 to 55% and 12 to 64% under RCP4.5 and RCP8.5, respectively. Similar to temperature, a higher level of multimodel agreement is observed in the winter season comparing to the annual scale (Figure 5.8), particularly under RCP8.5. On average and based on multimodel mean ensemble, the decrement in snow depth across

the province during the winter season is expected to be -19cm under RCP4.5 and -27cm under RCP8.5. Compared to the annual scale, winter's snow depth is more vulnerable to changes in climate conditions, showing higher relative decreases in the magnitude of the multimodel ensemble mean across most ecozones compared to the annual scale. Similar to the annual scale, the highest decrements in snow depth during the winter season are observed in EZ3 that are 23cm under RCP4.5 and 34cm under RCP8.5. Also, a higher level of multimodel agreement is observed looking at the projection of decrements in snow depth during the winter season compared to the annual scale, highlighting higher confidence in the projections.

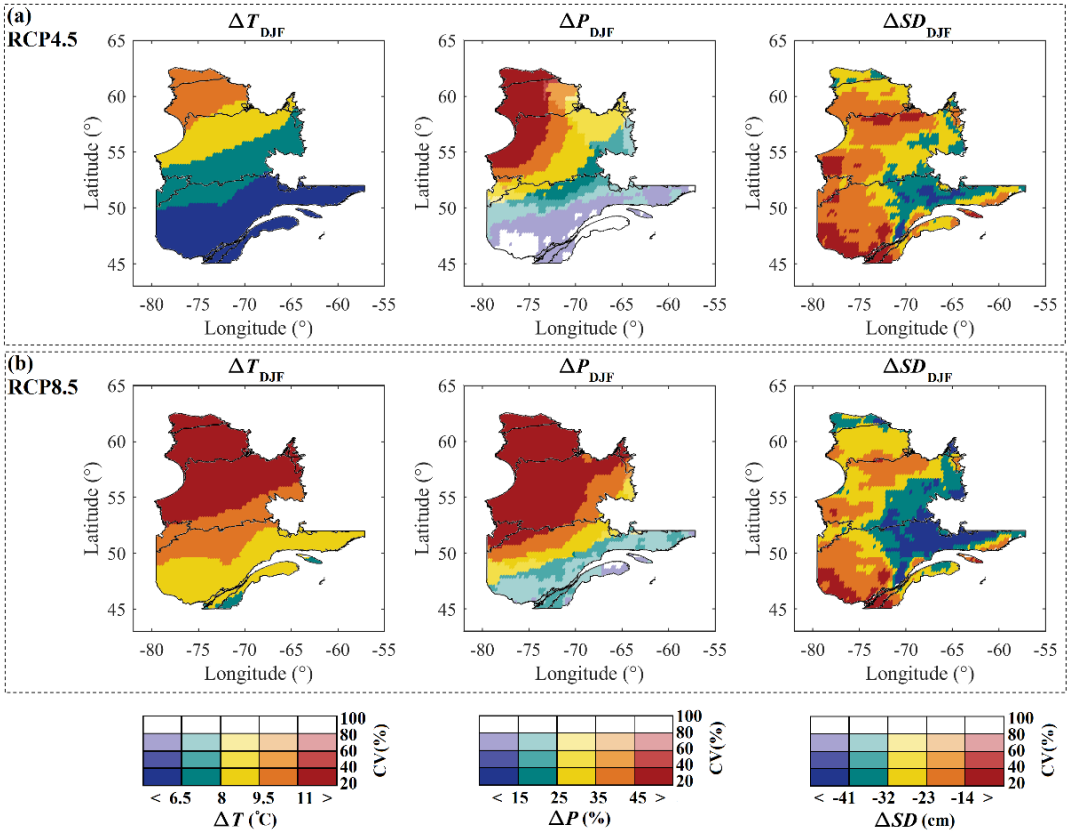

Figure 5.9 Changes in long-term winter's temperature (°C), precipitation (%), and snow depth (cm) during 2094-2100 under RCP 4.5 (top) and RCP 8.5 (bottom) scenarios, compared to the present day, portrayed during 1999-2005. Color hues show the change inferred from the multimodel mean ensemble of 20 GCMs, and saturation shows the agreement between multimodel projections.

5.6 Discussion

5.6.1 Assessing the need for downscaling

As noted above, one key issue is evaluating the need for further bias-correction. To formally inspect this, we feed the regressor models of snow depth once again with original NEX-GDDP data and compare the results with the snow depth simulations obtained using the bias-corrected NEX-GDDP data reported in Section 5.5 in terms of representing the dynamics of expected

monthly snow depth across each ecozone. Figure 5.10 summarizes the results of this comparison using Taylor Diagrams, which is an effective tool to integrated three different characteristics of the simulated snow depth in a single plot (see Jiang et al., 2020; L. Peng et al., 2018; Taylor, 2001). The top row (panel a) shows the Taylor Diagrams related to comparison between expected simulations and observations of temperature (left), precipitation (middle), and snow depth (right) using the original NEX-GDDP data over the testing period of 1999-2005. The bottom row (panel b) performs the same comparisons when the NEX-GDDP data are further bias-corrected. The three metrics summarized by each Taylor Diagram include the normalized standard deviation (radial distance from the origin), root mean square of error (RMSE; radial distance from the observed point), and correlation coefficient (cosine of azimuth angle). The color code corresponds to each ecozone and is defined in the legend. Dots with the same color show different GCMs in one particular ecozone. The closer the points are to the black dot on the *x*-axes, the better the simulations are.

Looking at Figure 5.10, it can be seen that bias-correcting the temperature and precipitation and feeding the regressors models of snow depth with these bias-corrected values improve all of the three considered characteristics. The least improvement while considering the bias-corrected values is observed looking at the monthly temperature. Using the original NEX-GDDP data, high compatibility with the observed values at the monthly temporal scale is observed (average correlation=0.94, RMSE=0.36, and standard deviation=0.97). Having said that, the quantile-based method for bias-correction of temperature exhibits higher correlation (average of 0.97), lower RMSE (average of 0.27), and normalized standard deviation closer to the observed values (average of 1.0). The variability between the results for different GCMs obtained using both original and bias-corrected temperature data are very similar for this variable. For monthly precipitation, an average correlation of 0.25, RMSE of 1.92, and standard deviation of 0.13 are observed while using the original NEX-GDDP data. However, these characteristics significantly improved when the bias-corrected data is taken into account (average Correlation=0.61, RMSE=1.21, and standard deviation=0.89). Higher correlation, lower RMSE, and closer normalized standard deviation for bias-corrected temperature compared to precipitation are consistent with many studies showing that the bias-corrected results obtained by precipitation correction methods demonstrate larger diversities than those produced by the temperature correction methods (Luo et al., 2018). Finally, looking at the monthly dynamics of snow depth, using gridded original NEX-GDDP climatic data the MLR models yield to the average Correlation=0.42, RMSE=1.84, and standard deviation=1.87. While using the bias-corrected climatic data as the input of regressor models of snow depth, on the other hand, the modeling performance is considerably improved in all of the studied ecozones and all considered 20 GCMs (average Correlation=0.82, RMSE=0.66, and standard deviation=0.81). While using the bias-corrected data, the variability in both precipitation and modeled snow depth is higher compared to the case of original NEX-GDDP data. The desirable performance using the bias-corrected temperature and precipitation, and corresponding modeled snow depth in representing the monthly characteristics of the observed period validates our assumption of the need for further bias-correction.

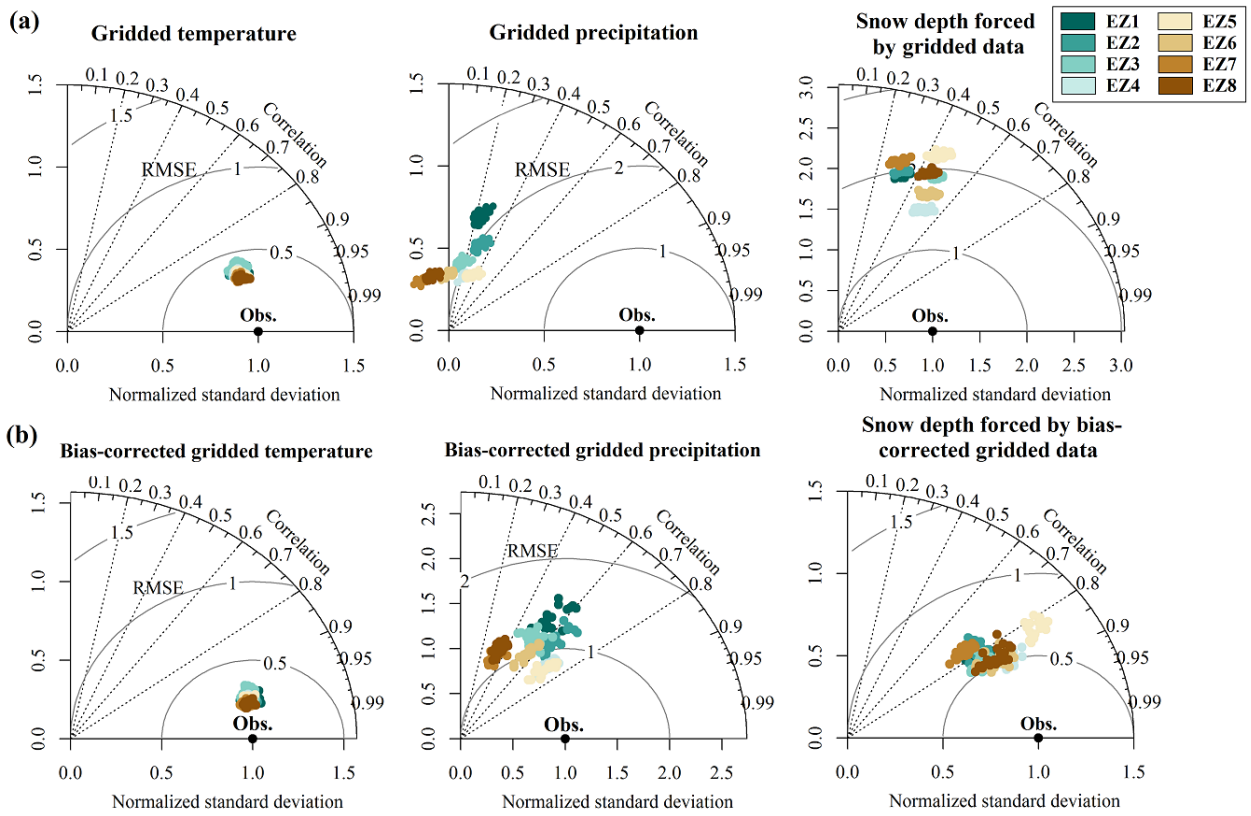

Figure 5.10 Taylor diagrams comparing observed gridded data against simulated temperature (left), precipitation (middle), and snow depth (right), obtained by (a) original NEX-GDDP data and (b) NEX-GDDP data that are further bias corrected. Colored dots represent the skill of 20 GCMs in capturing the expected snow depth across each ecozone

5.6.2 Evolution of snow depth in short-, mid-, and long-range futures

While Figures 5.8 and 5.9 show the changes in the long-range future compared to the present-day baseline using the GCM data, the pathways toward these changes are not investigated. Here, we look at how the changes in gridded snow depth evolve during short-range (2034-2040), mid-range (2064-2070), and long-range (2094-2100) futures compared to the present-day baseline (1999-2005). Figures 5.11 and 5.12 summarize the results of this analysis for annual and winter snow depth. In both figures, frames (a) and (b) are related to the simulation results under RCP4.5 and RCP8.5 respectively. In each frame, panels show the result for each ecozone ordered from the north to the south (i.e., EZ1 to EZ8) from the top left to the bottom right. Changes in future snow depth at each ecozone are shown in boxplots for the three time episodes considered. Whiskers illustrate the range of changes in the gridded snow depth obtained by the multimodel mean ensemble and dots show the expected change in the snow depth across the ecozone, inferred by the multimodel mean ensemble of simulated snow depth based on 20 downscaled and bias-corrected GCM simulations. In general, changes in annual snow depth are more vivid in northern ecozones (EZ1 to EZ4). The highest rate of change occurs in EZ3 and under long-range future,

where it is expected that on average the snow depth decrease by 13cm and 27cm under RCP4.5 and RCP8.5, respectively. It should be noted that there are ecozones in which some of the grids exhibit an increase in the snow depth. For instance, the average snow depth during the short-range future in EZ7 is expected to increase by 2cm under RCP4.5. In addition rates of decrement in annual snow depth increase in time, pointing at the possible amplifying impacts of climate change on the annual snow depth across the province.

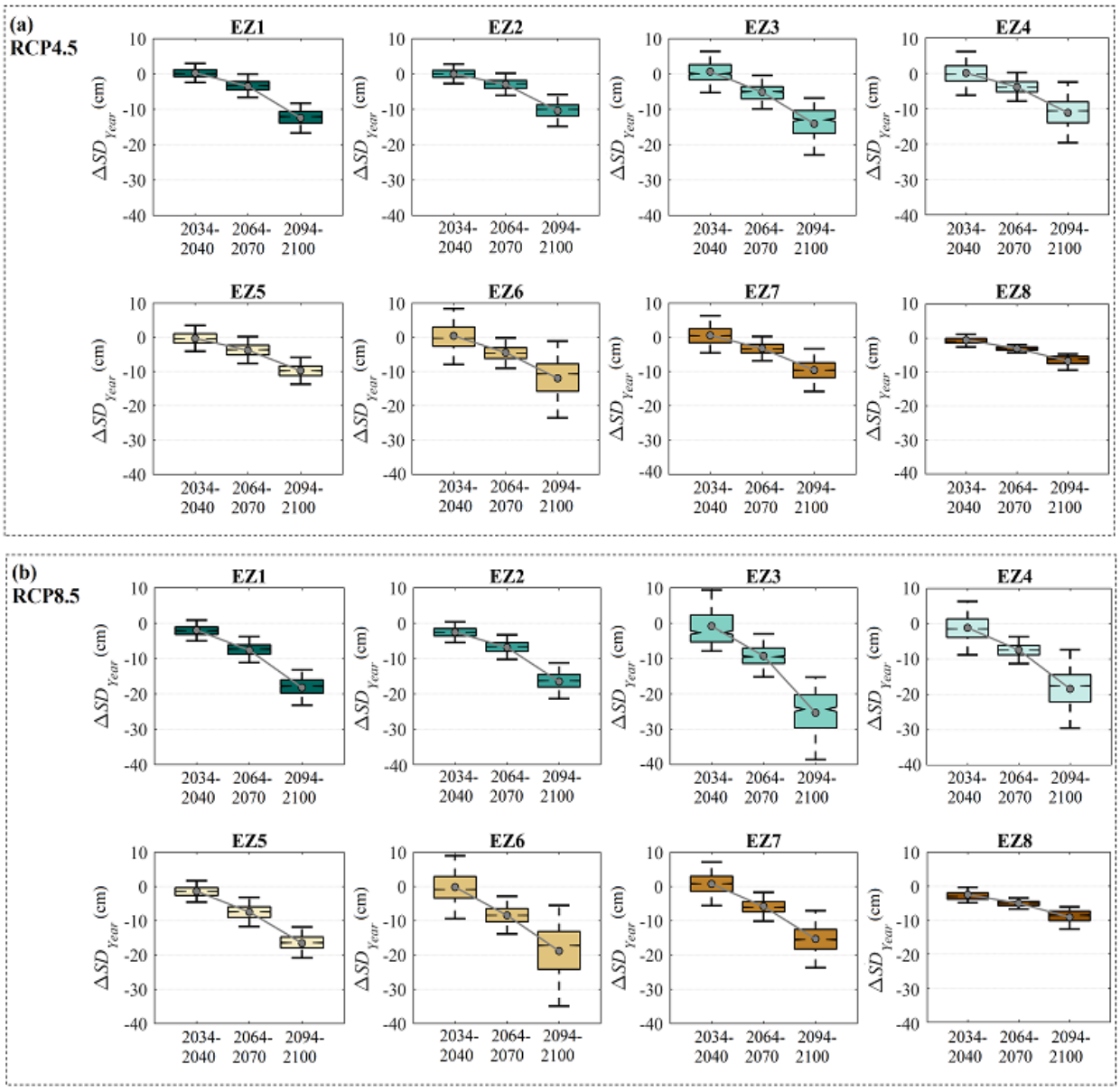

Figure 5.11 Changes in gridded annual snow depth under short-range (2034-2040), mid-range (2064-2070), and long-range (2084-2100) futures across Québec's ecozones under RCP4.5 (frame a) and RCP8.5 (frame b)

Similarly, we examine the evolution in future snow depth during the winter season across Québec's ecozones. Figure 5.12 summarizes the results. Again the northern ecozones show more severe decrements in future snow depth. The highest expected decrement occurring in EZ3 with 23cm and 34cm under RCP4.5 and RCP8.5, respectively. The temporal amplification in the snow depth decrements is also significant in southern ecozones. The highest rate of difference is observed in EZ6, in which the decrement in snow depth is around 21cm and 26cm RCP4.5 and RCP8.5, respectively.

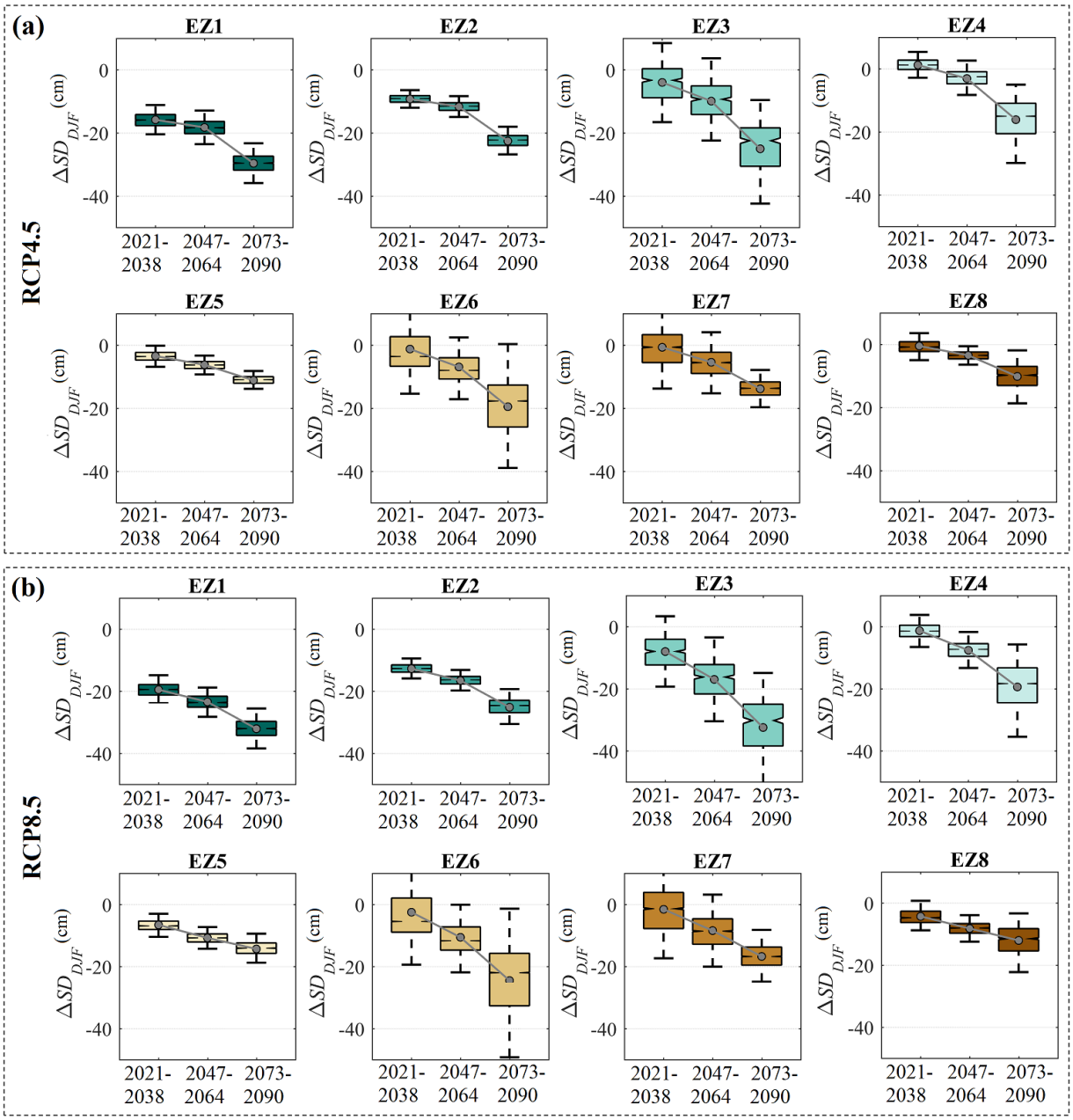

Figure 5.12 Changes in gridded snow depth during the winter season under short-range (2034-2040), mid-range (2064-2070), and long-range (2084-2100) futures across Québec's ecozones under RCP4.5 (frame a) and RCP8.5 (frame b)

5.6.3 The predictive uncertainty over observed and future periods

As the last step of our analysis, we aim to address the uncertainties related to MLR model parameters as well as uncertainties due to using different GCMs. For this purpose, the time series of expected observed monthly snow depth across each ecozone are compared with the simulated values using the bias-corrected climatic variables from different GCM models over the testing period of 1999-2005. Modeling the monthly snow depth using different GCMs provides an understanding of the predictive uncertainty. The parametric uncertainty associated with MLR model parameters is also considered as another part of this study. Figure 5.13 illustrates the response of snow depth models to the climatic inputs from each GCM as well as the 95% parametric uncertainty range obtained in each ecozone. The black solid lines display the expected observed values of monthly snow depth across different ecozones. The pink bounds correspond to the predictive uncertainty as a result of using different GCMs while the parametric uncertainty of MLR models is relaxed. The gray bounds correspond to the predictive uncertainty when both GCMs and the embedded parametric uncertainties in MLRs are considered.

To assess the parametric uncertainty, the 95% confidence intervals for model parameters are estimated at each grid using the maximum likelihood method during the calibration and then the expected values are obtained over each ecozone. Using these intervals, the monthly snow depth during the period of 1999-2005 is calculated considering a range of parameters between the obtained intervals of model parameters. The minimum and maximum bound from all GCMs are shown with the gray range. To quantitatively analyze the level of uncertainty we use the measure of Percentage Of Coverage (POC). POC assesses the number of observed data falling in the range of predictive and/or parametric uncertainties (Kasiviswanathan and Sudheer, 2013). Based on the results, it is evident that both of the gray and pink intervals contain most of the observed values. Looking at the pink bounds, i.e. the predictive uncertainty due to using different GCMs, the highest POC is observed in EZ6 with higher than 98% of points falling into the range of uncertainty bound. The lowest POC for pink bounds is observed in EZ3 with a POC of 85%. Moreover, the comparison of pink and gray bounds can provide an understanding of the contribution of the parametric uncertainty embedded in the MLR models to the total amount of predictive uncertainty. The narrower bounds are more preferable over large bounds indicating higher practical values. Looking at the gray bounds, the total predictive uncertainty considering both different GCM models and the parametric uncertainties in MLR models, although the POC is higher than 99% in all ecozones, the wide range of uncertainty due to the parameterization of MLR models (i.e. the difference between gray and pink bounds) in EZ3 and EZ6 made the modeling performance less desirable in these ecozones. However, the modeling practicality is considerably higher in EZ1, EZ2, and EZ8.

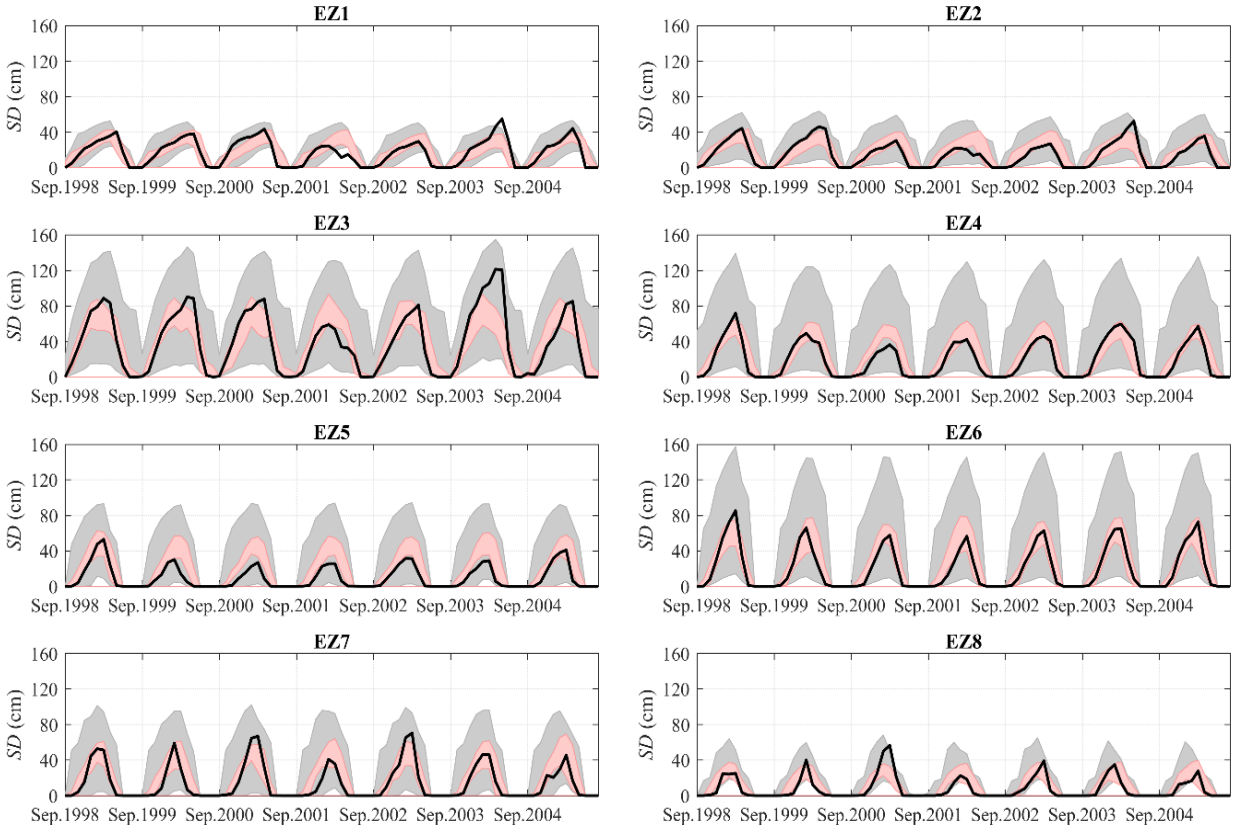

Figure 5.13 The predictive uncertainty of MLR models in representing the monthly snow depth over the ecozone scale during the period of 1999-2005. Black solid lines are the expected observed monthly snow depth across the ecozones. The pink and gray shadings cover the uncertainty due to employing climatic data from different GCMs and the 2.5th to 97.5th percentiles of parametric uncertainties of MLR model parameters for different GCMs, respectively.

The predictive uncertainty over the future period is also investigated at grid scale by obtaining the 95% confidence intervals for all considered GCMs over the long-range future (2094-2100). For this purpose, the multimodel mean changes in snow depth are obtained for the lower and upper bound of the predictive uncertainties at each grid. Figures 5.14 and 5.15 display the ranges of the multimodel mean changes in annual and winter's snow depth, respectively. The results for RCP4.5 and RCP8.5 are presented in the first and second rows in each figure, while the first and second columns correspond to the lower and upper bounds, respectively. The color hues are similar to those used to showcase the multimodel mean changes in annual and winter's snow depth for Figures 5.8 and 5.9. To analyze the range of predictive uncertainty we obtained the difference between the 2.5th and 97.5th uncertainty bounds at grid scale and then get the average values for each ecozone. Looking at the predictive uncertainties in annual snow depth under RCP4.5 (Figure 5.14, first row), the widest range is observed for EZ3 and EZ6 similar to the results over the historical period. In EZ3, for instance, the multimodel mean for the lower and upper bounds -3 and -23cm, showing an uncertainty bound of 23cm for RCP45. The lowest bounds, in this case, are observed in EZ8 and EZ1 with the lower and upper bounds ranging between -3 to -11cm and -9 to -18, respectively. Similarly, for RCP8.5 (Figure 5.14, second row), in EZ3, the uncertainty bound

is 26cm with the multimodel mean for the lower and upper bounds ranging from -4 and -31cm. The two ecozones having the narrowest predictive uncertainties bounds are EZ8 (with the bound of 12cm) and EZ1 (with the bound of 17cm). However, in this case, the overall predictive uncertainties are slightly higher compared to RCP4.5.

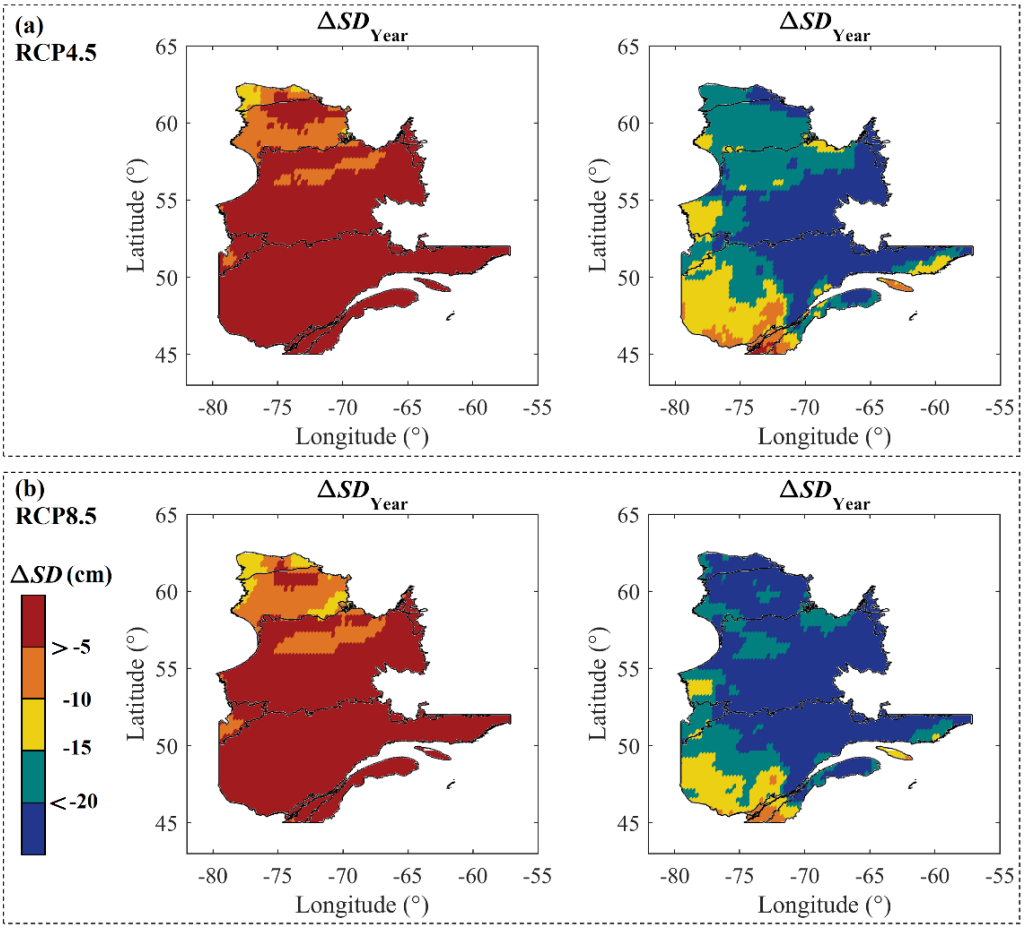

Figure 5.14 The predictive uncertainty of MLR models in representing the future annual snow depth over grid scale during the long-range future projections (2094-2100). Color hues show the multimodel mean change.

Looking at the uncertainty bounds for winter's snow depth (Figure 5.15), the uncertainty bounds are rather wider compared to the annual ranges. For RCP4.5 (Figure 5.15, first row), the range of predictive uncertainty is the lowest in EZ1, EZ2, and EZ8, with a bound of less than 18cm. The highest range of uncertainty bounds for the changes in winter's snow depth is observed in EZ3 and EZ7 with the lower and upper bounds ranging between -8 to -56 and -2 to -45, respectively. Finally, looking at the range of change in winter's snow depth under RCP8.5 (Figure 5.15, second row), it can be observed that the uncertainty bounds are slightly wider compared to that of RCP4.5. The lowest bounds, in this case, are observed in EZ1, and EZ8, with the bound of less than 23cm while the highest uncertainty is observed in EZ7 and EZ3 with the bounds of 58 and 51cm, respectively.

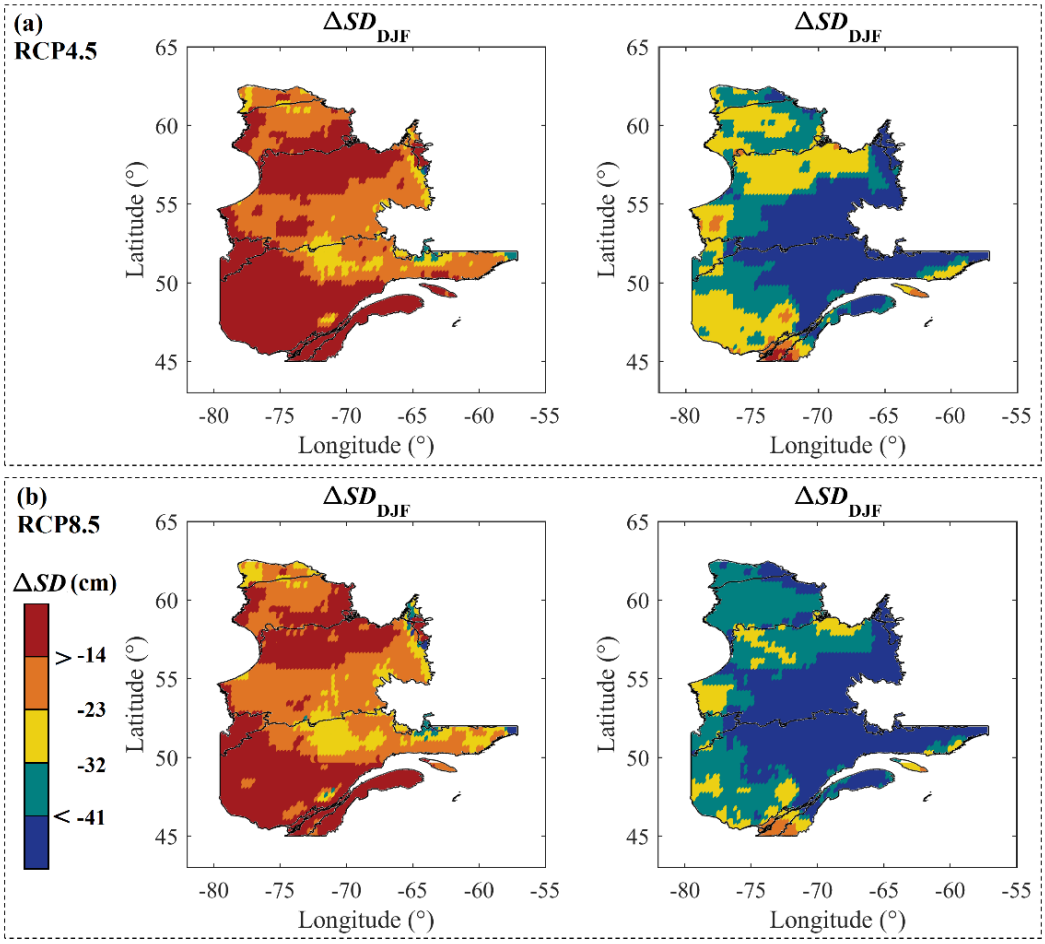

Figure 5.15 The predictive uncertainty of MLR models in representing the future winter's snow depth over grid scale during the long-range future projections (2094-2100). Color hues show the multimodel mean change.

5.7 Conclusions

FT dynamics are among the most important components of the cryosphere across higher latitudes, controlling the regional hydrology, phenology, and land-atmospheric interactions. Changes in FT characteristics can further create feedback effects with other elements of the environment. These changes can, for instance, unleash a substantial amount of greenhouse gas fluxes into the atmosphere due to the thawing of the previously frozen soil and consequently intensifying the rate of the warming climate. Due to these impacts, projecting the future FT dynamics is an important consideration point for advising land management and adaptation strategies in northern communities. The role of changing temperature and snow depth, as the two most important climatic drivers of landscape FT, has been the subject of many studies. Having said that, few challenges are in the way of projecting the future dynamics of FT characteristics under changing climate. First, the use of readily available downscaled data needs to be validated. Second, the future gridded snow depth dynamics must be projected. And third, any possible change in the dependence structure between temperature, snow depth, and FT dynamics must be quantified and taken into

account. In Part 1 of this double feature article, we address the first two highlighted challenges. Proposing a statistical framework, fusing MLR and an input selection scheme, we formally assessed the need for further bias correction of available downscaled data and consequently project the future dynamics of gridded monthly snow depth across different ecozones of the province of Québec, Canada.

First, we classify the form of precipitation using a simple Bayesian Classifier calibrated with station-based climate data. Due to the good performance of the calibrated classifier in modeling the form of precipitation over all of the considered stations, we upscaled the calibrated classifier to extract the threshold of temperature at which the type of precipitation is changing from snow to rain. The type of precipitation is then classified for all the grids across the province. The PCIS scheme is then used to obtain a unique set of predictors for all grids in each ecozone of the province. This regional input selection scheme allows for considering the role of ecosystem conditions, such as vegetation type, soil type, land cover, etc. in regulating the impacts of changing climate on the dynamics of snow depth. MLR models are then calibrated at grid scale using the observed gridded data. We show that calibrated MLRs can accurately quantify the monthly dynamics of snow depth with R^2 of 0.74 over the ecozones of Québec. Higher accuracy is observed in northern or southern ecozones compared to the central regions highlighting the better performance of the proposed statistical approach in smaller ecozones. The developed MLRs are then applied for projecting the future dynamics of snow depth over different future time episodes. For this purpose, we first quantify the modeling performance in representing the monthly dynamics of snow depth in case of using the bias-corrected climate data over the testing phase over the period of 1999-2005. Looking at the results, the proposed framework shows similar performance in modeling the total snow depth case of using bias-corrected values compared to the conditions in which the model is forced by observed gridded data, with an average relative error of less than 4% over the studied ecozones. The good performance of the MLR models in representing the monthly dynamics of the observed period while using the bias-corrected ensures the accurate projections of the future conditions. As the next step, we looked into the future changes in snow depth. The multimodel mean across all GCMs exhibits a number of robust large-scale features. In particular, an increasing rate of change in snow depth is observed moving from southern to northern ecozones. The highest decreasing magnitude of annual snow depth is projected for the Arctic Cordialla with an average decrease of 13cm to 27cmunder RCP4.5 and RCP8.5, respectively. Moreover, we further investigate the need for further bias-correction of already available downscaled climate data by assessing the performance of calibrated models in representing the monthly dynamics of snow depth in case of using both original *vs.* bias-corrected data sets. Based on our results, the developed models fed with already available downscaled data are not capable to capture the monthly dynamics of snow depth over the historical period over the testing period of 1999-2005. Hence, further bias-correction is required. In the case of using bias-corrected data, on the other hand, the good performance of developed MLRs ensures accurate projections of future conditions. Furthermore, we compared the changes in future snow depth over different future time episodes. Based on our results, the changes in annual and winter's snow depth show a significantly

amplifying pattern over time specifically across northern ecozones under RCP4.5 and RCP8.5. Finally, we looked into the predictive uncertainties related to the proposed framework. Based on our results, although the predictive uncertainty intervals contain most of the observed values, the narrower uncertainty bounds in Northern Arctic, Southern Arctic, and Mixed Wood Plains over observed and future periods show the higher practicability of the proposed framework in these ecozones.

Chapter 6.

A Multivariate Statistical Framework for Top-down Projections of Freeze-Thaw Characteristics under Changing Climate – Part 2: Development of a Time-varying Conditional Model and an Integrated Impact Assessment[6]

The contents of this chapter are in preparation as "A Multivariate Statistical Framework for Top-down Projections of Freeze-Thaw under Changing Climate Conditions – Part 2: Development of a Time-varying Conditional Model and an Integrated Impact Assessment" for submission to the Journal of Earth's Future.

Synopsis

The dynamics of Freeze-Thaw (FT) significantly impact eco-hydrological processes and socio-economic activities across cold regions. Climate change, however, greatly alters the FT dynamics through changes in the two influential hydroclimatic variables, namely air temperature and snow depth. Accurate quantification of the future state of FT dynamics, hence, is essential for advising adaptive strategies for future human developments and land management. Here, a statistical framework is proposed for the top-down projection of FT dynamics conditioned to a wide range of air temperature and snow depth scenarios over coarse spatial and temporal scales. The future projections of temperature and snow depth are obtained using a quantile-based bias-correction method as well as a statistical framework defined in Part 1 of this double feature paper. A time-varying copula-based approach is used to quantify the statistical characteristics of landscape FT based on joint characteristics of air temperature and snow depth. The model is equipped with a regression-based scheme to update the model parameters over time based on a set of hydroclimatic proxies as the model predictors. The model is then implemented for the projection of FT dynamics in the province of Québec, Canada. We investigate the changes in future FT characteristics conditioned to historical and future air temperature and snow depth scenarios. Results show that the proposed model can well capture the marginal and joint characteristics of FT dynamics, demonstrating $R^2 > 0.92$ and $NSE > 0.89$ in representing the observed annual number of frozen days. The model also performs well in representing the observed number of days with the transient state in winter with $R^2 > 0.89$ and $NSE > 0.72$. Looking at the future changes in studied FT characteristics over time demonstrates an amplification in the rate of changing FT dynamics due to changing climate. The result of impact assessment under future conditions demonstrates that in the northern ecozones the changes in the annual number of frozen days are more pronounced and are projected to decrease by more than 15 days due to 2℃ increasing temperature and 5cm decreasing snow depth. In the southern ecozones, however, changes in the number of days with the transient state in winter are more remarkable and are projected to increase more than 6 days

[6] Hatami, S., Nazemi, A. (2021). A Multivariate Statistical Framework for Top-down Projections of Freeze-Thaw under Changing Climate Conditions – Part 2: Development of a Time-varying Dependence Model and an Integrated Impact Assessment. *Earth's Future*, (In preparation).

due to 2℃ warming and 5cm decreasing snow depth. The proposed framework is globally relevant and can be employed for top-down impact assessment and to statistically address the compound impacts of changes in different variables on any environmental processes over any spatial and temporal scales.

6.1 Introduction

The dynamic of Freeze-Thaw (FT), as one of the most important land-surface characteristics, is greatly affected by climate change through changes in air temperature and snow depth (Plaza et al., 2019; C. Wang et al., 2019). Around one-third of the global land area exhibits seasonal FT transitions and these transitions are likely to show an increasing rate of change under future climate change (Shati et al., 2018). Regionally these changes differ, with generally larger changes in FT dynamics at northern latitudes due to greater rate of climate change in these regions (Kim et al., 2011). In high-latitude regions, mean annual surface air temperature increased at rates of up to $\sim 0.7^{\circ}C$ per decade during the latter half of the 20th century (Hansen et al., 1999; Smith et al., 2004). Increases in air temperature have resulted in increases in an active layer thickness of soil and permafrost degradation (Chen et al., 2003; T. Zhang, 2005). Decreasing snow depth, which exists between the atmosphere and the ground surface, is another key factor influencing the FT dynamics through changes in the ground thermal regime in cold regions (Atchley et al., 2016; T. Zhang, 2005). Such changes can alter FT dynamics which in turn may damage infrastructure (Nelson et al., 2001), impact on landscapes and ecosystem functioning (Frauenfeld et al., 2004; Smith et al., 2004; Wu et al., 2018), lead to the release of carbon stored in frozen soils (Kurganova et al., 2007), alter energy exchange between land and atmosphere (M. Yang et al., 2007), and influence biogeochemical processes (Duan et al., 2012; K. Yang et al., 2014). Hence, quantifying potential changes in FT characteristics under future climate conditions is essential for understating their diverse socioeconomic and environmental consequences, and to develop mitigating strategies to adapt to changing conditions (e.g., Zwissler et al., 2014).

Several methodologies have been suggested to assess the impacts of changing climate on FT dynamics. Based on International Panel for Climate Change (IPCC) suggestion, these approaches are mainly through a top-down (a.k.a, "scenario-led") impact assessment paradigm in which the downscaled GCM projections are often used in conjunction with impact models (IPCC, 2007, 2014, 2021). The impact assessment studies through scenario-led approaches can be categorized into two fundamental groups of temperature-based and RCP-based scenarios. In temperature-based top-down impact assessment, results are presented as a function of global mean warming above the present day to allow for systematic comparison of climate change impacts across temperature scenarios (e.g., Frieler et al., 2012; Schewe et al., 2014; Tang and Lettenmaier, 2012). In RCP-based impact assessment, the results are presented for short-, mid-, and long-range futures under different RCPs to allow for impact assessment conditioned to different emission pathway scenarios (Gusain et al., 2020; Lotze et al., 2019; Mehran et al., 2017). In classic top-down approaches, GCM projections serve as inputs to physically-based models embedded in land surface

models with which FT dynamics can be simulated (Huang et al., 2018). Such approaches require modeling of complex soil-water dynamics which includes water, heat, and solute transfer through conduction due to soil temperature profile and convection because of migration of water in the soil (Flerchinger and Saxton, 1989; Li et al., 2012; X. Zhang et al., 2021). Qi et al., (2016a,b), for instance, developed a physically-based soil temperature module to simulate the FT dynamics by considering the soil thermal status and snow insulation effects. Such physically-based approaches can often represent the FT dynamics accurately at a local scale by using the in-situ data (Walvoord and Kurylyk, 2016). However, capabilities for global monitoring to capture FT spatiotemporal dynamics are severely constrained by generally sparse global weather station networks, particularly at higher latitudes and elevations (Henry, 2008; Rawlins, M.A. et al., 2005; K. Wang et al., 2015). Additionally, these approaches are hugely data-intensive, subject to large uncertainty due to model structure and parametrization, and require site measurements and monitoring in a harsh environment and complex landscape at a regional scale. Such limitations preclude the understanding of soil FT dynamics and changes at large temporal and spatial scales.

In response to these limitations, alternative approaches for top-down impact assessment of FT dynamics have been suggested. These approaches are mainly through the use of GCM projection along with a statistically-based impact assessment paradigm (Hatami and Nazemi, 2019; Lemoine and Kapnick, 2016). Statistical approaches are generally more computationally efficient and require less data support than process-based models and thus often have a better transferability as well as scalability at large temporal and spatial scales (Ni et al., 2021; Zheng et al., 2020). The key advantage of such approaches is in providing the opportunity for the modeling of FT characteristics across coarser temporal and spatial scales instead of continuous modeling of FT dynamics using complex physically-based approaches. Sinha and Cherkauer (2008), for instance, used a statistical framework to analyze the changes in the FT states and the climatic factors such as air temperature and precipitation, demonstrating significant reductions in the number of frozen days along with increasing seasonal mean maximum temperature at all studied sites. Han et al. (2021) employed a machine-learning algorithm to characterize the spatiotemporal dynamics of FT at the largest lake in China, showing remarkable changes in the spatial distribution of FT dynamics in the early 21st century. Ni et al. (2021) used statistical and machine-learning approaches to simulate the present and future changes in an active layer of soil, demonstrating pronounced changes in a soil layer in the future. Despite many advances in the use of machine-learning approaches, such methodologies are limited in addressing uncertainty, and cannot fully reproduce the probabilistic dynamics of the hydroclimatological variables in time and space (Lall et al., 2016). Recently, copula-based models have gained popularity in hydroclimatology and applied in probabilistic analysis, prediction, and projection of hydroclimatic variables (Das et al., 2020; Genest et al., 2007; Nazemi and Elshorbagy, 2012, Nazemi et al., 2020; Pandey et al., 2018, Zaerpour et al., 2021b). Copula methodology – a generic multivariate approach to characterize statistical dependence – can bring a formal solution to the above-mentioned limitations and provide a basis for modeling FT dynamics conditioning to influencing climate variables. The main advantage of copula is its flexibility to model the dependence structure between different random variables independently of

their marginal distributions (Genest and Favre, 2007; Salvadori and De Michele, 2004). Providing distributional properties of involving variables, copula has been widely used in multivariate hydrological risk assessment. Additionally, copulas show that the exceedance probability of a multivariate event can emerge by an infinite number of possible combinations rather than from only the observed combination, thus they offer a more advanced approach to address uncertainties in the modeling of the hydroclimatological variables (Sadegh et al., 2017).

Despite the advances in copula-based approaches, there are two major drawbacks in the early applications of such models. Most of the studies focus only on bivariate copulas, limiting the potential for incorporating simulations of several climate mechanisms (Salvadori and De Michele, 2007; L. Zhang and Singh, 2006). Additionally, traditional copula-based methodologies are based on the fundamental assumption of statistical stationarity (Grimaldi et al., 2016; Hao and Singh, 2016). Under stationarity, it is assumed that probabilistic characteristics of hydrometeorological processes and the dependence structures between variables will not change over time. This is in contrast to the empirically observed time-varying dependence structures between hydroclimatic variables (Chebana and Ouarda, 2021; Dong et al., 2021; C. Jiang et al., 2015). Milly et al. (2005, 2008) argued that the fundamental assumption of stationarity has been influenced by climate change and human activities, and therefore it is no longer applicable for future projection of hydroclimatic variables (Chebana et al., 2013; Hao and Singh, 2015). Although modeling the nonstationary features of individual variables such as trends in the moments of a single variable are often taken into account in the literature (Prosdocimi et al., 2014; Read and Vogel, 2015; Serinaldi et al., 2018; Silva et al., 2012), yet it is not straightforward to model the nonstationarity in the dependence structure (Hao and Singh, 2016; Huser and Genton, 2016; Jonathan et al., 2014). Hence, suitable statistical advancements are required to identify and incorporate the nonstationarity features such as time-varying dependence structure for facilitating improved engineering design in a changing climate (Bender et al., 2014; Borgomeo et al., 2014; Rootzén and Katz, 2013; Sarhadi et al., 2016; Serinaldi and Kilsby, 2015).

Here, we propose a time-varying multivariate statistical framework for the top-down projection of FT dynamics under future changing conditions. For this purpose, we employ a dynamic vine-copula approach to characterize the future FT dynamics conditioning to the main influencing climatic variable. The copula method enables the modeling of symmetric/asymmetric dependence structure between climatic variables and FT dynamics. To account for the nonstationary dependence structure between hydroclimatological variables, we utilize a dynamic copula equipped with a regression-based statistical scheme to update the copula parameters over time. The proposed framework is then applied for future projection of FT dynamics at a large region in the northern latitude, i.e. the province of Québec – the largest province by area in Canada and the richest in terms of the ecosystem diversity and availability of freshwater resources. The remainder of the paper is structured as follows. Section 6.2 presents the proposed methodology. Section 6.3 introduces the data support. Section 6.4 and 6.5 provides the results and discuss the findings. Finally, Section 6.6 concludes the paper and outlines further researches.

6.2 A Framework for top-down projections of freeze-thaw

6.2.1 Rationale

As discussed in the "Scope and problem definition" in Part 1 of this paper, in Part 2 we aim at developing and applying a dynamic copula-based sampler to project the future dynamics of FT characteristics conditioned to temperature and snow depth. For this purpose, to match the size and centroid of FT characteristics, temperature, and snow depth, we first re-grid these data sets into a unique spatial and temporal scale. Then we extract a set of FT characteristics with physical relevance at grid scale. The properties of considered FT characteristics are thoroughly discussed in the "Data support and experimental setup" of this paper. To quantitatively describe the joint dependencies between the FT characteristics, temperature, and snow depth over the observed period, the copula methodology is used over each year at each specific region. Different probability distributions are tested to find the best fitted parametric distribution based on the Bayesian Information Criterion. To apply the copula methodology, we first investigate any possible changes in the dependence structure between temperature, snow depth, and FT characteristics over time at any specific region. In case of the availability or not availability of any significant change in dependence structure, dynamic or stationary copula models are proposed to describe the regional dependence between temperature, snow depth, and FT characteristics. If the dynamics copula models are chosen, the copula model's parameters are obtained for each year using the data from all grids in one region. Having the yearly model parameters, we can establish any statistical model (MLR in our case) for representing the model's parameters using a set of relevant hydroclimatic proxies. To describe the dynamics of the copula model's parameters using the MLR, we directly linked these parameters to the obtained hydroclimatic proxies through a dimensionless mapping using:

$$\Psi\{\theta_i(t)\} = f(\Psi\{\boldsymbol{X}(t)\}) \quad \textbf{(6.1)}$$

$\theta_i(t)$ are each of the copula's parameters and $\boldsymbol{X}(t)$ is the vector of relevant hydroclimatic proxies at any time step. The obtained results for model parameters are then back-transformed to the actual domain using the observed range of the parameters for each region. The calibrated models are then tested over the testing phase period to investigate the performance of MLR in capturing the yearly dynamics of the copula model's parameters. The performance of developed copula models is also investigated in capturing the marginal and joint characteristics of the two considered FT characteristics at any specific region.

In case of considering a dynamic copula approach, the developed MLRs for copula model parameters are fed with the future projections of the hydroclimatic proxies (using bias-corrected future projections of temperature and future projections of snow depth from Part 1) to obtain the copula model's parameters over the historical and future period at each specific region. Consequently, we update the copula models over the historical and future period assuming a fixed copula family. As the next step, the capability of copula models in representing the yearly

dynamics of FT characteristics over the historical period is validated. We then feed the updated copula models with future projections of temperature and snow depth and simulate the probability of yearly FT characteristics conditioned to future dynamics of temperature and snow depth over each specific region.

6.2.2 Assessing the empirical dependence and the changes in dependencies

To quantitively measure the interdependencies between FT characteristics, temperature, and snow depth, we use Kendall's tau dependence coefficient. Kendall's tau is a non-parametric dependence test with the empirical formulation as (Kendall, 1938):

$$\tau_{X,Y} = \frac{n_c - n_d}{\binom{n}{2}} \tag{6.2}$$

where n_c and n_d are the number of concordant and discordant pairs, respectively and X, Y are the pair of random variables (Genest and Favre, 2007). The significance of the dependence is evaluated by a formal p-value associated with Kendall's tau dependence coefficient. In this study, p-value = 0.05 is considered as the level of meaningful dependence. The regional dependence coefficients are obtained using the data from all grids in each region over each year.

To investigate any possible increasing or decreasing changes in the dependence structure over time, the regional interdependencies between FT characteristics, temperature, and snow depth are analyzed using Mann-Kendall and Sen's slope estimator (Gocic and Trajkovic, 2013; Kendall, 1975; Mann, 1945; Sen, 1968). The Mann-Kendall and Sen's Slope estimator are methods to statistically investigate possible changes in variables of interest. Mann-Kendall test is utilized in this study to determine the significance of trend and Sen's Slope estimator is applied to obtain the rate of change. The significance of the trend is assessed using the p-value associated with the Mann-Kendall test and is chosen in this paper as p-value = 0.1.

6.2.3 Modeling the interdependencies

The copula methodology is used to quantitatively describe the joint dependencies between FT characteristics, temperature, and snow depth. Copulas are continuous parametric functions to model the nonlinear interdependencies between sets of random variables. If $F_1(FT)$, $F_2(T)$, and $F_3(SD)$ are the marginal Cumulative Distribution Functions (CDFs) of FT characteristics (FT), mean temperature (T), and snow depth (SD), based on Sklar's theorem, the joint dependencies structure $F(FT, T, SD)$ can be described as:

$$F(FT, T, SD) = C\big(F_1(FT), F_2(T), F_3(SD)\big) \tag{6.3}$$

where C is the trivariate copula function (Sklar, 1959).

Here, we use canonical vine (C-vine), among different alternative multivariate copulas to develop the probabilistic model (Bedford and Cooke, 2002; Joe and Kurowicka, 2011; Hatami and Nazemi, 2021a). A *d*-dimensional C-vine structure is a combination of bivariate pairs of copulas arranged into $(d-1)$ trees. Each of the bivariate pairs of copula can belong to different parametric families. Using the C-vine copula the joint distribution between the studied variables can be described as:

$$f(FT,T,SD) = f_2(T) f_{3|2}(SD|v) f_{1|2,3}(FT|T,SD) \tag{6.4}$$

where the marginal PDFs are shown by $f(.)$. The conditional distributions can be estimated as (Aas et al., 2009):

$$\begin{aligned} f_{3|2}(SD|T) &= \frac{f(SD,T)}{f(T)} = \frac{c_{2,3}\big(F_2(T),F_3(SD)\big) f_2(T) f_3(SD)}{f_2(T)} \\ &= c_{2,3}\big(F_2(T),F_3(SD)\big) f_3(SD) \end{aligned} \tag{6.5}$$

and

$$\begin{aligned} f_{1|2,3}(FT|T,SD) &= \frac{f(FT,SD|T)}{f(SD|\bar{T})} = \frac{c_{1,3|2}\big(F(FT|T),F(SD|T)\big) f(FT|\bar{T}) f(SD|T)}{f(SD|T)} \\ &= c_{1,3|2}\big(F(FT|T),F(SD|T)\big) c_{1,2}\big(F_1(FT),F_2(T)\big) f_1(FT) \end{aligned} \tag{6.6}$$

where $c(\cdot)$ is the 3-dimensional copula density (Joe, 1997). As a result, the three dimensional joint density can be represented in terms of bivariate copulas as the following:

$$f(FT,T,SD) = f_1(FT).f_2(T).f_3(SD).c_{2,1}.c_{2,3}.c_{1,3|2} \tag{6.7}$$

where $c_{2,1}$, $c_{2,3}$ and $c_{1,3|2}$ are the densities of bivariate pairs. $c_{2,1}$ and $c_{2,3}$ are $c_{2,1}(F_2(T),F_1(FT))$ and $c_{2,3}(F_2(T),F_3(SD))$. $c_{1,3|2}$ are the conditional pairwise copulas between $F_1(FT)$ and $F_3(SD)$ conditional to $F_2(T)$ i.e. $c_{1,3|2}\big(F_1(FT),F_3(SD)|F_2(T)\big)$.

6.2.4 Representing the changes in copula parameters

As mentioned previously, the structure of the C-vine models fitted between three variables of FT, $\bar{T}$, and SD consists of a combination of three bivariate pairs of copulas with their associated parameters, arranged into two trees. However, the dependence structure between mentioned variables may change over time. To capture these changes in interdependencies between FT characteristics, temperature, and snow depth and consequently copula model parameters, we propose a statistical approach to capture the dynamics of copula models parameters using a group

of hydroclimatic proxies. Hence, after obtaining these copula parameters at each year over the observed period in each region, we utilize the MLR models to find the relationship between the hydroclimatic proxies, as model predictors, and copula model parameters, as the predictand. The MLR can be formulated as follows:

$$\theta_i(t) = \alpha_0 + \sum_{j=1}^{m} \alpha_j . x_j(t) + e(t) \quad \textbf{(6.8)}$$

where α_0 is the intercept, $\alpha_j, j = 1, \dots, m$ are the linear coefficients, m is the number of predictors and e is the error term in each time step. The MLR modeling is performed in dimensionless space, hence, the copula model parameters and all relevant hydroclimatic proxies are standardized into the range of [0.1 0.9]. The developed MLR models are then fed by yearly downscaled hydroclimatic proxies under different climatic conditions to model the copula parameters in each year over the future period. The standardized copula parameters are then rescaled into the original domain. The obtained future copula parameters are used to project the future FT characteristics conditional to future hydroclimatic conditions.

6.2.5 Top-down impact assessment

Using the final tree structure and updated C-vine model's parameters over the future period, the future FT characteristics conditional to air temperature and snow depth can be projected. The changes in FT characteristics corresponding to different hydroclimatic conditions can be studied by fusing the C-vine copula methodology with a top-down impact assessment scheme. The probability distribution of FT characteristics due to any known temperature and snow depth can be obtained through conditional modeling using the following equation:

$$h = F(FT|T, SD) = \frac{\partial C_{1,3|2}\big(F(FT|T), F(SD|T)\big)}{\partial F(SD|T)} \quad \textbf{(6.9)}$$

where $F(FT|T, SD)$ is the conditional distribution function,

$$F(FT|T) = h(FT|T) = \frac{\partial C_{1,2}\big(F(FT), F(T)\big)}{\partial F(T)} \quad \textbf{(6.10)}$$

and

$$F(SD|T) = h(SD|T) = \frac{\partial C_{3,2}\big(F(SD), F(T)\big)}{\partial F(T)} \quad \textbf{(6.11)}$$

Equation 6.9 can, hence, be rewritten as:

$$h = F(FT|T, SD) = h[h(FT|T)|h(SD|T)] \quad \textbf{(6.12)}$$

The estimated CDF of characteristics can be back-transformed to the quantile space using the inverse CDF function of fitted parametric distributions for FT, $\bar{T}$ and SD. This can be obtained using the inverse form of h-function given in Equation 6.12. The probability distribution of FT characteristics is then extracted using a Monte Carlo-based simulation to generate 1,000 random sets of FT characteristics under any temperature and snow depth condition (Roy and Gupta, 2021). Given random uniform random numbers of ε:

$$FT = F^{-1}\left\{h^{-1}\left[\left(h^{-1}\left(\varepsilon|h(SD|T)\right)\right)|T\right]\right\} \quad \textbf{(6.13)}$$

Comparing the probability distribution of observed FT characteristics with its probability distribution under the future hydroclimatic conditions provides a basis to illustrate how future changes in temperature and/or snow depth will result in changes in FT characteristics.

Having Equation 6.13, to perform top-down impact assessment we obtain the probability distribution of FT characteristics conditioned to scenarios of future temperature and snow depth. For this purpose, we obtain the future scenarios of temperature from a set of 20 GCMs under RCP4.5 and RCP8.5 – see Jaramillo and Nazemi (2018) and Hassanzadeh et al. (2019) for the specific model used. Regarding snow depth, we obtain the scenarios of future snow depth using the model developed in Part 1 of this double feature paper. The probability distribution of future FT characteristics is then extracted using a Monte Carlo-based simulation to generate 1,000 random sets of FT characteristics under any temperature and snow depth conditions using Equation 6.13 (Roy and Gupta, 2021). Firstly, in a RCP-based impact assessment, the changes in the long-range future compared to the present-day baseline and the pathways toward these changes are investigated. For this purpose, we look at how the changes in FT characteristics evolve during future time episodes. Secondly, to systematically quantify the impacts of changing temperature and consequently snow depth on future FT dynamics, a temperature-based approach is employed. We look into all plausible scenarios of change using the concept of the moving window (Jaramillo and Nazemi, 2018; Zaerpour et al., 2021a) and then categorize the future scenarios based on the degree of change in temperature.

6.3 Data support and experimental setup

6.3.1 Data support

The principal objective of this study is a global assessment of the impacts of climate change on FT characteristics across the province of Québec and its eight ecozones – see "Case study and data" in Part 1. For this purpose, a database consisting of the observed gridded climatic data, snow depth data, and FT data as well as future projections of climatic data had to be put together. The global landscape FT Earth System Data Record (FT-ESDR) is available at the National Snow and Ice

Data Center archive (https://doi.org/10.5067/MEASURES/CRYOSPHERE/nsidc-0477.004) is used to extract the FT characteristics in this study. FT-ESDR consists of the daily state of soil provided over 1979-2017 at the spatial resolution of 25×25 km^2 (Kim et al., 2011). Using 37GH, vertically polarized brightness temperature, the soil's state is classified into the classes of frozen (AM and PM frozen), non-frozen (AM and PM thawed), transitional (AM frozen and PM thawed), and inverse-transitional (AM thawed and PM frozen). Using this dataset, we obtain the annual number of frozen days (FD_{year}) and the number of transient days during winter season (FTD_{DJF}) as two of the most impactful FT characteristics on environmental processes as well as civil infrastructures (Ho and Gough, 2006; Sorensen et al., 2018; Zhang et al., 2017). The changes in the days with frozen state, for instance, can significantly impact the length of vegetation growth and consequently directly affect the agricultural activities (Margesin et al., 2007). These changes can, moreover, contribute to a higher rate of emission of greenhouse gasses due to permafrost thawing (Schuur et al., 2015). Furthermore, the increasing number of transient days can lead to soil erosion (Kimiaghalam et al., 2015) and increasing the deterioration rate of civil infrastructure (Roseen et al., 2012). The FD_{year} obtained at both grid and ecozone scale reveals the duration of the frozen period over each year (September - August) and can provide a basis to study the temporal and spatiotemporal variations in the length of the frozen period. The FTD_{DJF} shows the number of transient days, either as transitional or inverse-transitions. This FT characteristic is studied over the season winter (December, January, and February), where the highest interdependencies between the studied hydroclimatic variables and FTD_{DJF} are observed across both grid and ecozone scales.

The Global Meteorological Forcing Dataset (GMFD; Sheffield et al., 2006) as well as the Canadian Meteorological Center (CMC; (R. D. Brown and Brasnet, 2010) are used as the source of the observed temperature and snow depth data. Note that the observed period for all datasets (FT-ESDR, GMFD, and CMC) is considered as the common period of 1999-2016. The NASA Earth Exchange Global Daily Downscaled Projections dataset (NEX-GDDP; Thrasher et al., 2012) is used as the source of downscaled future projections of climate data. For further information on the hydroclimatic data sets over observed and future periods please refer to the "Case study and data" in Part 1 of this paper.

6.3.2 Experimental setup

To project the future dynamics of FT, the future temperature and snow depth are required. The bias-corrected temperature and projected snow depth using the proposed methodology in Part 1 of this double feature paper are used for this purpose. As the size and/or centroid of different sources of gridded data (temperature, snow depth, and FT characteristics) are not the same, *k*-nearest neighbor interpolation methodology is used to regrid these datasets into a similar scale (i.e. FT-ESDR dataset). The procedure of regriding is described in "Case study and data" of Part 1. We find k=4 as the optimum number of nearest neighbors to achieve the highest accuracy in modeling the statistical properties (i.e. mean, standard deviation, and skewness) of hydroclimatic variables

over different ecozones of Québec. The regridded estimations of studied hydroclimatic variables are then paired with FT characteristics, at the same temporal and spatial scales. Moreover, the copula methodology is sensitive to the existence of autocorrelation in considered variables. Hence, as the last step of the data processing, the temperature, snow depth, and FT characteristics at the ecozone scale are analyzed to investigate the presence of autocorrelation in any case. No significant autocorrelation structure is found in temperature, snow depth, and FT characteristics at studied temporal scales. To obtain the parametric distribution of involved variables (i.e. temperature, snow depth, and FT characteristics), different probability distributions are fitted to these variables by maximum likelihood estimation and the best fitted parametric distribution is selected. Normal, lognormal, Weibull, gamma, and exponential are considered as potential distributions and the Bayesian Information Criterion is used to select the best distribution among those fitted over each region. The CRAN R with the package of "fitdistrplus" is used for this purpose (Delignette-Muller and Dutang, 2015). In parallel, the possible change in dependence structure between involved variables is investigated. In case of the existence of significant changes in the dependence structure, dynamic copula modeling is proposed. The copula model parameters in which a significant trend is observed are updated over time using the regression-based approach. Expected yearly temperature, expected yearly snow depth, the standard deviation in temperature, the standard deviation in snow depth, dependence between temperature and snow depth, and time are considered as the potential predictors in the regression-based updating methodology. The PCIS onward selection approach is employed to find the effective predictors from the pool of potential variables – see Part 1 of this paper for more information on PCIS. Note that the copula model parameters are only updated for ecozones that a significant trend is observed in their corresponding dependence structures. When no significant trends are observed in the copula model parameters, the parameters are considered constant over time and are found by considering the expected of the parameters obtained using the available observed data from the whole 18-year period. The C-vine copulas are then used to model the interdependencies. The tree structure of the C-vine is based on the maximum spanning tree algorithm which enhances the ability of the model to decompose the multivariate probability structure. The copula parameters can be then chosen with respect to the interdependencies between the pairs (Dißmann et al., 2013). In C-vine copula models, there is a key variable that governs interactions in the data set. In this study, the temperature is considered as the main variable that triggers its interactions with FT characteristics and snow depth. Different copula families (i.e. Frank, Gaussian, Student t, Clayton, Gumbel, and Joe) are then tested to select the bivariate copulas with the best performance – see Nelsen (2006) for the formulation of these copulas. The bivariate copulas in the C-vine structure are parameterized using the Maximum log-Likelihood Method and considering the Bayesian Information Criterion as the goodness-of-fit measure (Sadegh et al., 2017). The C-vine copula modeling is conducted using CRAN R with the packages of VineCopula, CDVine, and copula (Brechmann and Schepsmeier, 2013; Schepsmeier et al., 2015; Yan, 2007). The performance of copula models is evaluated based on their capability in preserving the marginal and joint characteristics of the studied FT characteristics. Comparing the probability distribution of observed FT characteristics over the 7-year testing phase period of

1999-2005 with their probability distribution under the future hydroclimatic conditions provides a basis to illustrate how future changes in temperature and/or snow depth will result in changes in FT characteristics. The top-down impact assessment results are presented in two ways (1) the RCP-based representation and (2) the temperature-based representation. In RCP-based representation, results are analyzed and demonstrated under RCPs 4.5 and 8.5 for short-range, mid-range, and long-range future periods. These future periods include 7-year time episodes of short-range (2034-2040), mid-range (2064-2070), and long-range (2094-2100) futures compared to the present-day baseline (1999-2005) using the historical period of GCM models in which we analyze the impact of various temperature and snow depth scenarios. In temperature-based representation, we consider all the plausible scenarios of change in temperature and then categorize the future scenarios as a function of global mean warming above the present day. This will provide the capability to account for the independence of regional snow depth and FT characteristics changes of the rate of warming and allow for climate changes impact assessment across regions and scenarios.

6.4 Results

6.4.1 Quantifying changes in dependence structure

To inspect the spatiotemporal dynamics of interdependencies between FT characteristics, temperature, and snow depth, we take snapshots from these interdependencies year by year over all grids of each ecozone for the whole observed period. This results in a time series of dependencies at each ecozone, showing how the association between FT characteristics and temperature or snow depth evolves in time. The Kendall's tau is used to measure the interdependencies. The considered interdependencies are dependence between pairs of temperature and snow depth ($\tau_{T,SD}$), between FT characteristics and temperature ($\tau_{FT,T}$), and the conditional dependence between FT characteristics and snow depth conditional to temperature ($\tau_{FT,SD|T}$). These values correspond to the parameters of C-vine model (θ_1 to θ_3, respectively). To analyze the potential changes in the dependence structures over time, we use Mann-Kendall and Sen's slope estimator. Figure 6.1 summarizes the results of this experiment. The first row demonstrates the results of changes in the interdependencies between pairs of FD_{year}, temperature, and snow depth at the annual scale; whereas, the second row represents the changes in the interdependencies between pairs of FTD_{DJF}, temperature, and snow depth during winter. Each panel includes the results for one pair, in which rows are the results for each ecozone over the entire observed period. The blue and red colors on the left side of each panel show the negative and positive dependence; whereas, the green and orange colors on the right side of each panel show the negative and positive trends, respectively. The significant positive and negative trends at p-value=0.10 are distinguished by +/- signs within cells. As it can be observed, the dependencies are dynamic over time and space and there are ecozones in which the changes in the dependence structure are significant. In general, in most of the ecozones the interdependencies between at least

one pair of studied variables are significantly changing over time, indicating the need for accounting for a dynamic dependence structure in those regions. As expected, there is a negative dependence looking at $\tau_{T,SD}$ and $\tau_{FD,T}$ in the majority of cases (Panel a, left and mid columns). While the trends in $\tau_{T,SD}$ is mostly positive (significant trends in EZ1, EZ2, EZ3, EZ5, and EZ7), negative trends are observed for $\tau_{FD,T}$ (significant trends in EZ4 and EZ8). In regards to the conditional interdependence of $\tau_{FD,SD|T}$ the dependencies are mostly positive and a mix of positive and negative trends can be observed across ecozones (significant trends in EZ1, EZ3, and EZ4). As the second row represents, the $\tau_{FTD,T}$ during winter are often negative except in EZ2 and EZ4, in which a mixed of positive and negative dependencies can be observed over different snapshots. Similar to the annual scale, such interdependencies increase over time, particularly in EZ3 and EZ5 in which interdependencies are significantly strengthening. The $\tau_{FTD,T}$ are often positive across time and space, showing mixed decreasing/increasing trends over different ecozones where significant trends are observed in EZ1, EZ4, EZ6, and EZ8. Finally, the conditional dependencies of $\tau_{FTD,SD|T}$ are often negative and show a pattern of positive trends across most of the ecozones with significant trends observed only in EZ5.

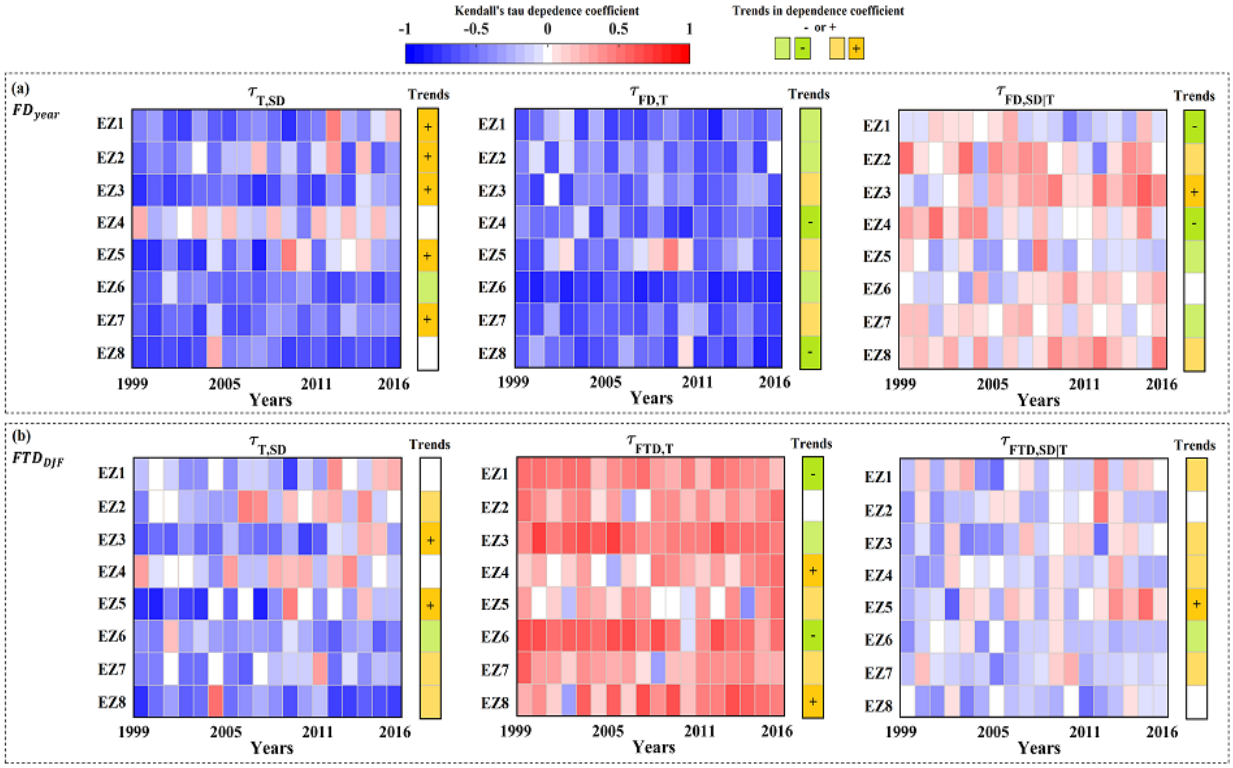

Figure 6.1 The changes in the observed interdependencies between temperature (T), snow depth (SD), and each of studied FT characteristics over time across Québec's ecozones. Blue and red colors show the negative and positive dependencies while green and orange colors display the negative and positive trends. The significant positive/negative trends at p-value=0.1 are identified by +/- signs within cells, respectively. The ecozones are sorted from north (top) to south (bottom).

6.4.2 Quantifying the C-vine modeling performance over the historical period

By identifying the interdependencies between FT characteristics, temperature, and snow depth, we can set up and evaluate our C-vine model in capturing the observed interdependencies. For this purpose, within each snapshot, the proposed model is parametrized and pairs of temperature, snow depth, and FT characteristics in each ecozone are randomly generated. Accordingly, 1,000 sets of variables of the same size as the observed data are sampled for each year. Then the value of Kendall's tau dependence using the simulated pairs is extracted. The range of expected values of sampled Kendall's tau is obtained for each year of the 18-year observed period. The simulated range is then compared with the observed values to assess the ability of the copula model in representing the observed dependencies. Results are summarized in Figure 6.2. Similar to Figure 6.1, the first row demonstrates the results for $\tau_{T,SD}$, $\tau_{FD,T}$, and the conditional dependence of $\tau_{FD,SD|T}$; whereas, the second row represents the results for interdependencies between the pairs of FTD_{DJF}, temperature, and snow depth during winter. The ranges of observed and simulated Kendall's tau are shown with gray and colored boxes, respectively. The color code corresponds to the colors used for identifying ecozones. The dots are the expected observed and simulated Kendall's tau values, respectively and the x-axis represents the different ecozones of Québec. As shown in Figure 6.2, the parametrized copulas can effectively represent the interdependencies between studied hydroclimatic variables and FT characteristics. Regarding the interdependence between hydroclimatic variables in the annual scale, an average Relative Error (RE) of 2.1%is observed in representing the $\tau_{T,SD}$ for all ecozones. The C-vine model can capture the interquartile range of observed with an average RE of less than 3.4%. Looking at FD_{year}, an average relative error of 2.4% is observed for the $\tau_{FD,T}$. Regarding the ranges of interquartiles for such interdependencies, the C-vine model can capture the observed ranges with average REs of 2.7%. Finally, for the conditional dependence of $\tau_{FD,SD|T}$, the RE considering the mean and interquartile range are 0.9% and 1.9%, respectively.

As the second row of Figure 6.2 shows, regarding the interdependence between FTD_{DJF} and the hydroclimatic variables in winter, an average RE of 0.8% is observed in representing the $\tau_{T,SD}$ for all ecozones. The observed interquartile range of this dependence can be captured with less than 1.2% RE. The average RE is 1%for representing the $\tau_{FTD,T}$ and the C-vine model can preserve the interquartile range of observed $\tau_{FTD,T}$ with REs of 1.1%. Regarding the conditional dependence of $\tau_{FTD,SD|T}$, the RE considering the mean and interquartile ranges are 0.7% and 1 %, respectively. Moreover, spatial patterns in the magnitude of dependencies between both FT characteristics, temperature, and snow depth are observed. Looking at Figure 6.2, there is a clear increase in the magnitude of dependencies by moving from the northern ecozones to the southern ones in many cases of dependencies between studied variables. The one-way ANOVA test is used to assess the difference between the estimated dependencies in different studied ecozones. Based on our results, The dependence between temperature (or snow depth) and both FD_{year} and FTD_{DJF} as well as the conditional dependence are unique across all considered ecozones of Québec. The significant differences between the dependencies of FT characteristics and temperature or snow depth in

different ecozones can reveal the role of ecosystem conditions (e.g. vegetation type, soil type, and land cover) in regulating the impacts of changing climate on FT dynamics. The high level of accuracy in representing the interdependencies between studied variables over the observed period justifies the application of the C-vine models for projecting the future FT dynamics due to future changes in temperature and snow depth throughout Québec.

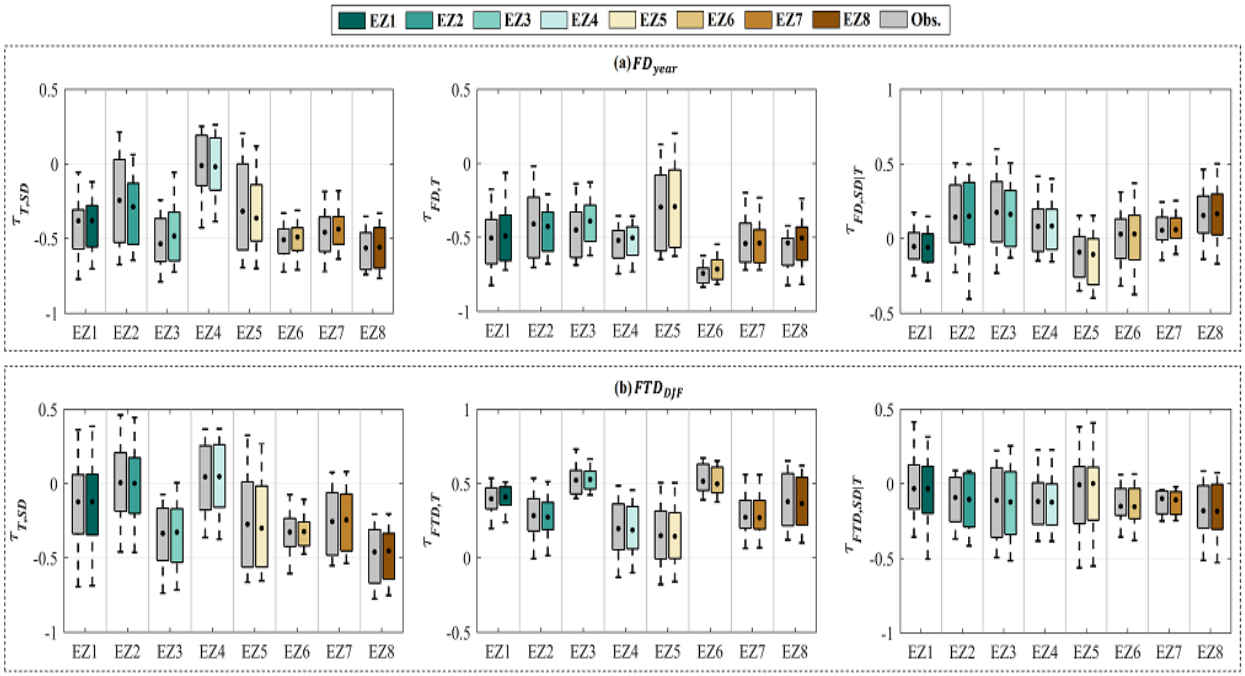

Figure 6.2 The modeling performance of the C-vine copula model in representing the Kendall's tau dependence coefficient between temperature (T), snow depth (SD), and each of the studied FT characteristics across Québec's ecozones.

We also assess the performance of the proposed model in capturing the time series of FT characteristics. Figure 6.3 summarizes the results. The first and second rows depict the performance in representing the time series of FD_{year} and FTD_{DJF} in terms of R^2, NSE, and RE in the long-term mean of FT characteristics. Similar to Figure 6.2, the x-axis is related to the result of each ecozone. In general, the performance of the proposed model in representing the FD_{year} is high, demonstrating $R^2 > 0.92$ and $NSE > 0.89$. The REs in representing the FD_{year} are low, showing the REs of less than 3% across all ecozones. The best performance is observed in EZ4 with $R^2 = 0.97, NSE = 0.96$, and $RE = 0.1\%$. Regarding the FTD_{DJF} as shown in the second row, the proposed model can capture the FTD_{DJF} time series with average $R^2 > 0.89$ and $NSE > 0.72$, and REs of less than 9.2%. The best performance in modeling the dynamics of FTD_{DJF} is also observed in EZ4 with $R^2 = 0.96, NSE = 0.94$, and $RE = -0.7\%$.

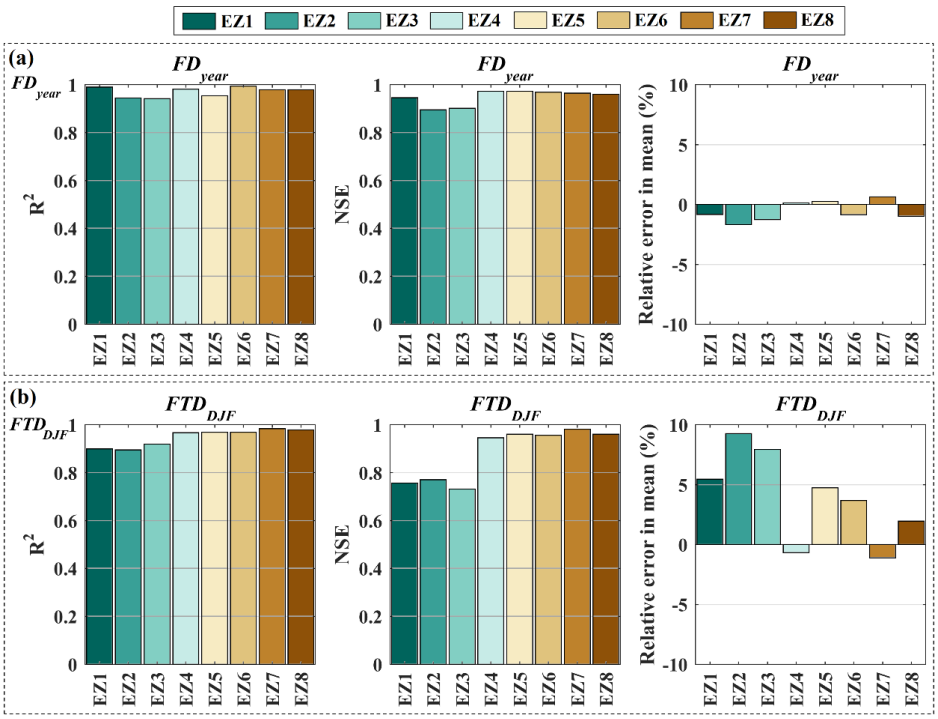

Figure 6.3 The modeling performance of the proposed model in representing the (a) FD_{year} and (b) FTD_{DJF} time series. The performance is evaluated in terms of R^2, NSE, and RE shown in left, middle, and right columns, respectively. The x-axis in each subplot depicts the results corresponding to different ecozones.

6.4.3 Estimation of time-varying model parameters

We demonstrated previously in Figure 6.1 that the structure of interdependencies between FT characteristics and hydroclimatic variables is changing with time. This requires the selection of predictors with which we can update the parameters of the proposed model. This is the first step towards the development of the time-varying model. In total, there are three parameters named as θ_1, θ_2, and θ_3 for the proposed model which need to be updated for each ecozone separately. As discussed in section 6.2.4, MLR is used to update the copula model parameters over time. Expected temperature, expected snow depth, the standard deviation in temperature, the standard deviation in snow depth, dependence between temperature and snow depth (i.e., $\tau_{T,SD}$), and time itself ($t = 1, \dots, 18$) are considered as the potential. The PCIS is employed to find the effective predictors from the pool of potential variables. Note that the copula model parameters are only updated for ecozones that a significant trend is observed in their corresponding dependence structures. For other ecozones, the copula model parameters are considered constant over time and are found by considering the expected of the parameters obtained by considering the available observed data from the whole period of 1999-2016. After selecting the best set of predictors for each parameter at each ecozone, the observed annual data over the period of 2006-2016 is used as the calibration period. The remaining of the observed period (1999-2005) is used to investigate the model performance during an independent testing phase. Nash–Sutcliffe coefficient of efficiency (NSE) is used to investigate the skills in representing the parmaeters' dynamics.

Figure 6.4 shows the NSE at the ecozones with significant trends during the testing phase, identified with colored bars. To provide a reference for the skills during the testing phase, the values corresponding to the best fit over the calibration phase are also depicted with solid black lines in each ecozone. The first and second rows display the performance of MLR in representing the three parameters of the proposed model including θ_1, θ_2, and θ_3 used for modeling of FD_{year} and FTD_{DJF}, respectively. The columns correspond to the three parameters. The x-axis is related to the result in each ecozone. Looking at this FT characteristic, the calibrated MLRs are found to be more accurate in the case of modeling θ_1 (expected NSE = 0.91) compared to θ_2 (expected NSE=0.69) and θ_3 (expected NSE = 0.60) in required ecozones over the testing phase. This is due to the strongly significant dependence between θ_1 and the $\tau_{T,SD}$ as one of the hydroclimatic predictors selected in case of modeling of θ_1. For θ_1, the highest accuracy of MLR models is observed in EZ1 with NSE = 0.91. Looking at θ_2, among EZ4 and EZ8, considerably better performance is observed in EZ4 with NSE = 0.85. Finally for θ_3 better performance is observed across EZ4 with NSE = 0.69. Similar to FD_{year}, higher accuracy is observed while modeling the dynamics of θ_1 compared to other model parameters in EZ3 (NSE = 0.89) and EZ5 (NSE = 0.93), looking at FTD_{DJF}. Regarding θ_2, expected NSE = 0.61 are obtained over considered ecozones, where MLR shows better performance in EZ8 (NSE = 0.74) compared to the other ecozones. Looking at θ_3, in EZ5 (the only considered ecozone with observed significant trend), the expected NSE = 0.61 is observed. Our analysis shows that the MLR model stands as an accurate model, capable of describing the dynamics of C-vine model parameters. This ability can provide a basis to extend the model application for updating the model parameters using the considered set of hydroclimatic predictors.

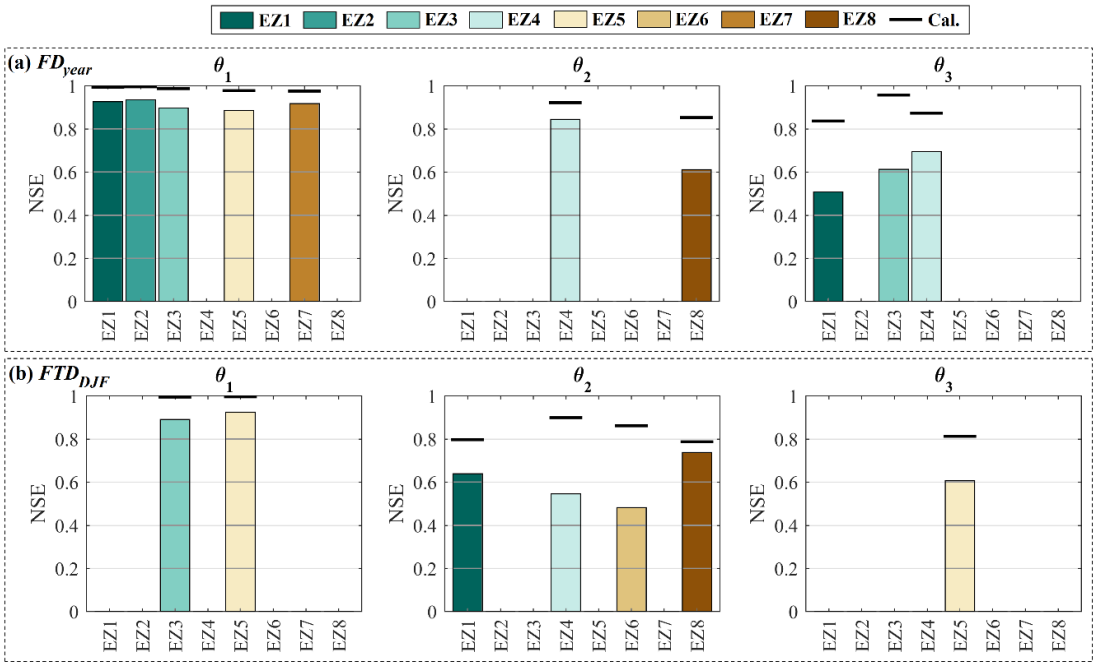

Figure 6.4 The modeling performance of the MLR model in representing the dynamics of model parameters for FD_{year} and FTD_{DJF} at ecozone scale based on the NSE during the testing phase.

6.4.4 Evaluating the time-varying copula performance in capturing the statistical characteristics of FT over the historical period

As the last step of model evaluation, the Taylor Diagram is used to assess the performance of the dynamic copula models in capturing the statistical characteristics of FD_{year} and FTD_{DJF} at the ecozone scale. Taylor Diagram can statistically summarize multiple aspects of the C-vine model in a single plot (Z. Jiang et al., 2020; Peng et al., 2018; Taylor, 2001). For this purpose, the simulated values of FT characteristics over the testing period of 1999-2005 of the historical period using the NEX-GDDP data as well as projected snow depth values (described in Part 1) are compared with the observed values obtained using the FT-ESDR dataset. Figure 6.5 presents the comparison results using the Taylor Diagram. The considered statistical metrics include the normalized standard deviation (radial distance from the origin), RMSE (radial distance from the observed point), and correlation coefficient (cosine of azimuth angle). The color code used corresponds to those used for identifying ecozones. Dots with the same color corresponds to different GCMs. It is observed that the proposed time-varying approach is capable of capturing the observed dynamics of FD_{year} (Figure 6.5.a) and FTD_{DJF} (Figure 6.5.b) with good performance. Looking at FD_{year}, for all considered GCMs and across all ecozones, the average correlation coefficient = 0.81, RMSE = 0.63 and standard deviation = 0.58 are observed. Higher performance is observed in EZ8, EZ2, EZ5, and EZ1, respectively, where the correlation coefficient higher than 0.75 is observed for all GCMs. For FTD_{DJF}, for all considered GCMs and in all ecozones, the average correlation coefficient = 0.84, RMSE = 0.72 and standard deviation = 0.61 are observed across different GCMs and ecozones. Looking at this FT characteristic, EZ1 is the ecozone with the highest accuracy among the studied ecozones, where the correlation coefficient higher than 0.85 is observed for all GCMs. The good performance of the dynamic copula models in representing the characteristics of the observed period ensures accurate projections of future conditions.

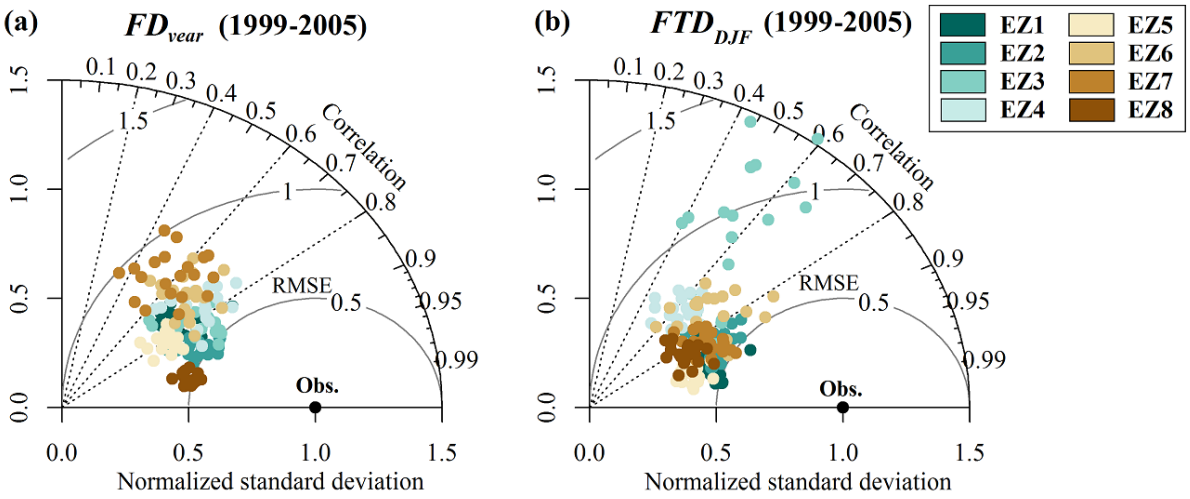

Figure 6.5 Taylor diagrams comparing simulated FD_{year} and FTD_{DJF} from 20 GCMs against observations during the historical period (1999-2005) over different ecozones. The observed values for the each FT characteristic is shown with the black dots on *x* axis.

6.4.5 Systematic assessment of error propagation

After model development and quantifying the modeling performance under historical conditions, in this section, we aim at analyzing the modeling sensitivity to different levels of complexity in the proposed framework. For this purpose, four levels of complexity are defined. The simplest form of model (Case 1) is considered as the one calibrated using the observed gridded temperature (GMFD) and snow depth (CMC) data records. In this case, the parameters of the copula models are obtained using the observed values in the C-vine structure. Case 2 is defined as the models calibrated using the observed gridded temperature and snow depth, while the model parameters are simulated using the MLR models. In Case 3, the gridded temperature data is used in parallel to the simulated snow depth using the modeling scheme proposed in Part 1 of this paper. The copula model parameters, in this case, are directly derived using the C-vine copula models. Finally, the most complex form (Case 4) is considered as the case of using the gridded temperature data, simulated snow depth data from Part 1, and simulated copula model parameters by MLR models. Figure 6.6 summarizes the results based on the absolute relative error in mean, in which panel (a) depicts the results for FD_{year} and panel (b) is related to FTD_{DJF} across the eight ecozones of Québec. The colors correspond to the ecozone presented in each arc of the circle. The results for Case 1 to Case 4 for each ecozone are presented with four bars with the same color, respectively.

Looking at the difference between the error corresponding to Case 1 to that of more complex cases the propagation of the error due to more complexity in the modeling scheme can be quantified. As can be seen from Panel a, the relative error in the mean of FD_{year} is considerably lower in Case 1 in all ecozones with an average of 0.8% while is it increasing moving to Case 4 with an average relative error of 1.3%. Based on the results, the relative error in the mean of FD_{year} is higher in EZ2 for all cases. Looking at the error propagation moving from Case 1 to Case 4 the difference between the relative errors in Case 1 compared to Case 4 is the highest in EZ2 and EZ6, respectively. In EZ2, where the highest errors are observed, the relative error in the mean is 1.5%, 2.4%, 1.9%, and 2.5% for Case 1 to Case 4, respectively. The highest similarity between the relative errors corresponding to different cases is observed in EZ7, EZ3, and EZ8. Considering the results for FTD_{DJF}, the propagation of error is more significant comparing to FD_{year} where the average relative errors in mean value over the ecozones are 3.2% and 6.7% for Case 1 and Case 4, respectively. Similarly, for FTD_{DJF} the highest relative errors in mean for almost all cases are observed in EZ2. However, the highest amount of error propagation is observed in EZ1 where the relative error in Case 4 is more than 7 times higher than that of Case 1. In contrast, in EZ7, EZ3, and EZ8 higher complexity in models (moving from Case 1 to Case 4) does not contribute to significant changes in relative errors.

Cases	Snow depth (SD)	Model parameter (θ)
1	Observed	Observed
2	Observed	Simulated
3	Simulated	Observed
4	Simulated	Simulated

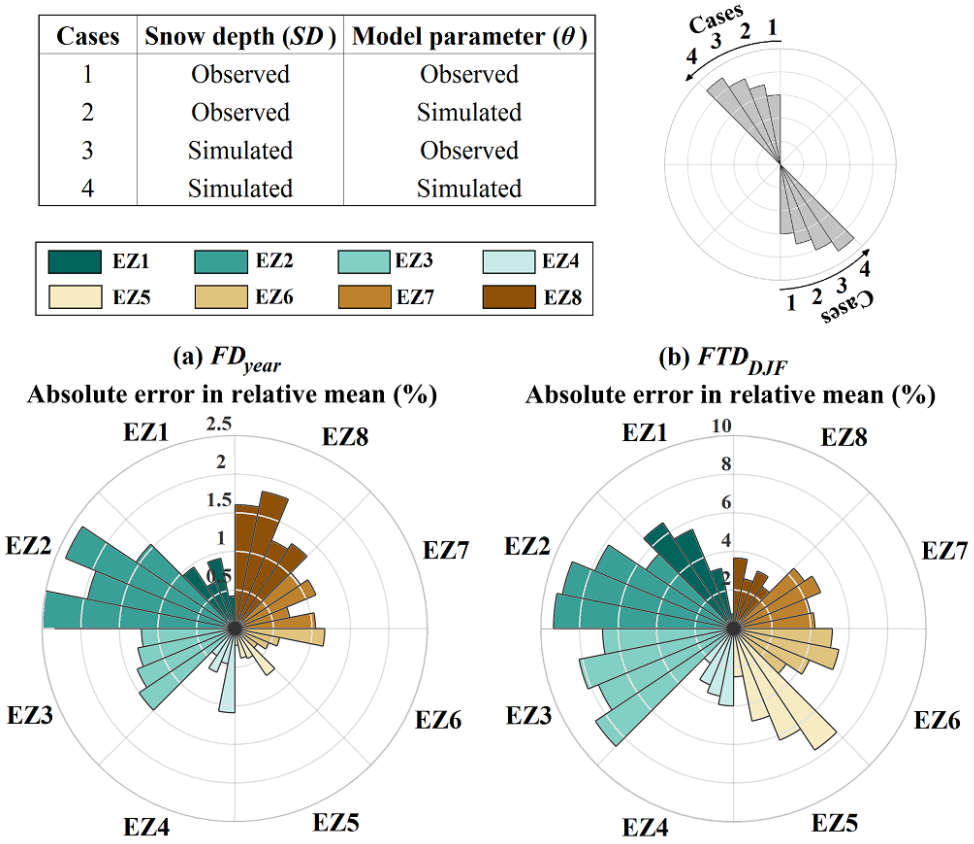

Figure 6.6 The modeling sensitivity to different levels of complexity for (a) FD_{year} and (b) FTD_{DJF}, based on absolute relative error in the mean. The colors correspond to each ecozone.

6.4.6 Evolution of FT characteristics in short-range, mid-range, and long-range futures

As the RCP-based impact assessment, the future changes in FD_{year} and FTD_{DJF} due to changing climate are investigated. For this purpose, we look at how the changes in gridded snow depth evolve during short-range (2034-2040), mid-range (2064-2070), and long-range (2094-2100) futures compared to the present-day baseline (1999-2005 of GCM projections). Figures 6.7 and 6.8 highlight the results of this analysis for FD_{year} and FTD_{DJF}. Panels (a) and (b) are related to the simulation results under RCP4.5 and RCP8.5 in which the results for ecozones ordered from north to south from EZ1 to EZ8 from the top left to the bottom right. The future ΔFD_{year} and ΔFTD_{DJF} at each ecozone are shown in boxplots for the three time episodes where whiskers span the range of changes in FT characteristics in each ecozone obtained by multimodel mean ensemble and dots show the expected of simulated values. Regarding ΔFD_{year}, there is a clear geographic distinction between future changes in ΔFD_{year} across different ecozones. In general, a higher ΔFD_{year} is observed in the northern ecozones including EZ1 to EZ4 with an average ΔFD_{year} of 29 to 31 days less FD_{year} for long-range future under RCP4.5. These changes vary between -35 to -41 days under RCP8.5 in northern ecozones. However, it should be noted that there are some ecozones that exhibit some increasing patterns in ΔFD_{year} over the short-range future, specifically under RCP4.5 scenario. Looking at ΔFD_{year} across the three time episodes provides insights into the rate of

change and possible amplification in future ΔFD_{year} over time. In general, the changes in ΔFD_{year} over time are more severe at the northern ecozones. However, the amplifications are mostly observed over southern ecozones such as E5, EZ6, and EZ7. Regarding FTD_{DJF} as Figure 8 shows, in general, more ΔFTD_{DJF} is expected in the southern ecozones, specifically in EZ7 and EZ8 with average of 11 to 10 more days with the transient state, respectively for the long-range future under RCP4.5. The increases in FTD_{DJF} over mentioned ecozones reach 13 days for EZ7 under RCP8.5. Additionally, the rate of changes over time is more severe in the southern ecozones while the highest amplification is observed in EZ7. Looking at the difference between short-, mid-, and long-range future ΔFTD_{DJF} demonstrates more amplification in the rate of ΔFTD_{DJF} under RCP8.5

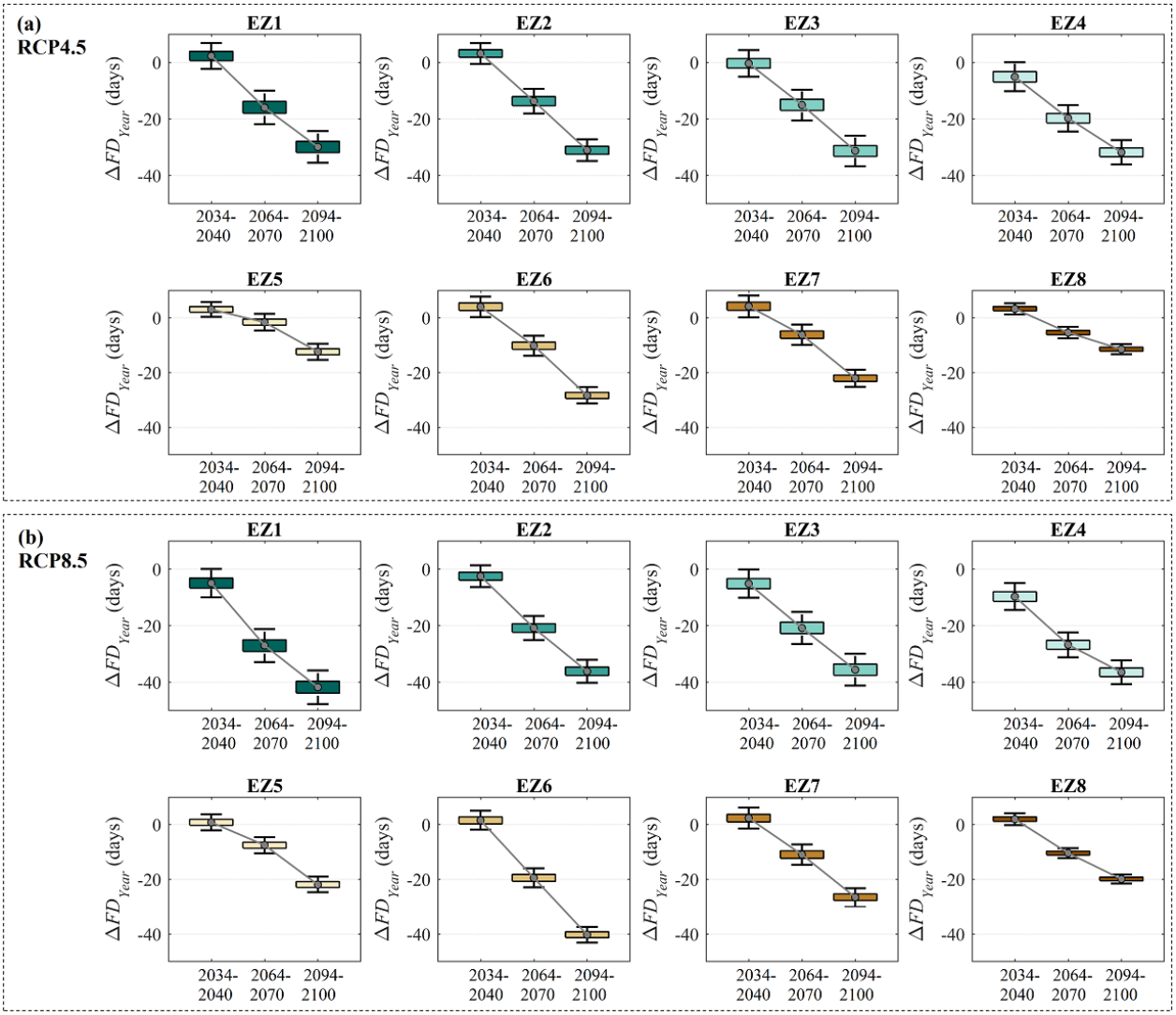

Figure 6.7 Changes in FD_{year} under short-range (2034-2040), mid-range (2064-2070), and long-range (2094-2100) future projections across Québec's ecozones under RCP4.5 (frame a) and RCP8.5 (frame b).

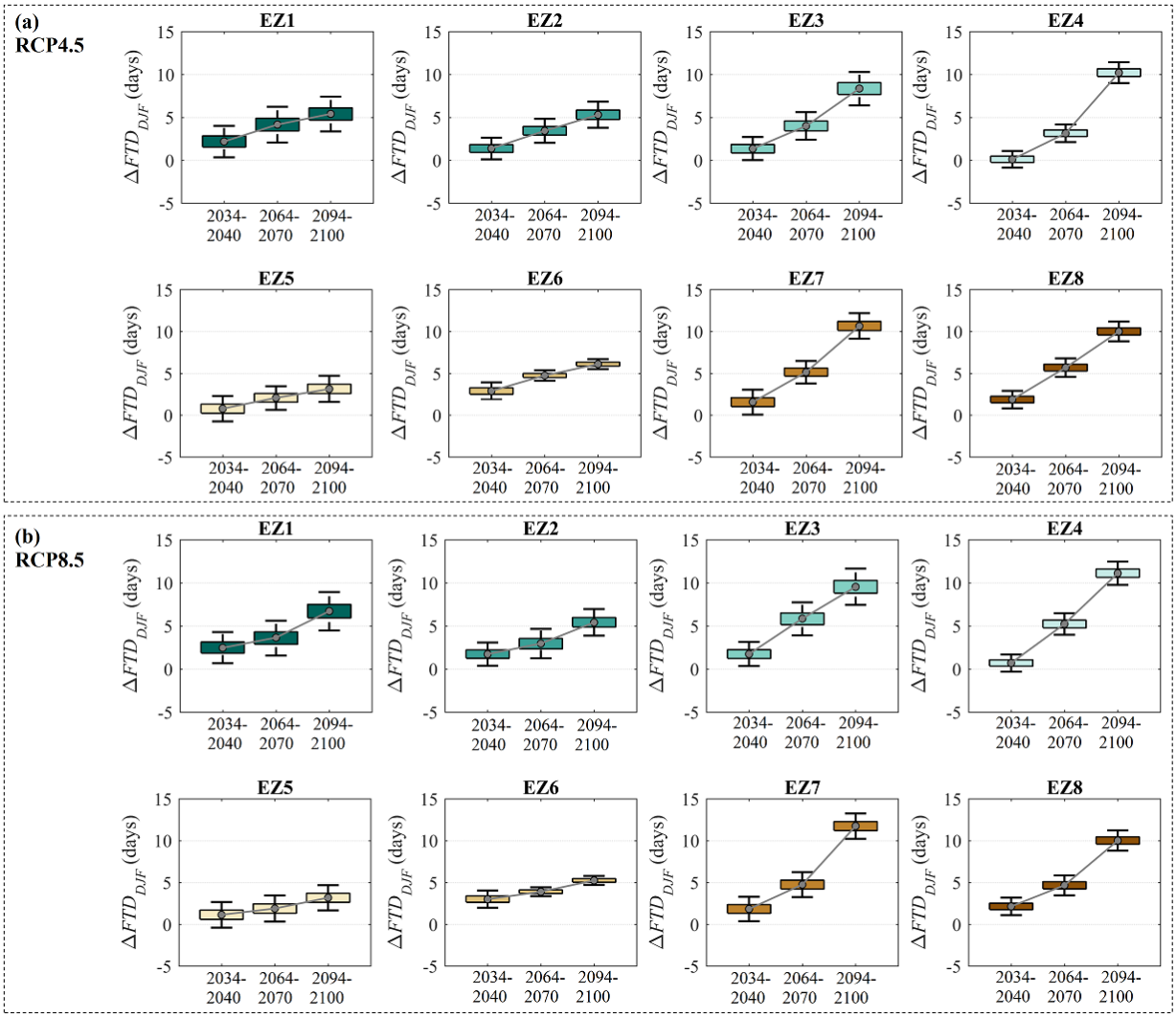

Figure 6.8 Changes in FTD_{DJF} under short-range (2034-2040), mid-range (2064-2070), and long-range (2094-2100) future projections across Québec's ecozones under RCP4.5 (frame a) and RCP8.5 (frame b).

6.5 Integrated impact assessment

6.5.1 Temperature control on snow depth and FT dynamics

To showcase how FT dynamics can change spatially due to unique changes in air temperature, we quantify the expected changes in the long-term average of FT characteristics in face of different future climatic scenarios compared to the present day. Similar to Part 1 of this article, the term "present day" refers to the 7-year historical period of GCM projections which is considered for the testing phase (1999-2005). The results are presented by a temperature-based impact assessment approach, i.e. as a function of regional change in temperature average, to allow for systematic comparison of temperature change impacts across different ecozones. Figure 6.9 summarizes the results of this analysis, in which the top row is the results for the snow depth in annual and winter named as SD_{year} and SD_{DJF}; and the bottom row is the results of FT characteristics including FD_{year}

and FTD_{DJF}, respectively. The rows in each subplot correspond to ecozones, sorted from north (top) to south (bottom); and columns are related to different levels of temperature change with the increment of 0.5°C for annual and 1°C for winter, sorted from left to right. Red (blue) color is the indicator of increasing (decreasing) changes in the long-term average of SD_{year}, SD_{DJF}, FD_{year}, or FTD_{DJF} at each ecozone. The size of the circles shows the likelihood of occurrence of events in each ecozone. A 7-year time frame is moved year-by-year through the future period of 2017-2100 and the changes in temperature, snow depth, and FT characteristic compared to the testing phase of the presnet day (1999-2005) are obtained. In total, considering 20 GCMs used in this study, the two RCP4.5 and RCP8.5, and different 7-year time episodes, we have $20 \times 2 \times 78$ future scenarios for temperature. The likelihood of occurance of each temperature scenario in the future is calculated based on the number of times that one temperature scenario happens in a specific interval divided by the total number of possible scenarios. It can be observed that as the changes in annual temperature increase, the likelihood of occurrence of temperature scenarios often decreases except in northern ecozones of EZ1 to EZ4 in which the likelihood of occurrence of warmer temperature is high, reaching the likelihood of higher than 12% for scenarios with more than 6℃ increase in annual temperature. Similarly, in the winter season, the likelihood of temperature changes higher than 6℃ also reaches 23% in EZ1. The temperatures scenarios with the changes in temperature between 1°C to 2.5°C are often the most probable scenarios in the annual scale; whereas, temperature changes between 1°C and 2°C are the scenarios with the highest probability in the future over winter. As the first row shows regarding ΔSD_{year} and ΔSD_{DJF}, in general, the magnitude of changes in snow depth due to the same level of warming temperature is higher in the northern ecozone with the highest decrease in ΔSD_{year} and ΔSD_{DJF} occurring in the EZ3, reaching 27cm and 36cm for temperature scenarios of warmings higher than 6°C and 10°C, respectively.

Regarding the ΔFD_{year}, in general, the magnitude of decreasing FD_{year} due to the same level of warming temperature is higher in the northern ecozones (i.e EZ1 to EZ4) with decreases higher than 33 days due to the temperature changes higher than 6℃. The changes in FD_{year} due to identical change in regional temperature is also considerably high in EZ6 ecozone located in the southern part of the province. Under 6°C increase in temperature, for instance, it is expected to have up to 42 fewer days with the frozen state in each year across EZ6. The likelihood of warmer temperature in EZ6, however, is low compared to the northern ecozones. Due to 2.5℃ warming, one of the most probable temperature scenarios at annual scale, the decrease in the long-term average of FD_{year} is ranging from 23 to 7 days moving from EZ1 to EZ8. The higher likelihood of significant decreases in days with frozen state in northern ecozone is of great importance due to the role of FT dynamics on land-atmospheric greenhouse gas emissions in these regions as a result of permafrost degradation (Carpino et al., 2018). Looking at FTD_{DJF}, in general, the magnitude of increasing FTD_{DJF} due to the same level of warming temperature is higher in southern ecozones of EZ7 and EZ8 as well as EZ4. The highest sensitivity of dynamics of FTD_{DJF} to changes in temperature is observed in EZ7 with ΔFTD_{DJF} of 14 days due to the temperature change of higher than 10℃. Under 2℃, one of the most probable scenarios of temperature change over the winter

season, the shifts in FTD_{DJF} range between 2 to 5 days. The higher sensitivity of FTD_{DJF} to changing temperature in the southern ecozones has an important implication due to its impacts on soil instability and infrastructure deterioration in the part of the province with the highest population already suffering from aging infrastructure (Doughty et al., 2013; Lewkowicz and Way, 2019).

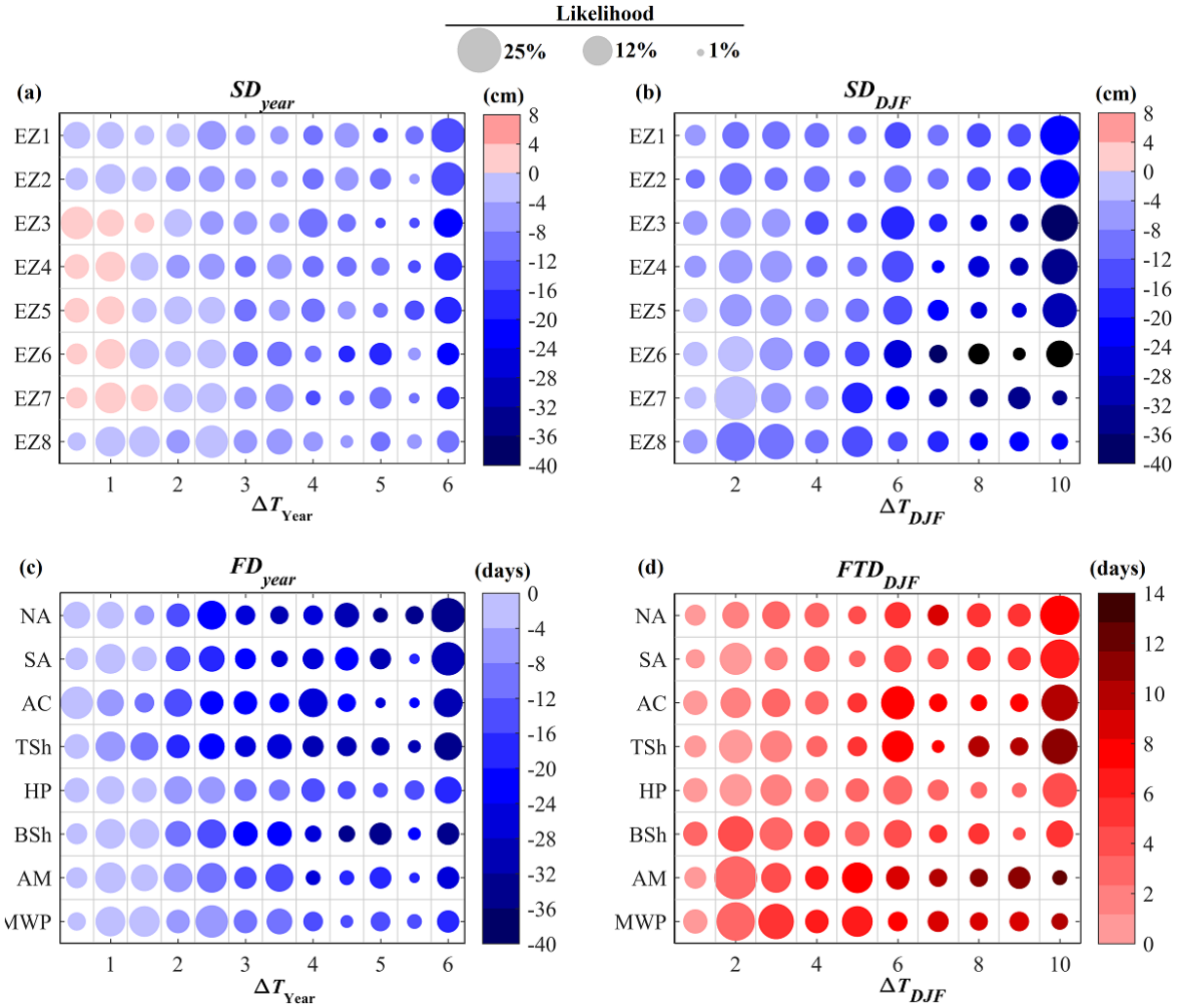

Figure 6.9 Changes in (a) annual snow depth, (b) winter's snow depth, (c) FD_{year}, and (d) FTD_{DJF} compared with the present day (1999-2005). Color codes at the right hand of each panel show the multimodel mean change of scenario. The likelihood of each event of changing temperature at different ecozones of Québec is shown with the size of the circles.

6.5.2 Compound control of changing temperature and snow depth on FT dynamics

Although in the previous section we studied the sensitivity of FT dynamics to different levels of changing temperature, however, the future shifts in studied FT characteristics due to compound changes in temperature and snow depth are not yet clear. Here, we further quantify and compare the changes in FT characteristics due to future projections of air temperature and snow depth at the ecozone scale. This comparison can address the alterations in studied FT characteristics under

compound changes in air temperature and snow depth. In Figures 6.10 and 6.11, we displayed the changes in FD_{year} and FTD_{DJF}, respectively. In each subplot, the x-axis shows the shifts in temperature under different climatic scenarios while the y-axis displays the corresponding shifts in snow depth (obtained using the methodology proposed in Part 1 of this paper) comparing to the present day. The color maps show the changes in FT characteristics in face of compound changes in climatic variables. The results for short-range (2034-2040), mid-range (2064-2070), and long-range (2094-2100) future projections are displayed with circles, triangles, and squares, respectively.

Considering FD_{year}, higher changes in temperature and snow depth comparing to the present day are happening in northern ecozones for most of the future climatic scenarios, hence the decrease in FD_{year} is higher in these regions. In EZ1 as one of the ecozones with the highest changes in FD_{year}, the mean ensemble of temperature and snow depth for different climatic scenarios over short-, mid-, and long-range time episodes changes with an average of 1.6, 3.8, and 5.5℃ warming and 1, 6, and 15 cm decrease in snow depth comparing to the present day. Mentioned changes in temperature and snow depth over EZ1, lead to an average decrease of 1, 16, and 36 days for FD_{year}. On the other hand, in EZ8 where the lowest shifts in FD_{year} are observed, both temperature and snow depth experience lower shifts in the mean ensemble of models (1.2, 2.5, and 4.4℃ warming and 1,4, and 8 cm less snow depth for short-, mid-, and long-range time episodes, respectively) which leads to +2, -10, and -16 days changes in FD_{year}.

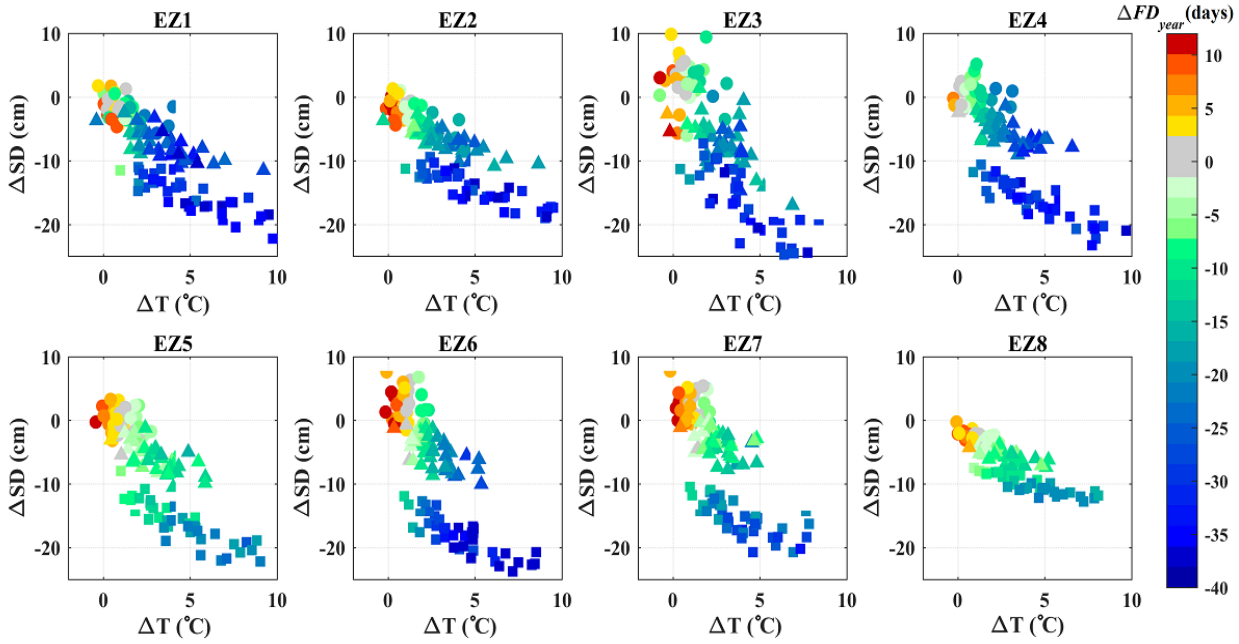

Figure 6.10 Control of changing temperature and snow depth on FD_{year} across different ecozones of Québec. The results for short-range (2034-2040), mid-range (2064-2070), and long-range (2094-2100) future projections are displayed with circles, triangles, and squares, respectively.

Looking at FTD_{DJF}, higher shifts in FTD_{DJF} are observed in the two southern ecozones of the province (i.e. EZ7 and EZ8) as well as EZ4. In EZ7, where the highest shifts in FTD_{DJF} are observed, an average change of 2.1, 4.4, and 8.3℃ warming and 1,8, and 23 cm less snow depth leads to an average increase of 2,5, and 12 days in FTD_{DJF}. As another important example, in EZ8, both temperature and snow depth experience lower shifts in the mean ensemble of models (2.1, 3.4, and 5.6℃ warming and 2, 5, and 14cm decrease in snow depth over short-, mid-, and long-range time episodes, respectively), while the FTD_{DJF} in this ecozone decrease significantly by an average of roughly 3, 6, and 10 days over the studied time episodes. The results of this section further highlight the high vulnerability of FTD_{DJF} to changing temperature and snow depth in the southern parts of the province. The observed spatial patterns in future FT characteristics due to changing climate can reveal the role of ecosystem conditions in regulating the impacts of changing temperature on snow depth and consequently FT dynamics.

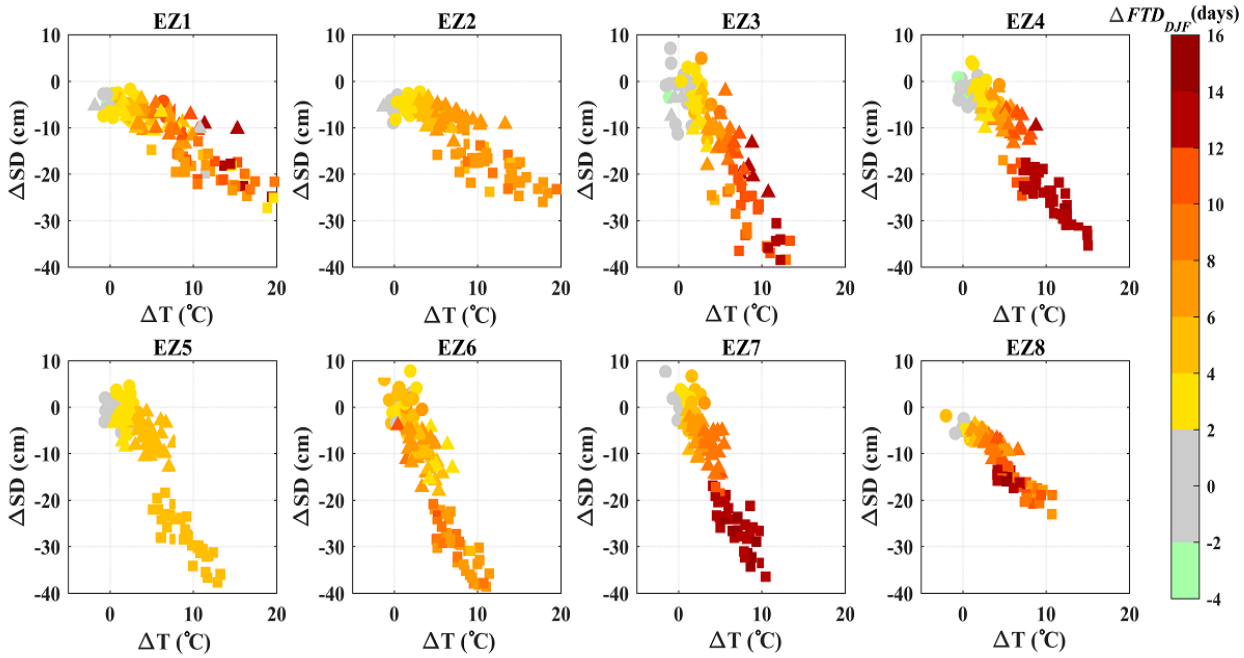

Figure 6.11 Control of changing temperature and snow depth on FTD_{DJF} across different ecozones of Québec. The results for short-range (2034-2040), mid-range (2064-2070), and long-range (2094-2100) future projections are displayed with circles, triangles, and squares, respectively.

6.5.3 Evolution of probability distribution of FT characteristics due to changing climate

As the last step of this study, the future dynamics of FD_{year} and FTD_{DJF} are investigated. The changes in FD_{year} is specifically looked into across EZ1, the northern ecozone of Québec, where the rate of changes due to changing temperature and snow depth is rather high and the uncertainty of the modeled snow depth is lower – see section "The predictive uncertainty over observed and future periods" of Part 1. For FTD_{DJF}, the results are studied over EZ8, the second southern ecozone of the province, due to the highest vulnerability of FTD_{DJF} to changing temperature and

snow depth and the low uncertainty in modeled snow depth in this ecozone. In Figure 6.12, we present the shifts in the probability distribution of FD_{year} given the different projections of hydroclimatic variables in EZ1. The right, middle, and left columns in Figure 6.12 show the changes in FD_{year} under short-range (2034-2040), mid-range (2064-2070), and long-range (2094-2100) future projections, respectively. The first and second row panels display the results corresponding to RCP4.5 and RCP8.5 scenarios. The probability distribution of FD_{year} under historical hydroclimatic conditions under present day using the multimodel mean ensemble of all GCM data isdisplayed with black lines. The solid vertical black lines show the mean value of FD_{year} over the historical period of GCMs. The solid and vertical dashed red (purple) lines show the probability corresponding to the multimodel mean ensemble for all GCM models in each time episode and its mean values under RCP4.5 (RCP8.5), respectively. The gray lines show the probability distribution of FT characteristics using over the historical period using the observed data.

The results clearly show the increasing magnitude of change in FD_{year} due to later time episodes. Looking at RCP4.5 scenarios, for instance, the projected FD_{year} over the short-range, mid-range, and long-range future show average change of +2, -18, and -30 days across EZ1. Looking at RCP8.5 scenarios higher magnitude of the shift in this FT characteristic is observed, showing the average of -4, -27, and -42 days change in FD_{year} due to short-range, mid-range, and long-range future projections. The higher shifts due to RCP8.5 are more significant over later time episodes. In the short-range future, for instance, the change in FD_{year} is 6 more days under RCP8.5 compared to RCP4.5. This change is 9 more days due to RCP8.5 compared to RCP4.5 in the mid-range future while it reaches 12 more days under RCP8.5 *vs.* RCP4.5 over the long-range future. Finally, considering the PDFs of simulated FD_{year} for different GCM models over the studied time episodes, the results highlight the higher variability in simulated time series over the short-range period. These variabilities are decreasing moving towards later time episodes. Furthermore, comparing the simulated PDFs obtained from RCP4.5 *vs.* RCP8.5 projections, it is observed that the variability of simulated FD_{year} is considerably higher for RCP4.5 projections.

Figure 6.13 shows the results for the same analysis for FTD_{DJF} across EZ8. The results highlight the higher changes in FTD_{DJF} over later time episodes. The projected FTD_{DJF} under RCP4.5 shows an increase of +2, +6, and +10 days in FTD_{DJF}, respectively. These changes are +2, +5, and +10 days for RCP8.5. Although similar changes in FTD_{DJF} under RCP4.5 and RCP8.5 are observed over both short-range and long-range futures, the amplifying impacts over time are only observed under RCP8.5. The variabilities in simulated time series are lower compared to that of FD_{year}. These variabilities are decreasing moving towards later time episodes. Comparing the variability in simulated time series for RCP4.5 and RCP8.5, higher variabilities are observed for RCP4.5 simulations.

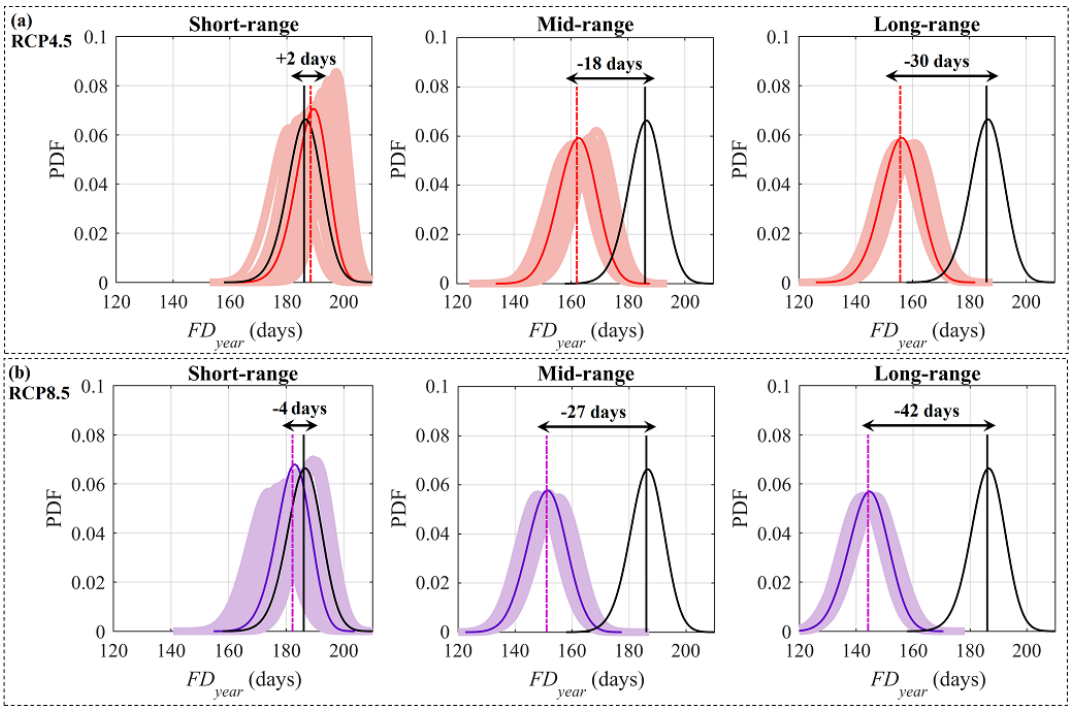

Figure 6.12 The Probability Density Functions (PDF) of FD_{year} in EZ1 given different climatic scenarios. Top row panels display the shifts in FD_{year} under RCP4.5 for long-range, mid-range and short-range time episodes. The panels in bottom row show the changes in FD_{year} under RCP8.5.

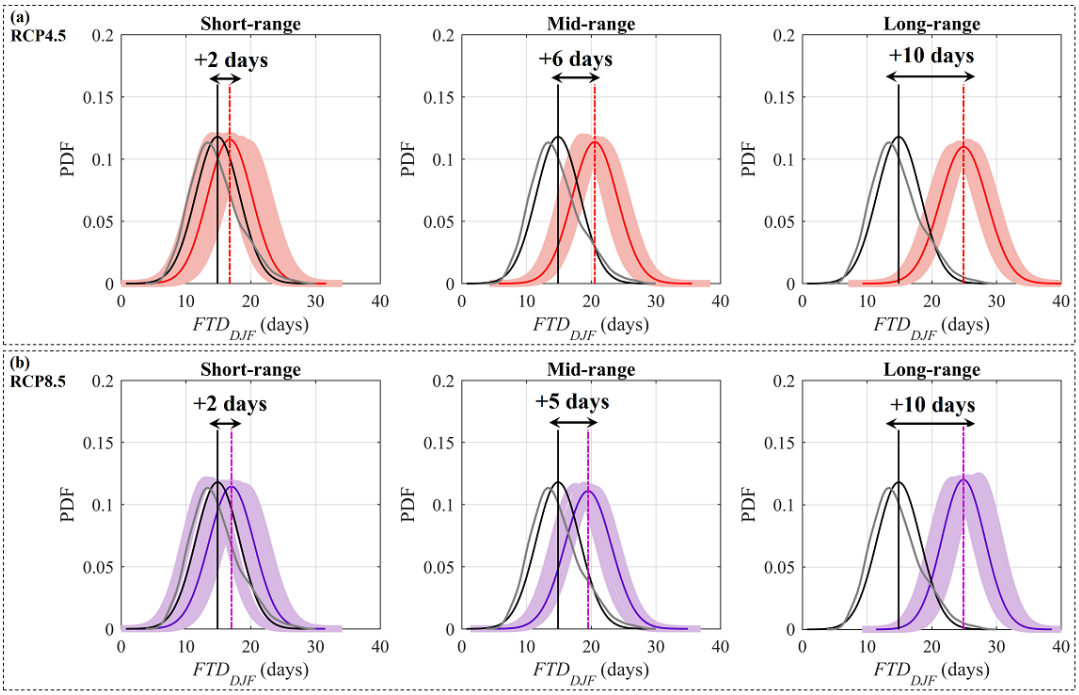

Figure 6.13 The Probability Density Functions (PDF) of FTD_{DJF} in EZ8 given different climatic scenarios. Top row panels display the shifts in FTD_{DJF} under RCP4.5 for long-range, mid-range and short-range time episodes. The panels in bottom row show the changes in FTD_{DJF} under RCP8.5.

6.6 Conclusions

FT dynamics are among the most important components of the cryosphere across higher latitudes, controlling the regional hydrology, phenology, and land-atmospheric interactions. Changes in FT characteristics can further create feedback effects with other elements of the environment. These changes can, for instance, unleash a substantial amount of greenhouse gas fluxes into the atmosphere due to the thawing of the previously frozen soil and consequently intensifying the rate of the warming climate. Due to these impacts, projecting the future FT dynamics is an important consideration point for advising land management and adaptation strategies in northern communities. The role of changing temperature and snow depth, as the two most important climatic drivers of landscape FT, has been the subject of many studies. Having said that, to the best of the authors' knowledge, there is not a study yet to address the compound impacts of changes in temperature and snow depth on FT characteristics across different spatiotemporal scales while considering the nonstationarity in the dependence structure between FT characteristics and impactful hydroclimatic variables. Here, we shift the focus of FT modeling from continuous descriptions of FT states to quantifications of statistical properties of FT characteristics across different temporal and spatial scales. Then using C-vine copula models we formally represent the interdependencies between the FT characteristics, temperature, and snow depth. Finally, we used a dynamic statistical model to project the future dynamics of FT due to future projections of temperature and snow depth. To account for any possible change in the dependence structure over the future period, the parameters of the proposed model are updated using one of the simplest, yet most widely used regression-based scheme. In our time-varying model, the parameters of the proposed model are directly linked to a set of relevant hydroclimatic variables, available from future projections of temperature and snow depth. To showcase the performance of the proposed model across a coarse spatial scale, we implemented the proposed model for the projection of FT dynamics across the province of Québec, Canada, the largest province of Canada with a landmass of 20% larger than Western Europe. The future projections of temperature and snow depth are obtained using a quantile-based bias-correction method as well as a statistical framework defined in Part 1 of this double feature paper.

Based on our results, the dependence structure between at least one pair of involved variables (i.e. temperature, snow depth, and FT characteristics) is changing significantly in almost all of the ecozones of Québec. This observation shed lights on the need for developing a time-varying model parametrization to update the model parameters over time. First, we evaluate the performance of the proposed model under historical condition. The calibrated model over the observed period performs well in capturing the marginal and joint characteristics of FT dynamics, demonstrating $R^2 > 0.92$, $NSE > 0.89$, and RE $< 3\%$ in representing the annual number of frozen days and $R^2 > 0.89$, $NSE > 0.72$ and RE $< 9.2\%$ in representing the number of days with transient state in winter. The regression-based scheme is also found to have a rather satisfactory accuracy in representing the changes in the model parameters while necessary with NSE higher than 70% in the most of the cases. Furthermore, the good performance of the model in representing the

dynamics of FT characteristics under historical condition ensures accurate projections over the future periods.

The proposed model provides a tool for a top-down impact assessment and understanding the control of changing temperature on snow depth and consequently FT characteristics through (1) RCP-based paradigm and (2) temperature-based approach. Looking at the results from the RCP-based approach, a spatial pattern in projected FT characteristics is observed in the future, showing that the changes in these characteristics are amplifying over time. The rate of amplification over time is higher in southern regions. Employing the temperature-based approach, spatial diversity is observed in the compound impacts of changing temperature and snow depth on studied FT characteristics. The impacts of warming temperature on the number of days with the transient state in winter, for instance, is more pronounced across southern ecozones of the province. The higher sensitivity of transient days to changing temperature in the southern ecozones can cause considerable damages to civil infrastructures in these highly populated regions already suffering from aging infrastructure. Moreover, the likelihood of future increasing temperature scenarios in the northern ecozones of the province is significantly higher. In some of these ecozones, the annual number of frozen days is projected to decrease by more than 33 days due to 6℃ increasing temperature. This is of great importance due to the role of this FT characteristic on greenhouse gas emissions as a result of permafrost degradation across the northern regions. The observed spatial patterns in control of changing climate on FT characteristics can reveal the role of physiographic features such as land cover, vegetation type, and soil type in regulating the impacts of changing climate on FT dynamics. Finally, our results demonstrate the intensifying changes in FT characteristics over time, while the departure between the results obtained for RCP8.5 *vs.* RCP4.5 is increasing over later time episodes. The results also highlight a decrease in the variability of future projection of FT characteristics in later time episodes.

The proposed framework is globally relevant and can be employed for top-down impact assessment and to statistically address the compound impacts of changes in different variables on any environmental processes over any spatial and temporal scales. The sensitivity of findings to data supports (i.e. FT data, hydroclimatic data, and the future projections), however, is not yet clear. This understanding is an essential step toward accurate uncertainty analysis of our findings. Moreover, the performance of this framework should be investigated across other regions with possibly different land-surface characteristics and more ecosystem diversity.

Chapter 7.
Conclusion and Future Research Need

This study established a global statistical framework to estimate the landscape Freeze-Thaw under changing climate; from characterizing the individual and compound impacts of changing temperature and snow depth on FT dynamics, to modeling the future snow depth, to projecting the future dynamics of FT under future climate conditions. To showcase the application of the proposed framework, the datasets of satellite-based FT, gridded observed hydroclimatic variables, and gridded downscaled climatic variables are paired over Québec, the largest province in Canada. As the size and centroid of gridded data are not the same, the raw data are regridded in a common grid system before further use. The entire landmass of Québec undergoes three states of FT during a typical year, including continuous periods of frozen and thawed states, divided by a transit period in which the landscape switches between frozen and thawed conditions throughout a diurnal cycle. As the area of Québec is massive and landscape characteristics are diverse, regional FT characteristics are subject to large spatial variability.

7.1 Key findings

Having said that, the main conclusions of the proposed framework conducted under this thesis can be summarized as follows:

- The dynamics of FT are largely governed by the near surface air temperature and snow depth. The changing climate can, hence, alter historical characteristics of FT quite substantially; and such changes have been already observed across cold regions. However, there are some drawbacks in conventional studies focusing on the control of changing climate of FT dynamics. First, the current understandings are mainly based on the in-situ measurements which suffer sparsity and local relevance. Moreover, the current dominant paradigm to assess the impacts of changing climate on FT dynamics is based on the use of physically-based algorithms. Such approaches are limited regionally due to poor process representations, the lack of scalability as well as limitations in data support at larger scales and model parametrization. Furthermore, it is not yet clear whether changes in the FT characteristics are solely due to changes in temperature and snow depth conditions; or, it is due to a more profound change in the relationship between these impactful variables and FT characteristics at the landscape scale. Finally, no studies investigate and take into account any possible changes in the dependence structure between temperature, snow depth, FT characteristics.

- Our findings highlight significant variations in the dependence structure between temperature, snow depth, and FT characteristics across time and space. The changes in the dependencies over different regions reveal the role of ecosystem conditions such as vegetation type, elevation, slope, and latitude in regulating the impact of temperature on FT characteristics. The changes in the dependence structure over time also highlight the revelation of climate change.

- The bivariate copula methodology is utilized in a bottom-up impact assessment setting to represent the control of temperature on FT dynamics. The response of FT characteristics to temperature change is found to be nonsymmetric across different temporal and spatial scales. The comparison of the change in the number of frozen days over the spring season under the unique degree alterations in expected temperature, for instance, shows the higher impacts of cooling *vs.* warming. Moreover, the changes in number of frozen days in spring due to identical change in regional temperature is considerably higher in northern ecozones, while the changes in number of thawed days in spring are more sensitive to changes in expected temperature in southern regions. I show that the impacts of a similar magnitude of temperature change are higher under more recent dependencies. These findings clearly point at the role of variations in marginal characteristics of temperature, as well as joint dependencies between temperature and FT characteristics causing a complex and multifaceted nature of temperature control on FT dynamics.

- The trivariate C-vine copula methodology is employed in the next step of this study to identify the compound impacts of changes in temperature and snow depth on FT patterns using a bottom-up impact assessment approach. Based on the results of this section, the simulations obtained by parametrized C-vine copulas can capture the marginal and joint characteristics of FT characteristics with high accuracy. The impacts of changing temperature and snow depth are found to be unique with a spatial divide in the FT response to changing climate conditions. The ecozonal uniqueness in the interdependencies between studied FT characteristics, temperature, and snow depth points at the role of ecosystem conditions in regulating the impact of changing climate conditions on FT characteristics. It is also shown that the nature of the FT response to changing temperature and snow depth conditions are significantly different and nonsymmetric across different regions and spatial scales. In general, it is concluded that the changes in FT characteristics are more intense due to rising temperature and/or thinning snow depth compared to corresponding scenarios with falling temperature and/or thickening snow depth, especially in regions with higher sensitivity in FT response. To increase the spatial resolution, the FT response to changing climate is also studied at the grids scale. The obtained results reveal the nonlinear amplifying responses of FT characteristics to compound changes in impactful climatic variables. The amplifying response is considered as the case where the response of FT to compound changes in temperature and snow depth is more severe than the cumulative response of FT due to changes in temperature and snow depth individually. These amplifying impacts can result in up to two weeks of alterations in the frozen period during a typical year in the north, and up to one week change in the transient period during a typical winter season in the three most populated regions of Québec, i.e., Montréal, Québec City, and Gatineau. While amplified shrinkage in the annual frozen period in the north can result in unprecedented changes in the northern environment under compound warming, the similar climatic condition can lead to additional stress to already aging infrastructures

in the south. The amplifying response is also observed in the likelihood of the number of transient days over the winter season exceeding the long-term historical values.

- A simple statistical framework, initially at station scale, is developed to describe the dynamics of snow accumulation and loss. This framework is then extended to a more global approach providing a statistical tool for projecting the future dynamics of snow depth. Fusing a forward input selection scheme with Multiple Linear Regression an accurate, parsimonious, and robust framework is proposed for representing the monthly dynamics of snow depth across 67 stations spanning throughout southern Canada. Comparison of model performance with a conceptual temperature-index model, the statistical approach outperforms in terms of accuracy in the majority of the considered stations. The proposed statistical model is also shown to be capable of being regionalized only with the three most primary geographic characteristics, i.e. latitude, longitude, and altitude, providing the opportunity of extending the use of the model in ungauged sites. The proposed methodology has enormous practical applications from being linked to monthly weather forecasts, to providing monthly predictions of the snow depth, to being fed by downscaled climate model outputs to project monthly snow depth under climate change conditions.

- The application of the proposed framework for modeling the monthly dynamics of snow depth at station scale is then extended from local to regional scale to project the future dynamics of snow depth at the grid scale. A set of algorithmic advancements are added to previously developed statistical frameworks for different purposes such as retrieval of the precipitation type (snow *vs.* rain) and potential bias correction for linking to climate projections rather than observation. The form of precipitation is classified using a simple Bayesian Classifier calibrated by the station-based climate data. The calibrated classifier in modeling the form of precipitation has a good performance over all of the considered stations. Hence, it is upscaled to a regional scale to extract the threshold of temperature at which the type of precipitation is changing from snow to rain. The type of precipitation is then classified for all the grids across the province. A regional input selection scheme is employed allowing for considering the role of ecosystem conditions in regulating the impacts of changing climate on the dynamics of snow depth. The models are calibrated at the grid scale using the observed gridded data. The calibrated MLRs show high accuracy in quantifying the observed dynamics of snow depth as well as representing the monthly dynamics of snow depth in case of using the bias corrected climate data over a common time period. The good performance of the MLR models in representing the monthly dynamics of the observed period while using the bias corrected climate data ensures the accurate projections of future conditions. Based on the results, the rate of change in snow depth increases moving from southern to northern regions. Moreover, the results highlight the need for further bias correction of already available downscaled climate data due to the low accuracy of snow depth models when fed with already available downscaled data. Finally, the changes in future snow depth are found to be amplified over time specifically

in northern parts of the province. Lower predictive and parametric uncertainties associated with the proposed framework are observed in the northern and southern parts of the province show the higher practicability of the proposed framework in these regions.

- As the last step of this study, the previously proposed algorithms are combined and revised to provide a global statistical framework for top-down projection of FT while taking into account the nonstationarity in the dependence structure between involving variables. The significant trends in the interdependencies between at least one pair of temperature, snow depth, and FT characteristics indicate the need for updating the model parameters over time. The proposed model is found to have high accuracy in capturing the marginal and joint characteristics of FT dynamics over the observed period as well as while being fed with bias corrected temperature and modeled snow depth over the historical period. The impacts of changing temperature and snow depth on FT characteristics over the future are represented in two ways: (1) RCP-based and (2) temperature-based each providing a unique way for the interpretation of the results. Using the RCP-based representation, for instance, an amplification in the changes in FT characteristics over time is observed. Employing the temperature-based representation, on the other hand, a spatial diversity is observed in the compound impacts of changing temperature and snow depth on studied FT characteristics. For instance, it is observed that in some of the northern regions of the province, the annual number of frozen days is projected to decrease by more than 15 days due to 2℃ increasing temperature. In the southern regions, however, the number of transient days in the winter season shows higher sensitivity to changing climate, projected to increase by more than 6 days due to 2℃ in some ecozones. Finally, our results demonstrate the intensifying changes in FT characteristics over time, while the departure between the results obtained for different carbon emission scenarios is increasing over later time episodes. The variability in the future projection of FT characteristics is also found to decrease over time. Although I only focus on the impacts imposed by changes in temperature and snow depth conditions and apply the proposed methodology only in the province of Québec, Canada, I make a particular effort to develop a generic framework that can include other variables and be applicable in other regions and/or globally.

7.2. Relevance to future engineering application

Understanding the impacts of changing climate on FT characteristics can provide invaluable knowledge for advising effective adaptation strategies for future human development and ecosystem functioning. This is due to the role of FT dynamics in controlling eco-hydrological processes and accordingly its impacts on human infrastructures and activities.

- As an important example of Freeze-Thaw implications, the changes in FT dynamics can lead to substantial environmental changes due to amplified rates of permafrost degradation. This is globally relevant due to massive land-induced carbon and nitrogen emissions from

the previously frozen land which can intensify the rate of global warming unprecedentedly. Having comprehensive information on the rate of greenhouse gasses emitted from frozen *vs.* thawed land, the future changes in land-induced greenhouse gas fluxes due to changing FT dynamics can be accurately quantified using the proposed framework. The Arctic Tundra biome, for instance, is known to be one of the main potential sources of carbon emission under warming climate, contributing to land-atmospheric emission of approximately 10 and 5.4 ($gCm^{-2}season^{-1}$) of CO_2-C and CH_4-C, respectively (Mcguire et al., 2012). Knowing the amount of land-atmospheric carbon release from a unit of unfrozen land over any temporal scale, the changes in FT characteristics (such as length of nonfrozen season) due to changing climate can be utilized to derive the positive and negative change in magnitude of net carbon release to the atmosphere.

- The agricultural activities and growing season are directly or indirectly affected by the dynamics of Freeze-Thaw. Soil freezing, for instance, directly damages agricultural products, increases crop mortality, and decreases yield. It also poses a seasonal constraint by altering the growing season. Indirectly, it also affects agricultural activities by changing soil moisture, bulk density, nutrients, and soil biotic factors. Having the information on future changes in FT characteristics such as length of frozen and thawed period and employing this information in integrated water recourses models (Hassanzadeh et al., 2014; Memarian et al., 2014) is, hence, of a great importance for advising land use and land management strategies in northern latitudes.

- Freeze-Thaw dynamics also act as a controller to various natural processes taking place in the critical zone of the soil, including bulk density and hydraulic conductivity that determine the storage and movement of moisture and nutrients. When soil freezes, hydraulic conductivity reduces, leading to decreasing infiltration and increasing surface transport. When the landscape thaws, water pathways are formed below and above the land surface; and in some regions, surface and sub-surface water reserves connect to one another. Using the information of the changes in soil infiltration and moisture due to changes in FT characteristics (Ding et al., 2019) and considering this information in different hydrological models (Unduche et al., 2018) provides essential understanding for operational flood forecasting across cold regions.

- Moreover, the increasing number of transient days can be potentially harmful to urban infrastructures including but not limited to roads, buildings, drainage systems, pipelines, and airports. In Montréal, for instance, it is shown that under the historical condition in the next 20 years, 216km out of the total length of the city pipeline (2719km) will need to be replaced while other 2400km will require repairing (Zangenehmadar et al., 2020). This rate will change due to changing climatic conditions impacting the damages to the pipeline system. As another example, a lower number of FT cycles due to the warming climate in Alaska is estimated to decrease the damages to the roads and airports by roughly 20-25 million dollars (reported in 2015 dollars) by the end of 2099 (Melvin et al., 2017). It is also

shown that even a few more days with transient state can significantly degrade the properties of the civil engineering materials such as Marshall stability of asphalt concrete (Özgan and Serin, 2013). Implementing the information on changes in FT characteristics (such as number of days with transient state) in already available engineering tools such as Infrastructure Planning Support System software (Chinowsky et al., 2013; Schweikert et al., 2014) provides invaluable knowledge on climate change damages to the infrastructure specifically in higher latitudes.

7.3. Limitations, challenges, and ways forward

While a number of methodological advancements have been made and several crucial understandings have been extracted throughout this study, further researches can be performed to address other aspects of the control of changing climate on FT dynamics:

- Although the proposed framework is applied across the province of Québec and using a particular dataset, it is globally relevant and can be implemented through pairing other relevant datasets too. However, it is not yet clear how much the findings are sensitive to these specific datasets, from which temperature, snow depth, and FT characteristics along with their joint dependencies are inferred. This is an important step towards quantifying uncertainty in our findings in Québec and should be also considered in other regions to give a broader perspective on the future changes in FT dynamics.

- Although here we rigorously looked into the interdependencies between involving climatic variables such as temperature, snow depth, and FT characteristics, the causal interaction of mentioned time series is not investigated. Using methodologies such as Granger causality statistical test (Granger, 1990) can provide invaluable information to go beyond the dependence structure and aim at a mechanistic reconstruction of causes and consequences in observed systems.

- For the studies related to the bottom-up impact assessments, the changes in the dependence structure have not been taken into the account. Having said that, based on the results from the final works, it is clearly shown that the dependencies between at least one pair of temperature, snow depth, and FT characteristics are changing over time. This further highlights the need for proposing a dynamic bottom-up impact assessment approach for better quantification of the impacts of changing climate on FT dynamics.

- Many studies show the importance of removing the temporal trends as well as autocorrelation from the series to obtain a stationary process (Cong and Brady, 2012; Jalili Pirani and Najafi, 2020; Manton et al., 2001). This is one of the assumptions that can be considered while employing the copula methodology in further studies. The Mann-Kendall trends test and Sen's slope estimator can be utilized to statistically estimate the trends in the time series (Kendall, 1975; Mann, 1945; Sen, 1968). Any present significant trends can

be removed by simple regression-based methods. The existence of autocorrelation can be detected by methods such as Box-Pierce and Ljung-Box tests (Box and Pierce, 1970; Ljung and Box, 1978) and procedures such as pre-whitening techniques can be used to remove any autocorrelation (Hobbs et al., 2013; Kwasnicka et al., 2017). Removing the autocorrelation and/or trend, however, will lead to difficulties in the interpretation of results as well as heterogeneity in the computation and impact assessment as it requires adding another parametric procedure.

- In this study, the bulk density of snow, as another important property of snow relating to its depth and mass, is not taken into the account. Hence, the compactness of snow is not considered while looking into snow depth as one of the main influential variables on the dynamics of FT characteristics. Various methodologies can be employed to extract the bulk density of snow having the snow depth and other data such as the date of the year and the geographic characteristics of the location (McCreight and Small, 2014; Sturm, 2010). Also, gridded snow water equivalent data, available from different sources such as CMC and MODIS, can be used to provide an understanding of the snow density at grid scale (Brown et al., 2003; Savtchenko et al., 2004). Hence, it is important to study the potential role of snow density in controlling the FT patterns. The proposed methodology can be then extended to a higher dimension to accommodate snow density as one of the influential drivers of FT dynamics.

- Adding other information of the physical characteristics such as soil and vegetation type, elevation, and slope to the proposed methodology may enhance the performance and accuracy. However, a few issues must be considered. First and foremost, statistical methodologies, such as the copula approach, is considering the physical characteristics at regional scale by means of model parametrization. Second, it must be taken into account that the involving variables in the proposed framework must be continuous in order to be added to the proposed approach. Finally, the data on physical characteristics of the land are mostly provided at finer spatial resolutions compared to what is used in this study. Hence, further data analysis is required before any source of new data is added to this framework.

- Among the known limitations of the proposed methodology, we can mention to the problem of top-down modeling uncertainty across the spatial scale. Due to model development over the regional scale, the FT characteristics at any specific grid is overlooked. This limits analyzing the impacts of changing climate on FT dynamics at local scale. Although, utilizing data sets with finer temporal variations can mathematically provide the capability to use the same methodology at finer spatial scales, however, the low dependencies among temperature, snow depth, and FT characteristics at the shorter time intervals such as daily scales will significantly degrade the copula modeling performance.

- Finally, although the proposed time-varying dependence model is capable of updating the model parameters over time, this study is performed at the regional scale. Closer looks at the FT responses at the grid scale can provide more accurate information at finer spatial resolutions. A new algorithm is required to update the parameters of the statistical models at each grid, due to the incapability to obtain the copula model parameters in each year at grid scale. To solve this problem, the concept of moving window can be used (Nazemi et al., 2017). For each grid, a timeframe with desirable length can be considered and then moved year-by-year in which the model parameters can be obtained. The regression-based scheme can be consequently employed to update the model parameters over time based on the set of hydroclimatic proxies in studied timeframes. However, a dataset with a longer available observed period is required to achieve better performance in modeling dependencies in each timeframe as well as calibrating the regression-based models for updating the parameters.

Bibliography

Aas, K., Berg, D., 2009. Models for construction of multivariate dependence - a comparison study. Eur. J. Financ. 15, 639–659. https://doi.org/10.1080/13518470802588767

Aas, K., Czado, C., Frigessi, A., Bakken, H., 2009. Pair-copula constructions of multiple dependence. Insur. Math. Econ. 44, 182–198. https://doi.org/10.1016/j.insmatheco.2007.02.001

Abrahart, R.J., Anctil, F., Coulibaly, P., Dawson, C.W., Mount, N.J., See, L.M., Shamseldin, A.Y., Solomatine, D.P., Toth, E., Wilby, R.L., 2012. Two decades of anarchy? Emerging themes and outstanding challenges for neural network river forecasting. Prog. Phys. Geogr. 36, 480–513. https://doi.org/10.1177/0309133312444943

Acar, E.F., Craiu, R. V, Yao, F., 2011. Dependence Calibration in Conditional Copulas : A Nonparametric Approach. Biometrics 67, 445–453. https://doi.org/10.1111/j.1541-0420.2010.01472.x

Adamowski, J., Fung Chan, H., Prasher, S. O., Ozga-Zielinski, B., Sliusarieva, A., 2012. Comparison of multiple linear and nonlinear regression, autoregressive integrated moving average, artificial neural network, and wavelet artificial neural network methods for urban water demand forecasting in Montreal, Canada. Water Resources Research. 48, 1.

Adamowski, J.F., 2008. Development of a short-term river flood forecasting method for snowmelt driven floods based on wavelet and cross-wavelet analysis 247–266. https://doi.org/10.1016/j.jhydrol.2008.02.013

Adler, R.F., Huffman, G.J., Chang, A., Ferraro, R., Xie, P.P., Janowiak, J., Rudolf, B., Schneider, U., Curtis, S., Bolvin, D., Gruber, A., Susskind, J., Arkin, P., Nelkin, E., 2003. The version-2 global precipitation climatology project (GPCP) monthly precipitation analysis (1979-present). J. Hydrometeorol. 4, 1147–1167. https://doi.org/10.1175/1525-7541(2003)004<1147:TVGPCP>2.0.CO;2

AghaKouchak, A., 2015. A multivariate approach for persistence-based drought prediction: Application to the 2010-2011 East Africa drought. J. Hydrol. 526, 127–135. https://doi.org/10.1016/j.jhydrol.2014.09.063

AghaKouchak, A., Bárdossy, A., Habib, E., 2010. Conditional simulation of remotely sensed rainfall data using a non-Gaussian v-transformed copula. Adv. Water Resour. 33, 624–634. https://doi.org/10.1016/j.advwatres.2010.02.010

AghaKouchak, A., Huning, L., Chiang, F., Sadegh, M., Vahedifard, F., Mazdiyasni, O., Moftakhari, H., Mallakpour, I., 2018. How do natural hazards cascade to cause disasters? Nature 458–460.

Ali, S.H., 2009. Mining, the environment, and indigenous development conflicts. University of Arizona Press.

Amir Jabbari, A., Nazemi, A., 2019. Alterations in Canadian Hydropower Production Potential Due to Continuation of Historical Trends in Climate Variables. Resources 8, 163. https://doi.org/10.3390/resources8040163

Anderson, E. A., 1976. A point of energy and mass balance model of snow cover. NOAA Technical Report NWS, 19, 1-150. National Oceanic and Atmospheric Administration, United State Department of Commerce.

Andrews, T. D., Kokelj, S. V., MacKay, G., Buysse, J., Kritsch, I., Andre, A., Lantz, T., 2016. Permafrost thaw and Aboriginal cultural landscapes in the Gwich'in Region,Canada. APT Bull. J. Preserv. Technol. 47, 15–22.

Anisimov, O.A., Nelson, F.E., 1996. Permafrost distribution in the Northern Hemisphere under scenarios of climatic change. Glob. Planet. Change 14, 59–72.

Arns, A., Dangendorf, S., Jensen, J., Talke, S., Bender, J., Pattiaratchi, C., 2017. Sea-level rise induced amplification of coastal protection design heights. Sci. Rep. 7, 40171. https://doi.org/10.1038/srep40171

Arsenault, R., Brissette, F. P., 2014. Continuous streamflow prediction in ungauged basins: The effects of equifinality and parameter set selection on uncertainty in regionalization approaches. Water Resources Research. 50, 7, 6135-6153.

Ashouri, H., Hsu, K.L., Sorooshian, S., Braithwaite, D.K., Knapp, K.R., Cecil, L.D., Nelson, B.R., Prat, O.P., 2015. PERSIANN-CDR: Daily precipitation climate data record from multisatellite observations for hydrological and climate studies. Bull. Am. Meteorol. Soc. 96, 69–83. https://doi.org/10.1175/BAMS-D-13-00068.1

Atchley, A.L., Coon, E.T., Painter, S.L., Harp, D.R., Wilson, C.J., 2016. Influences and interactions of inundation, peat, and snow on active layer thickness. Geophys. Res. Lett. https://doi.org/10.1002/2016GL068550

Atlas of Canada, Natural Resources Canada, 2016. <https://www.nrcan.gc.ca/maps-tools-and-publications/maps/atlas-canada/10784>.

Bach, F., 2017. Breaking the curse of dimensionality in regression. J. Mach. Learn. Res. 18, 629–681.

Bales, R. C., Hopmans, J. W., O'Geen, A. T., Meadows, M., Hartsough, P. C., Kirchner, P Hunsaker, C. T., Beaudette, D., 2011. Soil moisture response to snowmelt and rainfall in a Sierra Nevada mixed-conifer forest. Vadose Zone Journal. 10, 3, 786-799.

Bao, Y., Wen, X., 2017. Projection of China's near- and long-term climate in a new high-resolution daily downscaled dataset NEX-GDDP. J. Meteorol. Res. 31, 236–249. https://doi.org/10.1007/s13351-017-6106-6

Bárdossy, A., 2006. Copula-based geostatistical models for groundwater quality parameters. Water Resour. Res. 42, 1–12. https://doi.org/10.1029/2005WR004754

Bárdossy, A., Li, J., 2008. Geostatistical interpolation using copulas. Water Resour. Res. 44, 1–15. https://doi.org/10.1029/2007WR006115

Bárdossy, A., Pegram, G.G.S., 2009. Copula based multisite model for daily precipitation simulation. Hydrol. Earth Syst. Sci. 13, 2299–2314. https://doi.org/10.5194/hess-13-2299-2009

Barnes, W.L., Xiong, X.J., Salomonson, V. V., 2003. Status of Terra MODIS and Aqua MODIS. Adv. Sp. Res. 32, 2099–2106. https://doi.org/10.1109/igarss.2002.1025746

Barnett, T. P., Adam, J. C., Lettenmaier, D. P., 2005. Potential impacts of a warming climate on water availability in snow-dominated regions. Nature. 438, 7066, 303-309.

Bechmann, M.E., Kleinman, P.J.A., Sharpley, A.N., Saporito, L.S., 2005. Freeze-Thaw Effects on Phosphorus Loss in Runoff from Manured and Catch-Cropped Soils. J. Environ. Qual. 34,

2301–2309. https://doi.org/10.2134/jeq2004.0415

Bedford, B.Y.T.I.M., Cooke, R.M., 2002. Vines : A New Graphical Model for Dependent Random Variables Author (s): Tim Bedford and Roger M . Cooke Source : The Annals of Statistics , Vol . 30 , No . 4 (Aug ., 2002), pp . 1031-1068 Published by : Institute of Mathematical Statistics Stable URL. Ann. Stat. 30, 1031–1068.

Beier, N.A., Sego, D.C., 2009. Cyclic freeze-thaw to enhance the stability of coal tailings. Cold Reg. Sci. Technol. 55, 278–285. https://doi.org/10.1016/j.coldregions.2008.08.006

Bender, J., Wahl, T., Jensen, J., 2014. Multivariate design in the presence of non-stationarity. J. Hydrol. 514, 123–130. https://doi.org/10.1016/j.jhydrol.2014.04.017

Bengtsson, L., 1984. Modeling snowmelt induced runoff with short time resolution. Series A. 10, < http://lup.lub.lu.se/record/2836046 >.

Bennett, J.C., Grose, M.R., Post, D.A., Ling, F.L.N., Corney, S.P., Bindoff, N.L., 2011. Performance of quantile-quantile bias-correction for use in hydroclimatological projections. MODSIM 2011 - 19th Int. Congr. Model. Simul. - Sustain. Our Futur. Underst. Living with Uncertain. 2668–2675.

Berg, D., Aas, K., 2007. Models for construction of multivariate dependence. Prepr. Ser. Stat. Res. Rep. 15, 639–659. https://doi.org/10.1080/13518470802588767

Bergstrom, S., 1976. Development and application of a conceptual runoff model for Scandinavian catchments.

Bhave, A.G., Mishra, A., Raghuwanshi, N.S., 2014. A combined bottom-up and top-down approach for assessment of climate change adaptation options. J. Hydrol. 518, 150–161. https://doi.org/10.1016/j.jhydrol.2013.08.039

Bland, J.M., Altman, D.G., 1995. Multiple significance tests: the Bonferroni method. BMJ 310, 170.

Bochove, E. Van, Prevost, D., Pelletier, F., 2000. Effects of Freeze – Thaw and Soil Structure on Nitrous Oxide Produced in a Clay Soil. oil Sci. Soc. Am. J. 64, 1638–1643.

Bonan, G.B., 1989. A computer model of the solar radiation, soil moisture, and soil thermal regimes in boreal forests. Ecol. Modell. 45, 275–306.

Borgomeo, E., Hall, J.W., Fung, F., Watts, G., Colquhoun, K., Lambert, C., 2014. Risk-based water resources planning: Incorporating probabilistic nonstationary climate uncertainties. Water Resour. Res. https://doi.org/10.1002/2014WR015558

Bosson, E., Selroos, J.O., Stigsson, M., Gustafsson, L.G., Destouni, G., 2013. Exchange and pathways of deep and shallow groundwater in different climate and permafrost conditions using the Forsmark site, Sweden, as an example catchment. Hydrogeol. J. 21, 225–237. https://doi.org/10.1007/s10040-012-0906-7

Bouezmarni, T., Camirand Lemyre, F., Quessy, J.F., 2019. On the large-sample behavior of two estimators of the conditional copula under serially dependent data. Metrika 82, 823–841. https://doi.org/10.1007/s00184-019-00711-y

Box, G.E.P., Pierce, D.A., 1970. Distribution of residual autocorrelations in autoregressive-integrated moving average time series models. J. Am. Stat. Assoc. 65, 1509–1526. https://doi.org/10.1080/01621459.1970.10481180

Bracken, C., Holman, K.D., Rajagopalan, B., Moradkhani, H., 2018. A Bayesian Hierarchical Approach toMultivariate Nonstationary Hydrologic Frequency Analysis. Water Resour. Res. 243–255. https://doi.org/10.1002/2017WR020403

Braithwaite, R. J., Zhang, Y., 1999. Modelling changes in glacier mass balance that may occur as a result of climate changes. Geografiska Annaler: Series A, Physical Geography. 81, 4, 489-496.

Brasnett, B., 1999. A Global Analysis of Snow Depth for Numerical Weather Prediction. J. Appl. Meteorol. 38, 726–740.

Brechmann, E.C., Schepsmeier, U., 2013. CDVine: Modeling Dependence with C- and D-Vine Copulas in R Eike. J. Stat. Softw. 52.

Brown, P.J., Degaetano, A.T., 2011. Agricultural and Forest Meteorology A paradox of cooling winter soil surface temperatures in a warming northeastern United States. Agric. For. Meteorol. 151, 947–956. https://doi.org/10.1016/j.agrformet.2011.02.014

Brown, R.D., Brasnet, B., 2010. Canadian Meteorological Centre (CMC) Daily Snow Depth Analysis Data, Version 1, Boulder, Colorado USA. NASA National Snow and Ice Data Center Distributed Active Archive Center. https://doi.org/https://doi.org/10.5067/W9FOYWH0EQZ3

Brown, R.D., Brasnett, B., Robinson, D., 2003. Gridded North American monthly snow depth and snow water equivalent for GCM evaluation. Atmos. - Ocean 41, 1–14. https://doi.org/10.3137/ao.410101

Brown, R.D., Mote, P.W., 2009. The Response of Northern Hemisphere Snow Cover to a Changing Climate *. J. Clim. 22(8), 2124–2145. https://doi.org/10.1175/2008JCLI2665.1

Broxton, P.D., van Leeuwen, W.J.D., Biederman, J.A., 2019. Improving Snow Water Equivalent Maps With Machine Learning of Snow Survey and Lidar Measurements. Water Resour. Res. 55, 3739–3757. https://doi.org/10.1029/2018WR024146

Brubaker, K, Rango, A, Kustas, W, 1996. Incorporating radiation inputs into the snowmelt runoff model. Hydrological Processes. 10, 10, 1329-1343.

Bürger, G., 2014. Comment on “bias correction, quantile mapping, and downscaling: Revisiting the inflation issue.” J. Clim. 27, 1819–1820. https://doi.org/10.1175/JCLI-D-13-00184.1

Burles, K., and Boon, S., 2011. Snowmelt energy balance in a burned forest plot, Crowsnest Pass, Alberta, Canada. Hydrological Processes. 25, 19, 3012-3029.

Butterbach-bahl, K., Wolf, B., 2017. Greenhouse gases: Warming from freezing soils. Nat. Publ. Gr. 10, 248–249. https://doi.org/10.1038/ngeo2915

Cannon, A.J., Sobie, S.R., Murdock, T.Q., 2015. Bias correction of GCM precipitation by quantile mapping: How well do methods preserve changes in quantiles and extremes? J. Clim. 28, 6938–6959. https://doi.org/10.1175/JCLI-D-14-00754.1

Cao, B., Gruber, S., Zheng, D., Li, X., 2020. The ERA5-Land soil temperature bias in permafrost regions. Cryosph. 14, 2581–2595.

Carpino, O.A., Berg, A.A., Quinton, W.L., Adams, J.R., 2018. Climate change and permafrost thaw-induced boreal forest loss in northwestern Canada. Environ. Res. Lett. 13, 084018. https://doi.org/10.1088/1748-9326/aad74e

Cestnik, B., 1990. Estimating probabilities: A Crucial Task in Machine Learning. ECAI. 90, 147–149.

Chamberlain, E.J., Iskandar, I., Hunsicker, S.E., 1990. Effect of freeze-thaw cycles on the permeability and macrostructure of soils. Cold Reg. Res. Eng. Lab. 90, 145–155.

Chebana, F., Ouarda, T.B.M.J., 2021. Multivariate non-stationary hydrological frequency analysis. J. Hydrol. 593, 125907. https://doi.org/10.1016/j.jhydrol.2020.125907

Chebana, F., Ouarda, T.B.M.J., Duong, T.C., 2013. Testing for multivariate trends in hydrologic frequency analysis. J. Hydrol. 486, 519–530. https://doi.org/10.1016/j.jhydrol.2013.01.007

Chen, J.P., Zhong, I., Zhang, Y., Navar, D., Yeh, W.W., 2017. A decomposition-integration risk analysis method for real-time operation of a complex flood control system. Water Resour. Res. 53, 2490–2506. https://doi.org/10.1002/2016WR019842.Received

Chen, L., Chen, Z., Jia, G., Zhou, J., Zhao, J., Zhang, Z., 2020. Influences of forest cover on soil freeze-thaw dynamics and greenhouse gas emissions through the regulation of snow regimes: A comparison study of the farmland and forest plantation. Sci. Total Environ. 726, 138403. https://doi.org/10.1016/j.scitotenv.2020.138403

Chen, L., Qiu, H., Zhang, J., Singh, V.P., Zhou, J., Huang, K., 2019. Copula-based method for stochastic daily stream fl ow simulation considering lag-2 autocorrelation. J. Hydrol. 578, 123938. https://doi.org/10.1016/j.jhydrol.2019.123938

Chen, W., Zhang, Y., Cihlar, J., Smith, S.L., Riseborough, D.W., 2003. Changes in soil temperature and active layer thickness during the twentieth century in a region in western Canada. J. Geophys. Res. Atmos. https://doi.org/10.1029/2002jd003355

Cheng, L., Hoerling, M., Aghakouchak, A., Livneh, B., Quan, X.W., Eischeid, J., 2016. How has human-induced climate change affected California drought risk? J. Clim. 29, 111–120. https://doi.org/10.1175/JCLI-D-15-0260.1

Chiang, F., Mazdiyasni, O., AghaKouchak, A., 2018. Amplified warming of droughts in southern United States in observations and model simulations. Sci. Adv. 4, 1–7. https://doi.org/10.1126/sciadv.aat2380

Chinowsky, P.S., Price, J.C., Neumann, J.E., 2013. Assessment of climate change adaptation costs for the U.S. road network. Glob. Environ. Chang. 23, 764–773. https://doi.org/10.1016/j.gloenvcha.2013.03.004

Clow, D.W., 2010. Changes in the timing of snowmelt and streamflow in Colorado: A response to recent warming. J. Clim. 23, 2293–2306. https://doi.org/10.1175/2009JCLI2951.1

Cong, R.G., Brady, M., 2012. The interdependence between rainfall and temperature: Copula analyses. Sci. World J. 2012. https://doi.org/10.1100/2012/405675

Congreves, K.A., Wagner-Riddle, C., Si, B.C., Clough, T.J., 2018. Nitrous oxide emissions and biogeochemical responses to soil freezing-thawing and drying-wetting. Soil Biol. Biochem. 117, 5–15. https://doi.org/10.1016/j.soilbio.2017.10.040

Connon, R., Devoie, É., Hayashi, M., Veness, T., Quinton, W., 2018. The Influence of Shallow Taliks on Permafrost Thaw and Active Layer Dynamics in Subarctic Canada. J. Geophys. Res. Earth Surf. 123, 281–297. https://doi.org/10.1002/2017JF004469

Coops, N.C., Wulder, M.A., Duro, D.C., Han, T., Berry, S., 2008. The development of a Canadian

dynamic habitat index using multi-temporal satellite estimates of canopy light absorbance. Ecol. Indic. 8, 754–766. https://doi.org/10.1016/j.ecolind.2008.01.007

Cover, T.M., Hart, P.E., 1967. Nearest Neighbor Pattern Classification. IEEE Trans. Inf. theory 13, 21–27.

Crane-Droesch, A., 2018. Machine learning methods for crop yield prediction and climate change impact assessment in agriculture. Environ. Res. Lett. 13. https://doi.org/10.1088/1748-9326/aae159

Creel, K.A., 2020. Transparency in complex computational systems. Philos. Sci. 87, 568–589. https://doi.org/10.1086/709729

Das, J., Jha, S., Goyal, M.K., 2020. Non-stationary and copula-based approach to assess the drought characteristics encompassing climate indices over the Himalayan states in India. J. Hydrol. 580, 124356. https://doi.org/10.1016/j.jhydrol.2019.124356

De Michele, C., Salvadori, G., 2003. A Generalized Pareto intensity-duration model of storm rainfall exploiting 2-Copulas. J. Geophys. Res. 108, 1–11. https://doi.org/10.1029/2002JD002534

De Michele, C., Salvadori, G., Canossi, M., Petaccia, A., Rosso, R., 2005. Bivariate Statistical Approach to Check Adequacy of Dam Spillway. J. Hydrol. Eng. 10, 50–57. https://doi.org/10.1061/(ASCE)1084-0699(2005)10:1(50)

DeBeer, C.M., Pomeroy, J.W., 2017. Influence of snowpack and melt energy heterogeneity on snow cover depletion and snowmelt runoff simulation in a cold mountain environment. J. Hydrol. 553, 199–213. https://doi.org/10.1016/j.jhydrol.2017.07.051

Debele, B., Srinivasan, R., Gosain, A.K., 2010. Comparison of process-based and temperature-index snowmelt modeling in SWAT. Water Resour. Manag. 24, 1065–1088. https://doi.org/10.1007/s11269-009-9486-2

Delignette-Muller, M.L., Dutang, C., 2015. fitdistrplus: An R package for fitting distributions. J. Stat. Softw. 64, 1–34. https://doi.org/10.18637/jss.v064.i04

Derksen, C., Brown, R., 2012. Spring snow cover extent reductions in the 2008–2012 period exceeding climate model projections. Geophysical Research Letters. 39, 19.

Dettinger, M. D., Cayan, D. R. (1995)., Large-scale atmospheric forcing of recent trends toward early snowmelt runoff in California. Journal of Climate. 8, 3, 606-623.

Dile, Y.T., Srinivasan, R., 2014. Evaluation of CFSR climate data for hydrologic prediction in data-scarce watersheds: An application in the blue nile river basin. J. Am. Water Resour. Assoc. https://doi.org/10.1111/jawr.12182

Ding, B., Rezanezhad, F., Gharedaghloo, B., Van Cappellen, P., Passeport, E., 2019. Bioretention cells under cold climate conditions: Effects of freezing and thawing on water infiltration, soil structure, and nutrient removal. Sci. Total Environ. 649, 749–759. https://doi.org/10.1016/j.scitotenv.2018.08.366

Dißmann, J., Brechmann, E.C., Czado, C., Kurowicka, D., 2013. Selecting and estimating regular vine copulae and application to financial returns. Comput. Stat. Data Anal. 59, 52–69. https://doi.org/10.1016/j.csda.2012.08.010

Dobinski, W., 2011. Permafrost. Earth-Science Rev. 108, 158–169.

https://doi.org/10.1016/j.earscirev.2011.06.007

Dong, H., Huang, S., Fang, W., Leng, G., Wang, H., Ren, K., Zhao, J., Ma, C., 2021. Copula-based non-stationarity detection of the precipitation-temperature dependency structure dynamics and possible driving mechanism. Atmos. Res. 249, 105280. https://doi.org/10.1016/j.atmosres.2020.105280

Doughty, M., Eyles, N., Eyles, C., 2013. High-resolution seismic reflection profiling of neotectonic faults in Lake Timiskaming, Timiskaming Graben, Ontario-Quebec, Canada. Sedimentology 60, 983–1006. https://doi.org/10.1111/sed.12002

Duan, A., Wu, G., Liu, Y., Ma, Y., Zhao, P., 2012. Weather and Climate Effects of the Tibetan Plateau. Adv. Atmos. Sci. 29, 978–992. https://doi.org/10.1007/s00376-012-1220-y.1.Introduction

Edwards, A.C., Cresser, M.S., 1992. Freezing and Its Effect on Chemical and Biological Properties of Soil. Springer, New York, NY. https://doi.org/https://doi.org/10.1007/978-1-4612-2844-8_2

Edwards, P.N., 2011. History of climate modeling. Wiley Interdiscip. Rev. Clim. Chang. 2, 128–139. https://doi.org/10.1002/wcc.95

Ehret, U., Zehe, E., Wulfmeyer, V., Warrach-Sagi, K., Liebert, J., 2012. HESS Opinions "should we apply bias correction to global and regional climate model data?" Hydrol. Earth Syst. Sci. 16, 3391–3404. https://doi.org/10.5194/hess-16-3391-2012

Eisner, S., Voss, F., Kynast, E., 2012. Statistical bias correction of global climate projections - Consequences for large scale modeling of flood flows. Adv. Geosci. 31, 75–82. https://doi.org/10.5194/adgeo-31-75-2012

Elliott, A.C., Henry, H.A.L., 2009. Freeze – thaw cycle amplitude and freezing rate effects on extractable nitrogen in a temperate old field soil. Soil Biol. Biochem. 45, 469–476. https://doi.org/10.1007/s00374-009-0356-0

Entekhabi, D., Njoku, E.G., Houser, P., Spencer, M., Doiron, T., Kim, Y., Smith, J., Girard, R., Belair, S., Crow, W., Jackson, T.J., Kerr, Y.H., Kimball, J.S., Koster, R., McDonald, K.C., O'Neill, P.E., Pultz, T., Running, S.W., Shi, J., Wood, E., Van Zyl, J., 2004. The hydrosphere state (hydros) satellite mission: An earth system pathfinder for global mapping of soil moisture and land freeze/thaw. IEEE Trans. Geosci. Remote Sens. 42, 2184–2195. https://doi.org/10.1109/TGRS.2004.834631

Environment Canada. Historical Climate Data., 2016 <http://climate.weather.gc.ca/historical_data/search_historic_data_e.html> (Sep. 2016).

Essery, R., 1997. Modelling fluxes of momentum, sensible heat and latent heat over heterogeneous snow cover. Quarterly Journal of the Royal Meteorological Society. 123, 543, 1867-1883.

Essery, R., Pomeroy, J., Ellis, C., Link, T., 2008. Modelling longwave radiation to snow beneath forest canopies using hemispherical photography or linear regression. Hydrol. Process. An Int. J. 22, 2788–2800. https://doi.org/10.1002/hyp

Fang, S., Xu, L., Pei, H., Liu, Y., Liu, Z., Zhu, Y., Zhang, H., 2014. An integrated approach to snowmelt flood forecasting in water resource management. IEEE Transactions on Industrial Informatics. 10, 1, 548-558.

Fang, X., Luo, S., Lyu, S., 2019. Observed soil temperature trends associated with climate change in the Tibetan Plateau , 1960 – 2014. Theor. Appl. Climatol. 135, 169–181.

Farran, M., Zayed, T., 2009. Comparative Analysis of Life-Cycle Costing for Rehabilitating Infrastructure Systems. J. Perform. Constr. Facil. 23, 320–326. https://doi.org/10.1061/(asce)cf.1943-5509.0000038

Favre, A., Adlouni, S. El, Perreault, L., Thie, N., Bobe, B., 2004. Multivariate hydrological frequency analysis using copulas. Water Resour. Res. 40, 1–12. https://doi.org/10.1029/2003WR002456

Fekete, B.M., Vrsmarty, C.J., Lammers, R.B., 2001. Scaling gridded river networks for macroscale hydrology : Development , analysis , and control of error. Water Resour. Res. 37, 1955–1967.

Feng, D., Yi, J., Wang, D., Chen, L., 2010. Cold Regions Science and Technology Impact of salt and freeze – thaw cycles on performance of asphalt mixtures in coastal frozen region of China. Cold Reg. Sci. Technol. 62, 34–41. https://doi.org/10.1016/j.coldregions.2010.02.002

Flerchinger, G.N., Saxton, K.E., 1989. Simultaneous Heat and Water Model of a Freezing Snow-Residue-Soil System I. Theory and Development. Trans. ASAE 32, 565–571.

Fletcher, C.G., Kushner, P.J., Hall, A., Qu, X., 2009. Circulation responses to snow albedo feedback in climate change. Geophys. Res. Lett. 36, 2–5. https://doi.org/10.1029/2009GL038011

Foley, A.M., 2010. Uncertainty in regional climate modelling: A review. Prog. Phys. Geogr. 34, 647–670. https://doi.org/10.1177/0309133310375654

Francey, R.J., Trudinger, C.M., Van Der Schoot, M., Krummel, P.B., Steele, L.P., Langenfelds, R.L., 2010. Differences between trends in atmospheric CO 2 and the reported trends in anthropogenic CO 2 emissions. Tellus B 62, 316–328. https://doi.org/10.1111/j.1600-0889.2010.00472.x

Frauenfeld, O.W., Zhang, T., Barry, R.G., Gilichinsky, D., 2004. Interdecadal changes in seasonal freeze and thaw depths in Russia. J. Geophys. Res. Atmos. 109, 1–12. https://doi.org/10.1029/2003jd004245

Frieler, K., Meinshausen, M., Mengel, M., Braun, N., Hare, W., 2012. A scaling approach to probabilistic assessment of regional climate change. J. Clim. 25, 3117–3144. https://doi.org/10.1175/JCLI-D-11-00199.1

Funk, C., Peterson, P., Landsfeld, M., Pedreros, D., Verdin, J., Shukla, S., Husak, G., Rowland, J., Harrison, L., Hoell, A., Michaelsen, J., 2015. The climate hazards infrared precipitation with stations — a new environmental record for monitoring extremes. Sci. data 2, 1–21. https://doi.org/10.1038/sdata.2015.66

Galelli, S., Humphrey, G.B., Maier, H.R., Castelletti, A., Dandy, G.C., Gibbs, M.S., 2014. Environmental Modelling & Software An evaluation framework for input variable selection algorithms for environmental data-driven models. Environ. Model. Softw. 62, 33–51. https://doi.org/10.1016/j.envsoft.2014.08.015

Garen, D.C., Marks, D., 2005. Spatially distributed energy balance snowmelt modelling in a mountainous river basin : estimation of meteorological inputs and verification of model results. J. Hydrol. 315, 126–153. https://doi.org/10.1016/j.jhydrol.2005.03.026

Gebremichael, M., Krajewski, W.F., 2007. Application of Copulas to Modeling Temporal

Sampling Errors in Satellite-Derived Rainfall Estimates. J. Hydrol. Eng. 12, 404–408.

Genest, C., Favre, A.-C., 2007. Everything You Always Wanted to Know about Copula Modeling but Were Afraid to Ask. J. Hydrol. Eng. 12, 347–368. https://doi.org/10.1061/(ASCE)1084-0699(2007)12:4(347)

Genest, C., Favre, A.C., Béliveau, J., Jacques, C., 2007. Metaelliptical copulas and their use in frequency analysis of multivariate hydrological data. Water Resour. Res. 43, 1–12. https://doi.org/10.1029/2006WR005275

Genest, C., Rémillard, B., Beaudoin, D., 2009. Goodness-of-fit tests for copulas: A review and a power study. Insur. Math. Econ. 44, 199–213. https://doi.org/10.1016/j.insmatheco.2007.10.005

Genxu, W., Tianxu, M., Juan, C., Chunlin, S., Kewei, H., 2017. Processes of runoff generation operating during the spring and autumn seasons in a permafrost catchment on semi-arid plateaus. J. Hydrol. 550, 307–317. https://doi.org/10.1016/j.jhydrol.2017.05.020

Ghotbi, S., Wang, D., Singh, A., Blöschl, G., Sivapalan, M., 2020. A New Framework for Exploring Process Controls of Flow Duration Curves Water Resources Research. Water Resour. Res. 56, e2019WR026083. https://doi.org/10.1029/2019WR026083

Gibson, C.M., Brinkman, T., Cold, H., Brown, D., Turetsky, M., 2021. Identifying increasing risks of hazards for northern land-users caused by permafrost thaw: integrating scientific and community-based research approaches. Environ. Res. Lett. 16, 064047. https://doi.org/10.1088/1748-9326/abfc79

Gibson, C.M., Chasmer, L.E., Thompson, D.K., Quinton, W.L., Flannigan, M.D., Olefeldt, D., 2018. Wildfire as a major driver of recent permafrost thaw in boreal peatlands. Nat. Commun. 9. https://doi.org/10.1038/s41467-018-05457-1

Giles, D. E., Feng, H., Godwin, R. T., 2016. Bias-corrected maximum likelihood estimation of the parameters of the generalized Pareto distribution. Communications in Statistics-Theory and Methods. 45, 8, 2465-2483.

Giorgi, F., Jones, C., Asrar, G., 2009. Addressing climate information needs at the regional level: the CORDEX framework. … Organ. Bull. 58, 175–183.

Girard, C., Pulido-velazquez, M., Rinaudo, J., Pagé, C., 2015. Integrating top – down and bottom – up approaches to design global change adaptation at the river basin scale. Glob. Environ. Chang. 34, 132–146. https://doi.org/10.1016/j.gloenvcha.2015.07.002

Gizaw, M.S., Biftu, G.F., Gan, T.Y., Moges, S.A., Koivusalo, H., 2017. Potential impact of climate change on streamflow of major Ethiopian rivers. Clim. Change 143, 371–383. https://doi.org/10.1007/s10584-017-2021-1

Gocic, M., Trajkovic, S., 2013. Analysis of changes in meteorological variables using Mann-Kendall and Sen's slope estimator statistical tests in Serbia. Glob. Planet. Change 100, 172–182. https://doi.org/10.1016/j.gloplacha.2012.10.014

Goodbody, T.R.H., Tompalski, P., Coops, N.C., White, J.C., Wulder, M.A., Sanelli, M., 2020. Uncovering spatial and ecological variability in gap size frequency distributions in the Canadian boreal forest. Sci. Rep. 10, 1–12. https://doi.org/10.1038/s41598-020-62878-z

Grams, H.M., Kirstetter, P.-E., Gourley, J.J., 2016. Na ï ve Bayesian Precipitation Type Retrieval from Satellite Using a Cloud-Top and Ground-Radar Matched Climatology. J.

Hydrometeorol. 17, 2649–2665. https://doi.org/10.1175/JHM-D-16-0058.1

Granger, R. J., Gray, D. M., 1990. A net radiation model for calculating daily snowmelt in open environments. Hydrology Research. 21, 4-5, 217-234.

Grant, I., Jones, D., Wang, W., Fawcett, R., Barratt, D., 2008. Meteorological and Remotely Sensed Datasets for Hydrological Modelling : A Contribution to the Australian Water Availability Project, in: International Workshop on Hydrological Prediction: Modelling, Observation and Data Assimilation. Melborne, pp. 1–4.

Grimaldi, S., Petroselli, A., Salvadori, G., De Michele, C., 2016. Catchment compatibility via copulas: A non-parametric study of the dependence structures of hydrological responses. Adv. Water Resour. https://doi.org/10.1016/j.advwatres.2016.02.003

Grimaldi, S., Serinaldi, F., 2006. Design hyetograph analysis with 3-copula function. Hydrol. Sci. J. 51, 223–238. https://doi.org/10.1623/hysj.51.2.223

Grimaldi, S., Serinaldi, F., 2006b. Asymmetric copula in multivariate flood frequency analysis. Adv. Water Resour. 29, 1155–1167. https://doi.org/10.1016/j.advwatres.2005.09.005

Guo, D., Wang, A., Li, D., Hua, W., 2018. Simulation of Changes in the Near-Surface Soil Freeze/Thaw Cycle Using CLM4.5 With Four Atmospheric Forcing Data Sets. J. Geophys. Res. Atmos. 123, 2509–2523. https://doi.org/10.1002/2017JD028097

Guo, D., Yang, M., Wang, H., 2011. Sensible and latent heat flux response to diurnal variation in soil surface temperature and moisture under different freeze/thaw soil conditions in the seasonal frozen soil region of the central Tibetan Plateau. Environ. Earth Sci. 63, 97–107. https://doi.org/10.1007/s12665-010-0672-6

Guo, W., Liu, H., Anenkhonov, O.A., Shangguan, H., Sandanov, D. V, Yu, A., Hu, G., Wu, X., 2018. Agricultural and Forest Meteorology Vegetation can strongly regulate permafrost degradation at its southern edge through changing surface freeze-thaw processes. Agric. For. Meteorol. 252, 10–17. https://doi.org/10.1016/j.agrformet.2018.01.010

Gusain, A., Mohanty, M.P., Ghosh, S., Chatterjee, C., Karmakar, S., 2020. Capturing transformation of flood hazard over a large River Basin under changing climate using a top-down approach. Sci. Total Environ. 726, 138600. https://doi.org/10.1016/j.scitotenv.2020.138600

Hachem, S., Duguay, C.R., Allard, M., 2012. The Cryosphere Comparison of MODIS-derived land surface temperatures with ground surface and air temperature measurements in continuous permafrost terrain. Croysph. 6, 51–69. https://doi.org/10.5194/tc-6-51-2012

Haerter, J.O., Hagemann, S., Moseley, C., Piani, C., 2011. Climate model bias correction and the role of timescales. Hydrol. Earth Syst. Sci. 15, 1065–1079. https://doi.org/10.5194/hess-15-1065-2011

Haile, G.G., Tang, Q., Sun, S., Huang, Z., Zhang, X., Liu, X., 2019. Droughts in East Africa : Causes , impacts and resilience. Earth-Science Rev. 193, 146–161. https://doi.org/10.1016/j.earscirev.2019.04.015

Hamlet, A.F., Salathé, E.P., Carrasco, P., 2010. Statistical Downscaling Techniques for Global Climate Model Simulations of Temperature and Precipitation with Application to Water Resources Planning Studies 28.

Han, W., Huang, C., Gu, J., Hou, J., Zhang, Y., 2021. Spatial-temporal distribution of the freeze–

thaw cycle of the largest lake (Qinghai lake) in china based on machine learning and modis from 2000 to 2020. Remote Sens. https://doi.org/10.3390/rs13091695

Han, Y., Wang, Q., Xia, W., Liu, J., Wang, J., Chen, Y., Shen, J., 2020. Experimental study on the hydraulic conductivity of unsaturated dispersive soil with different salinities subjected to freeze-thaw. Journal of Hydrology, 583, 124297.

Hansen, J., Ruedy, R., Glascoe, J., Sato, M., 1999. GISS analysis of surface temperature change. J. Geophys. Res. Atmos. https://doi.org/10.1029/1999JD900835

Hao, Z., AghaKouchak, A., 2014. A Nonparametric Multivariate Multi-Index Drought Monitoring Framework. J. Hydrometeorol. 15, 89–101. https://doi.org/10.1175/JHM-D-12-0160.1

Hao, Z., Singh, V.P., 2015. Integrating entropy and copula theories for hydrologic modeling and analysis. Entropy. https://doi.org/10.3390/e17042253

Hao, Z., Singh, V.P., 2016. Review of dependence modeling in hydrology and water resources. Prog. Phys. Geogr. 40, 549–578. https://doi.org/10.1177/0309133316632460

Harding, R., Best, M., Blyth, E., Hagemann, S., kabat, P., Tallaksen, L.M., Warnaars, T., Wiberg, D., Weedon, G.P., Van Lanen, H., Ludwig, F., Haddeland, I., 2011. WATCH: Current knowledge of the terrestrial global water cycle. J. Hydrometeorol. 12, 1149–1156. https://doi.org/10.1175/JHM-D-11-024.1

Harrison, J.L., Sanders-DeMott, R., Reinmann, A.B., Sorensen, P.O., Phillips, N.G., Templer, P.H., 2020. Growing-season warming and winter soil freeze/thaw cycles increase transpiration in a northern hardwood forest. Ecology 101, 1–16. https://doi.org/10.1002/ecy.3173

Hassanzadeh, E., Elshorbagy, A., Nazemi, A., Jardine, T. D., Wheater, H., Lindenschmidt, K. E., 2017. The ecohydrological vulnerability of a large inland delta to changing regional streamflows and upstream irrigation expansion. Ecohydrology. doi: 10.1002/eco.1824.

Hassanzadeh, E., Elshorbagy, A., Wheater, H., Gober, P., 2014. Managing water in complex systems: An integrated water resources model for Saskatchewan, Canada. Environ. Model. Softw. 58, 12–26. https://doi.org/10.1016/j.envsoft.2014.03.015

Hassanzadeh, E., Elshorbagy, A., Wheater, H., Gober, P., 2016. A risk-based framework for water resource management under changing water availability, policy options, and irrigation expansion. Adv. Water Resour. 94, 291–306. https://doi.org/10.1016/j.advwatres.2016.05.018

Hassanzadeh, E., Nazemi, A., Elshorbagy, A., 2013. Quantile-based downscaling of precipitation using genetic programming: application to IDF curves in Saskatoon. Journal of Hydrologic Engineering, 10.1061/(ASCE)HE.1943-5584.0000854.

Hatami, S., Nazemi, A., 2019. Temperature Controls of the Freeze and Thaw Patterns in Québec, in: Canadian Society for Civil Engineering. Laval, Greater Montréal, pp. 1–7.

Hatami, S., Nazemi, A., 2021a. The Compound Impacts of Changing Temperature and Snow Cover on Freeze and Thaw Patterns across Québec, in: Geo-Extreme. ASCE, Savannah, Georgia.

Hatami, S, Nazemi. A., 2021b. A statistical framework for assessing temperature controls on landscape Freeze-Thaw: Application and implications in Québec, Canada (1979–2016). Journal of Hydrology 603 (2021): 126891.

https://doi.org/10.1016/j.jhydrol.2021.126891

Hatami, S., Nazemi, A., Amirjabbari, A., 2019a. Evolving Trends of Rain over Precipitation in Canadian Cold Season During the late 20th Century, in: Canadian Society for Civil Engineering. pp. 1–5.

Hatami, S., Zandmoghaddam, S., Nazemi, A., 2019b. Statistical Modeling of Monthly Snow Depth Loss in Southern Canada. J. Hydrol. Eng. 24, 1–13. https://doi.org/10.1061/(ASCE)HE.1943-5584.0001763.

Hayashi, M., Goeller, N., Quinton, William, L., Wright, N., 2007. A simple heat-conduction method for simulating the frost-table depth in hydrological models. Hydrol. Process. 21, 2610–2622. https://doi.org/10.1002/hyp.6792 A

Hayashi, M., Van der Kamp, G., 2000. Simple equations to represent the volume–area–depth relations of shallow wetlands in small topographic depressions. Journal of Hydrology, 237, 1, 74-85.

He, H., Dyck, M.F., Si, B.C., Zhang, T., Lv, J., Wang, J., 2015. Soil freezing – thawing characteristics and snowmelt infiltration in Cryalfs of Alberta, Canada. Geoderma Reg. 5, 198–208. https://doi.org/10.1016/j.geodrs.2015.08.001

He, Z.H., Parajka, J., Tian, F.Q., Blöschl, G., 2014. Estimating degree-day factors from MODIS for snowmelt runoff modeling. Hydrol. Earth Syst. Sci. 18, 4773–4789. https://doi.org/10.5194/hess-18-4773-2014

Helgason, W. D., Pomeroy, J. W., 2005. Uncertainties in estimating turbulent fluxes to melting snow in a mountain clearing. In Proc. 62nd Eastern Snow Conf, 129-138.

Hempel, S., Frieler, K., Warszawski, L., Schewe, J., Piontek, F., 2013. A trend-preserving bias correction – The ISI-MIP approach. Earth Syst. Dyn. 4, 219–236. https://doi.org/10.5194/esd-4-219-2013

Henry, H.A.L., 2007. Soil freeze – thaw cycle experiments : Trends , methodological weaknesses and suggested improvements 39, 977–986. https://doi.org/10.1016/j.soilbio.2006.11.017

Henry, H.A.L., 2008. Climate change and soil freezing dynamics : historical trends and projected changes. Clim. Change 87, 421–434. https://doi.org/10.1007/s10584-007-9322-8

Henry, H.A.L., 2013. Plant and Microbe Adaptations to Cold in a Changing World, Plant and Microbe Adaptations to Cold in a Changing World. Springer, New York, NY, New York. https://doi.org/10.1007/978-1-4614-8253-6

Hickel, K., Zhang, L., 2006. Estimating the impact of rainfall seasonality on mean annual water balance using a top-down approach. J. Hydrol. 331, 409–424. https://doi.org/10.1016/j.jhydrol.2006.05.028

Hirota, T., Iwata, Y., Hayashi, M., Suzuki, S., Hamasaki, T., Sameshima, R., Takayabu, I., 2006. Decreasing soil-frost depth and its relation to climate change in Tokachi, Hokkaido, Japan. J. Meteorol. Soc. Japan 84, 821–833. https://doi.org/10.2151/jmsj.84.821

Hirota, T., Usuki, K., Hayashi, M., Nemoto, M., Iwata, Y., Yanai, Y., Yazaki, T., Inoue, S., 2011. Soil frost control: Agricultural adaptation to climate variability in a cold region of Japan. Mitig. Adapt. Strateg. Glob. Chang. 16, 791–802. https://doi.org/10.1007/s11027-011-9296-8

Hjort, J., Karjalainen, O., Aalto, J., Westermann, S., Romanovsky, V.E., Nelson, F.E., Etzelmüller, B., Luoto, M., 2018. Degrading permafrost puts Arctic infrastructure at risk by mid-century. Nat. Commun. 1, 1–9. https://doi.org/10.1038/s41467-018-07557-4

Ho, E., Gough, W.A., 2006. Freeze thaw cycles in Toronto , Canada in a changing climate. Theor. Appl. Climatol. 83, 203–210. https://doi.org/10.1007/s00704-005-0167-7

Hobbs, N., Dixon, D., Johnston, M., Howie, K., 2013. Can the theory of planned behaviour predict the physical activity behaviour of individuals? Psychol. Heal. 28, 234–249. https://doi.org/10.1080/08870446.2012.716838

Hock, R., 2003. Temperature index melt modelling in mountain areas. Journal of Hydrology. 282, 1, 104-115.

Hodgson, M.E., 1989. Searching methods for rapid grid interpolation. Prof. Geogr. 41, 51–61.

Holder, R. L, 1985. Multiple regression in hydrology. Institute of hydrology.

Hsu, K. L., Gupta, H. V., Sorooshian, S., 1995. Artificial neural network modeling of the rainfall-runoff process. Water Resources Research. 31, 10, 2517-2530.

Hu, G., Zhao, L., Li, R., Wu, X., Wu, T., Xie, C., Zhu, X., Hao, J., 2020. Thermal properties of active layer in permafrost regions with different vegetation types on the Qinghai-Tibetan Plateau. Theor. Appl. Climatol. https://doi.org/10.1007/s00704-019-03008-2

Huang, J., Zhang, X., Zhang, Q., Lin, Y., Hao, M., Luo, Y., Zhao, Z., Yao, Y., Chen, X., Wang, L., Nie, S., Yin, Y., Xu, Y., 2017. Recently amplified arctic warming has contributed to a continual global warming trend. Nat. Clim. Chang. 1–6. https://doi.org/10.1038/s41558-017-0009-5

Huang, M., Ireson, A., Barbour, S.L., DeMars, S., Appels, W.M., 2018. Fully coupled heat and water dynamics modelling of a reclamation cover for oil sands shale overburden. J. Hydrol. 566, 250–263. https://doi.org/10.1016/j.jhydrol.2018.09.026

Huffman, G.J., Adler, R.F., Bolvin, D.T., Gu, G., Nelkin, E.J., Bowman, K.P., Hong, Y., Stocker, E.F., Wolff, D.B., 2007. The TRMM Multisatellite Precipitation Analysis (TMPA): Quasi-global, multiyear, combined-sensor precipitation estimates at fine scales. J. Hydrometeorol. 8, 38–55. https://doi.org/10.1175/JHM560.1

Huning, L.S., Aghakouchak, A., 2018. Mountain snowpack response to different levels of warming. Proc. Natl. Acad. Sci. 115, 1–6. https://doi.org/10.1073/pnas.1805953115

Huser, R., Genton, M.G., 2016. Non-Stationary Dependence Structures for Spatial Extremes. J. Agric. Biol. Environ. Stat. 21, 470–491. https://doi.org/10.1007/s13253-016-0247-4

Immerzeel, W. W., Droogers, P., De Jong, S. M., Bierkens, M. F. P., 2009. Large-scale monitoring of snow cover and runoff simulation in Himalayan river basins using remote sensing. Remote sensing of Environment. 113, 1, 40-49.

Ines, A.V.M., Hansen, J.W., 2006. Bias correction of daily GCM rainfall for crop simulation studies 138, 44–53. https://doi.org/10.1016/j.agrformet.2006.03.009

IPCC, Climate change 2013: The Physical Science Basis. Contribution of Working Group I to the Fifth Assessment Report of the Intergovernmental Panel on Climate Change, Stocker TF et al. (eds), Cambridge University Press, Cambridge, United Kingdom and New York, NY, USA, 1535 pp, 2013.

IPCC, 2021: Climate Change 2021: The Physical Science Basis. Contribution of Working Group I to the Sixth Assessment Report of the Intergovernmental Panel on Climate Change, Masson-Delmotte, V., P. Zhai, A. Pirani, S.L. Connors, C. Péan, S. Berger, N. Caud, Y. Chen, L. Goldfarb, M.I. Gomis, M. Huang, K. Leitzell, E. Lonnoy, J.B.R. Matthews, T.K. Maycock, T. Waterfield, O. Yelekçi, R. Yu, and B. Zhou, Cambridge University Press. In Press (2021).

Ireson, A.M., Barr, A.G., Johnstone, J.F., Mamet, S.D., van der Kamp, G., Whitfield, C.J., Michel, N.L., North, R.L., Westbrook, C.J., DeBeer, C., Chun, K.P., Nazemi, A., Sagin, J., 2015. The changing water cycle: the Boreal Plains ecozone of Western Canada. Wiley Interdiscip. Rev. Water 2, 505–521. https://doi.org/10.1002/wat2.1098

Iwata, Y., Hayashi, M., Suzuki, S., Hirota, T., 2010. Effects of snow cover on soil freezing , water movement , and snowmelt infiltration : A paired plot experiment. Water Resour. Res. 46, 1–11. https://doi.org/10.1029/2009WR008070

Jain, S., Salunke, P., Mishra, S.K., Sahany, S., Choudhary, N., 2019. Advantage of NEX-GDDP over CMIP5 and CORDEX Data: Indian Summer Monsoon. Atmos. Res. https://doi.org/10.1016/j.atmosres.2019.05.026

Jalili Pirani, F., Najafi, M.R., 2020. Recent Trends in Individual and Multivariate Compound Flood Drivers in Canada's Coasts. Water Resour. Res. 56, 1–20. https://doi.org/10.1029/2020WR027785

Jansson, J.K., Taş, N., 2014. The microbial ecology of permafrost. Nat. Rev. Microbiol. 12, 414–425.

Jaramillo, P., Nazemi, A., 2017. Assessing urban water security under changing climate : Challenges and ways forward. Sustain. Cities Soc. 1–12. https://doi.org/10.1016/j.scs.2017.04.005

Jeníček, M., Beitlerová, H., Hasa, M., Kučerová, D., Pevná, H., Podzimek, S., 2012. Modeling Snow Accumulation and Snowmelt Runoff- Present Approaches and Results. AUC Geographica. 47, 2, 15-24.

Jiang, C., Xiong, L., Xu, C.Y., Guo, S., 2015. Bivariate frequency analysis of nonstationary low-flow series based on the time-varying copula. Hydrol. Process. https://doi.org/10.1002/hyp.10288

Jiang, Z., Sharma, A., Johnson, F., 2020. Refining Predictor Spectral Representation Using Wavelet Theory for Improved Natural System Modeling. Water Resour. Res. 56, 1–17. https://doi.org/10.1029/2019WR026962

Joe, H., 1997. Multivariate models and multivariate dependence concepts. CRC Press.

Joe, H., Kurowicka, D. (Eds.), 2011. Dependence modeling: vine copula handbook. World Scientific.

Johansson, E., Gustafsson, L., Berglund, S., Lindborg, T., Selroos, J., Claesson, L., Destouni, G., 2015. Data evaluation and numerical modeling of hydrological interactions between active layer , lake and talik in a permafrost catchment , Western Greenland. J. Hydrol. 527, 688–703. https://doi.org/10.1016/j.jhydrol.2015.05.026

Johnson, F., Sharma, A., 2012. A nesting model for bias correction of variability at multiple time scales in general circulation model precipitation simulations. Water Resour. Res. https://doi.org/10.1029/2011WR010464

Johnson, S. L., Stefan, H. G., 2006. Indicators of climate warming in Minnesota: lake ice covers and snowmelt runoff. Climatic Change. 75, 4, 421-453.

Jonathan, P., Ewans, K., Randell, D., 2014. Non-stationary conditional extremes of northern North Sea storm characteristics. Environmetrics. https://doi.org/10.1002/env.2262

Jones, B.M., Grosse, G., Arp, C.D., Jones, M.C., Walter Anthony, K.M., Romanovsky, V.E., 2011. Modern thermokarst lake dynamics in the continuous permafrost zone, northern Seward Peninsula, Alaska. J. Geophys. Res. Biogeosciences 116, 1–13. https://doi.org/10.1029/2011JG001666

Jones, M.O., Kimball, J.S., Jones, L.A., 2013. Satellite microwave detection of boreal forest recovery from the extreme 2004 wildfires in Alaska and Canada. Glob. Chang. Biol. 19, 3111–3122. https://doi.org/10.1111/gcb.12288

Kane, D. L., Gieck, R. E., Hinzman, L. D., 1997. Snowmelt modeling at small Alaskan Arctic watershed. Journal of Hydrologic Engineering. 10.1061/(ASCE)1084-0699(1997)2:4(204).

Kang, E., Cheng, G., Song, K., Jin, B., Liu, X., Wang, J., 2005. Simulation of energy and water balance in Soil-Vegetation-Atmosphere Transfer system in the mountain area of Heihe River Basin at Hexi Corridor of northwest China. Sci. China, Ser. D Earth Sci. 48, 538–548. https://doi.org/10.1360/02yd0428

Kao, S., Govindaraju, R.S., 2008. Trivariate statistical analysis of extreme rainfall events via the Plackett family of copulas. Water Resour. Res. 44, 1–19. https://doi.org/10.1029/2007WR006261

Kao, S., Govindaraju, R.S., 2010. A copula-based joint deficit index for droughts. J. Hydrol. 380, 121–134. https://doi.org/10.1016/j.jhydrol.2009.10.029

Karger, D.N., Schmatz, D.R., Dettling, G., Zimmermann, N.E., 2020. High-resolution monthly precipitation and temperature time series from 2006 to 2100. Sci. Data 7, 1–10. https://doi.org/10.1038/s41597-020-00587-y

Karjalainen, O., Luoto, M., Aalto, J., Hjort, J., 2019. New insights into the environmental factors controlling the ground thermal regime across the Northern Hemisphere: A comparison between permafrost and non-permafrost areas. Cryosphere 13, 693–707. https://doi.org/10.5194/tc-13-693-2019

Karlsson, J.M., Lyon, S.W., Destouni, G., 2012. Thermokarst lake, hydrological flow and water balance indicators of permafrost change in Western Siberia. J. Hydrol. 464–465, 459–466. https://doi.org/10.1016/j.jhydrol.2012.07.037

Karlsson, J.M., Lyon, S.W., Destouni, G., 2013. Temporal behavior of lake size-distribution in a thawing permafrost landscape in northwestern Siberia. Remote Sens. 6, 621–636. https://doi.org/10.3390/rs6010621

Karlsson, J.M., Lyon, S.W., Destouni, G., 2013. Temporal behavior of lake size-distribution in a thawing permafrost landscape in northwestern Siberia. Remote Sens. 6, 621–636. https://doi.org/10.3390/rs6010621

Kasiviswanathan, K.S., Sudheer, K.P., 2013. Quantification of the predictive uncertainty of artificial neural network based river flow forecast models. Stoch. Environ. Res. Risk Assess. 27, 137–146. https://doi.org/10.1007/s00477-012-0600-2

Kasiviswanathan, K.S., Sudheer, K.P., 2016. Comparison of methods used for quantifying

prediction interval in artificial neural network hydrologic models. Model. Earth Syst. Environ. 2, 1–11. https://doi.org/10.1007/s40808-016-0079-9

Kattsov, V.M., Walsh, J.E., Chapman, W.L., Govorkova, V.A., Pavlova, T. V., Zhang, X., 2007. Simulation and projection of Arctic freshwater budget components by the IPCC AR4 global climate models. J. Hydrometeorol. 8, 571–589. https://doi.org/10.1175/JHM575.1

Kendall, A.M.G., 1938. A New Measure of Rank Correlation. Oxford Univ. Press behalf Biometrika Trust 30, 81–93.

Kendall, A.M.G., 1975. Rank correlation methods. Griffin & Co, London.

Kerr, J.T., Cihlar, J., 2004. Patterns and causes of species endangerment in Canada. Ecol. Appl. 14, 743–753. https://doi.org/10.1890/02-5117

Kharin, V. V., Zwiers, F.W., Zhang, X., Wehner, M., 2013. Changes in temperature and precipitation extremes in the CMIP5 ensemble. Clim. Change 119, 345–357. https://doi.org/10.1007/s10584-013-0705-8

Khedun, C.P., Mishra, A.K., Singh, V.P., Giardino, J.R., 2014. A copula-based precipitation forecasting model: Investigating the interdecadal modulation of ENSO's impacts on monthly precipitation. Water Resour. Res. 50, 580–600. https://doi.org/10.1002/2013WR013763

Khosravi, A., Nahavandi, S., Creighton, D., Atiya, A.F., 2011. Comprehensive review of neural network-based prediction intervals and new advances. IEEE Trans. Neural Networks 22, 1341–1356. https://doi.org/10.1109/TNN.2011.2162110

Kim, Y., Kimball, J.S., Du, J., Schaaf, C.L.B., Kirchner, P.B., 2018. Quantifying the effects of freeze-thaw transitions and snowpack melt on land surface albedo and energy exchange over Alaska and Western Canada. Environ. Res. Lett. 13. https://doi.org/10.1088/1748-9326/aacf72

Kim, Y., Kimball, J.S., Glassy, J., Du, J., 2017. An extended global Earth system data record on daily landscape freeze – thaw status determined from satellite passive microwave remote sensing. Earth Syst. Sci. Data 9, 133–147. https://doi.org/10.5194/essd-9-133-2017

Kim, Y., Kimball, J.S., McDonald, K.C., Glassy, J., 2011. Developing a Global Data Record of Daily Landscape Freeze/Thaw Status Using Satellite Passive Microwave Remote Sensing. Geosci. Remote Sensing, IEEE Trans. 49, 949–960. https://doi.org/10.1109/tgrs.2010.2070515

Kim, Y., Kimball, J.S., Robinson, D.A., Derksen, C., 2015. New satellite climate data records indicate strong coupling between recent frozen season changes and snow cover over high northern latitudes. Environ. Res. Lett. 10, 84004. https://doi.org/10.1088/1748-9326/10/8/084004

Kim, Y., Kimball, J.S., Xu, X., Dunbar, R.S., Colliander, A., Derksen, C., 2019. Global Assessment of the SMAP Freeze / Thaw Data Record and Regional Applications for Detecting Spring Onset and Frost Events. Remote Sens. 11. https://doi.org/https://doi.org/10.3390/rs11111317

Kim, Y., Kimball, J.S., Zhang, K., Didan, K., Velicogna, I., McDonald, K.C., 2014. Attribution of divergent northern vegetation growth responses to lengthening non-frozen seasons using satellite optical-NIR and microwave remote sensing. Int. J. Remote Sens. 35, 3700–3721. https://doi.org/10.1080/01431161.2014.915595

Kim, Y., Kimball, J.S., Zhang, K., McDonald, K.C., 2012. Satellite detection of increasing Northern Hemisphere non-frozen seasons from 1979 to 2008: Implications for regional vegetation growth. Remote Sens. Environ. 121, 472–487. https://doi.org/10.1016/j.rse.2012.02.014

Kimiaghalam, N., Goharrokhi, M., Clark, S.P., Ahmari, H., 2015. A comprehensive fluvial geomorphology study of riverbank erosion on the Red River in Winnipeg , Manitoba , Canada. J. Hydrol. 529, 1488–1498. https://doi.org/10.1016/j.jhydrol.2015.08.033

King, M., Altdorff, D., Li, P., Galagedara, L., Holden, J., Unc, A., 2018. Northward shift of the agricultural climate zone under 21st -century global climate change. Sci. Rep. 8, 7904. https://doi.org/10.1038/s41598-018-26321-8

Knoblauch, C., Beer, C., Liebner, S., Grigoriev, M.N., Pfeiffer, E.-M., 2018. Methane production as key to the greenhouse gas budget of thawing permafrost. Nat. Clim. Chang. 8, 309–312. https://doi.org/10.1038/s41558-018-0095-z

Koven, C.D., Riley, W.J., Stern, A., 2013. Analysis of permafrost thermal dynamics and response to climate change in the CMIP5 earth system models. J. Clim. 26, 1877–1900. https://doi.org/10.1175/JCLI-D-12-00228.1

Kraus, J.F., Benson, C.H., Erickson, A.E., Chamberlain, E.J., 1997. FREEZE-THAW CYCLING AND HYDRAULIC CONDUCTIVITY OF BENTONITIC BARRIERS. J. Geotech. Geoenvironmental Eng. 123, 229–238.

Kreyling, J., Beierkuhnlein, C., Pritsch, K., Schloter, M., Jentsch, A., 2008. Recurrent soil freeze – thaw cycles enhance grassland productivity 938–945.

Krogh, S.A., Pomeroy, J.W., Marsh, P., 2017. Diagnosis of the hydrology of a small Arctic basin at the tundra-taiga transition using a physically based hydrological model. J. Hydrol. 550, 685–703. https://doi.org/10.1016/j.jhydrol.2017.05.042

Kumar, M., Marks, D., Dozier, J., Reba, M., Winstral, A., 2013. Evaluation of distributed hydrologic impacts of temperature-index and energy-based snow models. Advances in Water Resources, 56, 77-89.

Kurganova, I., Teepe, R., Loftfield, N., 2007. Influence of freeze-thaw events on carbon dioxide emission from soils at different moisture and land use. Carbon Balance Manag. 2, 1–9. https://doi.org/10.1186/1750-0680-2-2

Kustas, W. P., Rango, A., Uijlenhoet, R., 1994. A simple energy budget algorithm for the snowmelt runoff model. Water Resources Research. 30, 5, 1515-1527.

Kuwajima, H., Tanaka, M., Okutomi, M., 2019. Improving transparency of deep neural inference process. Prog. Artif. Intell. https://doi.org/10.1007/s13748-019-00179-x

Kwasnicka, D., Dombrowski, S.U., White, M., Sniehotta, F.F., 2017. N-of-1 study of weight loss maintenance assessing predictors of physical activity, adherence to weight loss plan and weight change. Psychol. Heal. 32, 686–708. https://doi.org/10.1080/08870446.2017.1293057

Lall, U., Devineni, N., Kaheil, Y., 2016. An Empirical, Nonparametric Simulator for Multivariate Random Variables with Differing Marginal Densities and Nonlinear Dependence with Hydroclimatic Applications. Risk Anal. https://doi.org/10.1111/risa.12432

Larsen, K.S., Grogan, P., Jonasson, S., Michelsen, A., 2007. Respiration and microbial dynamics in two subarctic ecosystems during winter and spring thaw: Effects of increased snow depth.

Arctic, Antarct. Alp. Res. 39, 268–276. https://doi.org/10.1657/1523-0430(2007)39[268:RAMDIT]2.0.CO;2

Larsen, K.S., Jonasson, S., Michelsen, A., 2002. Repeated freeze-thaw cycles and their effects on biological processes in two arctic ecosystem types. Appl. Soil Ecol. 21, 187–195. https://doi.org/10.1016/S0929-1393(02)00093-8

Lawrence, D.M., Slater, A.G., Tomas, R.A., Holland, M.M., Deser, C., 2008. Accelerated Arctic land warming and permafrost degradation during rapid sea ice loss. Geophys. Res. Lett. 35. https://doi.org/10.1029/2008GL033985

Legates, D.R., McCabe Jr., G.J., 1999. Evaluating the Use of "Goodness of Fit" Measures in Hydrologic and Hydroclimatic Model Validation. Water Resour. Res. 35, 233–241. https://doi.org/10.1029/1998WR900018

Lemoine, D., Kapnick, S., 2016. A top-down approach to projecting market impacts of climate change. Nat. Clim. Chang. 6, 51–55.

Leong, M., Latif, A., Chua, V.P., Weng, N., 2017. Climate change impacts under CMIP5 RCP scenarios on water resources of the Kelantan River Basin , Malaysia. Atmos. Res. J. 189, 1–10. https://doi.org/10.1016/j.atmosres.2017.01.008

Lespinas, F., Fortin, V., Roy, G., Rasmussen, P., Stadnyk, T., 2015. Performance Evaluation of the Canadian Precipitation Analysis (CaPA). J. Hydrometeorol. 16, 2045–2064. https://doi.org/10.1175/JHM-D-14-0191.1

Lewkowicz, A.G., Way, R.G., 2019. Extremes of summer climate trigger thousands environment. Nat. Commun. 10, 1–11. https://doi.org/10.1038/s41467-019-09314-7

Li, H., Sheffield, J., Wood, E.F., 2010. Bias correction of monthly precipitation and temperature fields from Intergovernmental Panel on Climate Change AR4 models using equidistant quantile matching. Atmospheres 115. https://doi.org/10.1029/2009JD012882

Li, R., Shi, H., Flerchinger, G.N., Akae, T., Wang, C., 2012. Simulation of freezing and thawing soils in Inner Mongolia Hetao Irrigation District, China. Geoderma 173–174, 28–33. https://doi.org/10.1016/j.geoderma.2012.01.009

Liston, G. E., Sturm, M., 2002. Winter precipitation patterns in arctic Alaska determined from a blowing-snow model and snow-depth observations. Journal of Hydrometeorology. 3, 6, 646-659.

Liu, J., Wang, S., Yu, S., Yang, D., Zhang, L., 2009. Climate warming and growth of high-elevation inland lakes on the Tibetan Plateau. Glob. Planet. Change 67, 209–217. https://doi.org/10.1016/j.gloplacha.2009.03.010

Liu, J.N.K., Li, B.N.L., Dillon, T.S., 2001. An Improved Naïve Bayesian Classifier Technique Coupled With a Novel Input Solution Method. IEEE Trans. Syst. Man, Cybern. Part C (Applications Rev. 31, 249–256.

Liu, Y.R., Li, Y.P., Ma, Y., Jia, Q.M., Su, Y.Y., 2020. Development of a Bayesian-copula-based frequency analysis method for hydrological risk assessment – The Naryn River in Central Asia. J. Hydrol. 580, 124349. https://doi.org/10.1016/j.jhydrol.2019.124349

Liu, Z., Cheng, L., Hao, Z., Li, J., Thorstensen, A., Gao, H., 2018. A Framework for Exploring Joint Effects of Conditional Factors on Compound Floods. Water Resour. Res. 54, 2681–2696. https://doi.org/10.1002/2017WR021662

Ljung, G.M., Box, G.E.P., 1978. On a measure of lack of fit in time series models. Biometrika 65, 297–303. https://doi.org/10.1093/biomet/65.2.297

Lorenz, D.J., Nieto-Lugilde, D., Blois, J.L., Fitzpatrick, M.C., Williams, J.W., 2016. Downscaled and debiased climate simulations for North America from 21,000 years ago to 2100AD. Sci. Data 3, 1–19. https://doi.org/10.1038/sdata.2016.48

Lotze, H.K., Tittensor, D.P., Bryndum-Buchholz, A., Eddy, T.D., Cheung, W.W.L., Galbraith, E.D., Barange, M., Barrier, N., Bianchi, D., Blanchard, J.L., Bopp, L., Büchner, M., Bulman, C.M., Carozza, D.A., Christensen, V., Coll, M., Dunne, J.P., Fulton, E.A., Jennings, S., Jones, M.C., Mackinson, S., Maury, O., Niiranen, S., Oliveros-Ramos, R., Roy, T., Fernandes, J.A., Schewe, J., Shin, Y.J., Silva, T.A.M., Steenbeek, J., Stock, C.A., Verley, P., Volkholz, J., Walker, N.D., Worm, B., 2019. Global ensemble projections reveal trophic amplification of ocean biomass declines with climate change. Proc. Natl. Acad. Sci. U. S. A. 116, 12907–12912. https://doi.org/10.1073/pnas.1900194116

Luce, C. H., Tarboton, D. G., Cooley, K. R., 1998. The influence of the spatial distribution of snow on basin-averaged snowmelt. Hydrological Processes. 12, 1011, 1671-1683.

Luo, M., Liu, T., Meng, F., Duan, Y., Frankl, A., Bao, A., De Maeyer, P., 2018. Comparing bias correction methods used in downscaling precipitation and temperature from regional climate models: A case study from the Kaidu River Basin in Western China. Water 10. https://doi.org/10.3390/w10081046

Madadgar, S., Asce, S.M., Moradkhani, H., Wre, D., Asce, M., 2013. Drought Analysis under Climate Change Using Copula. J. Hydrol. Eng. 18, 746–759. https://doi.org/10.1061/(ASCE)HE.1943-5584

Madadgar, S., Asce, S.M., Moradkhani, H., Wre, D., Asce, M., 2013. Drought Analysis under Climate Change Using Copula. J. Hydrol. Eng. 18, 746–759. https://doi.org/10.1061/(ASCE)HE.1943-5584

Madadgar, S., Moradkhani, H., 2014. Spatio-temporal drought forecasting within Bayesian networks. J. Hydrol. 512, 134–146. https://doi.org/10.1016/j.jhydrol.2014.02.039

Mahalanobis, P.C., 1936. On the generalized distance in statistics.

Maity, R., Suman, M., Verma, N.K., 2016. Drought prediction using a wavelet based approach to model the temporal consequences of different types of droughts. J. Hydrol. 539, 417–428. https://doi.org/10.1016/j.jhydrol.2016.05.042

Mann, H.B., 1945. Nonparametric Tests Against Trend. Econometrica 13, 245. https://doi.org/10.2307/1907187

Manton, M.J., Della-Marta, P.M., Haylock, M.R., Hennessy, K.J., Nicholls, N., Chambers, L.E., Collins, D.A., Daw, G., Finet, A., Gunawan, D., Inape, K., Isobe, H., Kestin, T.S., Lefale, P., Leyu, C.H., Lwin, T., Maitrepierre, L., Ouprasitwong, N., Page, C.M., Pahalad, J., Plummer, N., Salinger, M.J., Suppiah, R., Tran, V.L., Trewin, B., Tibig, I., Yee, D., 2001. Trends in extreme daily rainfall and temperature in southeast Asia and the south Pacific: 1961-1998. Int. J. Climatol. 21, 269–284. https://doi.org/10.1002/joc.610

Maraun, D., 2013. Bias correction, quantile mapping, and downscaling: Revisiting the inflation issue. J. Clim. 26, 2137–2143. https://doi.org/10.1175/JCLI-D-12-00821.1

Margesin, R., Neuner, G., Storey, K.B., 2007. Cold-loving microbes , plants , and animals —

fundamental and applied aspects. Naturwissenschaften 94, 77–99. https://doi.org/10.1007/s00114-006-0162-6

Marks, D., Domingo, J., Susong, D., Link, T., Garen, D., 1999. A spatially distributed energy balance snowmelt model for application in mountain basins. Hydrological Processes, 13, 12-13, 1935-1959.

Marks, D., Kimball, J., Tingey, D., Link, T., 1998. The sensitivity of snowmelt processes to climate conditions and forest cover during rain-on-snow: a case study of the 1996 Pacific Northwest flood. Hydrological Processes. 12, 10, 1569-1587.

Marshall, I.B., Schut, P., Ballard, M., 1999. A national ecological framework for Canada: Attribute data. Ottawa/Hull, Canada.

May, R. J., Maier, H. R., Dandy, G. C., Fernando, T. G., 2008. Non-linear variable selection for artificial neural networks using partial mutual information. Environmental Modelling & Software. 23, 10, 1312-1326. https://doi.org/10.1016/j.envsoft.2008.03.007

May, R.J, Dandy, G., Maier, H., 2011. Review of input variable selection methods for artificial neural networks. Artificial neural networks-methodological advances and biomedical applications. InTech Open Access Publisher.

Mazdiyasni, O., AghaKouchak, A., 2015. Substantial increase in concurrent droughts and heatwaves in the United States. Proc. Natl. Acad. Sci. U. S. A. 112, 11484–11489. https://doi.org/10.1073/pnas.1422945112

McCartney, J.S., Jafari, N.H., Hueckel, T., Sánchez, M., Vahedifard, F., 2019. Emerging thermal issues in geotechnical engineering, in: Geotechnical Fundamentals for Addressing New World Challenges. pp. 275–317.

McCarty, J.L., Smith, T.E.L., Turetsky, M.R., 2020. Arctic fires re-emerging. Nat. Geosci. 13, 658–660. https://doi.org/10.1038/s41561-020-0641-y

Mccauley, C.A., White, D.M., Lilly, M.R., Nyman, D.M., 2002. A comparison of hydraulic conductivities , permeabilities and infiltration rates in frozen and unfrozen soils. Cold Reg. Sci. Technol. 34, 117–125.

McCreight, J.L., Small, E.E., 2014. Modeling bulk density and snow water equivalent using daily snow depth observations. Cryosphere 8, 521–536. https://doi.org/10.5194/tc-8-521-2014

McDonald, K.C., Kimball, J.S., Njoku, E., Zimmermann, R., Zhao, M., 2004. Variability in Springtime Thaw in the Terrestrial High Latitudes: Monitoring a Major Control on the Biospheric Assimilation of Atmospheric CO 2 with Spaceborne Microwave Remote Sensing. Earth Interact. 8, 1–23. https://doi.org/10.1175/1087-3562(2004)8<1:VISTIT>2.0.CO;2

Mcguire, A.D., Christensen, T.R., Hayes, D., Heroult, A., Euskirchen, E., Kimball, J.S., Koven, C., Lafleur, P., 2012. An assessment of the carbon balance of Arctic tundra : comparisons among observations , process models , and atmospheric inversions. Biogeosciences 9, 3185–3204. https://doi.org/10.5194/bg-9-3185-2012

Mearns, L., McGinnis, S., Arritt, R., Biner, S., Duffy, P., Gutowski, W., Held, I., Jones, R., Leung, R., Nunes, A., Snyder, M., 2007. The North American regional climate change assessment program dataset. Boulder, CO.

Mehran, A., AghaKouchak, A., Nakhjiri, N., Stewardson, M.J., Peel, M.C., Phillips, T.J., Wada, Y., Ravalico, J.K., 2017. Compounding Impacts of Human-Induced Water Stress and Climate

Change on Water Availability. Sci. Rep. https://doi.org/10.1038/s41598-017-06765-0

Meinshausen, M., Smith, S.J., Calvin, K., Daniel, J.S., Kainuma, M.L.T., Lamarque, J., Matsumoto, K., Montzka, S.A., Raper, S.C.B., Riahi, K., Thomson, A., Velders, G.J.M., van Vuuren, D.P.P., 2011. The RCP greenhouse gas concentrations and their extensions from 1765 to 2300. Clim. Change 109, 213–241. https://doi.org/10.1007/s10584-011-0156-z

Mekonnen, B. A., Nazemi, A., Mazurek, K. A., Elshorbagy, A., Putz, G., 2015. Hybrid modelling approach to prairie hydrology: fusing data-driven and process-based hydrological models. Hydrological Sciences Journal. 60, 9, 1473-1489.

Melvin, A.M., Larsen, P., Boehlert, B., Neumann, J.E., Chinowsky, P., Espinet, X., Martinich, J., Baumann, M.S., Rennels, L., Bothner, A., Nicolsky, D.J., Marchenko, S.S., 2017. Climate change damages to Alaska public infrastructure and the economics of proactive adaptation. Proc. Natl. Acad. Sci. 114, E122–E131. https://doi.org/10.1073/pnas.1611056113

Memarian, H., Balasundram, S.K., Abbaspour, K.C., Talib, J.B., Boon Sung, C.T., Sood, A.M., 2014. SWAT-based hydrological modelling of tropical land-use scenarios. Hydrol. Sci. J. 59, 1808–1829. https://doi.org/10.1080/02626667.2014.892598

Meshesha, T.W., Wang, J., Melaku, N.D., 2020. Modelling spatiotemporal patterns of water quality and its impacts on aquatic ecosystem in the cold climate region of Alberta, Canada. J. Hydrol. 587, 124952. https://doi.org/10.1016/j.jhydrol.2020.124952

Michaelides, R.J., Schaefer, K., Zebker, H.A., Parsekian, A., Liu, L., Chen, J., Natali, S., Ludwig, S., Schaefer, S.R., 2019. Inference of the impact of wildfire on permafrost and active layer thickness in a discontinuous permafrost region using the remotely sensed active layer thickness (ReSALT) algorithm. Environ. Res. Lett. 14. https://doi.org/10.1088/1748-9326/aaf932

Mills, B.N., Tighe, S.L., Andrey, J., Smith, J.T., Huen, K., 2009. Climate Change Implications for Flexible Pavement Design and Performance in Southern Canada. J. Transp. Eng. 135, 773–782. https://doi.org/10.1061/(ASCE)0733-947X(2009)135:10(773)

Milly, P.C.D., Betancourt, J., Falkenmark, M., Hirsch, R.M., Zbigniew, W., Lettenmaier, D.P., Stouffer, R.J., 2008. Stationarity Is Dead : Whither Water Management ? 573–574.

Milly, P.C.D., Dunne, K.A., Vecchia, A. V., 2005. Global pattern of trends in streamflow and water availability in a changing climate. Nature 438, 347–350. https://doi.org/10.1038/nature04312

Moghadas, S., Gustafsson, A. M., Muthanna, T. M., Marsalek, J., Viklander, M., 2016. Review of models and procedures for modelling urban snowmelt. Urban Water Journal. 13, 4, 396-411.

Mohamed, A.M.O., Hossein, M., Hassani, F.P., 2002. Hydro-mechanical evaluation of stabilized mine tailings. Environ. Geol. 41, 749–759. https://doi.org/10.1007/s00254-001-0458-y

Mohan, S., Ramsundram, N., 2016. Predictive Temporal Data-Mining Approach for Evolving Knowledge Based Reservoir Operation Rules. Water Resources Management. 30, 10, 3315-3330.

Moore, J. N., Harper, J. T., Greenwood, M. C., 2007. Significance of trends toward earlier snowmelt runoff, Columbia and Missouri Basin headwaters, western United States. Geophysical Research Letters, 34, 16.

Mu, C., Zhang, T., Wu, Q., Peng, X., Cao, B., Zhang, X., Cao, B., Cheng, G., 2015. Editorial :

Organic carbon pools in permafrost regions on the Qinghai – Xizang (Tibetan) Plateau. Croysph. 9, 479–486. https://doi.org/10.5194/tc-9-479-2015

Muerth, M.J., Gauvin St-Denis, B., Ricard, S., Velázquez, J.A., Schmid, J., Minville, M., Caya, D., Chaumont, D., Ludwig, R., Turcotte, R., 2013. On the need for bias correction in regional climate scenarios to assess climate change impacts on river runoff. Hydrol. Earth Syst. Sci. 17, 1189–1204. https://doi.org/10.5194/hess-17-1189-2013

Nakicenovic, N., Alcamo, J., Davis, G., De Vries, B., Fenhann, J., Gaffin, S., Gregory, K., Grubler, A., Jung, T.Y., Kram, T., 2000. A special report of Working Group III of the Intergovernmental Panel on Climate Change.

Nalley, D., Adamowski, J., Khalil, B. and Ozga-Zielinski, B., 2013. Trend detection in surface air temperature in Ontario and Quebec, Canada during 1967–2006 using the discrete wavelet transform. Atmospheric Research, 132, pp.375-398

Navarro-Racines, C., Tarapues, J., Thornton, P., Jarvis, A., Ramirez-Villegas, J., 2020. High-resolution and bias-corrected CMIP5 projections for climate change impact assessments. Sci. Data 7, 1–14. https://doi.org/10.1038/s41597-019-0343-8

Nayak, M.A., Villarini, G., 2018. Remote sensing-based characterization of rainfall during atmospheric rivers over the central United States. J. Hydrol. 556, 1038–1049. https://doi.org/10.1016/j.jhydrol.2016.09.039

Nazemi, A., Elshorbagy, A., 2012. Application of copula modelling to the performance assessment of reconstructed watersheds. Stoch. Environ. Res. Risk Assess. 26, 189–205. https://doi.org/10.1007/s00477-011-0467-7

Nazemi, A., Wheater, H.S., Chun, K.P., Bonsal, B., Mekonnen, M., 2017. Forms and drivers of annual streamflow variability in the headwaters of Canadian Prairies during the 20th century. Hydrol. Process. 31, 221–239. https://doi.org/10.1002/hyp.11036

Nazemi, A., Wheater, H.S., Chun, K.P., Elshorbagy, A., 2013. A stochastic reconstruction framework for analysis of water resource system vulnerability to climate-induced changes in river flow regime. Water Resour. Res. 49, 291–305. https://doi.org/10.1029/2012WR012755

Nazemi, A., Zaerpour, M., Hassanzadeh, E., 2020. Uncertainty in Bottom-Up Vulnerability Assessments of Water Supply Systems due to Regional Streamflow Generation under Changing Conditions. J. Water Resour. Plan. Manag. 146, 1–14. https://doi.org/10.1061/(ASCE)WR.1943-5452.0001149

Neitsch, S. L., Arnold, J. G., Kiniry, J. R., Williams, J. R., 2011. Soil and water assessment tool theoretical documentation version 2009. Texas Water Resources Institute.

Nelsen, R.B., 2006. An Introduction to Copulas. Springer, New York, NY, New York.

Nelson, F.E., Anisimov, O.A., Shiklomanov, N.I., 2001. Subsidence risk from thawing permafrost. Nature 410, 889–890. https://doi.org/10.1038/35073746

Ngai, S.T., Tangang, F., Juneng, L., 2017. Bias correction of global and regional simulated daily precipitation and surface mean temperature over Southeast Asia using quantile mapping method. Glob. Planet. Change 149, 79–90. https://doi.org/10.1016/j.gloplacha.2016.12.009

Nghiem, S. V, Hall, D.K., Mote, T.L., Tedesco, M., Albert, M.R., Keegan, K., Shuman, C.A., Digirolamo, N.E., Neumann, G., 2012. The extreme melt across the Greenland ice sheet in 2012 39, 6–11. https://doi.org/10.1029/2012GL053611

Nguyen-Huy, T., Deo, R.C., An-Vo, D.A., Mushtaq, S., Khan, S., 2017. Copula-statistical precipitation forecasting model in Australia's agro-ecological zones. Agric. Water Manag. 191, 153–172. https://doi.org/10.1016/j.agwat.2017.06.010

Ni, J., Wu, T., Zhu, X., Hu, G., Zou, D., Wu, X., Li, R., Xie, C., Qiao, Y., Pang, Q., Hao, J., Yang, C., 2021. Simulation of the Present and Future Projection of Permafrost on the Qinghai-Tibet Plateau with Statistical and Machine Learning Models. J. Geophys. Res. Atmos. 126. https://doi.org/10.1029/2020JD033402

Niu, F., Gao, Z., Lin, Z., Luo, J., Fan, X., 2019. Vegetation influence on the soil hydrological regime in permafrost regions of the Qinghai-Tibet Plateau, China. Geoderma 354, 113892. https://doi.org/10.1016/j.geoderma.2019.113892

Nourani, V., Jabbarian Paknezhad, N., Sharghi, E., Khosravi, A., 2019. Estimation of prediction interval in ANN-based multi-GCMs downscaling of hydro-climatologic parameters. J. Hydrol. 579, 124226. https://doi.org/10.1016/j.jhydrol.2019.124226

Ntokas, K.F.F., Odry, J., Boucher, M., Garnaud, C., 2021. Investigating ANN architectures and training to estimate snow water equivalent from snow depth. Hydrol. Earth Syst. Sci. 3017–3040. https://doi.org/10.5194/hess-25-3017-2021

Oh, D.H., Patton, A.J., 2013. Simulated Method of Moments Estimation for Copula-Based Multivariate Models. J. Am. Stat. Assoc. 108, 689–700. https://doi.org/10.1080/01621459.2013.785952

Östh, J., Clark, W.A. V, Malmberg, B., 2015. Measuring the Scale of Segregation Using k -Nearest Neighbor Aggregates. Geogr. Anal. 47, 34–49. https://doi.org/10.1111/gean.12053

Ouyang, F., Zhu, Y., Fu, G., 2015. Impacts of climate change under CMIP5 RCP scenarios on streamflow in the Huangnizhuang catchment. Stoch. Environ. Res. Risk Assess. 29, 1781–1795. https://doi.org/10.1007/s00477-014-1018-9

Özgan, E., Serin, S., 2013. Cold Regions Science and Technology Investigation of certain engineering characteristics of asphalt concrete exposed to freeze – thaw cycles. Cold Reg. Sci. Technol. 85, 131–136. https://doi.org/10.1016/j.coldregions.2012.09.003

Ozga-Zielinski, B., Ciupak, M., Adamowski, J., Khalil, B., Malard, J., 2016. Snow-melt flood frequency analysis by means of copula based 2D probability distributions for the Narew River in Poland. J. Hydrol. Reg. Stud. 6, 26–51. https://doi.org/10.1016/j.ejrh.2016.02.001

Pandey, P.K., Das, L., Jhajharia, D., Pandey, V., 2018. Modelling of interdependence between rainfall and temperature using copula. Model. Earth Syst. Environ. https://doi.org/10.1007/s40808-018-0454-9

Parajuli, A., Nadeau, D.F., Anctil, F., Parent, A.C., Bouchard, B., Girard, M., Jutras, S., 2020. Exploring the spatiotemporal variability of the snow water equivalent in a small boreal forest catchment through observation and modelling. Hydrol. Process. 34, 2628–2644. https://doi.org/10.1002/hyp.13756

Park, H., Kim, Y., Kimball, J.S., 2016a. Remote Sensing of Environment Widespread permafrost vulnerability and soil active layer increases over the high northern latitudes inferred from satellite remote sensing and process model assessments. Remote Sens. Environ. 175, 349–358. https://doi.org/10.1016/j.rse.2015.12.046

Park, H., Kim, Y., Kimball, J.S., 2016b. Widespread permafrost vulnerability and soil active layer

increases over the high northern latitudes inferred from satellite remote sensing and process model assessments. Remote Sens. Environ. 175, 349–358. https://doi.org/10.1016/j.rse.2015.12.046

Parry, M.L., 2019. Climate change and world agriculture. Routledge.

Patton, A.I., Rathburn, S.L., Capps, D.M., 2019. Geomorphology Landslide response to climate change in permafrost regions. Geomorphology 340, 116–128. https://doi.org/10.1016/j.geomorph.2019.04.029

Pavlovskii, I., Hayashi, M., Itenfisu, D., 2019. Midwinter melts in the Canadian prairies: Energy balance and hydrological effects. Hydrol. Earth Syst. Sci. 23, 1867–1883. https://doi.org/10.5194/hess-23-1867-2019

Peng, F., Xue, X., You, Q., Zhou, X., Wang, T., 2015. Warming effects on carbon release in a permafrost area of Qinghai-Tibet Plateau. Environ. Earth Sci. 73, 57–66. https://doi.org/10.1007/s12665-014-3394-3

Peng, L., Li, D., Sheffield, J., 2018. Drivers of Variability in Atmospheric Evaporative Demand: Multiscale Spectral Analysis Based on Observations and Physically Based Modeling. Water Resour. Res. 54, 3510–3529. https://doi.org/10.1029/2017WR022104

Peng, X., Frauenfeld, O., Cao, B., Wang, K., Wang, H., Su, H., Huang, Z., Yue, D., Zhang, T., 2016. Response of changes in seasonal soil freeze/thaw state to climate change from 1950 to 2010 across china. J. Geophys. Res. Earth Surf. 121, 1984–2000. https://doi.org/10.1002/2016JF003876

Peng, X., Zhang, T., Frauenfeld, O.W., Wang, K., Luo, D., Cao, B., Su, H., Jin, H., Wu, Q., 2018. Spatiotemporal changes in active layer thickness under contemporary and projected climate in the Northern Hemisphere. J. Clim. 31, 251–266. https://doi.org/10.1175/JCLI-D-16-0721.1

Pereira, G.A.A., Veiga, Á., Erhardt, T., Czado, C., 2017. A periodic spatial vine copula model for multi-site streamflow simulation. Electr. Power Syst. Res. 152, 9–17. https://doi.org/10.1016/j.epsr.2017.06.017

Plaza, C., Pegoraro, E., Bracho, R., Celis, G., Crummer, K.G., Hutchings, J.A., Pries, C.E.H., Mauritz, M., Natali, S.M., Salmon, V.G., Schädel, C., Webb, E.E., Schuur, E.A.G., 2019. Direct observation of permafrost degradation and rapid soil carbon loss in tundra. Nat. Geosci. 12, 627–631. https://doi.org/10.1038/s41561-019-0387-6

Pomeroy, J. W. Brun, E., 2001. Physical properties of snow. Snow Ecology: An interdisciplinary examination of snow-covered ecosystems, 45–126

Pomeroy, J. W., 1989. A process-based model of snow drifting. Annals of Glaciology. 13, 237-240.

Pomeroy, J. W., Fang, X., Williams, B., 2009. Impacts of climate change on Saskatchewan's water resources. Centre for Hydrology, University of Saskatchewan.

Pomeroy, J. W., Gray, D. M., Brown, T., Hedstrom, N. R., Quinton, W. L., Granger, R. J., Carey, S. K., 2007. The cold regions hydrological model: a platform for basing process representation and model structure on physical evidence. Hydrological Processes, 21(19), 2650-2667.

Pomeroy, J. W., Gray, D. M., Landine, P. G., 1993. The prairie blowing snow model: characteristics, validation, operation. Journal of Hydrology. 144, 1-4, 165-192.

Pomeroy, J. W., Li, L., 2000. Prairie and arctic areal snow cover mass balance using a blowing snow model. Journal of Geophysical Research: Atmospheres. 105, D21, 26619-26634.

Pomeroy, J. W., Toth, B., Granger, R. J., Hedstrom, N. R., Essery, R. L. H., 2003. Variation in surface energetics during snowmelt in a subarctic mountain catchment. Journal of Hydrometeorology. 4, 4, 702-719.

Poppel, B., Fægteborg, M., Siegstad, O., Snyder, H.T., 2015. The Arctic as a "hotspot" for natural extraction and global warming. Econ. North 129–135.

Porter, M., Lato, M., Quinn, P., Whittall, J., 2019. Challenges with use of risk matrices for geohazard risk management for resource development projects, in: Proceedings of the First International Conference on Mining Geomechanical Risk. Australian Centre for Geomechanics, pp. 71–84. https://doi.org/10.36487/acg_rep/1905_01_porter

Potter, N.J., Chiew, F.H.S., Charles, S.P., Fu, G., Zheng, H., Zhang, L., 2020. Bias in dynamically downscaled rainfall characteristics for hydroclimatic projections. Hydrol. Earth Syst. Sci. 24, 2963–2979. https://doi.org/10.5194/hess-24-2963-2020

Poulin, A., Huard, D., Favre, A., 2007. Importance of Tail Dependence in Bivariate Frequency Analysis. J. Hydrol. Eng. 12, 394–403.

Price, A. G., Dunne, T., 1976. Energy balance computations of snowmelt in a subarctic area. Water Resources Research. 12, 4, 686-694.

Prosdocimi, I., Kjeldsen, T.R., Svensson, C., 2014. Non-stationarity in annual and seasonal series of peak flow and precipitation in the UK. Nat. Hazards Earth Syst. Sci. 14, 1125–1144. https://doi.org/10.5194/nhess-14-1125-2014

Proverbs, T.A., Lantz, T.C., Lord, S.I., Amos, A., Ban, N.C., 2020. Social-Ecological Determinants of Access to Fish and Well-Being in Four Gwich'in Communities in Canada's Northwest Territories. Hum. Ecol. 48, 155–171. https://doi.org/10.1007/s10745-020-00131-x

Qi, J., Li, S., Li, Q., Xing, Z., Bourque, C.P.A., Meng, F.R., 2016a. A new soil-temperature module for SWAT application in regions with seasonal snow cover. J. Hydrol. 538, 863–877. https://doi.org/10.1016/j.jhydrol.2016.05.003

Qi, J., Li, S., Li, Q., Xing, Z., Bourque, C.P.A., Meng, F.R., 2016b. Assessing an Enhanced Version of SWAT on Water Quantity and Quality Simulation in Regions with Seasonal Snow Cover. Water Resour. Manag. 30, 5021–5037. https://doi.org/10.1007/s11269-016-1466-8

Qi, J., Zhang, X., Wang, Q., 2019. Improving hydrological simulation in the Upper Mississippi River Basin through enhanced freeze-thaw cycle representation. J. Hydrol. 571, 605–618. https://doi.org/10.1016/j.jhydrol.2019.02.020

Qi, J., Zhang, X., Wang, Q., 2019. Improving hydrological simulation in the Upper Mississippi River Basin through enhanced freeze-thaw cycle representation. J. Hydrol. 571, 605–618. https://doi.org/10.1016/j.jhydrol.2019.02.020

Qin, L., Zhai, C., Xu, J., Liu, S., Zhong, C., Yu, G., 2019. Evolution of the pore structure in coal subjected to freeze−thaw using liquid nitrogen to enhance coalbed methane extraction. J. Pet. Sci. Eng. 175, 129–139. https://doi.org/10.1016/j.petrol.2018.12.037

Qin, Y., Lei, H., Yang, D., Gao, B., Wang, Y., Cong, Z., Fan, W., 2016. Long-term change in the depth of seasonally frozen ground and its ecohydrological impacts in the Qilian Mountains,

northeastern Tibetan Plateau. J. Hydrol. 542, 204–221. https://doi.org/10.1016/j.jhydrol.2016.09.008

Qin, Z., Zou, X., Weng, F., 2012. Comparison between linear and nonlinear trends in NOAA-15 AMSU-A brightness temperatures during 1998-2010. Clim. Dyn. 39, 1763–1779. https://doi.org/10.1007/s00382-012-1296-1

Quick, M. C., Pipes, A., 1977. UBC Watershed Model/Le modèle du bassin versant UCB. Hydrological Sciences Journal. 22, 1, 153-161.

Rawlins, M.A., McDonald, K.C., Frolking, S., Lammers, R.B., Fahnestock, M., Kimball, J.S., Vörösmarty, C.., 2005. Remote sensing of snow thaw at the pan-Arctic scale using the SeaWinds scatterometer. J. Hydrol. 312, 294–311.

Raynolds, M.K., Walker, D.A., Ambrosius, K.J., Brown, J., Everett, K.R., Kanevskiy, M., Kofinas, G.P., Romanovsky, V.E., Shur, Y., Webber, P.J., 2014. Cumulative geoecological effects of 62 years of infrastructure and climate change in ice-rich permafrost landscapes, Prudhoe Bay Oilfield, Alaska. Glob. Chang. Biol. 20, 1211–1224. https://doi.org/10.1111/gcb.12500

Razavi, T., Coulibaly, P., 2012. Streamflow prediction in ungauged basins: review of regionalization methods. Journal of Hydrologic Engineering, 10.1061/(ASCE)HE.1943-5584.0000690

Read, L.K., Vogel, R.M., 2015. Reliability, return periods, and risk under nonstationarity. Water Resour. Res. https://doi.org/10.1002/2015WR017089

Ritter, A., Muñoz-Carpena, R., 2013. Performance evaluation of hydrological models: Statistical significance for reducing subjectivity in goodness-of-fit assessments. J. Hydrol. 480, 33–45. https://doi.org/10.1016/j.jhydrol.2012.12.004

Roach, T., Kapelan, Z., Ledbetter, R., Ledbetter, M., 2016. Comparison of Robust Optimization and Info-Gap Methods for Water Resource Management under Deep Uncertainty. J. Water Resour. Plan. Manag. 142, 1–13. https://doi.org/10.1061/(ASCE)WR.1943-5452.0000660

Romanovsky, V.E., Osterkamp, T.E., 1997. Freezing of the active layer on the coastal plain of the Alaskan Arctic. Permafr. Periglac. Process. 8, 23–44. https://doi.org/10.1002/(sici)1099-1530(199701)8:1<23::aid-ppp239>3.0.co;2-2

Rootzén, H., Katz, R.W., 2013. Design Life Level: Quantifying risk in a changing climate. Water Resour. Res. https://doi.org/10.1002/wrcr.20425

Roseen, R.M., Ballestero, T.P., Houle, J.J., Briggs, J.F., Houle, K.M., 2012. Water Quality and Hydrologic Performance of a Porous Asphalt Pavement as a Storm-Water Treatment Strategy in a Cold Climate. J. Environ. Eng. 138, 81–89.

Rosenzweig, C., Karoly, D., Vicarelli, M., Neofotis, P., Wu, Q., Casassa, G., Menzel, A., Root, T.L., Estrella, N., Seguin, B., Tryjanowski, P., Liu, C., 2008. Attributing physical and biological impacts to anthropogenic climate change. Nature 453, 353–358. https://doi.org/10.1038/nature06937

Rowe, J.S., Sheard, J.W., 1981. Ecological land classification: A survey approach. Environ. Manage. 5, 451–464. https://doi.org/10.1007/BF01866822

Roy, T., Gupta, H., 2021. How certain are our uncertainty bounds? Accounting for sample variability in Monte Carlo-based uncertainty estimates. Environ. Model. Softw. 136, 104931. https://doi.org/10.1016/j.envsoft.2020.104931

Sadegh, M., Ragno, E., Aghakouchak, A., 2017. Multivariate Copula Analysis Toolbox (MvCAT): Describing dependence and underlying uncertainty using a Bayesian framework. Water Resour. Res. 5166–5183. https://doi.org/10.1002/2016WR020242.Received

Sakizadeh, M., 2015. Assessment the performance of classification methods in water quality studies, A case study in Karaj River. Environ. Monit. Assess. 187, 573. https://doi.org/10.1007/s10661-015-4761-6

Salimi, A., Ziaii, M., Amiri, A., Hosseinjani Zadeh, M., Karimpouli, S., Moradkhani, M., 2018. Using a Feature Subset Selection method and Support Vector Machine to address curse of dimensionality and redundancy in Hyperion hyperspectral data classification. Egypt. J. Remote Sens. Sp. Sci. 21, 27–36. https://doi.org/10.1016/j.ejrs.2017.02.003

Salvadori, G., De Michele, C., 2004. Frequency analysis via copulas: Theoretical aspects and applications to hydrological events. Water Resour. Res. 40, 1–17. https://doi.org/10.1029/2004WR003133

Salvadori, G., De Michele, C., 2006. Statistical characterization of temporal structure of storms. Adv. Water Resour. 29, 827–842. https://doi.org/10.1016/j.advwatres.2005.07.013

Salvadori, G., De Michele, C., 2007. On the Use of Copulas in Hydrology : Theory and Practice. J. Hydrol. Eng. 12, 369–380.

Salvadori, G., De Michele, C., 2010. Multivariate multiparameter extreme value models and return periods : A copula approach. Water Resour. Res. 46. https://doi.org/10.1029/2009WR009040

Salvadori, G., Duranre, F., De Michele, C., Bernardi, M., Petrella, L., 2016. A multivariate copula-based framework for dealing with hazard scenarios and failure probabilities. Water Resour. Res. 3701–3721. https://doi.org/10.1002/2015WR017225.Received

Samuel, J., Coulibaly, P., Metcalfe, R. A., 2011. Estimation of continuous streamflow in Ontario ungauged basins: comparison of regionalization methods. Journal of Hydrologic Engineering. 10.1061/(ASCE)HE.1943-5584.0000338

Sarhadi, A., Ausín, M.C., Wiper, M.P., Touma, D., Diffenbaugh, N.S., 2018. Multidimensional risk in a nonstationary climate: Joint probability of increasingly severe warm and dry conditions. Sci. Adv. 4. https://doi.org/10.1126/sciadv.aau3487

Sarhadi, A., Burn, D.H., Concepcion Ausin, M., Wiper, M.P., 2016. Time-varying nonstationary multivariate risk analysis using a dynamic Bayesian copula. Water Resour. Res. 52, 2327–2349. https://doi.org/10.1111/j.1752-1688.1969.tb04897.x

Savtchenko, A., Ouzounov, D., Ahmad, S., Acker, J., Leptoukh, G., Koziana, J., Nickless, D., 2004. Terra and Aqua MODIS products available from NASA GES DAAC. Adv. Sp. Res. 34, 710–714. https://doi.org/10.1016/j.asr.2004.03.012

Schaefer, K., Lantuit, H., Romanovsky, V.E., Schuur, E.A.G., Witt, R., 2014. The impact of the permafrost carbon feedback on global climate. Environ. Res. Lett. 9. https://doi.org/10.1088/1748-9326/9/8/085003

Schaefer, K., Zhang, T., Bruhwiler, L., Barnett, A.P., 2011. Amount and timing of permafrost carbon release in. Tellus B 63, 165–180. https://doi.org/10.1111/j.1600-0889.2011.00527.x

Schepsmeier, U., Stoeber, J., Brechmann, E.C., Graeler, B., Nagler, T., Erhardt, T., Almeida, C., Min, A., Czado, C., Hofmann, M., Killiches, M., 2015. Package "VineCopula." R Packag. version 2.

Schewe, J., Heinke, J., Gerten, D., Haddeland, I., Arnell, N.W., Clark, D.B., Dankers, R., Eisner, S., Fekete, B.M., Colón-González, F.J., Gosling, S.N., Kim, H., Liu, X., Masaki, Y., Portmann, F.T., Satoh, Y., Stacke, T., Tang, Q., Wada, Y., Wisser, D., Albrecht, T., Frieler, K., Piontek, F., Warszawski, L., Kabat, P., 2014. Multimodel assessment of water scarcity under climate change. Proc. Natl. Acad. Sci. U. S. A. 111, 3245–3250. https://doi.org/10.1073/pnas.1222460110

Schultz, J., 2005. The ecozones of the world, 2nd ed. Springer Berlin Heidelberg, Berlin.

Schuur, E., McGuire, A., Schädel, C., Grosse, G., Harden, J., Hayes, D., Hugelius, G., Koven, C., Kuhry, P., Lawrence, D., Natali, S., 2015. Climate change and the permafrost carbon feedback. Nature 520, 171–179. https://doi.org/10.1038/nature14338

Schuur, E.A.G., Abbott, B., 2011. High risk of permafrost thaw. Nature 480, 32–33.

Schuur, E.A.G., Vogel, J.G., Crummer, K.G., Lee, H., Sickman, J.O., Osterkamp, T.E., 2009. The effect of permafrost thaw on old carbon release and net carbon exchange from tundra. Nature 459, 556–559. https://doi.org/10.1038/nature08031

Schweikert, A., Chinowsky, P., Espinet, X., Tarbert, M., 2014. Climate change and infrastructure impacts: Comparing the impact on roads in ten countries through 2100. Procedia Eng. 78, 306–316. https://doi.org/10.1016/j.proeng.2014.07.072

Sen, P.K., 1968. Estimates of the Regression Coefficient Based on Kendall's Tau. J. Am. Stat. Assoc. 63, 1379–1389. https://doi.org/10.1080/01621459.1968.10480934

Serinaldi, F., Grimaldi, S., 2007. Fully Nested 3-Copula : Procedure and Application on Hydrological Data. J. Hydrol. Eng. 12, 420–430.

Serinaldi, F., Kilsby, C.G., 2015. Stationarity is undead: Uncertainty dominates the distribution of extremes. Adv. Water Resour. 77, 17–36. https://doi.org/10.1016/j.advwatres.2014.12.013

Serinaldi, F., Kilsby, C.G., Lombardo, F., 2018. Untenable nonstationarity: An assessment of the fitness for purpose of trend tests in hydrology. Adv. Water Resour. 111, 132–155. https://doi.org/10.1016/j.advwatres.2017.10.015

Shafaei, M., Fakheri-Fard, A., Dinpashoh, Y., Mirabbasi, R., De Michele, C., 2017. Modeling flood event characteristics using D-vine structures. Theor. Appl. Climatol. 130, 713–724. https://doi.org/10.1007/s00704-016-1911-x

Shahrajabian, F., Behfarnia, K., 2018. The effects of nano particles on freeze and thaw resistance of alkali-activated slag concrete. Constr. Build. Mater. 176, 172–178. https://doi.org/10.1016/j.conbuildmat.2018.05.033

Sharma, S., Szele, Z., Schilling, R., Munch, J.C., Schloter, M., 2006. Influence of freeze-thaw stress on the structure and function of microbial communities and denitrifying populations in soil. Appl. Environ. Microbiol. 72, 2148–2154. https://doi.org/10.1128/AEM.72.3.2148-2154.2006

Shati, F., Prakash, S., Norouzi, H., Blake, R., 2018. Assessment of differences between near-surface air and soil temperatures for reliable detection of high-latitude freeze and thaw states. Cold Reg. Sci. Technol. 145, 86–92. https://doi.org/10.1016/j.coldregions.2017.10.007

Sheffield, J., Goteti, G., Wood, E.F., 2006. Development of a 50-year high-resolution global dataset of meteorological forcings for land surface modeling. J. Clim. 19, 3088–3111. https://doi.org/10.1175/JCLI3790.1

Sheffield, J., Wood, E.F., Roderick, M.L., 2012. Little change in global drought over the past 60 years. Nature 491, 435–438. https://doi.org/10.1038/nature11575

Shi, W., Huang, S., Liu, D., Huang, Q., Leng, G., Wang, H., Fang, W., Han, Z., 2020. Dry and wet combination dynamics and their possible driving forces in a changing environment. J. Hydrol. 589, 125211. https://doi.org/10.1016/j.jhydrol.2020.125211

Silva, A.T., Portela, M.M., Naghettini, M., 2012. Nonstationarities in the occurrence rates of flood events in Portuguese watersheds. Hydrol. Earth Syst. Sci. 16, 241–254. https://doi.org/10.5194/hess-16-241-2012

Singh, H., Najafi, M.R., 2020. Evaluation of gridded climate datasets over Canada using univariate and bivariate approaches: Implications for hydrological modelling. J. Hydrol. 584, 124673. https://doi.org/10.1016/j.jhydrol.2020.124673

Singh, H., Najafi, M.R., Cannon, A.J., 2021. Characterizing non-stationary compound extreme events in a changing climate based on large-ensemble climate simulations. Clim. Dyn. 56, 1389–1405. https://doi.org/10.1007/s00382-020-05538-2

Singh, P. R., Gan, T. Y., Gobena, A. K., 2005. Modified temperature index method using near-surface soil and air temperatures for modeling snowmelt in the Canadian prairies. Journal of Hydrologic Engineering, 10.1061/(ASCE)1084-0699(2005)10:5(405).

Sinha, T., Cherkauer, K.A., 2008. Time series analysis of soil freeze and thaw processes in Indiana. J. Hydrometeorol. 9, 936–950. https://doi.org/10.1175/2008JHM934.1

Sjursen, H., Michelsen, A., Holmstrup, M., 2005. Effects of freeze-thaw cycles on microarthropods and nutrient availability in a sub-Arctic soil. Appl. Soil Ecol. 28, 79–93. https://doi.org/10.1016/j.apsoil.2004.06.003

Sklar, M., 1959. Fonctions de repartition an dimensions et leurs marges, 8th ed. Publ. inst. statist. univ. Paris.

Skogland, T., Lomeland, S., Goksøyr, J., 1988. Respiratory burst after freezing and thawing of soil: experiments with soil bacteria. Soil Biol. Biochem. 20, 851–856.

Slater, A.G., Pitman, A.J., Desborough, C.E., 1998. Simulation of freeze-thaw cycles in a general circulation LI = Rne t - S ! (1-c •) - c o Tg. J. geop 103.

Smith, N. V., Saatchi, S.S., Randerson, J.T., 2004. Trends in high northern latitude soil freeze and thaw cycles from 1988 to 2002. J. Geophys. Res. D Atmos. 109, 1–14. https://doi.org/10.1029/2003JD004472

Sorensen, P.O., Finzi, A.C., Giasson, M.A., Reinmann, A.B., Sanders-DeMott, R., Templer, P.H., 2018. Winter soil freeze-thaw cycles lead to reductions in soil microbial biomass and activity not compensated for by soil warming. Soil Biol. Biochem. 116, 39–47. https://doi.org/10.1016/j.soilbio.2017.09.026

Srivastav, R.K., Sudheer, K.P., Chaubey, I., 2007. A simplified approach to quantifying predictive and parametric uncertainty in artificial neural network hydrologic models. Water Resour. Res. 43, 1–12. https://doi.org/10.1029/2006WR005352

Steinfeld, C.M.M., Sharma, A., Mehrotra, R., Kingsford, R.T., 2020. The human dimension of water availability : Influence of management rules on water supply for irrigated agriculture and the environment. J. Hydrol. 588, 125009. https://doi.org/10.1016/j.jhydrol.2020.125009

Stewart, I. T., Cayan, D. R., Dettinger, M. D., 2004. Changes in snowmelt runoff timing in western North America under a business as usual climate change scenario. Climatic Change, 62, 1-3, 217-232.

Stewart, I. T., Cayan, D. R., Dettinger, M. D., 2005. Changes toward earlier streamflow timing across western North America. Journal of Climate. 18, 8, 1136-1155.

Strum, M., Holmgren, J., Liston, G., 1995. A seasonal snow cover classification system for local to global applications. J. Clim. 8, 1261–1283.

Stuart, I.G., Jones, M.J., 2006. Movement of common carp , Cyprinus carpio , in a regulated lowland Australian river : implications for management. Fish. Manag. Ecol. 13, 213–219.

Sturm, M., Taras, B., Liston, G. E., Derksen, C., Jonas, T., Lea, J., 2010. Estimating snow water equivalent using snow depth data and climate classes. Journal of Hydrometeorology. 11, 6, 1380-1394.

Sunde, M.G., He, H.S., Hubbart, J.A., Urban, M.A., 2017. Integrating downscaled CMIP5 data with a physically based hydrologic model to estimate potential climate change impacts on streamflow processes in a mixed-use watershed. Hydrol. Process. 31, 1790–1803. https://doi.org/10.1002/hyp.11150

Sunyer, M.A., Hundecha, Y., Lawrence, D., Madsen, H., Willems, P., Martinkova, M., Vormoor, K., Bürger, G., Hanel, M., Kriaučiuniene, J., Loukas, A., Osuch, M., Yücel, I., 2015. Inter-comparison of statistical downscaling methods for projection of extreme precipitation in Europe. Hydrol. Earth Syst. Sci. 19, 1827–1847. https://doi.org/10.5194/hess-19-1827-2015

Takala, M., Pulliainen, J., Member, S., Metsämäki, S.J., Koskinen, J.T., 2009. Detection of Snowmelt Using Spaceborne Microwave Radiometer Data in Eurasia From 1979 to 2007. IEEE Trans. Geosci. Remote Sens. 47, 2996–3007.

Tang, Q., Lettenmaier, D.P., 2012. 21St Century Runoff Sensitivities of Major Global River Basins. Geophys. Res. Lett. 39, 1–5. https://doi.org/10.1029/2011GL050834

Tangborn, W. V., 1984. Prediction of glacier derived runoff for hydroelectric development. Geografiska Annaler. Series A. Physical Geography, 257-265.

Taormina, R., and Chau, K. W., 2015. Data-driven input variable selection for rainfall–runoff modeling using binary-coded particle swarm optimization and Extreme Learning Machines. Journal of Hydrology. 529, 1617-1632.

Tape, K.D., Gustine, D.D., Ruess, R.W., Adams, L.G., Clark, J.A., 2016. Range expansion of moose in arctic Alaska linked to warming and increased shrub habitat. PLoS One 11, 1–12. https://doi.org/10.1371/journal.pone.0152636

Tape, K.D., Jones, B.M., Arp, C.D., Nitze, I., Grosse, G., 2018. Tundra be dammed : Beaver colonization of the Arctic. Glob. Chang. Biol. 24, 4478–4488. https://doi.org/10.1111/gcb.14332

Tarboton, D. G., Luce, C. H., 1996. Utah energy balance snow accumulation and melt model (UEB). Utah Water Research Laboratory, Utah, USA.

Taylor, K.E., 2001. Summarizing multiple aspects of model performance in a Single Diagram. J. Geophys. Res. 106, 7183–7192.

Taylor, K.E., Stouffer, R.J., Meehl, G.A., 2012. An overview of CMIP5 and the experiment design.

Bull. Am. Meteorol. Soc. 93, 485–498. https://doi.org/10.1175/BAMS-D-11-00094.1

Tebaldi, C., Sansó, B., 2009. Joint projections of temperature and precipitation change from multiple climate models: A hierarchical Bayesian approach. J. R. Stat. Soc. Ser. A Stat. Soc. 172, 83–106. https://doi.org/10.1111/j.1467-985X.2008.00545.x

Teufel, B., Sushama, L., 2019. Abrupt changes across the Arctic permafrost region endanger northern development. Nat. Clim. Chang. 9, 858–862. https://doi.org/10.1038/s41558-019-0614-6

The Atlas of Canada 6th Edition 1999 – 2009, issue 6659, 2010.

Thomson, A.M., Calvin, K. V, Smith, S.J., Kyle, G.P., Volke, A., Patel, P., Delgado-arias, S., Bond-lamberty, B., Wise, M.A., Clarke, L.E., Edmonds, J.A., 2011. RCP4 . 5 : a pathway for stabilization of radiative forcing by 2100. Clim. Change 109, 77–94. https://doi.org/10.1007/s10584-011-0151-4

Thrasher, B., Maurer, E.P., McKellar, C., Duffy, P.B., 2012. Technical Note: Bias correcting climate model simulated daily temperature extremes with quantile mapping. Hydrol. Earth Syst. Sci. 16, 3309–3314. https://doi.org/10.5194/hess-16-3309-2012

Thrasher, B., Xiong, J., Wang, W., Melton, F., Michaelis, A., Nemani, R., 2013. Tracking historical papers and their citations. Eur. Sci. Ed. 38, 35–37. https://doi.org/10.1023/B

Tongal, H., Booij, M.J., 2017. Quantification of parametric uncertainty of ANN models with GLUE method for different streamflow dynamics. Stoch. Environ. Res. Risk Assess. 31, 993–1010. https://doi.org/10.1007/s00477-017-1408-x

Towler, E., Rajagopalan, B., Gilleland, E., Summers, R.S., Yates, D., Katz, R.W., 2010. Modeling hydrologic and water quality extremes in a changing climate: A statistical approach based on extreme value theory. Water Resour. Res. https://doi.org/10.1029/2009WR008876

Tran, A.P., Da, B., Bisht, G., Hubbard, S.S., 2018. Spatial and temporal variations of thaw layer thickness and its controlling factors identi fi ed using time-lapse electrical resistivity tomography and hydro-thermal modeling. J. Hydrol. 561, 751–763. https://doi.org/10.1016/j.jhydrol.2018.04.028

Trunk, G. V., 1979. A Problem of Dimensionality: A Simple Example. IEEE Trans. Pattern Anal. Mach. Intell. PAMI-1, 306–307. https://doi.org/10.1109/TPAMI.1979.4766926

Tucker, C.J., Pinzon, J.E., Brown, M.E., Slayback, D.A., Pak, E.W., Mahoney, R., Vermote, E.F., El Saleous, N., 2005. An extended AVHRR 8-km NDVI dataset compatible with MODIS and SPOT vegetation NDVI data. Int. J. Remote Sens. 26, 4485–4498. https://doi.org/10.1080/01431160500168686

Tucker, C.J., Pinzon, J.E., Brown, M.E., Slayback, D.A., Pak, E.W., Mahoney, R., Vermote, E.F., El Saleous, N., 2005. An extended AVHRR 8-km NDVI dataset compatible with MODIS and SPOT vegetation NDVI data. Int. J. Remote Sens. 26, 4485–4498. https://doi.org/10.1080/01431160500168686

Unduche, F., Tolossa, H., Senbeta, D., Zhu, E., 2018. Evaluation of four hydrological models for operational flood forecasting in a Canadian Prairie watershed. Hydrol. Sci. J. 63, 1133–1149. https://doi.org/10.1080/02626667.2018.1474219

Uppala, S.M., Kållberg, P.W., Simmons, A.J., Andrae, U., da Costa Bechtold, V., Fiorino, M., Gibson, J.K., Haseler, J., Hernandez, A., Kelly, G.A., Li, X., Onogi, K., Saarinen, S., Sokka,

N., Allan, R.P., Andersson, E., Arpe, K., Balmaseda, M.A., Beljaars, A.C.M., van de Berg, L., Bidlot, J., Bormann, N., Caires, S., Chevallier, F., Dethof, A., Dragosavac, M., Fisher, M., Fuentes, M., Hagemann, S., Hólm, E., Hoskins, B.J., Isaksen, L., Janssen, P.A.E.M., Jenne, R., McNally, A.P., Mahfouf, J.F., Morcrette, J.J., Rayner, N.A., Saunders, R.W., Simon, P., Sterl, A., Trenberth, K.E., Untch, A., Vasiljevic, D., Viterbo, P., Woollen, J., 2005. The ERA-40 re-analysis. Q. J. R. Meteorol. Soc. 131, 2961–3012. https://doi.org/10.1256/qj.04.176

Uss, M. L., Vozel, B., Lukin, V. V., Chehdi, K., 2012. Maximum likelihood estimation of spatially correlated signal-dependent noise in hyperspectral images. Optical Engineering. 51, 11, 111712-1.

Vahedifard, F., AghaKouchak, A., Ragno, E., Shahrokhabadi, S., Mallakpour, I., 2017. Lessons from the Oroville dam. Science (80-.). 355, 1139–1140.

Valeo, C., Ho, C. L. I., 2004. Modelling urban snowmelt runoff. Journal of Hydrology. 299, 3, 237-251.

Verdhen, A., Chahar, B. R., Sharma, O. P., 2013. Springtime snowmelt and streamflow predictions in the Himalayan Mountains. Journal of Hydrologic Engineering. 10.1061/(ASCE)HE.1943-5584.0000816.

Verleysen, M., François, D., Simon, G., Wertz, V., 2003. On the effects of dimensionality on data analysis with neural networks, in: International Work-Conference on Artificial Neural Networks. Springer Berlin Heidelberg, pp. 105–112. https://doi.org/10.1007/3-540-44869-1_14

Vicuña, S., Garreaud, R. D., McPhee, J., 2011. Climate change impacts on the hydrology of a snowmelt driven basin in semiarid Chile. Climatic Change. 105, 3, 469-488.

Vogel, M.M., Orth, R., Cheruy, F., Hagemann, S., Lorenz, R., van den Hurk, B.J.J.M., Seneviratne, S.I., 2017. Regional amplification of projected changes in extreme temperatures strongly controlled by soil moisture-temperature feedbacks. Geophys. Res. Lett. 44, 1511–1519. https://doi.org/10.1002/2016GL071235

Wagener, T., Wheater, H. S., Gupta, H. V., 2004. Rainfall-runoff modelling in gauged and ungauged catchments, Modelling Ungauged Catchments – Regional Procedures, 169-240.

Wagner-Riddle, C., Congreves, K.A., Abalos, D., Berg, A.A., Brown, S.E., Ambadan, J.T., Gao, X., Tenuta, M., 2017. Globally important nitrous oxide emissions from croplands induced by freeze-thaw cycles. Nat. Geosci. 10, 279–283. https://doi.org/10.1038/ngeo2907

Walter, M. T., Brooks, E. S., McCool, D. K., King, L. G., Molnau, M., Boll, J., 2005. Process-based snowmelt modeling: does it require more input data than temperature-index modeling? Journal of Hydrology. 300, 1-4, 65-75.

Walvoord, M.A., Kurylyk, B.L., 2016. Hydrologic Impacts of Thawing Permafrost—A Review. Vadose Zo. J. 15, 0. https://doi.org/10.2136/vzj2016.01.0010

Walz, J., Knoblauch, C., Böhme, L., Pfeiffer, E.M., 2017. Regulation of soil organic matter decomposition in permafrost-affected Siberian tundra soils - Impact of oxygen availability, freezing and thawing, temperature, and labile organic matter. Soil Biol. Biochem. 110, 34–43. https://doi.org/10.1016/j.soilbio.2017.03.001

Wang, C., Wang, Z., Kong, Y., Zhang, F., Yang, K., Zhang, T., 2019. Most of the Northern Hemisphere Permafrost Remains under Climate Change. Sci. Rep. 9, 1–10.

https://doi.org/10.1038/s41598-019-39942-4

Wang, G., Hongchang, H., Taibin, L., 2009. The influence of freeze – thaw cycles of active soil layer on surface runoff in a permafrost watershed. J. Hydrol. 375, 438–449. https://doi.org/10.1016/j.jhydrol.2009.06.046

Wang, J., Luo, S., Li, Zhaoguo, Wang, S., Li, Zhenhua, 2019. The freeze/thaw process and the surface energy budget of the seasonally frozen ground in the source region of the Yellow River. Theor. Appl. Climatol. 138, 1631–1646. https://doi.org/10.1007/s00704-019-02917-6

Wang, K., Zhang, T., Zhong, X., 2015. Changes in the timing and duration of the near-surface soil freeze/thaw status from 1956 to 2006 across China. Cryosphere 9, 1321–1331. https://doi.org/10.5194/tc-9-1321-2015

Wang, M., Meng, S., Sun, Y., Fu, H., 2018. Shear strength of frozen clay under freezing-thawing cycles using triaxial tests. Earthq. Eng. Eng. Vib. 17, 761–769. https://doi.org/10.1007/s11803-018-0474-5

Wang, W., Dong, Z., Zhu, F., Cao, Q., Chen, J., Yu, X., 2018. A Stochastic Simulation Model for Monthly River Flow in Dry Season. Water 10, 1654. https://doi.org/10.3390/w10111654

Wang, X., Chen, R., Liu, G., Yang, Y., Song, Y., Liu, J., Liu, Z., Han, C., Liu, X., Guo, S., Wang, L., Zheng, Q., 2019. Spatial distributions and temporal variations of the near-surface soil freeze state across China under climate change. Glob. Planet. Change 172, 150–158. https://doi.org/10.1016/j.gloplacha.2018.09.016

Warszawski, L., Frieler, K., Huber, V., Piontek, F., Serdeczny, O., Schewe, J., 2014. The inter-sectoral impact model intercomparison project (ISI-MIP): Project framework. Proc. Natl. Acad. Sci. U. S. A. 111, 3228–3232. https://doi.org/10.1073/pnas.1312330110

Weedon, G.P., Balsamo, G., Bellouin, N., Gomes, S., Best, M.J., Viterbo, P., 2014. The WFDEI meteorological forcing data set: WATCH Forcing Data methodology applied to ERA-Interim reanalysis data. Water Resour. Res. 50, 7505–7514. https://doi.org/10.1002/2014WR015638.Received

Wei, P., Ouyang, W., Gao, X., Hao, F., Hao, Z., Liu, H., 2017. Modified control strategies for critical source area of nitrogen (CSAN) in a typical freeze-thaw watershed. J. Hydrol. 551, 518–531. https://doi.org/10.1016/j.jhydrol.2017.06.026

Wei, Z., Dong, W., 2015. Assessment of simulations of snow depth in the Qinghai-Tibetan Plateau using CMIP5 multi-models. Arctic, Antarct. Alp. Res. 47, 611–625. https://doi.org/10.1657/AAAR0014-050

Weng, L., Wu, Z., Taheri, A., Liu, Q., Lu, H., 2020. Deterioration of dynamic mechanical properties of granite due to freeze-thaw weathering: Considering the effects of moisture conditions. Cold Reg. Sci. Technol. 176, 103092. https://doi.org/10.1016/j.coldregions.2020.103092

Wentzell, P.D., Darren, T.A., Kowalski, B.R., 1997. Maximum likelihood multivariate calibration. Anal. Chem. 69, 2299–2311.

White, M.A., de Beurs, K.M., Didan, K., Inouye, D.W., Richardson, A.D., Jensen, O.P., O'Keefe, J., Zhang, G., Nemani, R.R., van Leeuwen, W.J.D., Brown, J.F., de Wit, A., Schaepman, M., Lin, X., Dettinger, M., Bailey, A.S., Kimball, J., Schwartz, M.D., Baldocchi, D.D., Lee, J.T., Lauenroth, W.K., 2009. Intercomparison, interpretation, and assessment of spring phenology

in North America estimated from remote sensing for 1982-2006. Glob. Chang. Biol. 15, 2335–2359. https://doi.org/10.1111/j.1365-2486.2009.01910.x

Wiken, E.B., 1986. Terrestrial Ecozones Of Canada. Environment Canada, Lands Directorate.

Williams, C.M., Henry, H.A.L., Sinclair, B.J., 2015. Cold truths: How winter drives responses of terrestrial organisms to climate change. Biol. Rev. 90, 214–235. https://doi.org/10.1111/brv.12105

Williams, C.N., Basist, A., Peterson, T.C., Grody, N., 2000. Calibration and Verification of Land Surface Temperature Anomalies Derived from the SSM / I. Bull. Am. Meteorol. Soc. 81, 2141–2156.

Williams, D.L., Goward, S., Arvidson, T., 2006. Landsat : Yesterday, Today, and Tomorrow. Photogramm. Eng. Remote Sens. 72, 1171–1178.

Wolf, B., Zheng, X., Brüggemann, N., Chen, W., Dannenmann, M., Han, X., Sutton, M.A., Wu, H., Yao, Z., Butterbach-Bahl, K., 2010. Grazing-induced reduction of natural nitrous oxide release from continental steppe. Nature 464, 881–884. https://doi.org/10.1038/nature08931

Wu, F., Peng, C., Zhu, J., Zhang, J., Tan, B., Yang, W., 2014. Impact of changes in freezing and thawing on foliar litter carbon release in alpine$/$subalpine forests along an altitudinal gradient in the eastern Tibetan Plateau. Biogeosciences Discuss. 11, 9539–9564. https://doi.org/10.5194/bgd-11-9539-2014

Wu, Q., Zhang, T., 2010. Changes in active layer thickness over the Qinghai - Tibetan Plateau from 1995 to 2007. J. Geophys. Res. Atmos. 115, 1–12. https://doi.org/10.1029/2009JD012974

Wu, Y., Ouyang, W., Hao, Z., Lin, C., Liu, H., Wang, Y., 2018. Assessment of soil erosion characteristics in response to temperature and precipitation in a freeze-thaw watershed. Geoderma 328, 56–65. https://doi.org/10.1016/j.geoderma.2018.05.007

Yan, J., 2007. Enjoy the joy of copulas: With a package copula. J. Stat. Softw. 21, 1–21. https://doi.org/10.18637/jss.v021.i04

Yang, K., Wu, H., Qin, J., Lin, C., Tang, W., Chen, Y., 2014. Recent climate changes over the Tibetan Plateau and their impacts on energy and water cycle: A review. Glob. Planet. Change 112, 79–91. https://doi.org/10.1016/j.gloplacha.2013.12.001

Yang, M., Yao, T., Gou, X., Hirose, N., Fujii, H.Y., Hao, L., Levia, D.., 2007. Diurnal freeze/thaw cycles of the ground surface on the Tibetan Plateau. Chinese Sci. Bull. 52, 136–139.

Yates, D., Sieber, J., Purkey, D., Huber-Lee, A., 2005. WEAP21—A demand-, priority-, and preference-driven water planning model: part 1: model characteristics. Water International. 30, 4, 487-500.

Yi, Y., Kimball, J.S., Rawlins, M.A., Moghaddam, M., Euskirchen, E.S., 2015. The role of snow cover affecting boreal-arctic soil freeze-thaw and carbon dynamics. Biogeosciences 12, 5811–5829. https://doi.org/10.5194/bg-12-5811-2015

Yi, Y., Kimball, J.S., Reichle, R.H., 2014. Spring hydrology determines summer net carbon uptake in northern ecosystems. Environ. Res. Lett. 9. https://doi.org/10.1088/1748-9326/9/6/064003

Young, K. L., 2006. Assessment .f snow storage and ground ice melt in High Arctic environments. Hydrological Processes. 20, 12, 2643-2645.

Yue, S., 2001. A bivariate gamma distribution for use in multivariate flood frequency analysis. Hydrol. Process. 15, 1033–1045. https://doi.org/10.1002/hyp.259

Zaerpour, M., Hatami, S., Sadri, J., Nazemi, A., 2021a. A global algorithm for identifying changing streamflow regimes: application to Canadian natural streams (1966–2010). Hydrology and Earth System Sciences, 25(9), 5193-5217. https://doi.org/10.5194/hess-25-5193-2021, 2021.

Zaerpour, M., Papalexiou, S. M., & Nazemi, A., 2021b. Informing Stochastic Streamflow Generation by Large-Scale Climate Indices at Single and Multiple Sites. Advances in Water Resources, 104037. https://doi.org/10.1016/j.advwatres.2021.104037.

Zandmoghaddam, S., Nazemi, A., Hassanzadeh, E., Hatami, S., 2019. Representing Local Dynamics of Water Resource Systems through a Data-Driven Emulation Approach. Water Resour. Manag. 33, 3579-3594.

Zangenehmadar, Z., Moselhi, O., Golnaraghi, S., 2020. Optimized planning of repair works for pipelines in water distribution networks using genetic algorithm. Eng. Reports 2, 1–11. https://doi.org/10.1002/eng2.12179

Zapata, C.E., Houston, W.N., 2008. Calibration and validation of the enhanced integrated climatic model for pavement design. Transportation Research Board.

Zaremehrjardy, M., Razavi, S., Faramarzi, M., 2020. Assessment of the cascade of uncertainty in future snow depth projections across watersheds of mountainous, foothill, and plain areas in northern latitudes. J. Hydrol. 125735. https://doi.org/10.1016/j.jhydrol.2020.125735

Zhang, K., Kimball, J.S., Zhao, M., Oechel, W.C., Cassano, J., Running, S.W., 2007. Sensitivity of pan-Arctic terrestrial net primary productivity simulations to daily surface meteorology from NCEP-NCAR and ERA-40 reanalyses. J. Geophys. Res. 112, 1–14. https://doi.org/10.1029/2006JG000249

Zhang, L., Singh, V.P., 2006. Bivariate Flood Frequency Analysis Using the Copula Method. J. Hydrol. Eng. 11, 150–164. https://doi.org/10.1061/(ASCE)1084-0699(2006)11

Zhang, P., Wittmann, F.H., Vogel, M., Müller, H.S., Zhao, T., 2017. Influence of freeze-thaw cycles on capillary absorption and chloride penetration into concrete. Cem. Concr. Res. 100, 60–67. https://doi.org/10.1016/j.cemconres.2017.05.018

Zhang, T., 2005. Influence of the seasonal snow cover on the ground thermal regime: An overview. Rev. Geophys. 43. https://doi.org/10.1029/2004RG000157

Zhang, T., Armstrong, R.L., 2001. Soil Freeze/Thaw Cycles Over Snow Free Land Detected By Passive Microwave Remote Sensing. Geophys. Res. Lett. 28, 763–766.

Zhang, T., Barry, R.G., Armstrong, R.L., Zhang, T., Barry, R.G., Armstrong, R.L., Barry, R.G., Armstrong, R.L., 2011. Application of Satellite Remote Sensing Techniques to Frozen Ground Studies. Polar Geogr. 0513. https://doi.org/10.1080/789610186

Zhang, X., Wu, Y., Zhai, E., Ye, P., 2021. Coupling analysis of the heat-water dynamics and frozen depth in a seasonally frozen zone. J. Hydrol. 593, 125603. https://doi.org/10.1016/j.jhydrol.2020.125603

Zhang, Y., Wang, S., Barr, A.G., Black, T.A., 2008. Impact of snow cover on soil temperature and its simulation in a boreal aspen forest. Cold Reg. Sci. Technol. 52, 355–370. https://doi.org/10.1016/j.coldregions.2007.07.001

Zhang, Z.L., Cui, Z.D., 2017. Analysis of microscopic pore structures of the silty clay before and after freezing–thawing under the subway vibration loading. Environ. Earth Sci. 76, 1–17. https://doi.org/10.1007/s12665-017-6879-z

Zhao, L., Wu, Q., Marchenko, S.S., Sharkhuu, N., 2010. Thermal State of Permafrost and Active Layer in Central Asia during the International Polar Year. Permafr. Periglac. Process. 21, 198–207. https://doi.org/10.1002/ppp.688

Zheng, D., Velde, R. Van Der, Su, Z., Wen, J., Wang, X., Yang, K., 2018. Impact of soil freeze-thaw mechanism on the runoff dynamics of two Tibetan rivers. J. Hydrol. 563, 382–394. https://doi.org/10.1016/j.jhydrol.2018.06.024

Zheng, G., Yang, Y., Yang, D., Dafflon, B., Yi, Y., Zhang, S., Chen, D., Gao, B., Wang, T., Shi, R., Wu, Q., 2020. Remote sensing spatiotemporal patterns of frozen soil and the environmental controls over the Tibetan Plateau during 2002–2016. Remote Sens. Environ. 247, 111927. https://doi.org/10.1016/j.rse.2020.111927

Zheng, X., Flerchinger, G.N., 2001. Infiltration into Freezing and Thawing Soils under Differing Field Treatments. J. Irrig. Drain. Eng. 6, 150–158.

Zhou, Z., Yi, S., Chen, J., Ye, B., Sheng, Y., Wang, G., Ding, Y., 2015. Responses of Alpine Grassland to Climate Warming and Permafrost Thawing in Two Basins with Different Precipitation Regimes on the Qinghai-Tibetan Plateaus. Arctic, Antarct. Alp. Res. 47, 125–131. https://doi.org/10.1657/AAAR0013-098

Zuzel, J. F., Cox, L. M., 1975. Relative importance of meteorological variables in snowmelt. Water Resources Research. 11, 1, 174-17

Zwissler, B., Oommen, T., Vitton, S., 2014. A Study of the Impacts of Freeze-Thaw on Cliff Recession at the Calvert Cliffs in Calvert County, Maryland. Geotech. Geol. Eng. 32, 1133–1148. https://doi.org/10.1007/s10706-014-9792-1.

Appendix A.

Hatami, S., Nazemi, A., 2021. A statistical framework for assessing temperature controls on landscape freeze-thaw: application and implications in Québec, Canada (1979-2016). *Journal of Hydrology*, 126891.

The published version of this paper is available through:

https://www.sciencedirect.com/science/article/pii/S0022169421009410

DOI:

https://doi.org/10.1016/j.jhydrol.2021.126891

Appendix B.

Hatami, S., Nazemi, A., 2019. Temperature controls of the freeze and thaw patterns in Québec. CSCE2019 Conference Proceedings, Montréal, Canada.

CSCE Annual Conference
Growing with youth – Croître avec les jeunes

Laval (Greater Montreal)
June 12 - 15, 2019

TEMPERATURE CONTROLS OF THE FREEZE AND THAW PATTERNS IN QUEBEC

Hatami, S.[1,2] and Nazemi, A.[1]

[1] Department of Building, Civil and Environmental Engineering, Concordia University, Montreal, Quebec, Canada.
[2] s_hatam@encs.concordia.ca

Abstract: Accurate quantification of Freeze and Thaw (FT) dynamics is essential for better understanding of environmental processes and socio-economic activities across cold regions. However, climate variability and change can significantly perturb the characteristics of FT patterns, which can in turn result in profound alterations in land-surface characteristics. Investigating the control of temperature on FT is therefore an important step toward advising effective adaptation strategies for future human developments at higher latitudes. There are, however, a number of deficiencies associated with in-situ measurement of FT in terms of temporal and spatial extent of data as well as limitations in extending the local data to regional knowledge. To avoid these gaps, we use gridded remotely sensed FT data record and pair them with gridded surface air temperature data to quantify the association between temperature and FT patterns across Quebec during 1979 to 2016. We study the joint dependence between annual temperature and FT patterns and analyze its variability over time and space. Considering the changes in copula parameters, we address the role of geographic characteristics on altering the temperature control on FT. The copula methodology is employed to formally quantify temperature control on FT dynamics at the annual scale. We conclude that copulas provides a generic tool for assessing the future FT according to future projections of temperature.

Keywords: Freeze and Thaw dynamics, Gridded remotely sensed data, Copula, Climate variability and change

1 INTRODUCTION

Landscape Freeze and Thaw (FT) is one of most important cryosphere processes in cold region. This is due to the impacts of FT on formation of environmental processes and socio-economic activities (Williams, et al. 2015; Entekhabi et al. 2004). Although many hydroclimate variables such as snow depth and precipitation are effective on FT patterns, the timing and distribution of FT dynamics are majorly controlled by near surface air temperature (Frauenfeld et al. 2004). As a result, the changes in air temperature can perturb the characteristics of FT patterns over time and space. These changes are specifically observed across northern regions and during cold season (Henry 2008). There are, however, known deficiencies in in-situ data measurements such as being constraint in capturing spatial and temporal patterns of climate and FT states through the usage of station-scale measurements, particularly at higher latitudes with extremely sparse measurement network (Takala et al. 2009). Furthermore, interpolating the available data from weather stations into data-sparse regions can result in ignoring the role of geographic characteristics on the FT patters, particularly over larger scales (Williams et al. 2000). Satellite microwave data can overcome the limitations of in-situ measurmens by providing a synoptic monitoring technology for understanding the spatiotemporal variability of FT patterns. Continuous, remotely sensed time series of daily FT states have become recently available (Park et al. 2016) and can be paired with gridded temperature data to explore the statistical association between temperature and FT patterns. To evaluate

the control of temperature on FT formally, their joint dependencies must be taken into account. Copula provides a powerful statistical framework for modeling these interdependencies (Nazemi and Elshorbagy 2012). In this study, the copula methodology is employed to quantify the temperature control on different FT characteristics over Quebec. To showcase the utility of copula methodology, we address the impacts of 1° warming on annual FT characteristics over different spatial scales and within different time period.

2 DATA AND CASE STUDY

The FT data used in this study consists of classified remotely-sensed FT data, available from the newest version of FT Earth System Data Record (FT-ESDR; Kim et al., 2011). The data is based on retrieval of bi-daily FT states, using calibrated bi-daily (AM and PM) brightness temperature (Nghiem et al. 2012). Brightness temperature is essentially a physical temperature related to land-surface thermal emission. The changes in emissivity due to its sensitivity to water content in snow or ice as well as available information on temperature across the landscape enable the usage of brightness temperature in detection and mapping of FT. The daily FT state in relation to brightness temperature is then classified into four discrete classes, namely frozen (AM and PM frozen), non-frozen (AM and PM non-frozen), transitional (AM frozen and PM non-frozen) and inverse-transitional (AM non-frozen and PM frozen). This data is available publically at the daily scale and at 25 km × 25 km spatial resolution for the period of 1979 to 2016 (McDonald et al. 2004; check https://doi.org/10.5067/MEASURES/CRYOSPHERE/nsidc-0477.004). From this data, we extracted number of frozen (NF) and number of thawed (NT) days in each year (September- August) and paired it with historical gridded maximum and minimum daily temperature provided by Global Meteorological Forcing Dataset (http://hydrology.princeton.edu/data.pgf.php; see Sheffield et al. 2006) during the same period. The average of mean daily temperature over each year (September- August) is then obtained as the mean yearly temperature (T_{mean}) in each grid. Indeed, the yearly data period starts from September 1979 (beginning of FT year of 1980) to August 2016 (end of FT year of 2016). We then re-gridded the temperature data using the *k*-nearest neighbourhood to match them with FT gridded data. We then analyze the dependency between annual FT variables (i.e. NF and NT) and annual T_{mean} across Quebec and its eight ecozones, namely Arctic Cordillera (AC), Northern Arctic (NA), Southern Arctic (SA), Taiga Shield (TS), Boreal Shield (BS), Atlantic Maritime (AM), Mixed Wood Plains (MWP) and Hudson Plains (HP). Addressing temperature control on FT patterns over Quebec, the largest province in Canada, has a large diversity in climate and vegetation type over this region. This diversity can cause divergent environmental responses to climate change, which can impact the frequency and extent of FT patterns in different ways. Accurate quantification of changes in FT patterns different ecozones can be therefore essential for sustainable development in Quebec.

3 METHODOLOGY

We first analyze the statistical dependence between considered FT variable with T_{mean} using Kendall's Tau dependence coefficient (Kendall 1938) over the period of 1980 to 2016. To explore the potential changes in the dependence in time, we also divided the total period into two equal 18-year periods, one from 1980 to 1997 and the other from 1998 to 2016. We then use copula methodology to assess the temperature control on FT characteristics over different ecozones and Quebec as a whole. The copula methodology provides a powerful tool to model the joint dependencies among random variables, stating that the joint cumulative distribution function of any given pair of continuous random variables $(\boldsymbol{X}, \boldsymbol{Y})$, can be written as follows (Genest and Favre 2007):

$$[1] \quad H(\boldsymbol{X}, \boldsymbol{Y}) = C\big(F(\boldsymbol{X}), G(\boldsymbol{Y})\big)$$

where $H(\boldsymbol{X}, \boldsymbol{Y})$ is the joint dependence; $F(\boldsymbol{X})$ and $G(\boldsymbol{Y})$ are the marginal distributions; and C is the copula function. C is a continuous function, coupling a set of cumulative marginal distributions to form a cumulative joint distribution. Gaussian, Frank and Clayton copula families are analyzed to find the best competitive copula model. To provide a notion for alterations in dependencies with latitude, longitude and elevation, we developed a set of regional copula models based on all grid cells, located in each of the eight ecozones. The copula parameter for each ecozone is then compared with the average geographic characteristics of that ecozone to inspect the role of geographic characteristics on altering the temperature control on the FT variables. Using the regional copula models developed, we then address what 1° warming means to FT

variables across different ecozones based on the dependence observed in the whole period as well as the first and the second half-periods. For this purpose, the probability distribution of NF and NT are obtained based on the long-term T_{mean} and 1° warmer climate (long-term T_{mean}+1°) across two different ecozones over Quebec. The same analysis is performed to derive the probability of the FT characteristics in one particular ecozone but over two different time episodes to find the impacts of warming on interdependencies between temperature and FT patterns over time.

4 RESULTS AND DISCUSSION

4.1 Dependency between FT Characteristics and Mean Temperature

Figure 1 summarizes the results of the dependency analysis between the annual mean temperature and the number of frozen days (first row) and thawed days (second row) in each year. Red color spectrum is an indicator of positive dependencies while blue color shows negative Kendall's Tau dependence coefficient at the grid scale. We also look into the potential change in the dependency between temperature and FT characteristics by recalculating the dependence in the first and second half of the study periods. Based on the results, high number of grids are showing significant dependency between the NF and NT with T_{mean} , which is observed over 90 and 84 percent of grids, respectively, during the whole data period. Having said that, the dependency between FT characteristics and temperature is variant over considered time episodes, specifically across southern and central Quebec. In the Boreal Shield for instance, the number of grids with significant dependencies between NF and mean annual temperature is almost doubled in second half period, in comparison to the first half.

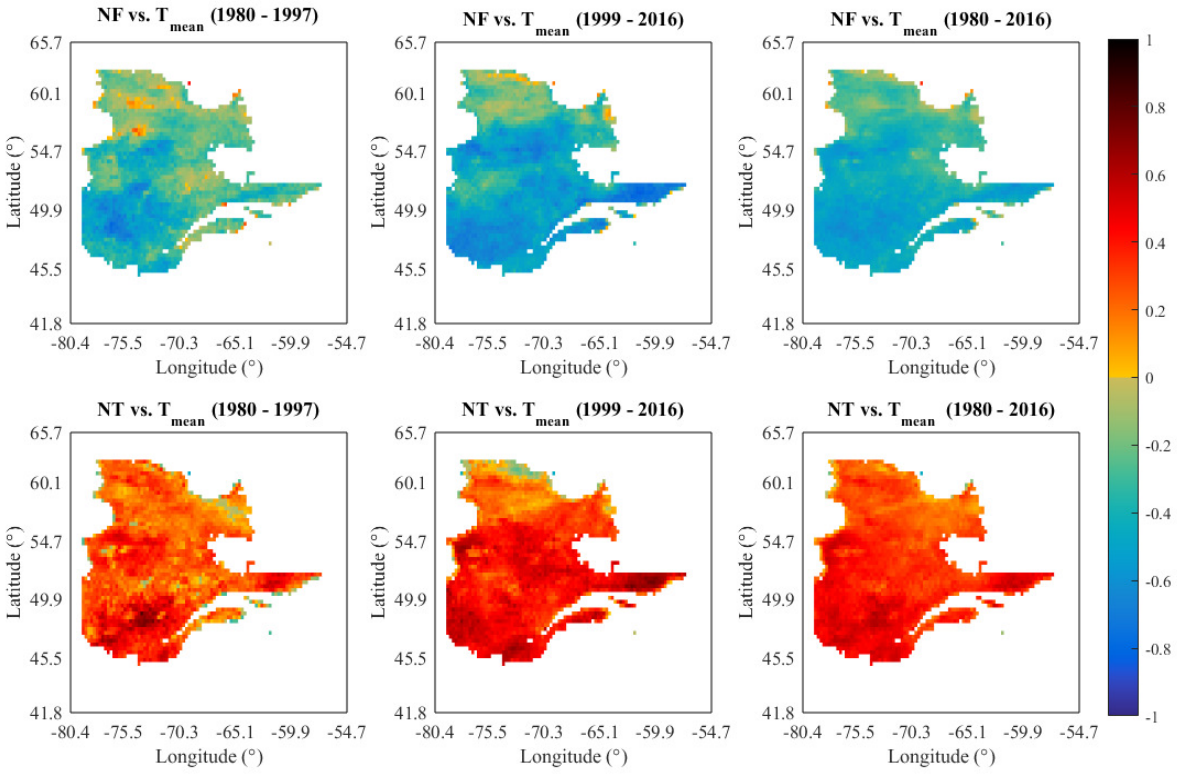

Figure 1: Kendall's tau dependence coefficient between NF and T_{mean} (first row) as well as NT and T_{mean} (second row) over the first half (1980-1997), second half (1998-2016) and whole study period (1980-2016).

4.2 Copula Modelling for Investigating the Temperature Control on FT Characteristics

Based on the results from previous section, there is significant dependence between temperature and FT characteristics over most of the Quebec area; and therefore, there is a copula model that can statistically describe the temperature control on the FT patterns. We compare, three competitive copulas to assess the impacts of change in annual T_{mean} on FT characteristics. For this purpose, the Gaussian, Frank and Clayton copulas are fitted on the data at the grid scale. To fit the copula models, first marginal temperature and FT characteristics should be transformed using their cumulative distributions functions and then copula structures are used to assess the dependencies between marginal distributions. After fitting copula models on marginal data in each grid, the simulated Kendall's Tau is compared to the observed dependence and the error in simulated dependence is calculated. The boxplot of errors in simulated Kendall's Tau over each ecozone are estimated for three copulas – see Figure 2. These boxplots can provide a notion for copula modelling performance to capture the interdependencies between mean annual temperature and FT characteristics in grids over different regional scales (i.e. 8 ecozones and Quebec as a whole). As can be easily investigated, the Clayton copula has considerably lower power in modelling the interdependencies between both NF and T_{mean} as well as NT and T_{mean} due to higher error values in modeled Kendall's Tau (with average error of -0.4 over grids covering Quebec for NF and T_{mean} and average error of roughly 0.1 in Quebec for NT and T_{mean}). Comparing the Gaussian and Frank copula, it can be seen that Frank copula is more robust due to having narrower boxplots over most ecozones as well as across the whole Quebec. As a result, hereafter we limit our discussion only to Frank copula.

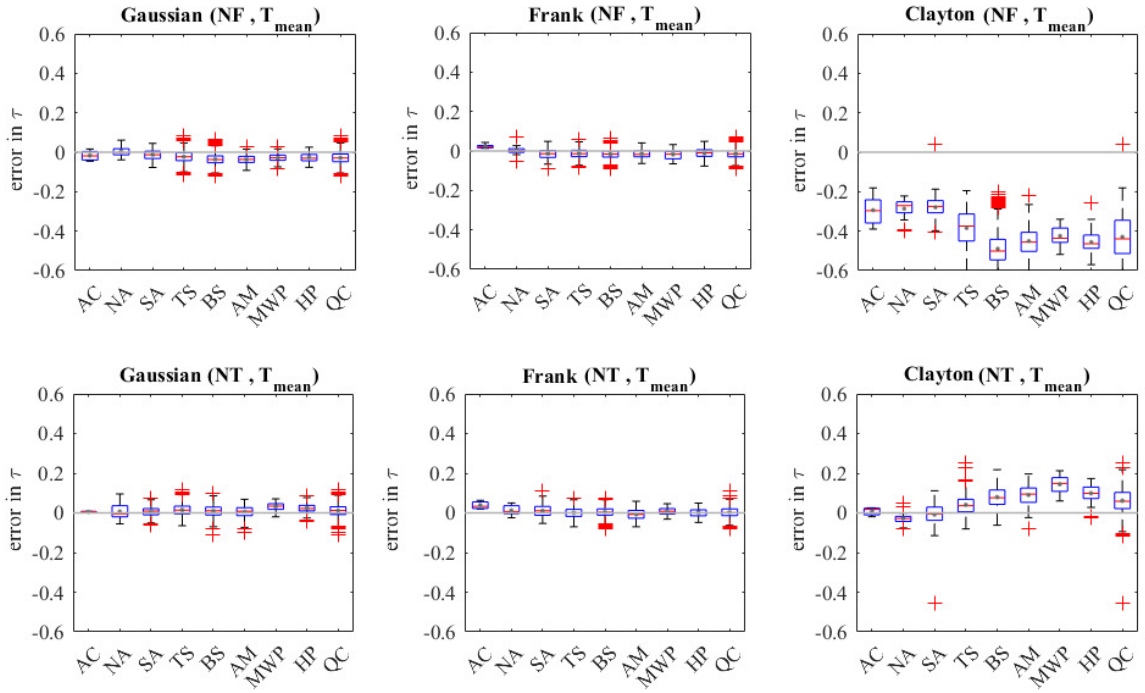

Figure 2: Boxplot of error in reconstructing interdependencies between NF and T_{mean} (first row) as well as NT and T_{mean} (second row) in different Quebec's ecozones and the province of Quebec as a whole using Gaussian (first column), Frank (second column) and Clayton (third column) copulas.

4.3 Alteration in Temperature Control on FT with Geographic Characteristics

To inspect the dependency between geographic dependencies and the Kendall's dependence coefficient, we matched the parameters of regional copula models at each ecozone with area-averaged geographic characteristics, namely latitude, longitude and altitude. The significance of dependencies is also evaluated using the formal *p*-values. Figure 3 illustrates the relationship between regional Frank copula parameter and geographic characteristics at ecozones over three considered time episodes (i.e. 1980-2016, 1980-1998 and 1999-2016). On top of each panel, the Kendall's Tau between regional copula parameter and

geographic characteristics over the whole period of study is reported along with the associated *p*-value in parentheses. As can be clearly seen, the latitude is the most significantly dependant geographic characteristic altering the copula parameter and consequently the temperature control on both NF and NT. Considering these observations, it can be argued that the regional dependencies between FT variables and temperature are mostly related to the latitude of corresponding regions comparing to the other two geographic characteristics. Moreover, the results show almost the same patterns over different time episodes.

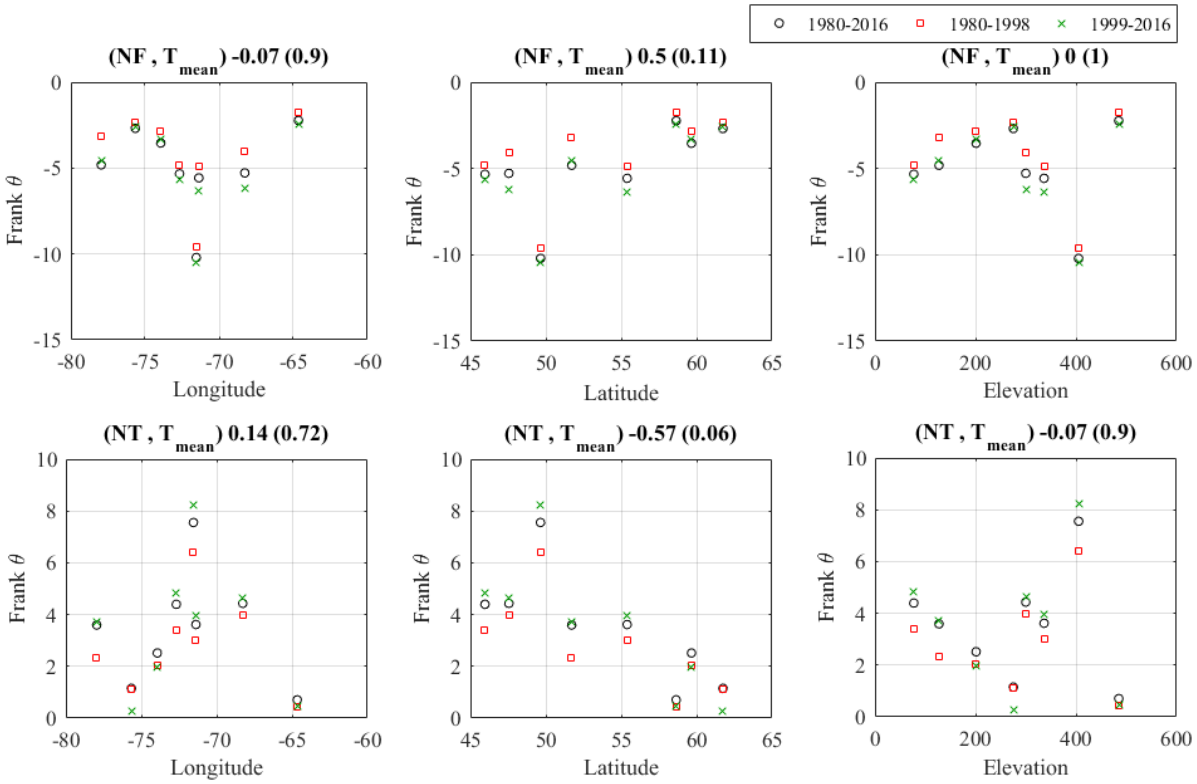

Figure 3: Dependence between the regional copula parameter and three geographic characteristics within different time period; columns are related to longitude, latitude and elevation from left to right whereas rows are related to the copula model parameter fitted on NF and T_{mean} (first row) and NT and T_{mean} (second row).

4.4 Change in FT characteristics in face of 1 ℃ Warming

By having the regional copula models, it would be possible to address the impacts of 1 ℃ warming across each ecozone. To assess these impacts, the probability distribution of NF and NT are obtained based on long-term T_{mean} as well as long-term T_{mean}+1 ℃ across different spatial scales and in different time periods. The analysis is performed once to evaluate the effects of 1 ℃ warmer climate across two different ecozones of Quebec with rather the same area and once over the first and second half-periods over MWP ecozone. The panels in the first row of Figure 4, show the changes in probability of NF and NT while long-term and 1 ° warmer average temperature is happening across two different ecozones of Quebec (i.e. Mixed Wood Plains and Hudson Palins). The probability distributions clearly illustrate the more vulnerability of both considered FT characteristics across MWP ecozone in case of 1 ° increase in long-term T_{mean}. To evaluate the temperature control on FT patterns within different time episodes, the imposed shifts in the probability distribution of NF and NT as a result of changes in temperature are also depicted – see second row panels of Figure 4. Based on this comparison, there is a significant difference in shifts of NF and NT probability distributions between two time episodes. This analysis clearly shows the greater shifts in probability distribution of both FT characteristics over the second half of the time period (1999-2016). Considering this

observations, it can be argued that the joint dependencies between temperature and FT characteristics are changing over time.

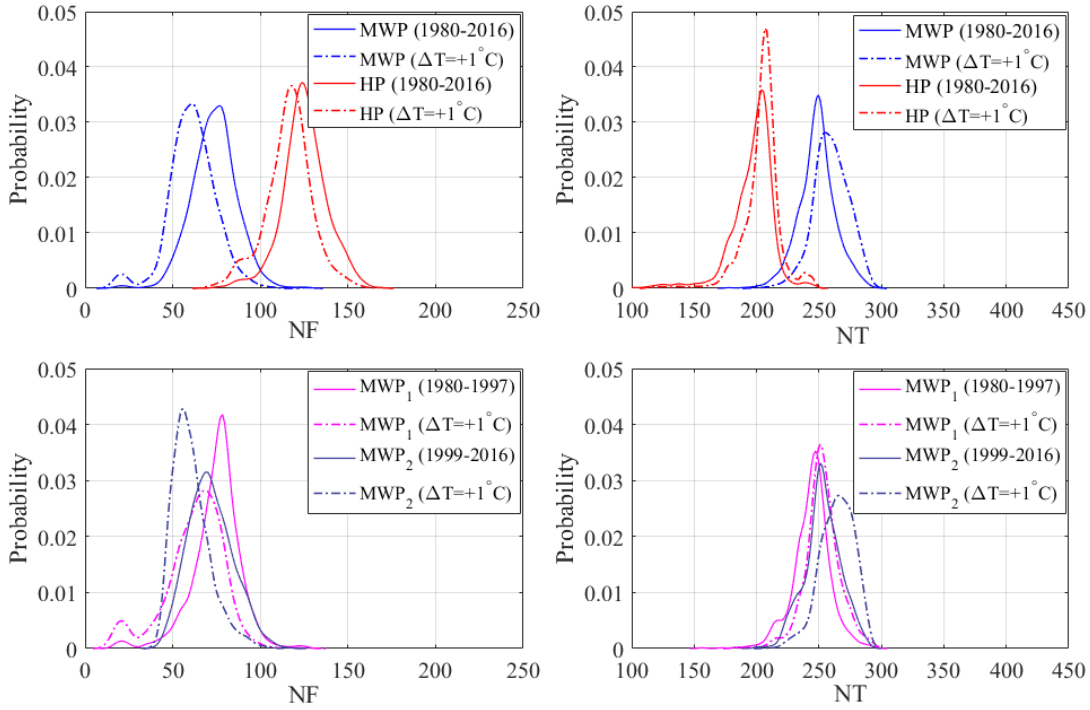

Figure 4: Impacts of 1℃ warming on NF (first column) and NT (second column) across different spatial scales (first row) and over different time periods (second row).

5 SUMMARY AND CONCLUSION

Quantifying the temperature controllers of FT patterns is of a great importance for advising a set of effective adaptation strategies for future human developments in cold regions due to the great impact of FT dynamics on hydrological and environmental processes. However, the timing and distribution of this patterns have been subjected to significant change across different temporal and spatial scales. In this study, the copula methodology is employed to provide a notion for temperature control on annual FT characteristics throughout Quebec. We also inspect the alteration in the model parameters with latitude, longitude and elevation as well as the impacts of 1° warming on FT variables across considered spatial scales as well as different time episodes. Considering the results of dependencies between FT characteristics and mean annual temperature, it is concluded that both FT variables are significantly dependent to T_{mean} in more than 84 percent of grids covering the province of Quebec. However, it is noted that these dependencies are variant in different periods. Three competitive copula models are considered to model the joint dependency between FT variables and temperature. Comparing these copula models, it is noted that the Frank copula has significantly better performance in capturing the dependence between temperature and FT characteristics in grid scale across most of the ecozones as well as the Quebec as a whole. Further studies on alterations in model parameters with geographic characteristics, show the latitude as the most significantly dependant geographic characteristic altering the copula parameter at regional-scale and accordingly the temperature control on both NF and NT. Nonetheless, it seems to be no variation in the dependencies between the geographic characteristics and temperature control on FT patterns over different time episodes, at least at the ecozone scale. We also show the vulnerability of FT characteristics to 1° increment in long-term temperature over time and space and concluded that the changes in long-term mean annual temperature do not have the same effects on FT characteristics across different ecozones. Moreover, it is concluded that the positive shift in temperature would be more impactful on probability distribution of both NF and NT during the second half of the study period, showing the possibility of changes in joint dependencies between temperature and FT characteristics over time. Considering our results, the

copula modelling can provide a formal basis for assessing the change in FT patterns due to changing temperature. However, further investigations are required to fully establish the copula modelling capability to address the impacts of temperature change on FT patterns in other temporal and/or spatial scales. Studying the control of other hydro-climatic variables (e.g. snow depth) on FT characteristics is another interesting research topic that would be the next step in our future studies.

6 REFERENCES

Entekhabi, Dara, Eni G. Njoku, Paul Houser, Michael Spencer, Terence Doiron, Yunjin Kim, Joel Smith, et al. 2004. The Hydrosphere State (Hydros) Satellite Mission: An Earth System Pathfinder for Global Mapping of Soil Moisture and Land Freeze/thaw. *IEEE Transactions on Geoscience and Remote Sensing*, **42** (10):2184–95. https://doi.org/10.1109/TGRS.2004.834631.

Frauenfeld, Oliver W., Tingjun Zhang, and Roger G. Barry. 2004. Interdecadal Changes in Seasonal Freeze and Thaw Depths in Russia. *Journal of Geophysical Research,* **109** (D5):D05101. https://doi.org/10.1029/2003JD004245.

Genest, Christian, and Anne-Catherine Favre. 2007. Everything You Always Wanted to Know about Copula Modeling but Were Afraid to Ask. *Journal of Hydrologic Engineering*, **12** (4):347–68. https://doi.org/10.1061/(ASCE)1084-0699(2007)12:4(347).

Henry, Hugh A L. 2008. Climate Change and Soil Freezing Dynamics : Historical Trends and Projected Changes. Climatic Change, 87:421–34. https://doi.org/10.1007/s10584-007-9322-8.

Kendall, Author M G. 1938. A New Measure of Rank Correlation. *Oxford University Press on Behalf of Biometrika Trust*, **30** (1):81–93. http://www.jstor.org/stable/2332226.

Kim, Youngwook, John S Kimball, Joseph Glassy, and Jinyang Du. 2017. An Extended Global Earth System Data Record on Daily Landscape Freeze – Thaw Status Determined from Satellite Passive Microwave Remote Sensing. *Earth System Science Data*, **9** (1):133–47. https://doi.org/10.5194/essd-9-133-2017.

McDonald, Kyle C., John S. Kimball, Eni Njoku, Reiner Zimmermann, and Maosheng Zhao. 2004. Variability in Springtime Thaw in the Terrestrial High Latitudes: Monitoring a Major Control on the Biospheric Assimilation of Atmospheric CO 2 with Spaceborne Microwave Remote Sensing. *Earth Interactions*, **8** (20):1–23. https://doi.org/10.1175/1087-3562(2004)8<1:VISTIT>2.0.CO;2.

Nazemi, Alireza, and Amin Elshorbagy. 2012. Application of Copula Modelling to the Performance Assessment of Reconstructed Watersheds. *Stochastic Environmental Research and Risk Assessment*, **26** (2):189–205. https://doi.org/10.1007/s00477-011-0467-7.

Nghiem, S V, D K Hall, T L Mote, M Tedesco, M R Albert, K Keegan, C A Shuman, N E Digirolamo, and G Neumann. 2012. The Extreme Melt across the Greenland Ice Sheet in 2012. *Geophysical Research Letters*, **39** (September):6–11. https://doi.org/10.1029/2012GL053611.

Park, Hotaek, Youngwook Kim, and John S. Kimball. 2016. Widespread Permafrost Vulnerability and Soil Active Layer Increases over the High Northern Latitudes Inferred from Satellite Remote Sensing and Process Model Assessments. *Remote Sensing of Environment*, **175**. Elsevier Inc.:349–58. https://doi.org/10.1016/j.rse.2015.12.046.

Sheffield, Justin, Gopi Goteti, and Eric F. Wood. 2006. Development of a 50-Year High-Resolution Global Dataset of Meteorological Forcings for Land Surface Modeling. *Journal of Climate*, **19** (13):3088–3111. https://doi.org/10.1175/JCLI3790.1.

Takala, Matias, Jouni Pulliainen, Senior Member, Sari J Metsämäki, and Jarkko T Koskinen. 2009. Detection of Snowmelt Using Spaceborne Microwave Radiometer Data in Eurasia From 1979 to 2007. *IEEE Transactions on Geoscience and Remote Sensing*, **47** (9):2996–3007.

Williams, Caroline M., Hugh A.L. Henry, and Brent J. Sinclair. 2015. Cold Truths: How Winter Drives Responses of Terrestrial Organisms to Climate Change. *Biological Reviews*, **90** (1):214–35. https://doi.org/10.1111/brv.12105.

Williams, Claude N, Alan Basist, Thomas C Peterson, and Norman Grody. 2000. Calibration and Verification of Land Surface Temperature Anomalies Derived from the SSM / I. *Bulletin of the American Meteorological Society*, **81** (9):2141–56. %5C%5CIBSERVER%5CID_enl%5CBulletin_of_the_American_Meteorological_Society%5C2000%5C081-09-2141.pdf.

Appendix C.

Hatami, S., Nazemi, A., 2021. On Complex Responses of Landscape Freeze-Thaw to Compound Climatic Changes: Lines of Evidence from Québec, Canada. *Scientific Reports*, (Submitted on June 9th).

On Complex Responses of Landscape Freeze-Thaw to Compound Climatic Changes: Lines of Evidence from Québec, Canada

Shadi Hatami[1] & Ali Nazemi[1]*

Cycles of Freeze-Thaw (FT) are among the key landscape processes in cold regions. Under current global warming, understanding the alterations in FT characteristics is of a great importance for advising land management strategies in northern latitudes. Using a generic statistical approach, we address the impacts of changing air temperature and snow depth on FT responses across Québec, a Canadian province ~2.5 times larger than France. Our findings show significant yet complex responses of landscape FT to changing climate conditions. We note a vivid spatial divide between northern and southern regions and point out two important features, namely non-symmetry and nonlinearity, in the FT response. In general, the response of sensitive FT characteristics to changing climate is more intense under warming compared to corresponding cooling conditions. In addition, FT responses include nonlinearity, meaning that compounding changes in temperature and snow depth have more severe impacts compared to the cumulative response when temperature and/or snow depth change separately. These nonsymmetric and nonlinear responses have important implications for the future environment and socio-economy in a thawing Québec. Our study provides a fresh look at complex landscape responses to climatic changes in Québec and a generic methodology that can be applied in other regions.

Introduction

Freeze-Thaw (FT) dynamics, i.e. the fluctuations of soil state between frozen and thawed conditions[1], is one of the most important land-surface characteristics in northern regions, which plays a major role in determining soil properties[2], hydrologic response[3] as well as ecosystem diversity and productivity[4]. Due to these critical impacts, FT dynamics are among key considerations for human activities such as agriculture[5] as well as the construction and operation of infrastructures in cold regions[6]. Heightened climate variability and change, however, have significantly affected soil temperature patterns and consequently the dynamics of FT cycles[7]. Changing climate can impact FT patterns in several ways. Increasing air temperature, for instance, can affect the FT dynamics through decreasing the length of frozen season[8], increasing depth of the active soil layer[9], and permafrost retreat[10]. Decreasing snow depth, in parallel, reduces the thermal insulation of soil interface with atmosphere and increases soil vulnerability to fluctuations in air temperature[11]. This can in turn contribute to decreasing frost depth and increasing the frequency of swinging in FT states[12]. Climate-induced changes in FT dynamics, therefore, can result in widespread alterations in regional hydrology[13], phenology[14], geology[15], water quantity, and quality[16] as well as socio-economic activities[17]. In addition, some of these alterations can create feedback effects with other elements of the environment. For instance, thawing landscapes

[1]Department of Building, Civil, and Environmental Engineering, Concordia University, 1455 De Maisonneuve Blvd. W. Montréal, Québec, H3G 1M8, Canada.
* Corresponding author; Email: ali.nazemi@concordia.ca

in northern regions can affect the climate system through the emission of an excessive amount of greenhouse gas fluxes[18], which can intensify the rate of global warming unprecedentedly[19]. These impacts together can pose challenges to northern communities, where not only natural processes and socio-economic activities but also cultural values and ways of life are strongly tied with dynamics of FT cycles[20].

One example of such regions is the province of Québec in Canada. Spanning from 57º 15ˈ to 79º 23ˈwest and 44º 59ˈ to 62º 09ˈ north[21], Québec is the largest Canadian province and the richest in terms of the ecosystem diversity and availability of freshwater resources. Almost the entire 1,542,056 km^2 of the Québec's landmass undergoes three states of FT during a typical year, including continuous periods of frozen and thawed states, divided by a transit period in which the landscape switches between frozen and thawed conditions throughout a diurnal cycle. Having said that, as the area is massive and landscape characteristics are diverse, regional FT characteristics are subject to large spatial variability[22,23]. This becomes crucial in light of significant alterations in regional temperature and snow depth[24], the two most influential climatic controls of FT at larger temporal and spatial scales[8,11,15]. At this stage, similar to many other cold regions, it is not yet clear how FT cycles across Québec respond to individual and compound changes in temperate and snow depth. This is a major gap as urgent management decisions are required to face the consequences of the thawing landscape in Québec and other regions in Canada, Alaska, Russia, and Northern Europe.

The knowledge gap in accounting FT response to changing climate stems from different sources. Firstly, most of our current findings are based on in-situ data that are rather sparse spatially and discontinuous temporally[8,25]. Secondly, in order to quantify the impact of changing climate on FT dynamics, physically-based approaches, implemented in the current generation of land-surface schemes, are typically used. Despite current advancements, this framework is rather incomplete due to limitations in both data availability and modeling capability[26]. While in-situ data provide valuable information on the local control of climate on FT dynamics, the lack of data, especially in higher latitudes, pose significant constraints on the ability of in-situ data to capture the characteristics of changing FT patterns in time and space[27]. In addition, while physically-based models are theoretically sound, they often suffer from oversimplified process representations and require large data support that are often unavailable.

We argue that recent advancements in remote sensing technology along with the advent of powerful statistical tools can address some of the above limitations. On the one hand, satellite remote sensing data can overcome the limitations in in-situ observation of FT state at larger spatial and temporal scales, by providing a synoptic and continuous monitoring of FT dynamics. This can provide an opportunity to systematically inspect temporal and spatial dependencies in FT dynamics, and their dependence with relevant climate variables[15,28]. On the other hand, if the purpose of modeling is shifted from continuous representations of FT states to representations of FT characteristics, then various statistical frameworks with much more flexibility can be used to describe functional links between FT and climate characteristics.

One approach of such kinds is the copula methodology, a formal framework to represent statistical dependence, which is widely used in recent hydrologic and environmental studies[29,30]. Copulas can provide a generic solution to formal conditioning of FT states to marginal and joint characteristics of temperature, snow depth, and other relevant variables if needed. The data support

for setting up such a framework is currently available through various publicly available gridded data[31–33]. This allows for setting up a bottom-up impact assessment framework, with which the impacts of changing climatic conditions on FT characteristics can be quantified systematically across different spatial and temporal scales – see Methods below.

Results

Québec includes eight ecozones that are regions with similar land, soil, vegetation, and climatic characteristics[34]. From the north to south, these ecozones include Northern Arctic (EZ1), Southern Arctic (EZ2), Arctic Cordillera (EZ3), Taiga Shield (EZ4), Hudson Plains (EZ5), Boreal Shield (EZ6), Atlantic Maritime (EZ7), and Mixed Wood Plains (EZ8), respectively[35] – see Fig. 1 below.

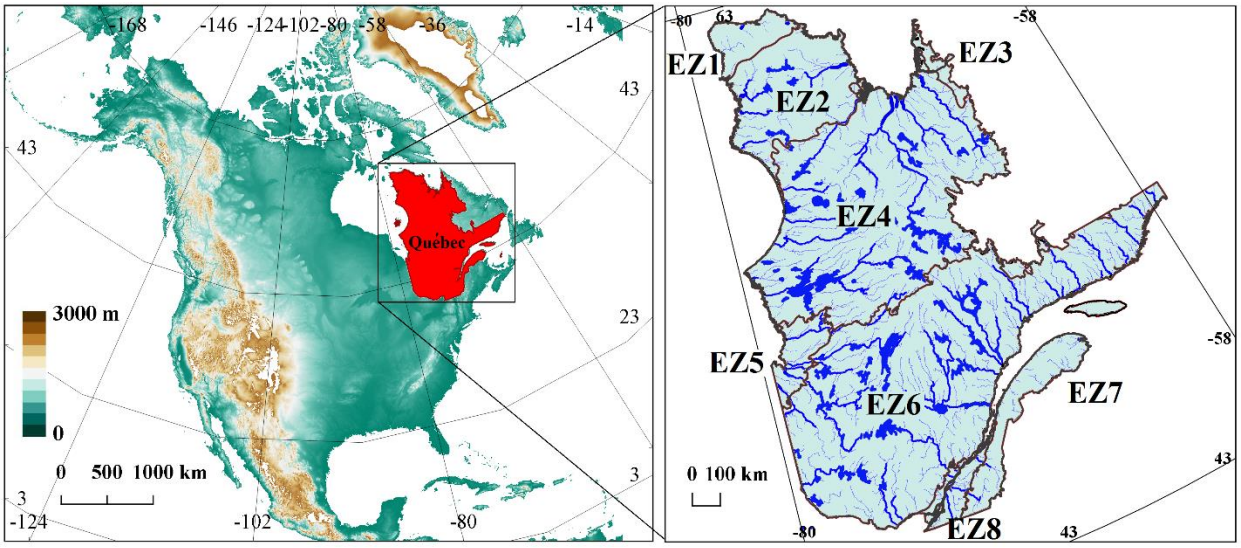

Figure 1. The province of Québec in Canada and its eight ecozones.

In each ecozone, the annual number of Frozen Days (FD_{year}) and the number of transient days in the winter season (December, January, and February; FTD_{DJF}) at grid scale are extracted. In line with earlier studies[36,37], our empirical results also show that these characteristics are the two most sensitive regional FT characteristics to changes in climate conditions, and demonstrate the strongest interdependence with temperature and snow depth at common scales and across the eight ecozones. These FT characteristics have also direct implications for land management. The changing annual number of frozen days can affect the length of phenological and agricultural activities[38], accessibility to natural resources[39], and the emission of greenhouse gasses from thawing permafrost[40]. In addition, the increasing number of transient days can be a proxy for land subsidence and erosion[41] as well as the deterioration rate of civil infrastructures such as buildings, roads, and pipelines[17].

By applying the proposed framework (see Methods below), FT characteristics at each ecozone can be conditioned to air temperature and snow depth using developed copula models[42,43]. Before applying these models for impact assessments, we evaluate their performance in representing the marginal and joint characteristics of the two considered FT characteristics, observed across the eight ecozones. Figure 2 summarizes the results, in which the top row depicts the results for the

annual number of frozen days (FD_{year}) and the bottom row is related to the number of transient days during the winter season (FTD_{DJF}). In each row, panels from left to right show the expected estimations (bars) and observed values (thresholds) for the mean, standard deviation, and skewness of the considered FT characteristics as well as their dependence with temperature and snow depth across the eight ecozones. Figure 2 clearly shows that the parametrized copulas can effectively represent the first three moments of the empirical probability distributions of both FT characteristics considered. For FD_{year}, the overall expected relative error of 0.2%, 2.2%, and 13.5% is observed for mean, standard deviation, and skewness, respectively. For FTD_{DJF}, the overall expected relative error for the first three moments are 0.4%, 1.1%, and 3.1%. Apart from statistical moments of marginal variables, the interdependencies between FD_{year}, temperature, and snow depth are preserved with average relative errors of 0.7% and 1.1%, respectively. Average relative errors of 0.9% and 1.1% are also observed for the interdependencies between FTD_{DJF}, temperature, and snow depth. These modeling efficiencies in reconstructing the historical FT characteristics justify the application of the proposed framework for assessing the compounding impacts of changing temperature and snow depth on the considered FT characteristics.

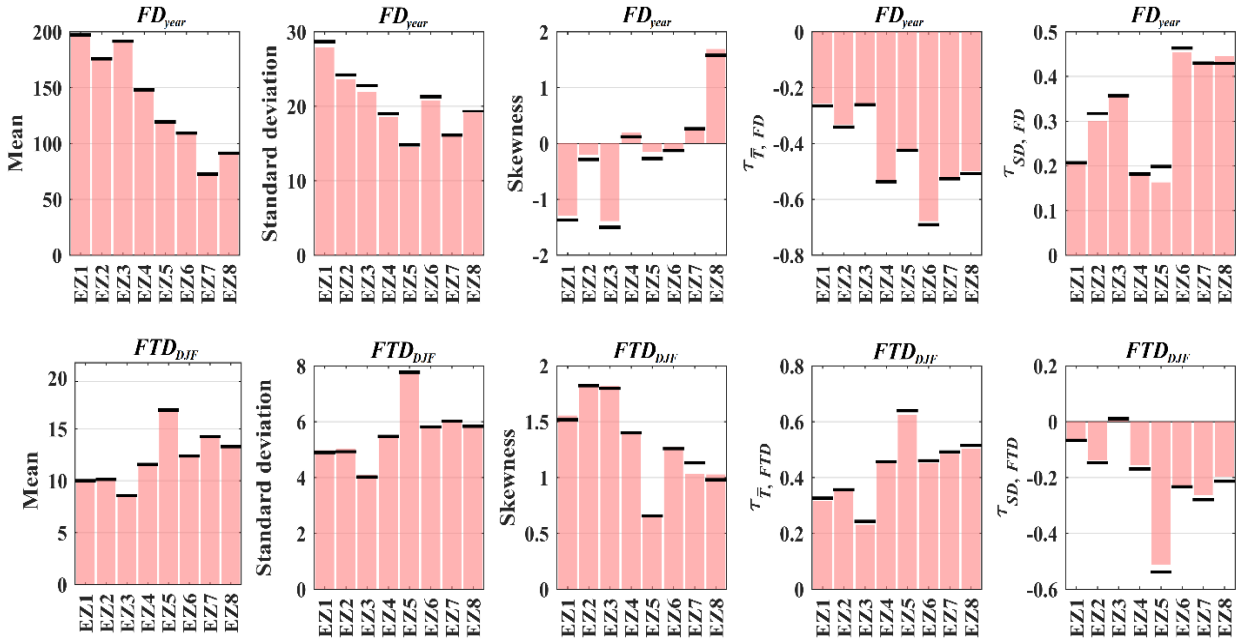

Figure 2. Observed (thick threshold lines) *vs.* simulated values (pink bars) for mean, standard deviation, skewness, as well as Kendall's tau dependencies between FT characteristics, temperature and snow depth across eight ecozones of Québec, displayed from left to right. The top and bottom rows depict the results for the number of frozen days in a typical year (FD_{year}) and the number of transient days in a typical winter season (FTD_{DJF}), respectively.

Apart from benchmarking the performance of copula models in reconstructing the historical dependencies between FT characteristics and climatic conditions, Fig. 2 shows a clear increase in the magnitude of dependencies between FD_{year} and both temperature and snow depth by moving from north to south. Similarly, the magnitude of dependence between FTD_{DJF} and considered climatic drivers generally increases in southern ecozones. Using the one-way ANOVA test, we

assess the differences between the estimated dependencies across different ecozones. The results highlight the uniqueness of interdependencies between FD_{year}, temperature, and snow depth across all ecozones. In addition, dependencies between FTD_{DJF} and climate drivers are almost unique. The only statistically significant similarity is in the case of FTD_{DJF} and temperature in EZ4 and EZ6. Significant variations in the dependencies between FT characteristics and hydroclimatic drivers can reveal the effect of ecosystem conditions on regulating the impacts of changing condition on FT characteristics. To showcase this empirically, we consider two compound scenarios related to opposing warming and cooling conditions. These scenarios include changes of 2°C increase in long-term mean temperature along with 10 cm thinner snow on the ground (compound warming), as well as 2°C decrease in long-term mean temperature along with 10 cm thicker snow on the ground (compound cooling). Figure 3 summarizes the results of this impact assessment and compares them with historical conditions, where whiskers span the range of expected FT characteristics obtained by 1,000 resampling trials – see Methods for the proposed assessment framework.

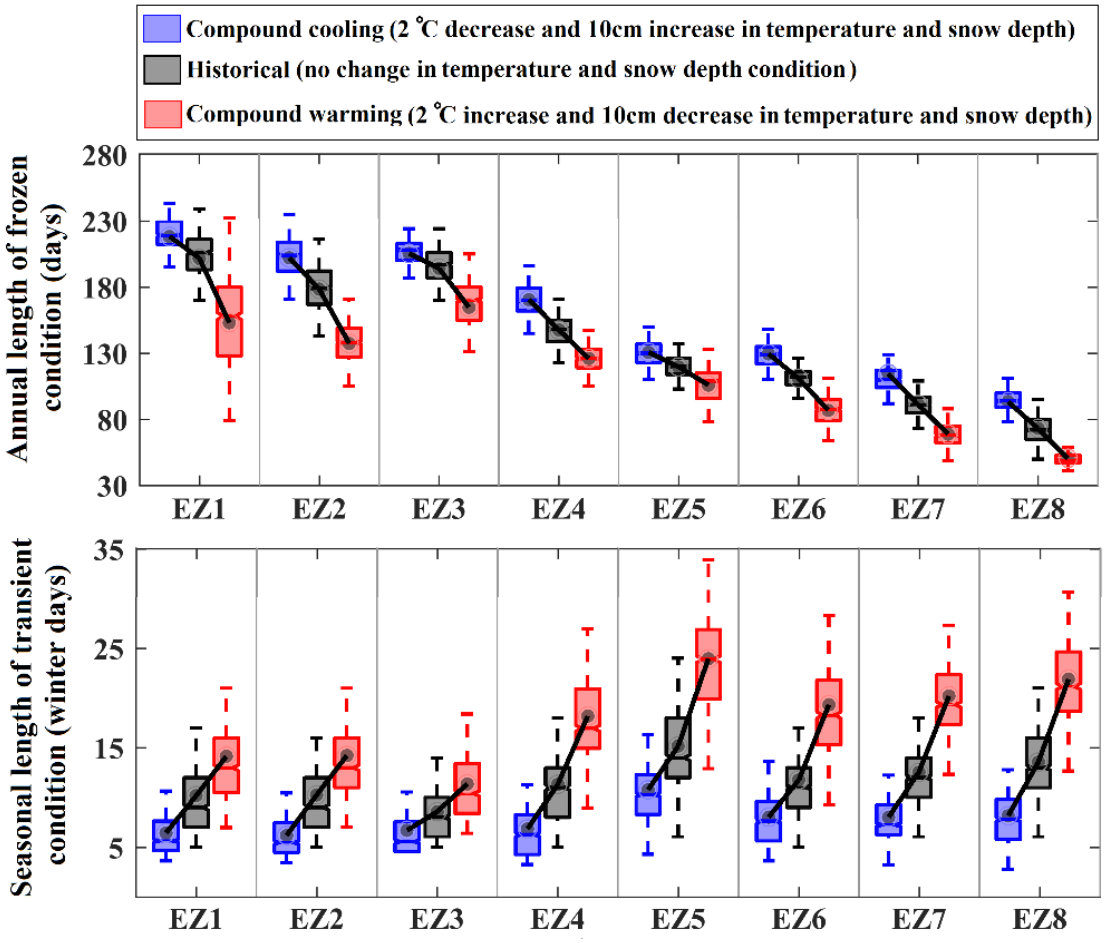

Figure 3. The response of FD_{year} (top row) and FTD_{DJF} (bottom row) to opposite compound scenarios of change in temperature and snow depth conditions. Historical as well as compound cooling and warming scenarios are shown with grey, blue and red boxplots obtained by 1,000 resamples. Dots signifies the simulated mean ensemble of FT characteristics at each ecozone.

In this figure, historical baseline (no change condition) along with compound cooling and warming scenarios are shown with gray, blue, and red colors, respectively. Black dots signify the mean ensembles of simulated values. Using Fig. 3, a couple of key findings are made. First, there is a clear geographic departure between FT responses to unique compound changes in temperature and snow depth. While the response of FD_{year} to compound cooling and warming is more vivid in the north, the impacts on FTD_{DJF} are more highlighted in the south. Considering FD_{year} and under compound warming conditions, on average between 48 (EZ1) to 22 (EZ8) fewer days with the frozen condition is expected in a typical year. The north-south decline in the response of FD_{year} is less obvious under compound cooling conditions, ranging from roughly 10 (EZ5) to 34 (EZ2) days extension in frozen conditions per year. Considering FTD_{DJF}, in contrast, the impact of compound warming increases by moving from north to south. Under this scenario and on average, it is expected to have 10 more days during a typical winter with the transient condition in EZ8, where the majority of Québec's population is inhabited, as appose to only 5 days in EZ1. Under cooling conditions, this change ranges from roughly 2 (EZ3) to 6 (EZ8) fewer days with transient conditions in a typical winter. These spatially heterogeneous impacts on FT characteristics under unique compound changes in temperature and snow depth can reveal how changes in ecozonal features (e.g. vegetation type, soil type, land cover, regional climate, etc.) can regulate FT responses to compound changes in temperature and snow depth.

Second, Fig. 3 clearly shows that in those ecozones in which FT characteristics are more sensitive to compound changes, responses to opposite warming and cooling scenarios become more non-symmetric and are more intense under the compound warming compared to the compound cooling scenario. For instance, looking at FD_{year}, the absolute shift under compound warming scenario is 30 days more in the Northern Arctic (EZ1), compared to the shift due to compound cooling scenario in the same ecozone. The higher impact of warming on FD_{year} in northern ecozones is of great importance in the context of the land-atmospheric Carbon emissions due to permafrost degradation[44]. Similarly, in the case of FTD_{DJF}, the magnitude of positive shift due to the compound warming scenario is about 4 days more in the Mixed Wood Plains (EZ8) compared to the opposite negative shift caused by the compound cooling scenario. More sensitivity to the compound warmings has important implications regarding soil stability[45] and deterioration of critical infrastructure[46] that are currently under pressure due to aging[47].

To better understand climate controls on FT characteristics, we consider additional compound and individual changes in temperature and snow depth by mixing-and-matching long-term shifts in mean temperature, ranging from $-2℃$ to $+2℃$ (sampled every 0.5º C), and mean snow depth, ranging from -10 cm to 10 cm (sampled every 2.5 cm). This results into 81 different scenarios, with which FD_{year} in the Northern Arctic (EZ1) and FTD_{DJF} in the Mixed Wood Plains (EZ8) are conditioned. We choose these two ecozones due to their largest sensitivity in changing hydroclimatic conditions with respect to FD_{year} and FTD_{DJF} (see Fig. 3); and accordingly, they can better reveal how marginal and joint variations in temperature and snow depth can result into alterations of FT characteristics. Figure 4 presents the results of this analysis, in which the top (panels a to c) and the bottom rows (panels d to f) depict the results related to FD_{year} and FTD_{DJF}, respectively. Panels a and d show response surfaces for changes in FT characteristics with respect to changes in temperature and snow depth.

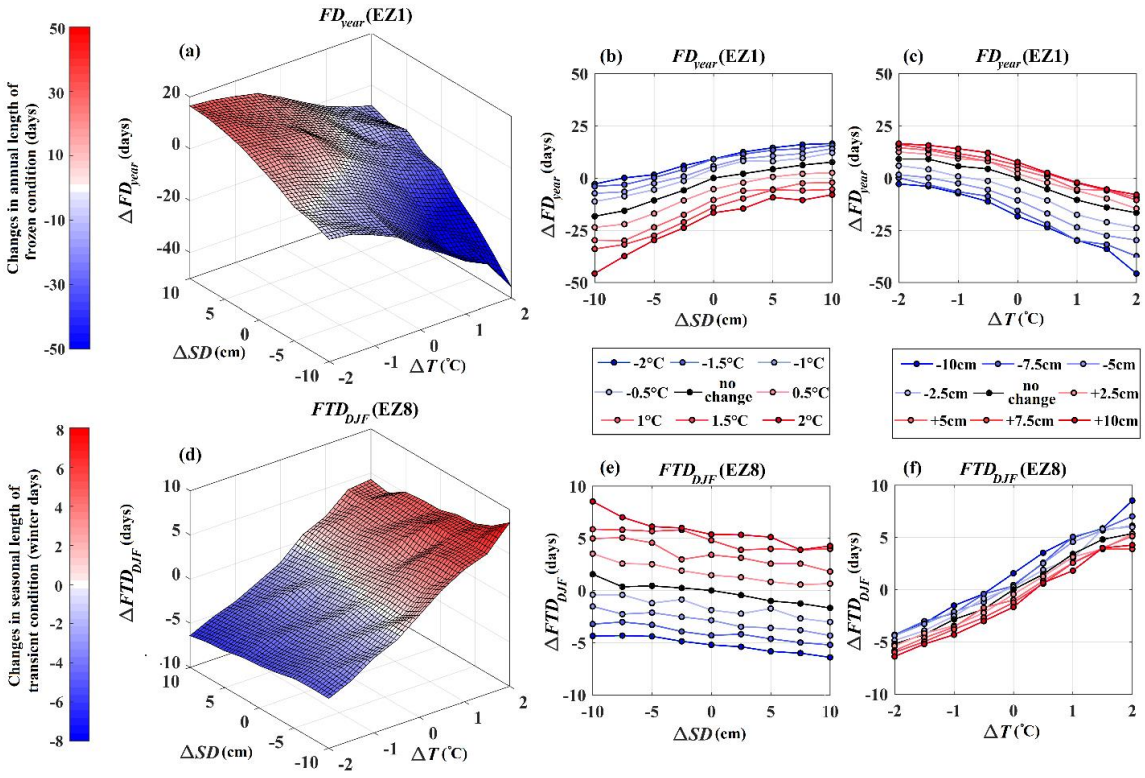

Figure 4. The response surfaces of FD_{year} in the Northern Arctic (EZ1, panel a) and FTD_{DJF} in the Mixed Wood Plains (EZ8, panel d) along with marginal sensitivity analyses to $\pm$2ºC change in temperature (panels b and c) and $\pm$10 cm change in snow depth (panels e and f) conditions.

These response surfaces are reconstructed using the proposed C-vine copula and 1,000 resampling – see Methods below. Panels b and e, as well as c and f, show the partial derivatives of these response surfaces, derived at known temperature and snow depth conditions, respectively. Looking at the results obtained for FD_{year} across EZ1 (Fig. 4, first row), several interesting observations can be made. First and foremost, the non-symmetric response of FT characteristics to warming *vs.* cooling is again revealed itself and is even more vivid in this round of analysis. While cooler temperature and inclined snow depth increase the length of the frozen period in a typical year by around 18 days, warmer temperature and declined snow depth can decrease the length of the annual frozen period by around 48 days. Projections of response surfaces, shown in panels (b) and (c), clearly present higher sensitivity of FD_{year} to warmer temperatures and thinner snow depth. Second, despite having different signs, the magnitude of interdependencies with temperature and snow depth is more or less the same (-0.27 and 0.22, respectively; see Fig. 2); and therefore, the sensitivity of FD_{year} to changes in temperature and snow depth are rather similar. The expected change in FD_{year} under constant temperature conditions when snow depth is varying from -10 cm to 10 cm of its long-term average value is about 25 days (Fig. 4b). Similarly, the expected change in FD_{year} under constant snow depth when the temperature is shifted from -2°C to +2°C of the annual long-term average is about 30 days (Fig. 4c). Having said that, it should be mentioned that the impacts of both snow depth and temperature variations are intensified as the temperature warms and snow depth declines. This is another line of evidence for non-symmetric marginal impacts that is further controlled by the state of other driving variables.

Similar rationale can be used to interpret the results obtained for FTD_{DJF} across the Mixed Wood Plains (EZ8; the bottom row of Fig. 4). The changes in the expected FTD_{DJF} range from 9 more transient days under warmer climate with declined snow depth to 7 fewer days with transient days under cooler climate with inclined snow depth on the ground. This observation again points at the non-symmetric response of the FT characteristics, although it is less obvious compared to FD_{year} across EZ1. In this case, however, the dependence between FTD_{DJF} and temperature is stronger than the dependence between FTD_{DJF} and snow depth; and therefore, this FT characteristic is more sensitive to temperature changes, compared to changes in the snow depth. As an example, the expected magnitude of change in FTD_{DJF} is roughly about 5 days under constant temperature conditions (Fig. 4e), while it is about 12 days under constant snow depth conditions (Fig. 4f). Similar to the case of FD_{year} across EZ1, the marginal impacts of change in snow depth are more intense under a warmer climate, ranging from 3 days under 2ºC cooling *vs.* 6 days under 2ºC warming. This is the case also for the marginal impacts of change in temperature under declined snow depth conditions, although with less vividity.

Discussion

The results provided above illustrate two important findings. First, the impacts of changing temperature and snow depth conditions on FT characteristics are rather unique spatially, with different manifestations and natures of response in northern and southern regions. Second, non-symmetric responses to compound warming and cooling conditions are seen across different FT characteristics and/or regions. In general, when there is a significant sensitivity to changing climate, the response is more intense under warmer and/or declined snow depth conditions. In this section, we look at another key feature of FT responses to compound changes in temperature and snow depth, which is rather overlooked in current literature. One key feature of the response to compound events is the nonlinear nature of the response, meaning that the impact of compound events can be more intense compared to the cumulative impacts of individual events when occurring independently[48,49]. Here we formally address the nonlinearity in FT responses at the grid resolution, by inspecting the deviation from the superposition principle of linear systems. This is through simulating FT responses to historical baseline and six opposing individual and compound scenarios of change in temperature and snow depth. Table 1 summarizes these scenarios.

Table 1. Individual and compound climate scenarios considered for addressing the nonlinear response of FT characteristics to individual and compound changes in temperature and snow depth conditions across Québec and at the grid scale.

Scenario description	Type	Notation
Long-term means of temperature and snow depth	Historical baseline (no-change)	(0,0)
2°C cooler compared to the long-term mean	Individual (cooling only)	(-2,0)
10 cm thicker snow compared to long-term mean	Individual (thickening snow cover only)	(0,10)
2°C cooler and 10 cm thicker snow compared to long-term means	Compound (cooling)	(-2,10)
2°C warmer compared to the long-term mean	Individual (warming only)	(2,0)
10 cm thinner snow compared to long-term mean	Individual (thinning snow cover only)	(0,-10)
2°C cooler and 10 cm thicker snow compared to long-term means	Compound (warming)	(2,-10)

In brief, we address the non-linearity in FT responses by comparing the expected values of FD_{year} under individual and compound changes in temperature and snow depth under cooling and warming conditions. For cooling, we compare the response to (-2,10) at each grid with the summation of the expected FD_{year} under corresponding (-2,0) and (0,10). Similarly for warming, we compare the (2,-10) with the summation response to (2,0) and (0,-10). Theoretically at each grid, the variation in FD_{year} under individual and compound scenarios compared to historical conditions, i.e. ΔFD_{year}, can have one of the following three conditions: (1) linear response, meaning either $\Delta FD_{year}(-2,10) = \Delta FD_{year}(-2,0) + \Delta FD_{year}(0,10)$ under cooling and/or $\Delta FD_{year}(2,-10) = \Delta FD_{year}(2,0) + \Delta FD_{year}(0,-10)$ under warming; (2) nonlinear dumping response, meaning either $\Delta FD_{year}(-2,10) < \Delta FD_{year}(-2,0) + \Delta FD_{year}(0,10)$ under cooling or $\Delta FD_{year}(2,-10) > \Delta FD_{year}(2,0) + \Delta FD_{year}(0,-10)$ under warming; or (3) nonlinear amplifying response, meaning either $\Delta FD_{year}(-2,10) > \Delta FD_{year}(-2,0) + \Delta FD_{year}(0,10)$ under cooling or $\Delta FD_{year}(2,-10) < \Delta FD_{year}(2,0) + \Delta FD_{year}(0,-10)$ under warming. Figure 5 summarizes the results of this analysis. The maps in the top row demonstrate the results related to deviation from the superposition principle at the grid scale under compound cooling (left column) and warming (right column). Under compound cooling, shades of blue and red show amplifying and dumping effects; whereas for compound warming, these colors represent dumping and amplifying effects, respectively. The white color highlights grids in which a linear response is observed. Black dots show the grids where the autocorrelation is present in temperature data and accordingly these grids are excluded from our assessment. The bar charts in the bottom row show the percentage of grids at each ecozone, where amplification in compound response is observed.

Considering this figure, although the amplified response of FD_{year} to compound changes is observed across the province, it is mainly concentrated in the northern ecozones for both cooling and warming scenarios. Looking at both compound cooling and warming, more than 70% of the area in the three northern ecozones, i.e. Northern Arctic (EZ1), Southern Arctic (EZ2), Arctic Cordillera (EZ3) demonstrate an amplified response. While the expected values for amplifying effect, i.e. $\Delta FD_{year}(-2,10) - \Delta FD_{year}(-2,0) - \Delta FD_{year}(0,10)$ in EZ1, EZ2, and EZ3 are 5, 8, and 7 days, respectively, the amplified cooling effect can reach up to 16 days in some grids in northern ecozones. In contrast, the percentage of grids with amplified effect reduces to less than 10% in the EZ7 – see Fig. 5c. Similar findings are obtained with regard to the compound warming scenario, although it should be noted that in contrast to compound cooling, the amplification can also dominate the response of FD_{year} in the south, e.g. in EZ8 (see Fig. 5d). Having said that, still more amplifications are observed in the three northern ecozones – see Fig. 5d. Although the expected values for amplified warming, i.e. $\Delta FD_{year}(2,-10) - \Delta FD_{year}(2,0) - \Delta FD_{year}(0,-10)$ are -4, -6, and -6 days in EZ1, EZ2, and EZ3, the amplified response can get to -11 days in a grid located in Southern Arctic. In addition, the percentage of areas with amplified warming is considerably lower in EZ4 to EZ7 with roughly 40% of grids showing some amplified response to compound warming. This finding has some important implications for the thawing landscape in the northern regions and a wide suite of environmental change that can be initiated by the amplified response of FT to compound warming. On the one hand, an amplified response can facilitate the access to untapped natural resources of the north and may unleash an opportunity for northern agriculture. On the other hand, however, it

intensifies permafrost degradation, which results in unprecedented emissions of greenhouse gasses[18,19,40].

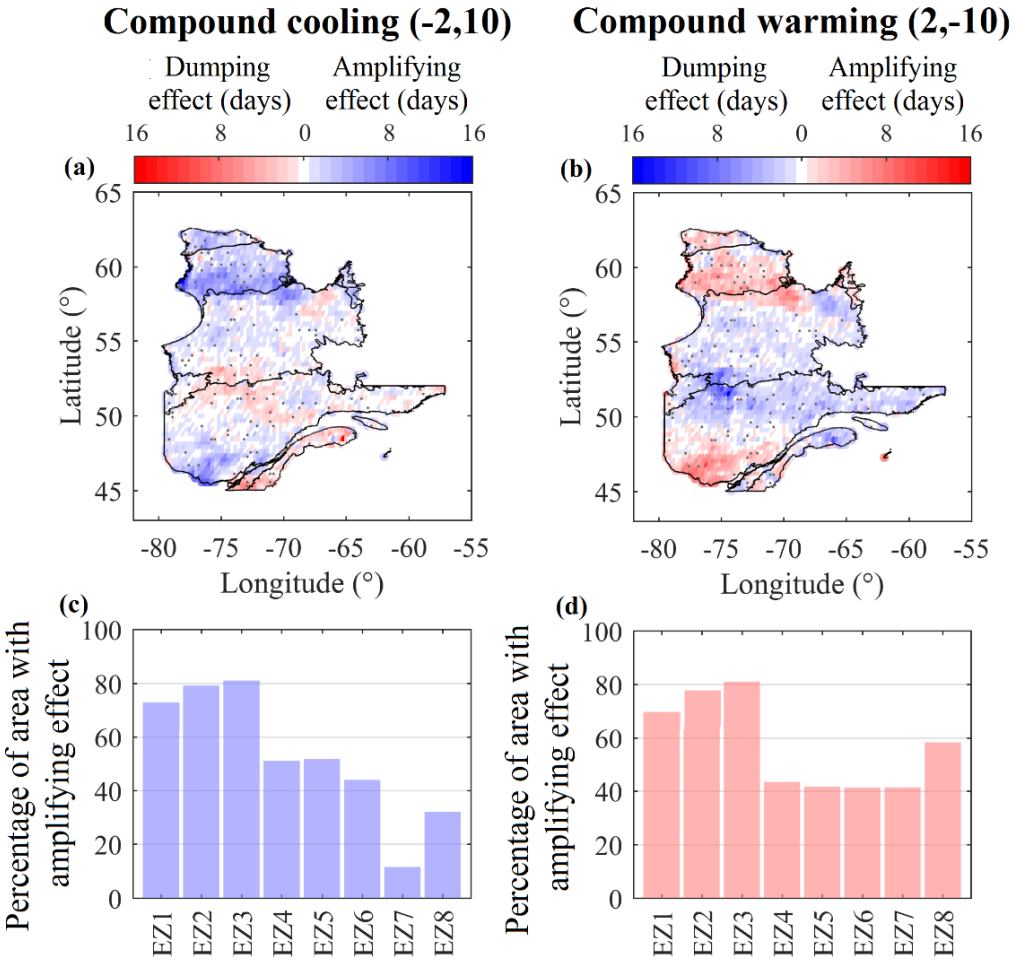

Figure 5. The nonlinear response of FD_{year} to considered compound cooling (left column) and warming (right column). Nonlinear responses are manifested by amplifying and dumping effects in the length of the frozen period (top row). In each map, black dots show the grids that are excluded from the study due to the existence of autocorrelation in temperature data. In the bottom row, the percentage of areas in each ecozone with an amplified response is shown.

In parallel to amplified responses in the north, the dumping effect dominates the FD_{year} response in the southern ecozones, with the exception of EZ8 under compound warming. For both cooling and warming scenarios, the most severe dumping effect is observed in the Atlantic Maritime (EZ7), with the expected and extreme dumping of -5 and -9 days under compound cooling as well as 6 and 10 days under compound warming respectively. While southern regions demonstrate significantly less amplification in FD_{year} response, it should be noted that the sensitivity of FD_{year} to compound changes in the hydroclimate conditions is rather marginal compared to northern regions. Accordingly, we look at the gridded response of FTD_{DJF} to individual and compound scenarios of change in the three most populated zones of Québec, i.e. Montréal (the grid including 45.5017ºN, 73.5673ºW), Québec City (the grid including 46.8139ºN, 71.2080ºW) and Gatineau (the grid including 45.4765ºN, 75.7013ºW). These cities are all located in the Mixed Wood Plains (EZ8), where the most significant sensitivity in the response of FTD_{DJF}

to compound changes in temperature and snow depth conditions is observed – See Fig 3. Figure 6 presents the shifts in the mean and exceedance probabilities of FTD_{DJF}, i.e. ΔFTD_{DJF}, given 7 different hydroclimatic conditions in Montréal (first row), Québec City (second row), and Gatineau (third row). From left to right, the first three columns show the changes in Probability Density Functions (PDFs) of FTD_{DJF} under (+2,0) and (-2,0), (0,-10) and (0,+10), as well as (+2,-10) and (-2,+10), respectively. The right column compares the hypothetical linear response, i.e. $\Delta FTD_{DJF}(-2,0) + \Delta FTD_{DJF}(0,10)$ in the case of compound cooling and $\Delta FTD_{DJF}(2,0) + \Delta FTD_{DJF}(0,-10)$ in the case of compound warming, with expected values of $\Delta FTD_{DJF}(-2,10)$ and $\Delta FTD_{DJF}(2,-10)$, respectively.

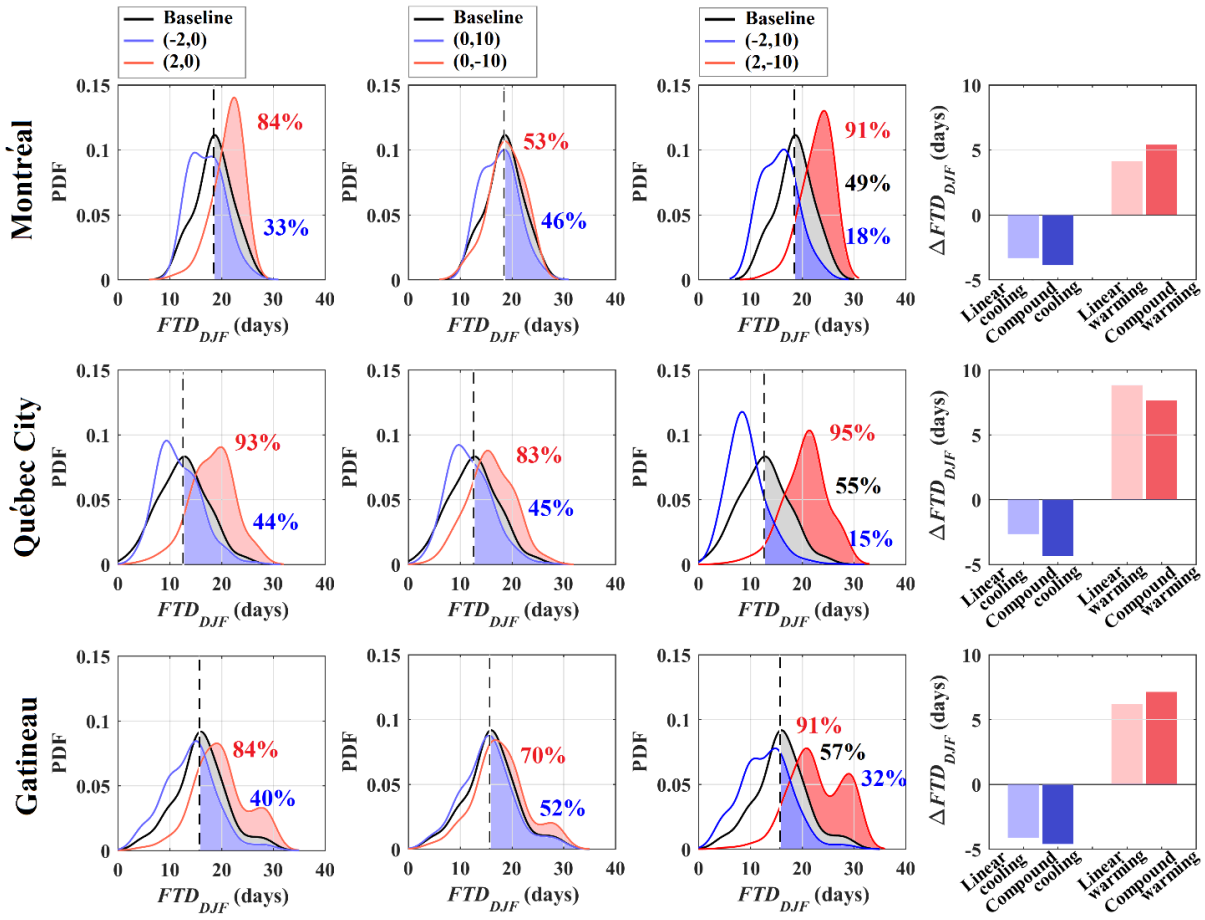

Figure 6. The Probability Density Functions of FTD_{DJF} along with the likelihood of exceeding the corresponding long-term historical values in Montréal (first row), Québec City (second row), and Gatineau (third row) given opposite individual and compound scenarios for climatic changes, shown in the first, second and third columns from the left, respectively. The nonlinear response of FTD_{DJF} to considered compound cooling and warming are demonstrated in the far right column.

The PDFs of FTD_{DJF} for warming, cooling, and no-change conditions are shown in red, blue, and black colors respectively; and the expected historical value of FTD_{DJF} are identified with vertical dashed lines. The highlighted regions in each PDF show likelihoods for FTD_{DJF} exceeding the long-term historical mean of FTD_{DJF} under the considered warming (red) or cooling (blue)

conditions. In each panel of the right column, light colored bars show hypothetical linear responses under cooling (blue) and warming (red) conditions. Dark colored bars, in contrast, show the expected responses under compound cooling (blue) and warming (red) conditions obtained by the C-vine copula models. Both non-symmetric and nonlinear responses of FTD_{DJF} to individual and compound cooling and warming scenarios are revealed in the three cities. Under individual scenarios, the shift in the mean of FTD_{DJF} is at least 4 days higher under (2,0) comparing to (-2,0), although these shifts are relatively symmetric under (0,-10) and (0,10). Under compound changes, the shift in the mean of FTD_{DJF} is approximately twice higher under (2,-10) comparing to (-2,10). The non-symmetric response of FTD_{DJF} to compound events is also manifested in the exceedance probabilities. For instance, in Montréal the exceedance probability of FTD_{DJF} changes by 42% under (2,-10), while the corresponding shift in the exceedance probability under (-2,10) is only -31%. This is another line of evidence for complex responses of FT characteristics to compound cooling and warming. Comparing the expected compound responses with hypothetical linear responses under cooling and warming scenarios, an amplified response to compound cooling is observed in all three cities with expected values of -2, -3, and -1 days in Montréal, Québec City, and Gatineau, respectively. Considering the compound warming scenario, the amplifying effect in Montréal and Gatineau are 2 and 1 days, respectively. It should be noted however that a dumping effect of -1 day is observed in Québec City under the considered compound warming. It should be noted that the nonlinearity in the response transcends to exceedance probabilities as well. In Montréal, for instance, the amplifying effects in exceedance probabilities under compound cooling and warming conditions are -12% and +3%, respectively. The amplifying response of FTD_{DJF} to compound warming in a place like Montréal has an important relevance to the current revelation of climate change, manifested by warmer temperature and less snowfall[50]. Montréal marks one of the most populated regions in Canada with a high concentration of aging infrastructures, vulnerable to increasing FTD_{DJF}. In Montréal, for instance, it is shown that under the historical condition, 216 km length of the city's watermains need to be replaced while another 2,400 km will require repairing[51]. This rate will significantly change under increasing FTD_{DJF}. Findings in other cold regions indicate that more swings in FT cycles can translate to multiple million dollars to infrastructure maintenance and repair[17]. In addition, it is shown that the results of the Marshall stability test of asphalt concrete reduce by up to 57% when the materials are exposed to only 6 more transient days[52]. This can pressurize aging infrastructures and built environments[53].

Summary and concluding remarks

Landscape FT is arguably the most important land-surface feature in cold regions, controlling physical, biological, and socio-economic processes along with their interactions with other elements of the environment. Historical characteristics of FT, however, are under unprecedented alterations due to climate change, which has important implications for land and resource management in the north. Despite existing understandings of the impact of changing climate on FT cycles, current assessment frameworks are rather limited. On the one hand in-situ data networks, often used as the main data support for understanding FT responses to changing climate conditions, are rather sparse and therefore fail to provide a synoptic view on different modes of responses. On the other hand, the current projection paradigm based on the use of physically-based land-surface models is incomplete due to several assumptions and/or simplifications in the

conceptualization, representation, and parametrization of the interacting processes that determine the state of FT at a given time and space. Our points of innovation are in the use of satellite remote-sensing data in conjunction with a formal statistical technique to overcome some of the above-mentioned limitations, at least at coarser spatial and temporal scales. First, we propose pairing gridded FT characteristics obtained from satellite retrievals with corresponding gridded data of temperature and snow depth, the two most influential hydroclimatic drivers of FT, to study the linkage between FT and climate characteristics at a common scale. Second, we suggest C-vine copulas to develop a conditional model, with which the impacts of individual and compound changes in temperature and snow depth on FT characteristics can be assessed and quantified probabilistically.

We showcase the application of this framework in the province of Québec, Canada, a sub-country jurisdiction with an area comparable to Mongolia, the 18th largest country in the world. We show that the simulations obtained by parametrized C-vine copulas can capture the empirical moments of observed FT characteristics as well as the interdependencies between FT, temperature and snow depth characteristics during 1998 to 2016. The application of the proposed framework for assessing the impact of individual and compound changes in temperature and snow depth reveals some important features of the FT response to climatic changes that have remained rather overlooked. First, we highlight an ecozonal uniqueness in the interdependencies between FT characteristics, temperature, and snow depth, pointing at the role of ecosystem conditions in regulating the impact of changing climate conditions on FT characteristics. Moreover, a north-south divide in the FT response to changing climate conditions is observed. While the impacts of changing climate conditions are manifested in the annual extent of the frozen period in northern regions, it is revealed through alteration in the extent of the transient period during a typical winter season in the south. Through sampling the response surfaces related to FD_{year} in Northern Arctic and FTD_{DJF} in Mixed Wood Plains, we also demonstrate a different nature of the response to changing temperature and snow depth conditions between the north and the south. Having said that, our results show a nonsymmetric response to changing temperature and snow depth conditions despite differences in FT variables, regions, and/or spatial scales. In general, where there is a considerable sensitivity in FT response, the alteration due to rising temperature and/or thinning snow depth is more intense compared to corresponding scenarios with falling temperature and/or thickening snow depth. Closer looks at the FT responses at the grid scale also revealed nonlinear, mainly amplifying, responses of FT characteristics to compound changes in climate conditions. This means that the response of FT to compound changes in temperature and snow depth is often more severe than the cumulative response of FT to changes in temperature and snow depth individually. These amplifying impacts can result in up to two weeks of alterations in the frozen period during a typical year in the north, and up to one week change in the transient period during a typical winter season in the three most populated regions of Québec, i.e., Montréal, Québec City, and Gatineau. While amplified shrinkage in the annual frozen period in the north can result into unprecedented changes in the northern environment under compound warming, the similar climatic condition can result into additional stress to already aging infrastructures in the south. We also show that the amplified response is not only observed in the expected values of the transient period in a typical winter, but also in the likelihood of this FT characteristic exceeding the long-term historical values.

Our proposed methodology is generic and can be applied globally. We encourage inspecting the non-symmetry, nonlinearity, and spatial variability of FT response to changing climate conditions in other Canadian regions and globally. In the context of Québec, landscape responses to freeze and thaw can have a wide range of implications from endangering already aging and vulnerable community infrastructures to substantial environmental changes due to amplified rates of permafrost degradation. The later can be even globally relevant due to massive land-induced carbon emissions. Facing these challenges requires integrated and inclusive, approaches that are supported by scientific information. As far as providing scientific information is concerned, we will soon report the application of the proposed framework for estimating future FT characteristics in Québec using available downscaled climate projections: *donc à bientôt!*

Methods

Data support. We use the global landscape FT Earth System Data Record (FT-ESDR) available from the publicly available archive of the National Snow and Ice Data Center (https://doi.org/10.5067/MEASURES/CRYOSPHERE/nsidc-0477.004). This dataset includes the daily state of soil at the spatial resolution of 25×25 km^2 over the period of 1979-2017. The remotely-sensed brightness temperature is used to classify FT states into four distinct classes of frozen (AM and PM frozen), non-frozen (AM and PM thawed), transitional (AM frozen and PM thawed), and inverse-transitional (AM thawed and PM frozen)[54]. We categorize transitional and inverse-transitional states into one combined transient state that shows whether landscape switches between the frozen and thawed conditions in a diurnal cycle. Knowing the gridded daily states of FT, FT characteristics, in this paper FD_{year} and FTD_{DJF}, can be extracted at the grid scale or each ecozone, and accordingly paired with corresponding gridded temperature and snow depth data. For air temperature data, we use the Global Meteorological Forcing Dataset (GMFD) provided by Princeton University available at https://hydrology.princeton.edu/data.pgf.php. GMFD dataset is constructed by blending the reanalysis data from the National Centers for Environmental Prediction, National Center for Atmospheric Research with a group of recent global observation-based data[32]. GMFD provides daily maximum and minimum air temperature at 0.25°×0.25° for the period of 1948-2016. The daily mean temperature is calculated by averaging the daily maximum and minimum temperature at each grid. Monthly snow depth data are obtained from the Canadian Meteorological Center (CMC; https://doi.org/10.5067/W9FOYWH0EQZ3). CMC dataset is constructed by combining the information from in-situ snow depth measurements with optimal interpolation results of a simple physical snow accumulation and melt model[33]. The data is provided for the period of 1998-2020 with the grid resolution of 24×24 km^2 across the northern hemisphere.

As the grid size and centroid locations of the three considered data sources are not the same, we implement *k*-nearest neighbor interpolation to re-grid the three data sets into a unique spatial scale and over the common period of 1998-2016. In brief, the *k*-nearest neighbor is a non-parametric approach to estimate a variable in a given point in time and space based on its neighboring values[55]. The nearest neighbors are identified as those with the smallest Euclidian distance to the center of a reference grid, here the grid of FT to which climate data are re-gridded. After finding the optimal nearest neighbors, a weighted averaging is applied to rescale the variables. The weight function gains its maximum value where the distance from the interpolated

point is zero and decreases as the distance increases[56]. By implementing some numerical experiments, we find k=4 as the optimal number of nearest neighbors to achieve the highest accuracy in modeling the mean and standard deviation of temperature and snow depth over different ecozones of Québec. The re-gridded monthly mean temperature and monthly mean snow depth are then matched with the corresponding FD_{year} and FTD_{DJF} at the same temporal and spatial scales. Before developing copula models, we investigate the existence of autocorrelation in temperature, snow depth, and FT characteristics and exclude those grids in which the autocorrelation is significant. We find that this is the case in less than 17% of grids, and only for annual temperature. These grids are excluded from our analysis.

Proposed copula-based impact assessment framework. To model the joint dependencies between FT characteristics, air temperature, and snow depth, trivariate copulas can be used. Based on the Sklar's Theorem, the joint dependencies between FT characteristics (FT), mean temperature ($\bar{T}$), and snow depth (SD) can be described as:

$$F(FT, \bar{T}, SD) = C\big(F_1(FT), F_2(\bar{T}), F_3(SD)\big) \quad (1)$$

where $F_1(FT)$, $F_2(\bar{T})$ and $F_3(SD)$ are the Cumulative Distribution Functions (CDFs) for FT, $\bar{T}$ and SD, respectively and C is the trivariate copula function[57]. Among different alternative multivariate copulas, we employ canonical vine (C-vine) to represent joint distribution between the three above-mentioned variables in Eq. 1[58]. In brief, C-vine copulas decompose a high-dimensional joint distribution into a $d(d-1)/2$ bivariate pairs of copulas arranged into $(d-1)$ trees; and accordingly the joint distribution between FT, $\bar{T}$ and SD can be described as:

$$f(FT, \bar{T}, SD) = f_2(\bar{T}) f_{3|2}(SD|\bar{T}) f_{1|2,3}(FT|\bar{T}, SD) \quad (2)$$

where $f(.)$ is the marginal PDFs and the conditional distributions that can be estimated as[59]:

$$\begin{aligned} f_{3|2}(SD|\bar{T}) &= \frac{f(SD, \bar{T})}{f(\bar{T})} = \frac{c_{2,3}\big(F_2(\bar{T}), F_3(SD)\big) f_2(\bar{T}) f_3(SD)}{f_2(\bar{T})} \\ &= c_{2,3}\big(F_2(\bar{T}), F_3(SD)\big) f_3(SD) \end{aligned} \quad (3)$$

and

$$\begin{aligned} f_{1|2,3}(FT|\bar{T}, SD) &= \frac{f(FT, SD|\bar{T})}{f(SD|\bar{T})} = \frac{c_{1,3|2}\big(F(FT|\bar{T}), F(SD|\bar{T})\big) f(FT|\bar{T}) f(SD|\bar{T})}{f(SD|\bar{T})} \\ &= c_{1,3|2}\big(F(FT|\bar{T}), F(SD|\bar{T})\big) c_{1,2}\big(F_1(FT), F_2(\bar{T})\big) f_1(FT) \end{aligned} \quad (4)$$

where $c(\cdot)$ is the 3-dimensional copula density. As a result, the three dimensional joint density can be represented in terms of bivariate copulas as the following[60]:

$$f(FT, \bar{T}, SD) = f_1(FT).f_2(\bar{T}).f_3(SD).c_{2,1}.c_{2,3}.c_{1,3|2} \quad (5)$$

where $c_{2,1}(F_2(\bar{T}), F_1(FT))$ and $c_{2,3}(F_2(\bar{T}), F_3(SD))$ are simply written as $c_{2,1}$ and $c_{2,3}$; and the conditional pairwise copulas between $F_1(FT)$ and $F_3(SD)$ conditional to $F_2(\bar{T})$, i.e.

$c_{1,3|2}\left(F_1(FT), F_3(SD)|F_2(\bar{T})\right)$ is shown by $c_{1,3|2}$. In addition, $c_{2,1}$, $c_{2,3}$ and $c_{1,3|2}$ are the densities of bivariate pairs. Having the C-vine copulas, the probability distribution of FT characteristics due to different quantitative change in temperature and snow depth can be obtained through conditional modeling as:

$$h = F(FT|\bar{T}, SD) = \frac{\partial C_{1,3|2}\left(F(FT|\bar{T}), F(SD|\bar{T})\right)}{\partial F(SD|\bar{T})} \quad (6)$$

where $F(FT|\bar{T}, SD)$ is the conditional distribution function. Moreover,

$$F(FT|\bar{T}) = h(FT|\bar{T}) = \frac{\partial C_{1,2}\left(F(FT), F(\bar{T})\right)}{\partial F(\bar{T})} \quad (7)$$

and

$$F(SD|\bar{T}) = h(SD|\bar{T}) = \frac{\partial C_{3,2}\left(F(SD), F(\bar{T})\right)}{\partial F(\bar{T})} \quad (8)$$

Using Eqs. 7 and 8, Eq. 6 can be rewritten as:

$$h = F(FT|\bar{T}, SD) = h[h(FT|\bar{T})|h(SD|\bar{T})] \quad (9)$$

The estimated CDF of characteristics can be back transformed to the original quantile space using the inverse CDF function, assuming empirical distributions for FT, $\bar{T}$ and SD at each ecozone. The inverse form of *h*-function given in Eq. 9 is applied for this purpose. To extract the probability distribution of FT characteristics, a Monte Carlo-based simulation is adopted by generating 1,000 random set of FT characteristics under known values of temperature and snow depth[61]. Given random uniform random numbers of ε, given FT characteristics can be sampled as:

$$FT = F^{-1}\left\{h^{-1}\left[\left(h^{-1}\left(\varepsilon|h(SD|\bar{T})\right)\right)|\bar{T}\right]\right\} \quad (10)$$

Computer models for conducting this simulations are developed in *CRAN R* with the use of packages of *VineCopula*, *CDVine*, and *copula*[62–64]. Tree structures for C-vine copulas are selected based on the maximum spanning tree algorithm, in which copula parameters are chosen with respect to the interdependencies between pairwise variables[65]. A set of well-known parametric copula families (i.e. Frank, Gaussian, Student t, Clayton, Gumbel, and Joe) are used to develop, falsify and select pairwise bivariate copulas. The formulations of these copulas are provided in detail in other sources[30]. These copulas are parameterized using the Maximum log-Likelihood Method and considering the Bayesian information criteria as the Goodness of Fit[66]. The pool of developed structures at each ecozone are then compared and evaluated based on their capability in representing the marginal FT characteristics and preserving empirical dependencies between a given FT characteristic and $\bar{T}$ or *SD*. Dependencies are quantified using the Kendall's tau non-parametric dependence measure and the associated hypothetical test[67]. The best C-vine copula structure is then used for conditioning the control of compounding changes in temperature and snow depth on FT characteristics. The one-way ANalysis Of VAriance (ANOVA) with Bonferroni correction is used to formally examine any change in the estimated dependencies across different spatial regions[68].

References

1. Frauenfeld, O. W., Zhang, T. & Barry, R. G. Interdecadal changes in seasonal freeze and thaw depths in Russia. *J. Geophys. Res.* **109**, D05101 (2004).
2. Mccauley, C. A., White, D. M., Lilly, M. R. & Nyman, D. M. A comparison of hydraulic conductivities , permeabilities and infiltration rates in frozen and unfrozen soils. *Cold Reg. Sci. Technol.* **34**, 117–125 (2002).
3. Jones, B. M. *et al.* Modern thermokarst lake dynamics in the continuous permafrost zone, northern Seward Peninsula, Alaska. *J. Geophys. Res. Biogeosciences* **116**, 1–13 (2011).
4. Jansson, J. K. & Taş, N. The microbial ecology of permafrost. *Nat. Rev. Microbiol.* **12**, 414–425 (2014).
5. Margesin, R., Neuner, G. & Storey, K. B. Cold-loving microbes , plants , and animals — fundamental and applied aspects. *Naturwissenschaften* **94**, 77–99 (2007).
6. Hjort, J. *et al.* Degrading permafrost puts Arctic infrastructure at risk by mid-century. *Nat. Commun.* **1**, 1–9 (2018).
7. Plaza, C. *et al.* Direct observation of permafrost degradation and rapid soil carbon loss in tundra. *Nat. Geosci.* **12**, 627–631 (2019).
8. Henry, H. A. L. Climate change and soil freezing dynamics : historical trends and projected changes. *Clim. Change* **87**, 421–434 (2008).
9. Wu, Q. & Zhang, T. Changes in active layer thickness over the Qinghai - Tibetan Plateau from 1995 to 2007. *J. Geophys. Res. Atmos.* **115**, 1–12 (2010).
10. Schuur, E. A. G. *et al.* The effect of permafrost thaw on old carbon release and net carbon exchange from tundra. *Nature* **459**, 556–559 (2009).
11. Iwata, Y., Hayashi, M., Suzuki, S. & Hirota, T. Effects of snow cover on soil freezing , water movement , and snowmelt infiltration : A paired plot experiment. *Water Resour. Res.* **46**, 1–11 (2010).
12. Zhang, T. Influence of the seasonal snow cover on the ground thermal regime: An overview. *Rev. Geophys.* **43**, (2005).
13. Liu, J., Wang, S., Yu, S., Yang, D. & Zhang, L. Climate warming and growth of high-elevation inland lakes on the Tibetan Plateau. *Glob. Planet. Change* **67**, 209–217 (2009).
14. Williams, C. M., Henry, H. A. L. & Sinclair, B. J. Cold truths: How winter drives responses of terrestrial organisms to climate change. *Biol. Rev.* **90**, 214–235 (2015).
15. Park, H., Kim, Y. & Kimball, J. S. Widespread permafrost vulnerability and soil active layer increases over the high northern latitudes inferred from satellite remote sensing and process model assessments. *Remote Sens. Environ.* **175**, 349–358 (2016).
16. Meshesha, T. W., Wang, J. & Melaku, N. D. Modelling spatiotemporal patterns of water quality and its impacts on aquatic ecosystem in the cold climate region of Alberta , Canada. *J. Hydrol.* **587**, 124952 (2020).
17. Melvin, A. M. *et al.* Climate change damages to Alaska public infrastructure and the economics of proactive adaptation. *Proc. Natl. Acad. Sci.* **114**, E122–E131 (2017).
18. Wagner-Riddle, C. *et al.* Globally important nitrous oxide emissions from croplands induced by freeze-thaw cycles. *Nat. Geosci.* **10**, 279–283 (2017).
19. Schaefer, K., Lantuit, H., Romanovsky, V. E., Schuur, E. A. G. & Witt, R. The impact of the permafrost carbon feedback on global climate. *Environ. Res. Lett.* **9**, (2014).
20. Andrews, T. D. *et al.* Permafrost thaw and Aboriginal cultural landscapes in the Gwich'in Region,Canada. *APT Bull. J. Preserv. Technol.* **47**, 15–22 (2016).
21. *Atlas of Canada*. (Natural Resources Canada, 2016).

22. Hatami, S. & Nazemi, A. Temperature Controls of the Freeze and Thaw Patterns in Quebec. in *Canadian Society for Civil Engineering* 1–7 (2019).
23. Hatami, S. & Nazemi, A. The Compound Impacts of Changing Temperature and Snow Cover on Freeze and Thaw Patterns across Québec. in *Geo-Extreme* (ASCE, 2021).
24. Amir Jabbari, A. & Nazemi, A. Alterations in Canadian Hydropower Production Potential Due to Continuation of Historical Trends in Climate Variables. *Resources* **8**, 163 (2019).
25. Fang, X., Luo, S. & Lyu, S. Observed soil temperature trends associated with climate change in the Tibetan Plateau , 1960 – 2014. *Theor. Appl. Climatol.* **135**, 169–181 (2019).
26. Walvoord, M. A. & Kurylyk, B. L. Hydrologic Impacts of Thawing Permafrost — A Review. *Vadose Zo. J.* **15**, (2016).
27. Zhang, K. *et al.* Sensitivity of pan-Arctic terrestrial net primary productivity simulations to daily surface meteorology from NCEP-NCAR and ERA-40 reanalyses. *J. Geophys. Res.* **112**, 1–14 (2007).
28. Tucker, C. J. *et al.* An extended AVHRR 8-km NDVI dataset compatible with MODIS and SPOT vegetation NDVI data. *Int. J. Remote Sens.* **26**, 4485–4498 (2005).
29. Favre, A., Adlouni, S. El, Perreault, L., Thie, N. & Bobe, B. Multivariate hydrological frequency analysis using copulas. *Water Resour. Res.* **40**, 1–12 (2004).
30. Nelsen, R. B. *An Introduction to Copulas*. (Springer, New York, NY, 2006).
31. Kim, Y., Kimball, J. S., McDonald, K. C. & Glassy, J. Developing a Global Data Record of Daily Landscape Freeze/Thaw Status Using Satellite Passive Microwave Remote Sensing. *Geosci. Remote Sensing, IEEE Trans.* **49**, 949–960 (2011).
32. Sheffield, J., Goteti, G. & Wood, E. F. Development of a 50-year high-resolution global dataset of meteorological forcings for land surface modeling. *J. Clim.* **19**, 3088–3111 (2006).
33. Brown, R. D. & Brasnet, B. *Canadian Meteorological Centre (CMC) Daily Snow Depth Analysis Data, Version 1*. *Boulder, Colorado USA. NASA National Snow and Ice Data Center Distributed Active Archive Center* (2010). doi:https://doi.org/10.5067/W9FOYWH0EQZ3
34. Schultz, J. *The ecozones of the world*. (Springer Berlin Heidelberg, 2005).
35. Wiken, E. B. *Terrestrial Ecozones Of Canada*. (1986).
36. Sorensen, P. O. *et al.* Winter soil freeze-thaw cycles lead to reductions in soil microbial biomass and activity not compensated for by soil warming. *Soil Biol. Biochem.* **116**, 39–47 (2018).
37. Zhang, P., Wittmann, F. H., Vogel, M., Müller, H. S. & Zhao, T. Influence of freeze-thaw cycles on capillary absorption and chloride penetration into concrete. *Cem. Concr. Res.* **100**, 60–67 (2017).
38. Sharma, S., Szele, Z., Schilling, R., Munch, J. C. & Schloter, M. Influence of freeze-thaw stress on the structure and function of microbial communities and denitrifying populations in soil. *Appl. Environ. Microbiol.* **72**, 2148–2154 (2006).
39. Poppel, B., Fægteborg, M., Siegstad, O. & Snyder, H. T. The Arctic as a 'hotspot' for natural extraction and global warming. *Econ. North* 129–135 (2015).
40. Schuur, E. *et al.* Climate change and the permafrost carbon feedback. *Nature* **520**, 171–179 (2015).
41. Kimiaghalam, N., Goharrokhi, M., Clark, S. P. & Ahmari, H. A comprehensive fluvial geomorphology study of riverbank erosion on the Red River in Winnipeg , Manitoba , Canada. *J. Hydrol.* **529**, 1488–1498 (2015).

42. Nazemi, A., Wheater, H. S., Chun, K. P. & Elshorbagy, A. A stochastic reconstruction framework for analysis of water resource system vulnerability to climate-induced changes in river flow regime. *Water Resour. Res.* **49**, 291–305 (2013).
43. Liu, Z. *et al.* A Framework for Exploring Joint Effects of Conditional Factors on Compound Floods. *Water Resour. Res.* **54**, 2681–2696 (2018).
44. Carpino, O. A., Berg, A. A., Quinton, W. L. & Adams, J. R. Climate change and permafrost thaw-induced boreal forest loss in northwestern Canada. *Environ. Res. Lett.* **13**, 084018 (2018).
45. Lewkowicz, A. G. & Way, R. G. Extremes of summer climate trigger thousands environment. *Nat. Commun.* **10**, 1–11 (2019).
46. Roseen, R. M., Ballestero, T. P., Houle, J. J., Briggs, J. F. & Houle, K. M. Water Quality and Hydrologic Performance of a Porous Asphalt Pavement as a Storm-Water Treatment Strategy in a Cold Climate. *J. Environ. Eng.* **138**, 81–89 (2012).
47. Doughty, M., Eyles, N. & Eyles, C. High-resolution seismic reflection profiling of neotectonic faults in Lake Timiskaming, Timiskaming Graben, Ontario-Quebec, Canada. *Sedimentology* **60**, 983–1006 (2013).
48. Mazdiyasni, O. & AghaKouchak, A. Substantial increase in concurrent droughts and heatwaves in the United States. *Proc. Natl. Acad. Sci. U. S. A.* **112**, 11484–11489 (2015).
49. Chiang, F., Mazdiyasni, O. & AghaKouchak, A. Amplified warming of droughts in southern United States in observations and model simulations. *Sci. Adv.* **4**, 1–7 (2018).
50. Hatami, S., Nazemi, A. & Amirjabbari, A. Evolving Trends of Rain over Precipitation in Canadian Cold Season During the late 20th Century. in *Canadian Society for Civil Engineering* 1–5 (2019).
51. Zangenehmadar, Z., Moselhi, O. & Golnaraghi, S. Optimized planning of repair works for pipelines in water distribution networks using genetic algorithm. *Eng. Reports* **2**, 1–11 (2020).
52. Özgan, E. & Serin, S. Cold Regions Science and Technology Investigation of certain engineering characteristics of asphalt concrete exposed to freeze – thaw cycles. *Cold Reg. Sci. Technol.* **85**, 131–136 (2013).
53. Farran, M. & Zayed, T. Comparative Analysis of Life-Cycle Costing for Rehabilitating Infrastructure Systems. *J. Perform. Constr. Facil.* **23**, 320–326 (2009).
54. Kim, Y., Kimball, J. S., Glassy, J. & Du, J. An extended global Earth system data record on daily landscape freeze – thaw status determined from satellite passive microwave remote sensing. *Earth Syst. Sci. Data* **9**, 133–147 (2017).
55. Cover, T. M. & Hart, P. E. Nearest Neighbor Pattern Classification. *IEEE Trans. Inf. theory* **13**, 21–27 (1967).
56. Fekete, B. M., Vrsmarty, C. J. & Lammers, R. B. Scaling gridded river networks for macroscale hydrology : Development , analysis , and control of error. *Water Resour. Res.* **37**, 1955–1967 (2001).
57. Sklar, M. *Fonctions de repartition an dimensions et leurs marges*. (Publ. inst. statist. univ. Paris, 1959).
58. Bedford, B. Y. T. I. M. & Cooke, R. M. Vines : A New Graphical Model for Dependent Random Variables Author (s): Tim Bedford and Roger M . Cooke Source : The Annals of Statistics , Vol . 30 , No . 4 (Aug ., 2002), pp . 1031-1068 Published by : Institute of Mathematical Statistics Stable URL. *Ann. Stat.* **30**, 1031–1068 (2002).
59. Aas, K., Czado, C., Frigessi, A. & Bakken, H. Pair-copula constructions of multiple

dependence. *Insur. Math. Econ.* **44**, 182–198 (2009).
60. Joe, H. *Multivariate models and multivariate dependence concepts*. (CRC Press, 1997).
61. Roy, T. & Gupta, H. How certain are our uncertainty bounds? Accounting for sample variability in Monte Carlo-based uncertainty estimates. *Environ. Model. Softw.* **136**, 104931 (2021).
62. Schepsmeier, U. *et al.* Package 'VineCopula'. *R Packag. version* **2**, (2015).
63. Brechmann, E. C. & Schepsmeier, U. CDVine: Modeling Dependence with C- and D-Vine Copulas in R Eike. *J. Stat. Softw.* **52**, (2013).
64. Yan, J. Enjoy the joy of copulas: With a package copula. *J. Stat. Softw.* **21**, 1–21 (2007).
65. Dißmann, J., Brechmann, E. C., Czado, C. & Kurowicka, D. Selecting and estimating regular vine copulae and application to financial returns. *Comput. Stat. Data Anal.* **59**, 52–69 (2013).
66. Sadegh, M., Ragno, E. & Aghakouchak, A. Multivariate Copula Analysis Toolbox (MvCAT): Describing dependence and underlying uncertainty using a Bayesian framework. *Water Resour. Res.* 5166–5183 (2017). doi:10.1002/2016WR020242.Received
67. Kendall, A. M. G. A New Measure of Rank Correlation. *Oxford Univ. Press behalf Biometrika Trust* **30**, 81–93 (1938).
68. Nazemi, A., Zaerpour, M. & Hassanzadeh, E. Uncertainty in Bottom-Up Vulnerability Assessments of Water Supply Systems due to Regional Streamflow Generation under Changing Conditions. *J. Water Resour. Plan. Manag.* **146**, 1–14 (2020).

Acknowledgments

The financial support of this study is provided by multiple sources including Fond de Recherche Nature et technologies through Établissement de la relève professorale award, Canada Natural Science and Engineering Research Council through Discovery Grant Program, New Frontiers in Exploration as well as Concordia University. To Warren, Nick, Yasha and brotherhood of men.

Authors' contribution

S.H. and A.N. conceived the study. S.H. led the technical work, data analysis and preparation of all figures. S.H. and A.N. wrote, reviewed and revised the paper and contributed to the discussions. A.N. supervised the work and led funding acquisition.

Competing interests

Authors declare no competing interests

Data availability

All data used in this study along with additional data related to elevation, land-use and land-cover, as well as existing in-situ climatic and hydrometric networks are available through the Cold Region Data Accessibility Portal for Québec (CRDAP – QC; http://wscc.encs.concordia.ca/home.html).

Appendix D.

Hatami, S., Nazemi, A., 2021. The Compound Impacts of Changing Temperature and Snow Cover on Freeze and Thaw Patterns across Québec. Geo-Extreme 2021, Savannah, Georgia. (Accepted).

The Compound Impacts of Changing Temperature and Snow Cover on Freeze and Thaw Patterns across Québec

Shadi Hatami[1], and Ali Nazemi[2*]

[1]Ph.D. Candidate, Dept. of Building, Civil and Environmental Engineering, Concordia University, Montreal, QC, Canada H3G 1M8; email: s_hatam@encs.concordia.ca
[2]Associate Professor, Dept. of Building, Civil and Environmental Engineering, Concordia University, Montreal, QC, Canada H3G 1M8; (corresponding author); email: ali.nazemi@concordia.ca; ORCID: https://orcid.org/0000-0002-8393-5519

ABSTRACT

Seasonal Freeze-Thaw cycles (*FT*) is a key to environmental processes and socioeconomic activities across northern latitudes. The large-scale dynamics of *FT* are mainly governed by near surface air temperature and snow depth. We argue that this physical control can be empirically characterized, represented, and simulated by the trivariate dependence structure between *FT*, temperature and snow depth. To showcase this, we consider the large-scale gridded data of these variables over Québec, Canada, and use canonical vine copulas to formulate the trivariate interdependence between *FT*, temperature and snow depth in different grids and ecozones. Our results reveal different dependence structures across Québec ecozones, pointing at the role of landscape in regulating the impacts of snow depth and temperature on *FT*. Having the trivariate dependence, we use a bottom-up impact assessment approach to address the alterations in *FT* characteristics under single and compound changes in the temperature and snow depth conditions.

INTRODUCTION

Cycles of Freeze-Thaw (*FT*) are among the most important cryosphere processes in cold regions and have major roles in controlling regional hydrology (Karlsson et al. 2012), phenology (Williams et al. 2015), soil stability (Teufel and Sushama 2019), permafrost extent (Schuur et al. 2009), as well as land-atmospheric interactions (Schuur et al. 2015). *FT* dynamics, therefore, matter to socio-economic development and ecosystem functioning in northern regions. It is now well understood that among different climatic variables, *FT* dynamics are majorly controlled by near surface air temperature and snow depth (Hatami and Nazemi 2019, Henry 2008). As a result, increasing variability and change in these climatic variables can perturb *FT* dynamics over time and space (Klein Tank and Können 2003). However, the simultaneous changes in temperature and snow depth can create feedback effects; and these feedbacks are not yet fully understood. For example, a warmer temperature deepens the active soil layer and speeds up thawing. If this coincides with a heavy snowfall,

heat in the soil is trapped by the snow cover and intensifies thawing. Modeling such feedback effects are not trivial because they are not fully represented in the current physically-based models and their representations very much depend on the details in the landscape, from which very limited in-situ observations are available. As a result, current generation of process-based models are largely incapable to represent such dynamics individually or in coupled forms and therefore their simulations entail a large uncertainty (Wang et al. 2016).

The purpose of this study is to address the current limitations in modeling *FT* dynamics over the Province of Québec in Canada. To overcome the issue of data availability as well as known deficiencies in in-situ data measurements, we use gridded remotely-sensed satellite *FT* data (Takala et al. 2009). To tackle the limitations in process-based modeling, we shift the purpose of modeling from dynamic modeling of *FT* states to modeling *FT* characteristics over a fixed temporal and spatial scale. Accordingly, we propose an empirical approach using a copula-based methodology to simulate the characteristics of gridded *FT* based on corresponding gridded temperature and snow depth through conditional probability modeling (Nazemi and Elshorbagy 2012). This empirical model is then used to model the changes in *FT* characteristics conditioned to various climatic scenarios. To showcase the suitability of the proposed framework, we only focus on annual number of thawed days (*TD*) across different grids and ecozones in Québec. We specifically tackle the following three questions: (1) How can copulas capture the interdependencies between *FT* characteristics and climatic variables? (2) To what extent can changes in temperature and/or snow depth affect *TD* across Québec? and (3) How much does this control changes in space?

DATA AND CASE STUDY

The proposed study is conducted across the Province of Québec, the second largest province in Canada with a large ecosystem diversity. The province is divided into eight distinct ecological units namely, Northern Arctic (EZ1), Southern Arctic (EZ2), Arctic Cordillera (EZ3), Taiga Shield (EZ4), Hudson Plains (EZ5), Boreal Shield (EZ6), Atlantic Maritime (EZ7) and Mixed Wood Plains (EZ8) sorted from north to the south shown in Figure 1– see Wiken (1986).

We use remotely-sensed gridded daily data of the FT Earth System Data Record (FT-ESDR). This dataset includes the state of soil among four distinct classes of frozen (AM and PM frozen), thawed (AM and PM thawed), transitional and inverse transitional (AM thawed and PM frozen or vice versa) at spatial resolution of 25×25 km (Kim et al. 2017). The data is publically available and can be obtained from the National Snow and Ice Data Center archive (https://doi.org/10.5067/MEASURES/CRYOSPHERE/nsidc-0477.004). Using the composite daily state of Freeze-Thaw, we extract annual number of *TD* (September-August). We match this data with 0.25º ×0.25º gridded daily maximum and minimum temperature from Global Meteorological Forcing Dataset (GMFD; http://hydrology.princeton.edu/data.php; Sheffield et al. 2006), provided by Princeton

University, from which mean daily temperature is calculated. Monthly snow depth is also obtained from the Canadian Meteorological Center (CMC; https://doi.org/10.5067/W9FOYWH0EQZ3) with spatial resolution of 24×24 km (Brown 2010). The common period of data among the three data set is 1998-2016. The climatic data are regridded to match the grid scale of the *FT* data. The *k*-nearest neighbor interpolation methodology is used for this purpose (Fekete et al. 2001).

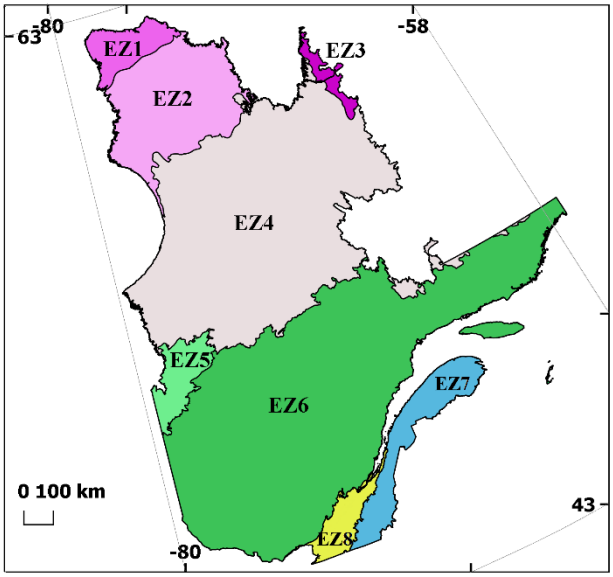

Figure 1. The terrestrial ecozones of Québec and their corresponding color-code.

METHODOLOGY

We first analyze the statistical interdependencies between pairs of climatic variables and *TD* using Kendall's tau dependence test. The significance of dependence is evaluated by a formal *p*-value; and *p*-values less than 0.05 is considered as statistically significant. The study is only conducted where the dependencies between *TD* and at least one of the climatic variables are found to be significant. This condition is hold in 90% of grids across Québec. Moreover, due to the sensitivity of copula methodologies to existence of autocorrelation in the input data, the data sets of *TD*, temperature and snow depth are tested against existence of autocorrelation. Based on our results, the autocorrelation is only found to be present in less than 17% of grids looking at annual temperature. We do not include these grids in our analyses.

Using copulas, the interdependencies between two or more of continuous random variables can be modeled (Nazemi et al. 2013, 2020). Here, the application of C-vine copula is proposed to model the joint dependencies between *TD*, temperature ($\bar{T}$) and snow depth (*SD*). If X, Y and Z are three random variables with marginal probability distributions of $F_1(X)$, $F_2(Y)$ and $F_3(Z)$, the joint dependencies $H(X,Y,Z)$ can be described as (Sklar 1959):

$$H(X,Y,Z) = C\{F_1(X), F_2(Y), F_3(Z)\} \quad (1)$$

where C is the trivariate copula function. Here we use C-vine copula to model this trivariate dependence. In simple words, a *d*-dimensional C-vine structure decomposes the multivariate density into *d*(*d*-1)/2 pairs of bivariate copulas, which are arranged into *d*-1 trees (Xiong et al. 2014). In our setting the multivariate density of *TD*, temperature and snow depth can be formulated as follows, where the pairwise dependence between variables are captured by bivariate copulas:

$$H(TD,\bar{T},SD) = F_1(TD).F_2(\bar{T}).F_3(SD).C_{21}.C_{23}.C_{13|2} \quad (2)$$

$C_{21}\{F_2(\bar{T}), F_1(TD)\}$ and $C_{23}\{F_2(\bar{T}), F_3(SD)\}$ are simply written as C_{21} and C_{23}. The conditional pair-copula between $F_1(TD)$ and $F_3(SD)$ conditional to $F_2(\bar{T})$ i.e. $C_{13|2}\{F_1(TD), F_3(SD)|F_2(\bar{T})\}$ is also shown by $C_{13|2}$. Constructing, parametrizing and simulating with the C-vine copula is conducted using CRAN with the packages of *VineCopula*, *CDVine* and *copula* developed in *R* programming language (Brechmann and Schepsmeier 2013, Schepsmeier et al. 2015, Yan 2007). Different bivariate copula families are tested to select the one with the best performance in capturing the mean, standard deviation and skewness of observed *TD* as well as preserving the joint interdependencies between *TD* and studied climatic variables. Among several options, Frank copula is found as the best copula family for modeling theses joint interdependencies across the Province of Québec.

By having the C-vine model, the corresponding probability distribution of *TD* to any temperature and/or snow depth can be obtained through conditional probability modeling. Accordingly, we design a bottom-up impact assessment scheme, in which the probability of *TD* can be stochastically generated through the conditional resampling from the copula space using different climatic scenarios. Different scenarios of changing climate are considered where the shifts in temperature can be either -2°C, 0°C, or +2°C and changes in snow depth can be either -10cm, 0cm, or +10cm of the long-term mean values. These climatic scenarios are summarized in Table 1. Accordingly the change in the probability distribution of annual *TD* can characterize the extent to which *TD* responds to changing climate. To account for sampling uncertainty, we repeat the conditional resampling 1000 times.

Table 1. Climatic Scenarios considered in this study.

Name	*Description*
Scenario-A	Long-term average of observed temperature and snow depth
Scenario-B	2°C warmer temperature
Scenario-C	10cm less snow depth
Scenario-D	2°C warmer temperature and 10cm less snow depth
Scenario-E	2°C cooler temperature
Scenario-F	10cm more snow depth
Scenario-G	2°C cooler temperature and 10cm more snow depth

RESULTS AND DISCUSSION

Modeling performance: For the sake of brevity, here we only present the validation of trivariate copula models at the ecozone-scale. To evaluate the performance of C-vine copula models, first the probability distribution of *TD* at each ecozone is obtained by resampling from the copula space, conditioned to the observed climate data. Accordingly the first three moments of the observed and simulated distributions of historical *TD* (i.e. mean, standard deviation and skewness) are compared at every ecozone. In addition, we also look at the capability of developed copula models in preserving the interdependencies between *TD* and the considered climatic variables at each ecozone. Figure 2 summarizes our finding and compares the observed (x-axis) versus simulated (y-axis) values of the above five criteria across different ecozones of Québec (color-code). This figure validates the accurate performance of copula methodology in reproducing the key probabilistic characteristics of historical *TD* across Québec's ecozone (panels a, b and c). It also highlights the desirable performance of proposed methodology in capturing the dependencies between *TD* and temperature (figure (d)) as well as *TD* and snow depth (figure (e)). We perform the same analysis at the grid-scale, verifying the good performance of C-vine copula models to describe this trivariate dependence at the smaller grid-scale too.

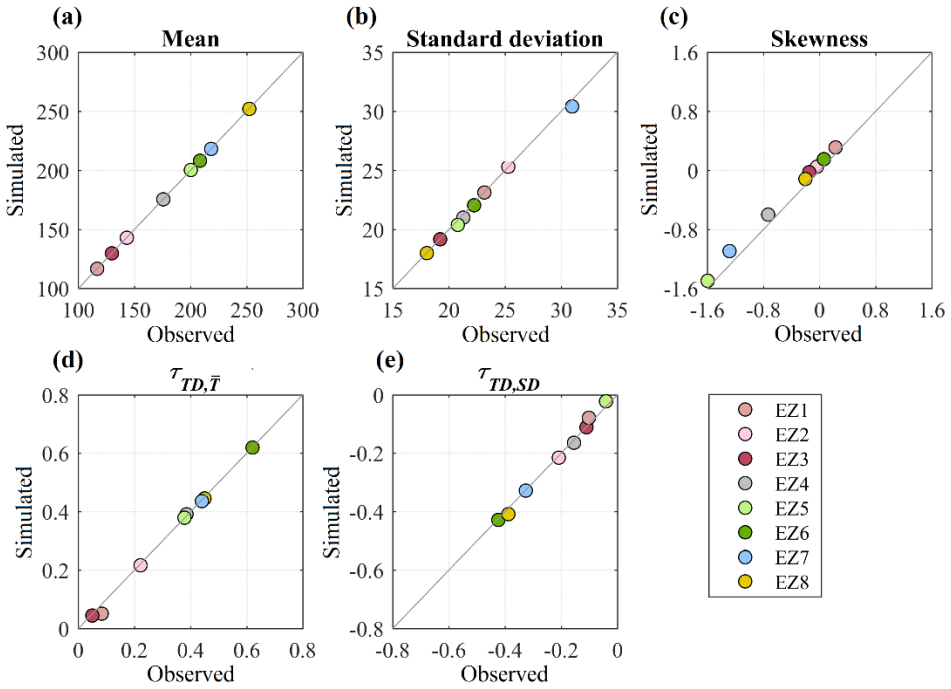

Figure 2. The observed (x-axis) versus simulated (y-axis) *TD* characteristics across Québec's ecozones. Observed and simulated values are compared based on the mean, standard deviation and skewness of *TD* in figures (a) to (c), respectively along with the dependencies between *TD* and temperature ($\bar{T}$) and *TD* and snow depth (*SD*) in figures (d) and (e), respectively. Ecozones are shown by different colors matching the color coding provided in Figure 1.

Climate control on annual *TD* at grid-scale: By having a validated C-vine copula, the model can be used to condition *TD* to changes in climate variables. Figure 3 shows changes in historical *TD* under Scenarios B to G (panels a to f, respectively) at the grid-scale. The spectrums of red and blue colors display the positive and negative changes in historical *TD* under six considered climatic scenarios. Black dots indicate the grids where autocorrelation is significant in annual temperature series and are not included in our study. Our simulations suggest that climatic condition corresponding to Scenario-B causes an average increase of 10 days extension in the thawed period over the Province of Québec. Larger changes in *TD* due to this climatic scenario are mainly observed in southern ecozones, specifically at EZ6 with a 14-day increase. For Scenario-C, the average increase in *TD* is approximately 4 days across the province, which is around half of the increase, corresponding to Scenario-B. In addition, simulated changes in *TD* under Scenario-C are the highest at EZ8, EZ7 and EZ2, experiencing 11, 7 and 6 days extension in *TD*. Decreases in *TD* are also observed at grids across southern parts of EZ4, EZ5 and northern parts of EZ6. The compound impact of 2°C warmer temperature and 10cm less snow depth (Scenario-D) leads to average increase of 15 days across Québec, where the control of this climatic condition is found to be the highest at southern ecozones. Changes in annual *TD* under Scenario-D range from 0 (EZ1) to 21 (EZ8) more days with thawed state. Looking at a cool climatic condition associated with Scenario-E, the annual *TD* shortens roughly 9 days across Québec. Higher sensitivities are observed in southern ecozones of the province, where the magnitude of change reaches over 13 days in EZ8. Scenario-F leads on average to 4 days shorter annual *TD* over the province. However, looking at this climatic condition, the highest changes in *TD* are observed across EZ2 and EZ8 with 8 and 7 days shortened *TD* period. Finally, under Scenario-G (i.e. compound impact of 2°C cooler temperature and 10cm more snow depth), the average of *TD* decreases roughly 15 days over Québec. An increasing effect in the control of this climatic condition on *TD* is observed by moving from northern to southern ecozones with 23, 15 and 13 days shortened *TD* periods in EZ8, EZ7 and EZ6, respectively. Spatially heterogeneous changes in *TD* highlight the role of land surface characteristics such as land cover and vegetation type on climate control on *FT* dynamics.

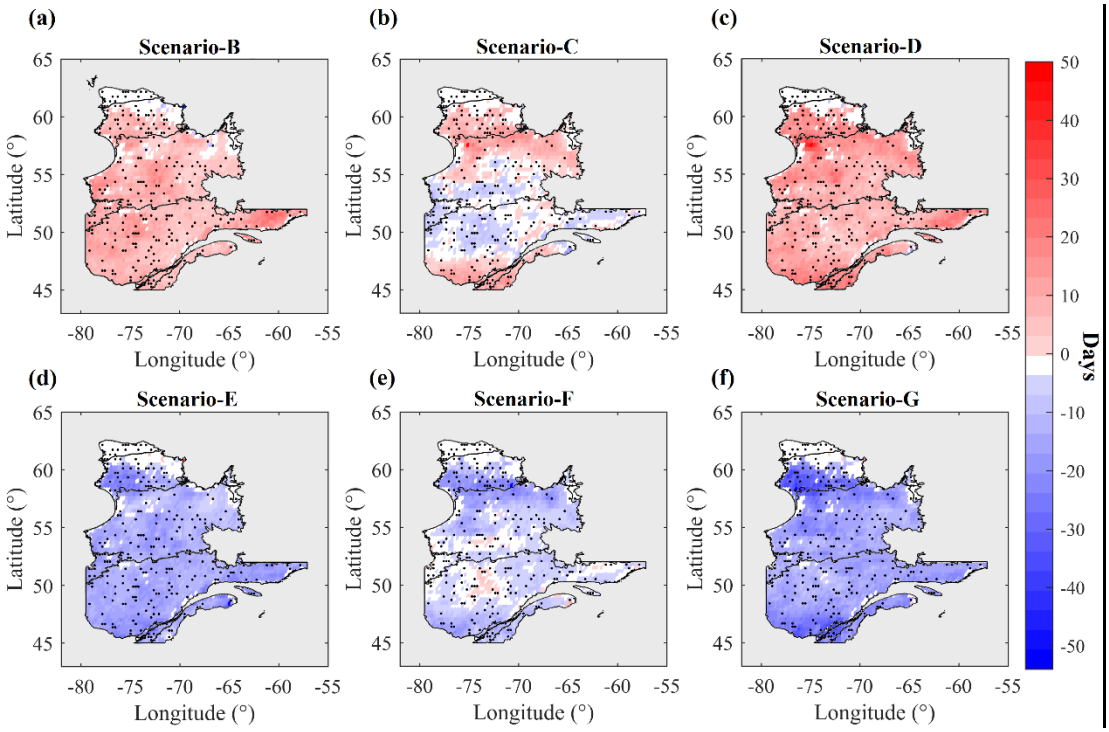

Figure 3. Changes in annual *TD* under Scenario-B (a), Scenario-C (b), Scenario-D (c), Scenario-E (d), Scenario-F (e) Scenario-G (f). Red (blue) color shows extension (shortening) in *TD* period compared to the historical condition.

Spatial variability in climatic control on *TD*. As the last step of this study, the control of the two considered extreme compound climatic scenarios, i.e. Scenario-D and Scenario-G, on annual *TD* is investigated at the ecozone-scale. Figure 4 shows the changes in annual *TD* at each ecozone under (1) a warmer condition with less snow depth on the ground as well as (2) a colder condition with more snow depth on the ground. Boxplots show the range of possible *TD* at each ecozone under considered climatic scenarios, obtained from simulated probability distributions of *TD* in each ecozone. Scenario-A, Scenario-D and Scenario-G are identified with black, red and blue colors, respectively. The dot in each boxplot signifies the mean values at each ecozone. Figure 4 provides an opportunity to compare the possible changes in annual *TD* at each ecozone due to the same magnitude of positive and negative changes in temperature and snow depth. Comparing the shifts in minimum, maximum and the range of the boxplots, we can further analyze (i) the changes in intensity of extreme high and low *TD* events under changing climate as well as (ii) the changes in the variability of climate control on *TD* at each ecozone. Comparing the changes in annual *TD* under Scenario-D and Scenario-G shows the higher impacts of the cooling in northern ecozones of Québec. This is different in southern ecozones where the magnitude of shift under warmer climatic scenario is mostly higher. Moreover, moving from the northern ecozones to southern ones, the compound impact of a 2°C warmer temperature and 10cm less snow depth (Scenario-D) on extreme high *TD* events increases. The extreme high events of *TD* observed across EZ6, EZ7 and EZ8

experience 34, 20 and 15 days extensions, respectively under this climatic scenario. The impacts of Scenario-G on extreme high events of annual *TD*, however, does not follow any regional pattern where the highest sensitivities are observed in EZ2 and EZ4 with 18 and 32 days shortened *TD*. Considering the extreme low events of *TD* among northern ecozones, Scenario-D is found to be more impactful (e.g. 26 and 35 days extended *TD* over EZ2 and EZ4, respectively). In contrast, the sensitivity of the extreme low events of *TD* is found to be much higher to Scenario-G across southern ecozones, where from 25 to 70 days decrements in *TD* are observed across four southern ecozones of Québec. Finally, looking at the range of the boxplots, thicker boxes of simulated *TD* corresponding to Scenario-G over EZ4, EZ5 and EZ7 highlight the higher variability in the control of this climatic scenario on the annual *TD*. The variations in climate control on *TD* extremes verifies the impacts of different land-surface characteristics on *FT* dynamics.

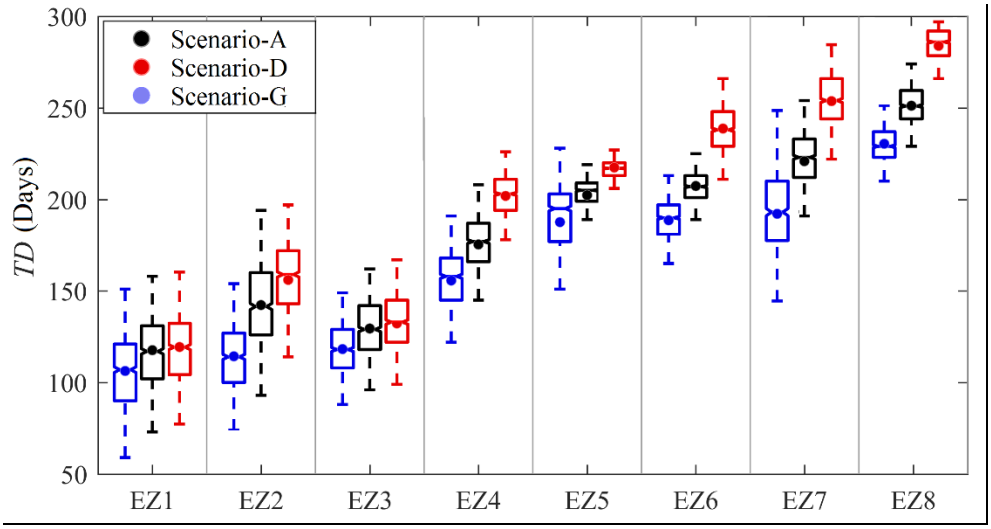

Figure 4. The compound impact of 2 °C warming (cooling) and 10cm less (more) snow depth on annual *TD* displayed in red (blue) over different ecozones of Québec. In each boxplot, the dot signifies the expected values for *TD* at ecozone-scale. The boxplots with black color show the simulated *TD* in each ecozone under historical conditions.

SUMMARY AND CONCLUSION

In the presence of climate change, quantifying the control of climatic characteristics on *FT* dynamics is an important consideration for future socio-economic development and ecosystem functioning across northern regions. However, existing process-based models are not able to fully represent the dynamics of *FT*. In this study, a copula-based methodology is employed to investigate the control of the most important climatic drivers, namely temperature and snow depth, on the annual characteristics of *TD*. Based on our results, C-vine copula methodology is found to have a desirable accuracy in

modeling the trivariate dependencies between *TD*, temperature and snow depth. Accordingly, by defining six climatic scenarios, we show that *TD*, whether considered at the grid-scale or at the ecozone-scale, is more sensitive to change in climatic condition in southern regions in almost all considered scenarios. It is also shown that the impacts of warming temperature and thinner snowpack on annual *TD* are higher in southern eozones of Québec comparing to the same magnitude of cooling temperature and thicker snow depth. In contrast, the *TD* characteristics is found to be more sensitive to cooling temperature and more snow depth, comparing to a warmer temperature and thinner snowpack in northern ecozones.

Identifying the changes in *FT* characteristic due to changing climate is important for understanding the future of active soil in cold regions. This understanding is essential for quantifying the changes in greenhouse gas emissions across northern latitudes as a results of thawed permafrost and hence of a great importance for developing and evaluating climate change mitigation policies (Burke et al. 2017). Furthermore as we shown, a warmer climate is associated with higher number of *TD*. This can lead to longer growing season altering agricultural activities (King et al. 2018), but also can create vulnerability in northern infrastructure (Hjort et al. 2018). Given the generality of this framework, the proposed methodology can be applied to any other scales, temporally and spatially and in other regions or globally, as far the data resolution allows. It can also provide a novel framework for improved diagnosis of changes in other environmental processes due to changing climate.

REFERENCES

Brechmann, E., & Schepsmeier, U. (2013). Cdvine: "Modeling dependence with c-and d-vine copulas in r." *Journal of statistical software*, 52(3), 1-27.

Brown, R. D. and B. B. (2010). Canadian Meteorological Centre (CMC) Daily Snow Depth Analysis Data, Version 1. https://doi.org/https://doi.org/10.5067/W9FOYWH0EQZ3

Burke, E. J., Ekici, A., Huang, Y., Chadburn, S. E., Huntingford, C., Ciais, P., ... Krinner, G. (2017). "Quantifying uncertainties of permafrost carbon–climate feedbacks." *Biogeosciences*, 14(12), 3051-3066.

Fekete, B. M., Vrsmarty, C. J., and Lammers, R. B. (2001). "Scaling gridded river networks for macroscale hydrology: Development, analysis, and control of error." *Water Resources Research*, 37(7), 1955–1967.

Hatami, S., and Nazemi, A. (2019). "Temperature Controls of the Freeze and Thaw Patterns in Québec." In *Canadian Society for Civil Engineering* (pp. 1–7). Laval. http://www.csceproceedings.ca/conferences/CSCE2019/papers/PaperPDFversion_7_0513041747.pdf (retrieved on 2020-10-28)

Henry, H. A. L. (2008). "Climate change and soil freezing dynamics : historical trends and projected changes." *Climatic Change*, 87, 421–434. https://doi.org/10.1007/s10584-007-9322-8

Hjort, J., Karjalainen, O., Aalto, J., Westermann, S., Romanovsky, V. E., Nelson, F.

E., ... Luoto, M. (2018). “Degrading permafrost puts Arctic infrastructure at risk by mid-century.” *Nature communications*, 9(1), 1-9.

Karlsson, J. M., Lyon, S. W., and Destouni, G. (2012). “Thermokarst lake, hydrological flow and water balance indicators of permafrost change in Western Siberia.” *Journal of Hydrology*, 464–465, 459–466. https://doi.org/10.1016/j.jhydrol.2012.07.037

Kim, Y., Kimball, J. S., Glassy, J., and McDonald, K. C. (2017). MEaSUREs Global Record of Daily Landscape Freeze/Thaw Status, Version 4. https://doi.org/https://doi.org/10.5067/MEASURES/CRYOSPHERE/nsidc-0477.004

King, M., Altdorff, D., Li, P., Galagedara, L., Holden, J., and Unc, A. (2018). “Northward shift of the agricultural climate zone under 21st-century global climate change.” *Scientific reports*, 8(1), 7904.

Klein Tank, A. M. G., and Können, G. P. (2003). “Trends in Indices of daily temperature and precipitation extremes in Europe, 1946-99.” *Journal of Climate*, 16(22), 3665–3680. https://doi.org/10.1175/1520-0442(2003)016<3665:TIIODT>2.0.CO;2

Nazemi, A., and Elshorbagy, A. (2012). “Application of copula modelling to the performance assessment of reconstructed watersheds.” *Stochastic environmental research and risk assessment*, 26(2), 189-205.

Nazemi, A., Wheater, H. S., Chun, K. P., and Elshorbagy, A. (2013). “A stochastic reconstruction framework for analysis of water resource system vulnerability to climate-induced changes in river flow regime.” *Water Resources Research*, 49(1), 291–305. https://doi.org/10.1029/2012WR012755

Nazemi, A., Zaerpour, M., and Hassanzadeh, E. (2020). “Uncertainty in Bottom-Up Vulnerability Assessments of Water Supply Systems due to Regional Streamflow Generation under Changing Conditions.” *Journal of Water Resources Planning and Management*, 146(2), 1–14. https://doi.org/10.1061/(ASCE)WR.1943-5452.0001149

Schepsmeier, U., Stoeber, J., Brechmann, E. C., Graeler, B., Nagler, T., Erhardt, T., ... Killiches, M. (2015). “Package ‘VineCopula’.” *R package version*, 2(5).

Schuur, E. A. G., Vogel, J. G., Crummer, K. G., Lee, H., Sickman, J. O., and Osterkamp, T. E. (2009). “The effect of permafrost thaw on old carbon release and net carbon exchange from tundra.” *Nature*, 459(7246), 556–559. https://doi.org/10.1038/nature08031

Schuur, E., McGuire, A., Schädel, C., Grosse, G., Harden, J., Hayes, D., … Natali, S. (2015). “Climate change and the permafrost carbon feedback.” *Nature*, 520(7546), 171–179. https://doi.org/10.1038/nature14338

Sheffield, J., Goteti, G., and Wood, E. F. (2006). “Development of a 50-year high-resolution global dataset of meteorological forcings for land surface modeling.” *Journal of Climate*, 19(13), 3088–3111. https://doi.org/10.1175/JCLI3790.1

Sklar, M. (1959). *Fonctions de repartition an dimensions et leurs marges* (8th ed.). Publ. inst. statist. univ. Paris.

Takala, M., Pulliainen, J., Member, S., Metsämäki, S. J., and Koskinen, J. T. (2009). "Detection of Snowmelt Using Spaceborne Microwave Radiometer Data in Eurasia From 1979 to 2007." *IEEE Transactions on Geoscience and Remote Sensing*, 47(9), 2996–3007.

Teufel, B., and Sushama, L. (2019). "Abrupt changes across the Arctic permafrost region endanger northern development." *Nature Climate Change*, 9(11), 858-862.

Wang, W., Rinke, A., Moore, J. C., Cui, X., Ji, D., Li, Q., ... McGuire, A. D. (2016). "Diagnostic and model dependent uncertainty of simulated Tibetan permafrost area." *The Cryosphere* (Online), 10(1).

Wiken, E. B. (1986). *Terrestrial Ecozones Of Canada*.

Williams, C. M., Henry, H. A. L., and Sinclair, B. J. (2015). "Cold truths: How winter drives responses of terrestrial organisms to climate change." *Biological Reviews*, 90(1), 214–235. https://doi.org/10.1111/brv.12105

Xiong, L., Yu, K., and Gottschalk, L. (2014). "Estimation of the distribution of annual runoff fromclimatic variables using copulas Lihua." *Water Resources Research*, 50(9), 7134–7152. https://doi.org/10.1002/2013WR015159.Received

Yan, J. (2007). "Enjoy the joy of copulas: with a package copula." *Journal of Statistical Software*, 21(4), 1-21.

Appendix E.

Hatami, S., Zandmoghaddam, S., Nazemi, A., 2019. Statistical modeling of monthly snow depth loss in southern Canada. *Journal of Hydrologic Engineering*, 24(3), 04018071.

The published version of this paper is available through:

https://ascelibrary.org/doi/full/10.1061/%28ASCE%29HE.1943-5584.0001763

DOI:

https://doi.org/10.1061/(ASCE)HE.1943-5584.0001763

Supplemental Materials

Table S1. The name, location, elevation, data availability and the data span of calibration and testing phase for each station.

ID	Name	Latitude	Longitude	Altitude	Data availability (years)	Calibration period	Test period
1	Prince Rupert	54.29	-130.44	35.4	44	1963-1997	1998-2006
2	Port Hardy	50.68	-127.37	21.6	67	1947-2000	2001-2013
3	Campbell River	49.95	-125.27	108.8	42	1966-1999	2000-2007
4	Comox	49.72	-124.90	25.6	69	1947-2001	2002-2015
5	Nanaimo Airport	49.05	-123.87	28	53	1955-1996	1997-2007
6	Victoria	48.65	-123.43	19.5	67	1947-2000	2001-2013
7	Vancouver	49.20	-123.18	4.3	70	1947-2002	2003-2016
8	Prince George	53.89	-122.68	691.3	64	1947-1997	1998-2010
9	Abbotsford	49.03	-122.36	59.1	66	1947-1999	2000-2012
10	Kamloops	50.70	-120.44	345.3	64	1952-2002	2003-2015
11	Penticton airport	49.46	-119.60	344.4	67	1947-2000	2001-2013
12	Kelowna	49.96	-119.38	429.5	37	1969-1998	1999-2005
13	Castlegar	49.30	-117.63	495.6	41	1967-1999	2000-2007
14	Calgary	51.11	-114.02	1084.1	75	1941-2000	2001-2015
15	Edmonton	53.32	-113.58	723.3	55	1961-2004	2005-2015
16	Lethbridge	49.63	-112.80	928.7	61	1947-1995	1996-2007
17	Moose Jaw	50.33	-105.57	576.7	45	1954-1989	1990-1998
18	Regina	50.43	-104.67	577.6	62	1947-1996	1997-2008
19	Peace Garden	49.00	-100.05	693.4	33	1969-1994	1995-2001
20	Brandon	49.91	-99.95	409.4	64	1952-2002	2003-2015
21	Winnipeg Richardson	49.92	-97.23	238.7	68	1941-1994	1995-2008
22	Kenora	49.79	-94.37	409.7	69	1947-2001	2002-2015
23	Red Lake	51.07	-93.79	385.9	55	1959-2002	2003-2013
24	Fort Frances	48.65	-93.43	342	31	1977-2001	2002-2007
25	Dryden	49.78	-92.83	371.9	60	1935-1985	1986-1997

Table S1. Continued

ID	Name	Latitude	Longitude	Altitude	Data availability (years)	Calibration period	Test period
26	Dryden A	49.83	-92.74	412.7	35	1971-1998	1999-2005
27	Sioux Lookout	50.12	-91.90	383.1	61	1955-2003	2004-2015
28	Thunder Bay	48.37	-89.33	199	58	1947-1992	1993-2004
29	Sault Ste Marie	46.48	-84.51	192	54	1962-2004	2005-2015
30	Windsor	42.28	-82.96	189.6	69	1947-2001	2002-2015
31	Pelee	41.78	-82.68	174	16	1980-1992	1993-1995
32	Gore Bay	45.88	-82.57	193.5	47	1948-1985	1986-1994
33	Sarnia	42.99	-82.30	180.6	40	1968-1999	2000-2007
34	London	43.03	-81.15	278	56	1947-1991	1992-2002
35	Wiarton	44.75	-81.11	222.2	68	1948-2001	2002-2015
36	Greater Sudbury	46.63	-80.80	348.4	61	1955-2003	2004-2015
37	Hamilton	43.17	-79.93	237.7	54	1962-2004	2005-2015
38	Toronto Lester B. Pearson	43.68	-79.63	173.4	67	1947-2000	2001-2013
39	North Bay	46.36	-79.42	370.3	68	1947-2000	2001-2014
40	Billy Bishop Toronto City Airport	43.63	-79.40	76.5	34	1962-1988	1989-1995
41	Muskoka District Municipality	44.97	-79.30	281.9	59	1947-1993	1994-2005
42	St. Catharines	43.20	-79.17	97.8	30	1972-1995	1996-2001
43	Peterborough	44.23	-78.37	191.4	38	1970-1999	2000-2007
44	Trenton	44.12	-77.53	86.3	69	1947-2001	2002-2015
45	Kingston	44.22	-76.60	92.4	30	1968-1991	1992-1997
46	Ottawa	45.32	-75.67	114	69	1947-2001	2002-2015
47	Montréal-Mirabel	45.67	-74.03	82.6	34	1976-2002	2003-2009
48	Montréal-Pierre Elliott Trudeau	45.47	-73.75	36	69	1947-2001	2002-2015
49	Montreal St. Hubert	45.52	-73.42	27.4	56	1950-1994	1995-2005
50	Sherbrooke	45.43	-71.68	241.4	33	1963-1988	1989-1995
51	Quebec City	46.80	-71.38	74.4	50	1947-1986	1987-1996
52	Bagotville	48.33	-71.00	159.1	66	1950-2002	2003-2015

Table S1. Continued

ID	Name	Latitude	Longitude	Altitude	Data availability (years)	Calibration period	Test period
53	Baie-comeau	49.13	-68.20	21.6	53	1948-1989	1990-2000
54	Fredericton	45.87	-66.53	20.7	57	1952-1997	1998-2008
55	Charlo	47.98	-66.33	40.2	37	1967-1996	1997-2003
56	Sept-Îles	50.22	-66.27	54.9	56	1947-1991	1992-2002
57	Yarmouth	43.83	-66.09	43	61	1955-2003	2004-2015
58	Saint John	45.32	-65.89	108.8	64	1952-2002	2003-2015
59	Greenwood	44.98	-64.92	28	67	1948-2001	2002-2014
60	Moncton	46.11	-64.68	70.7	66	1947-1999	2000-2012
61	Halifax Regional Municipality	44.88	-63.50	145.4	55	1961-2002	2003-2015
62	Dartmouth (Shearwater)	44.63	-63.50	44	56	1952-1996	1997-2007
63	Charlottetown	46.29	-63.13	48.8	69	1947-2001	2002-2015
64	Sydney	46.17	-60.05	61.9	69	1947-2001	2002-2015
65	Stephenville	48.53	-58.55	24.7	69	1947-2001	2002-2015
66	Gander	48.95	-54.58	151.2	69	1947-2001	2002-2015
67	St. Johns	47.62	-52.74	140.5	69	1947-2001	2002-2015

Table S2. The evaluation criteria for G1, G2, L1 and L2 models in calibration (Cal.) and testing phase.

ID	R^2				*NSE*				*BIC*				R^2				*NSE*				*BIC*			
	G1		L1		G1		L1		G1		L1		G2		L2		G2		L2		G2		L2	
	Cal.	Test	Cal.	Test	Cal.	Test	Cal.	Test	Cal.	Test	Cal.	Test	Cal.	Test	Cal.	Test	Cal.	Test	Cal.	Test	Cal.	Test	Cal.	Test
1	0.94	0.91	0.94	0.91	0.94	0.91	0.94	0.91	1020	971	1003	953	0.95	0.92	0.95	0.92	0.95	0.92	0.95	0.92	962	941	942	918
2	0.97	0.91	0.97	0.91	0.97	0.90	0.97	0.91	748	782	728	740	0.97	0.91	0.97	0.91	0.97	0.91	0.97	0.91	716	750	697	727
3	0.81	0.93	0.82	0.90	0.81	0.92	0.82	0.89	1121	812	1093	872	0.87	0.91	0.89	0.88	0.86	0.89	0.89	0.86	1036	873	987	926
4	0.92	0.96	0.92	0.97	0.92	0.96	0.92	0.97	1603	800	1585	658	0.92	0.97	0.93	0.97	0.92	0.96	0.93	0.97	1563	755	1518	656
5	0.88	0.73	0.88	0.73	0.88	0.71	0.88	0.72	1302	1432	1281	1405	0.90	0.74	0.89	0.76	0.90	0.74	0.89	0.76	1238	1392	1228	1344
6	0.89	0.96	0.89	0.96	0.89	0.95	0.89	0.95	1193	767	1175	766	0.91	0.95	0.91	0.95	0.91	0.94	0.91	0.94	1108	874	1092	820
7	0.89	0.89	0.89	0.89	0.89	0.88	0.89	0.88	1410	1062	1389	1041	0.91	0.93	0.91	0.92	0.91	0.92	0.91	0.92	1328	857	1281	888
8	0.75	0.78	0.76	0.78	0.75	0.78	0.76	0.78	1902	1720	1897	1724	0.72	0.70	0.71	0.71	0.71	0.70	0.71	0.71	1940	1819	1952	1820
9	0.86	0.87	0.86	0.87	0.86	0.86	0.86	0.87	1518	1296	1497	1262	0.87	0.90	0.88	0.90	0.87	0.90	0.88	0.90	1476	1178	1445	1154
10	0.74	0.67	0.74	0.67	0.74	0.67	0.74	0.67	1562	1436	1546	1413	0.78	0.71	0.77	0.73	0.77	0.70	0.77	0.72	1505	1379	1524	1356
11	0.87	0.90	0.87	0.91	0.87	0.90	0.87	0.90	1278	999	1262	978	0.88	0.91	0.88	0.89	0.88	0.90	0.88	0.89	1246	983	1226	1045
12	0.82	0.87	0.82	0.87	0.82	0.87	0.82	0.86	919	697	907	699	0.83	0.88	0.82	0.87	0.83	0.88	0.82	0.87	896	663	906	676
13	0.84	0.88	0.84	0.88	0.84	0.88	0.84	0.88	1335	1159	1320	1148	0.83	0.90	0.84	0.91	0.83	0.90	0.84	0.91	1335	1093	1326	1077
14	0.76	0.85	0.76	0.85	0.76	0.84	0.76	0.84	1561	1477	1556	1464	0.78	0.84	0.78	0.84	0.77	0.84	0.78	0.84	1530	1461	1526	1470
15	0.65	0.60	0.64	0.60	0.65	0.59	0.64	0.60	1465	1521	1462	1514	0.56	0.58	0.59	0.58	0.56	0.58	0.58	0.58	1525	1524	1519	1532
16	0.78	0.79	0.79	0.79	0.78	0.79	0.79	0.79	1377	1083	1363	1084	0.79	0.85	0.79	0.84	0.78	0.85	0.79	0.84	1365	953	1353	980
17	0.77	0.72	0.76	0.70	0.77	0.71	0.76	0.69	1027	1087	1019	1088	0.73	0.68	0.74	0.67	0.73	0.67	0.74	0.67	1054	1107	1052	1122
18	0.59	0.60	0.59	0.60	0.59	0.60	0.59	0.60	1593	1513	1587	1508	0.53	0.44	0.54	0.48	0.53	0.40	0.54	0.44	1629	1649	1629	1628
19	0.97	0.98	0.97	0.97	0.97	0.97	0.97	0.97	81	43	70	25	0.96	0.99	0.97	0.97	0.96	0.98	0.97	0.97	93	9	74	29
20	0.59	0.44	0.60	0.45	0.59	0.43	0.60	0.45	1503	1682	1500	1669	0.50	0.38	0.51	0.39	0.49	0.37	0.50	0.37	1566	1704	1559	1699
21	0.56	0.56	0.58	0.55	0.56	0.56	0.58	0.54	1627	1678	1618	1696	0.48	0.42	0.49	0.43	0.48	0.42	0.49	0.43	1671	1759	1666	1753
22	0.50	0.58	0.51	0.59	0.50	0.55	0.51	0.55	2197	2018	2196	2030	0.39	0.57	0.44	0.57	0.39	0.56	0.44	0.56	2262	2000	2247	2019
23	0.55	0.58	0.56	0.62	0.55	0.57	0.56	0.59	1728	1664	1726	1651	0.42	0.61	0.42	0.66	0.39	0.60	0.40	0.65	1808	1629	1809	1588
24	0.49	0.67	0.44	0.70	0.49	0.51	0.44	0.53	515	499	505	476	0.40	0.26	0.39	0.25	0.39	-0.04	0.39	-0.01	522	559	522	555
25	0.48	0.42	0.49	0.38	0.48	0.35	0.49	0.28	998	851	989	861	0.31	0.20	0.31	0.20	0.21	-0.21	0.21	-0.14	1055	943	1050	927
26	0.49	0.75	0.51	0.75	0.49	0.71	0.51	0.70	1132	993	1126	1003	0.45	0.60	0.44	0.60	0.44	0.60	0.43	0.60	1142	1051	1150	1055

Table S2. Continued

ID	R2				NSE				BIC				R2				NSE				BIC			
	G1		L1		G1		L1		G1		L1		G2		L2		G2		L2		G2		L2	
	Cal.	Test	Cal.	Test	Cal.	Test	Cal.	Test	Cal.	Test	Cal.	Test	Cal.	Test	Cal.	Test	Cal.	Test	Cal.	Test	Cal.	Test	Cal.	Test
27	0.52	0.60	0.52	0.61	0.52	0.58	0.52	0.59	2116	1983	2113	1975	0.43	0.60	0.44	0.56	0.41	0.57	0.42	0.53	2181	1975	2178	2017
28	0.64	0.62	0.64	0.61	0.64	0.58	0.64	0.58	1687	1517	1684	1508	0.54	0.45	0.54	0.45	0.53	0.38	0.53	0.38	1753	1623	1753	1623
29	0.76	0.83	0.76	0.83	0.76	0.83	0.76	0.82	1863	1850	1853	1840	0.75	0.82	0.75	0.82	0.74	0.82	0.75	0.82	1883	1849	1871	1855
30	0.92	0.96	0.92	0.96	0.92	0.96	0.92	0.96	1327	1328	1313	1306	0.93	0.97	0.93	0.97	0.93	0.97	0.93	0.97	1282	1228	1266	1194
31	0.90	0.19	0.91	0.50	0.90	-0.65	0.91	0.39	87	136	78	108	0.88	0.75	0.97	0.81	0.87	0.73	0.96	0.78	88	90	63	89
32	0.68	0.74	0.67	0.74	0.68	0.73	0.67	0.74	1648	1657	1644	1641	0.68	0.79	0.68	0.79	0.68	0.79	0.68	0.79	1633	1577	1623	1564
33	0.83	0.80	0.82	0.80	0.83	0.78	0.82	0.79	914	1060	910	1044	0.85	0.78	0.85	0.78	0.85	0.75	0.85	0.76	875	1081	859	1060
34	0.90	0.93	0.89	0.93	0.90	0.92	0.89	0.93	1474	1306	1472	1273	0.90	0.91	0.90	0.92	0.90	0.91	0.90	0.91	1461	1364	1449	1320
35	0.87	0.87	0.87	0.87	0.87	0.87	0.87	0.87	2395	2347	2384	2320	0.88	0.88	0.88	0.87	0.88	0.88	0.88	0.87	2362	2299	2355	2331
36	0.68	0.79	0.68	0.79	0.68	0.77	0.68	0.77	2106	1954	2100	1943	0.69	0.79	0.69	0.77	0.69	0.78	0.68	0.75	2092	1925	2118	1990
37	0.90	0.63	0.89	0.64	0.90	0.62	0.89	0.63	1110	1524	1115	1505	0.90	0.67	0.90	0.68	0.90	0.66	0.90	0.67	1089	1481	1091	1473
38	0.87	0.80	0.87	0.80	0.87	0.78	0.87	0.79	1509	1746	1506	1727	0.88	0.82	0.88	0.82	0.88	0.82	0.88	0.82	1460	1669	1447	1657
39	0.63	0.72	0.64	0.71	0.63	0.70	0.64	0.70	2394	2439	2383	2434	0.62	0.74	0.60	0.74	0.61	0.74	0.60	0.74	2402	2355	2432	2377
40	0.91	0.93	0.90	0.93	0.91	0.93	0.90	0.93	709	648	698	611	0.91	0.92	0.91	0.93	0.91	0.92	0.91	0.92	694	653	675	628
41	0.71	0.82	0.70	0.85	0.71	0.81	0.70	0.84	2086	2031	2088	1954	0.71	0.85	0.71	0.85	0.71	0.85	0.71	0.85	2077	1927	2086	1946
42	0.90	0.98	0.90	0.98	0.90	0.98	0.90	0.98	661	456	643	440	0.91	0.98	0.91	0.98	0.91	0.97	0.91	0.98	649	510	628	452
43	0.70	0.82	0.69	0.83	0.70	0.79	0.69	0.79	1122	1033	1113	1015	0.72	0.72	0.73	0.74	0.72	0.72	0.73	0.74	1096	1087	1093	1070
44	0.90	0.89	0.90	0.89	0.90	0.88	0.90	0.89	1511	1579	1510	1552	0.90	0.90	0.91	0.90	0.90	0.90	0.91	0.90	1498	1496	1484	1485
45	0.90	0.76	0.89	0.76	0.90	0.76	0.89	0.76	774	888	768	862	0.90	0.79	0.90	0.78	0.90	0.78	0.90	0.78	757	856	741	841
46	0.73	0.69	0.72	0.70	0.73	0.67	0.72	0.68	2290	2346	2284	2323	0.73	0.72	0.73	0.72	0.73	0.71	0.73	0.71	2274	2273	2283	2282
47	0.74	0.60	0.73	0.61	0.74	0.59	0.73	0.61	956	1062	952	1051	0.72	0.67	0.73	0.67	0.72	0.67	0.73	0.67	956	1017	958	1020
48	0.78	0.87	0.78	0.87	0.78	0.86	0.78	0.87	2182	1941	2180	1928	0.82	0.87	0.82	0.87	0.82	0.86	0.82	0.87	2092	1928	2076	1907
49	0.76	0.77	0.76	0.77	0.76	0.77	0.76	0.76	1737	1720	1724	1707	0.77	0.75	0.78	0.75	0.77	0.75	0.78	0.75	1706	1730	1689	1721
50	0.71	0.84	0.70	0.83	0.71	0.83	0.70	0.83	1196	1105	1187	1096	0.71	0.86	0.72	0.86	0.71	0.86	0.71	0.86	1181	1062	1184	1064
51	0.65	0.67	0.65	0.68	0.65	0.67	0.65	0.68	1882	1737	1873	1718	0.66	0.63	0.65	0.59	0.65	0.59	0.65	0.56	1872	1794	1873	1814
52	0.67	0.49	0.68	0.48	0.67	0.43	0.68	0.42	2278	2360	2270	2370	0.65	0.52	0.65	0.54	0.64	0.50	0.65	0.53	2297	2296	2296	2278
53	0.67	0.68	0.67	0.71	0.67	0.67	0.67	0.70	1413	1355	1397	1322	0.62	0.64	0.63	0.67	0.61	0.59	0.63	0.66	1438	1391	1436	1361

Table S2. Continued

ID	R2				NSE				BIC				R2				NSE				BIC			
	G1		L1		G1		L1		G1		L1		G2		L2		G2		L2		G2		L2	
	Cal.	Test	Cal.	Test	Cal.	Test	Cal.	Test	Cal.	Test	Cal.	Test	Cal.	Test	Cal.	Test	Cal.	Test	Cal.	Test	Cal.	Test	Cal.	Test
54	0.76	0.86	0.76	0.86	0.76	0.82	0.76	0.83	1862	1689	1853	1654	0.76	0.80	0.76	0.81	0.76	0.79	0.76	0.81	1851	1715	1854	1703
55	0.70	0.67	0.69	0.66	0.70	0.63	0.69	0.63	1435	1496	1429	1485	0.68	0.66	0.68	0.67	0.67	0.66	0.68	0.67	1443	1470	1435	1457
56	0.50	0.58	0.49	0.61	0.50	0.56	0.49	0.60	2390	2194	2384	2155	0.47	0.55	0.47	0.57	0.45	0.51	0.47	0.55	2411	2222	2419	2206
57	0.92	0.93	0.92	0.93	0.92	0.92	0.92	0.92	1629	1636	1622	1618	0.93	0.94	0.93	0.94	0.93	0.94	0.93	0.94	1572	1555	1556	1545
58	0.83	0.62	0.82	0.64	0.83	0.60	0.82	0.62	1868	2188	1868	2153	0.84	0.66	0.83	0.69	0.84	0.66	0.83	0.69	1828	2114	1840	2082
59	0.90	0.79	0.90	0.78	0.90	0.78	0.90	0.77	1858	2117	1853	2116	0.90	0.77	0.90	0.78	0.90	0.77	0.90	0.77	1842	2120	1844	2123
60	0.80	0.75	0.79	0.76	0.80	0.74	0.79	0.75	2380	2373	2371	2352	0.80	0.75	0.80	0.78	0.80	0.75	0.80	0.78	2366	2348	2368	2306
61	0.89	0.90	0.89	0.90	0.89	0.90	0.89	0.90	1532	1441	1529	1431	0.91	0.92	0.91	0.91	0.91	0.93	0.90	0.91	1475	1359	1466	1362
62	0.92	0.86	0.92	0.86	0.92	0.86	0.92	0.86	1347	1453	1342	1428	0.93	0.89	0.94	0.89	0.93	0.89	0.93	0.89	1273	1353	1253	1344
63	0.76	0.68	0.76	0.68	0.76	0.66	0.76	0.66	2409	2612	2403	2605	0.78	0.68	0.77	0.71	0.78	0.67	0.77	0.70	2348	2592	2357	2532
64	0.84	0.88	0.84	0.87	0.84	0.88	0.84	0.87	2312	2229	2297	2223	0.87	0.89	0.87	0.89	0.87	0.89	0.87	0.89	2216	2154	2197	2130
65	0.72	0.37	0.72	0.39	0.72	0.34	0.72	0.36	1972	2385	1960	2366	0.72	0.49	0.70	0.51	0.71	0.48	0.69	0.50	1963	2299	1973	2274
66	0.74	0.46	0.75	0.47	0.74	0.44	0.75	0.46	2574	3021	2557	3001	0.78	0.50	0.78	0.52	0.78	0.47	0.77	0.50	2497	2985	2505	2964
67	0.82	0.78	0.82	0.79	0.82	0.78	0.82	0.79	2336	2569	2323	2552	0.83	0.78	0.83	0.78	0.83	0.78	0.83	0.77	2285	2566	2289	2565

Appendix F.

A Multivariate Statistical Framework for Top-down Projections of Freeze-Thaw under Changing Climate Conditions – Part 1: Key Considerations and Development of a Gridded Snow Depth Model

Table F1. The name, location, elevation, and data availability of the utilized stations

ID	Name	Ecozone	Latitude	Longitude	Altitude	Data Period	Data Availability (years)
1	Montréal-Mirabel	EZ8	45.67	-74.03	82.6	1976-2009	34
2	Montréal-Pierre Elliott Trudeau	EZ8	45.47	-73.75	26	1947-2019	69
3	Montreal-St. Hubert	EZ8	45.52	-73.42	27.4	1950-2005	56
4	Sherbrooke	EZ7	45.43	-71.68	241.4	1963-1995	33
5	Québec City	EZ8	46.8	-71.38	74.4	1947-1996	50
6	Bagotville	EZ6	48.33	-71	159.1	1950-2015	66
7	Baie-comeau	EZ6	49.13	-68.2	21.6	1948-2000	53
8	Sept-Îles	EZ6	50.22	-66.27	54.09	1947-2002	56
9	Fermont	EZ6	52.8	-67.08	594.4	1976-2004	20
10	Harrington Harbour	EZ6	50.53	-59.5	7.6	1950-1974	20